Technische Universität München
Lehrstuhl für Theoretische Informationstechnik

Spatial Interference Management for OFDM-Based Cellular Networks

Lars Thiele

Vollständiger Abdruck der von der Fakultät für Elektrotechnik und Informationstechnik der Technischen Universität München zur Erlangung des akademischen Grades eines

Doktor-Ingenieurs (Dr.-Ing.)

genehmigten Dissertation.

Vorsitzender:	Univ.-Prof. Dr. techn. Josef A. Nossek
Prüfer der Dissertation:	
	1. Univ.-Prof. Dr.-Ing. Dr. rer. nat. Holger Boche
	2. Prof. Dr. Robert W. Heath Jr., The University of Texas at Austin, USA

Die Dissertation wurde am 05.11.2012 bei der Technischen Universität München eingereicht und durch die Fakultät für Elektrotechnik und Informationstechnik am 11.06.2013 angenommen.

To my family

Zusammenfassung

Der stetig steigende Kapazitätsbedarf zellularer Systeme setzt einen Betrieb im Bereich hoher spektraler Effizienz und somit von benachbarten Basisstationen im selben Frequenzbereich voraus. Die hierdurch entstehende Interferenz wird jedoch schnell zum limitierenden Faktor. Um verschiedene Konzepte zum räumlichen Interferenzmanagement entwickeln und bewerten zu können, haben wir eine System-Simulations-Kette entwickelt. Diese ermöglicht einen direkten Vergleich der Ergebnisse. Als Basis untersuchen wir Konzepte zur Interferenzunterdrückung am Empfänger und zur Nutzung von Mehrnutzerdiversität. Diese kann bereits mit einfachen Verfahren wie frequenzselektivem Scheduling und Umschalten von Übertragungsmodi unter Verwendung von Limited-Feedback Precoding genutzt werden. Im zweiten Schritt entwickeln wir Systemkonzepte zur Koordination von benachbarten Basisstationen, die auf voller Kanalkenntnis beruhen. Hier wird die Interferenz benachbarter Basisstationen mittels Zero-Forcing Precoding bereits sendeseitig verhindert. Die oberen Schranken der Systemkapazität des Broadcast-Kanals bestimmen wir mittels Dirty-Paper Precoding.

Abstract

In order to satisfy the continually increasing capacity demands of emerging wireless services, future mobile cellular networks shall operate with full frequency reuse to achieve high spectral efficiencies. However, inter-cell interference becomes soon a limiting factor. To evaluate various system concepts for spatial interference management on a multi-cell basis, we developed a system-level simulation tool chain. This tool chain covers state-of-the-art channel modeling as well as physical and medium access control layer emulations. As a main contribution of this thesis, we aim at direct and quantitative comparison of the different interference management techniques. Our study covers interference canceling receivers as well as frequency selective scheduling and MIMO mode switching to enable multi-user diversity under limited feedback precoding. The commonly used full channel knowledge assumption is used for the concept of base station coordination, while closed-loop joint transmit beam-forming removes the co-channel interference between neighboring base stations. Finally, non-linear dirty paper precoding, known to achieve the broadcast channel capacity, delivers the upper bound for our studies.

Contents

1

Introduction

1.1 Motivation

In order to satisfy the continually increasing capacity demands of emerging wireless services, future mobile cellular networks shall operate with full frequency reuse to achieve high spectral efficiencies. However, inter-cell interference becomes soon a limiting factor. Tools such as hybrid ARQ, turbo coding, adaptive modulation and coding as well as multiple-input multiple-output (MIMO)-orthogonal frequency division multiplex (OFDM) and multiuser scheduling reach a network performance that can hardly be enhanced further from a single-cell point of view. Various methods to combat co-channel interference (CCI) in cellular MIMO systems are summarized in [ACH07], ranging from interference canceling receivers over multi-user diversity to closed-loop joint transmit beam-forming from multiple base stations (BSs). The joint transmission approach falls in the group of coordinated multi-point (CoMP) transmission, where multiple BSs transmit in a coordinated manner so that multiple data streams can be delivered simultaneously to different users in adjacent cells with reduced CCI. In the Third Generation Partnership Project (3GPP) standardization activities concerning Long Term Evolution - Advanced (LTE-A) [TR 09], CoMP is considered as a tool to improve the coverage of high data rates and cell edge throughput. For CoMP MIMO, channel state information at the transmitter (CSIT) from multiple BSs and user equipments (UEs) is required. This can be achieved by measuring the channel in reverse direction and exploiting reciprocity of time division duplex (TDD) systems. In frequency division duplex (FDD) systems, which are in the focus of this work, the channel is measured in the downlink direction at the UE side and then channel state information (CSI) is fed back via the uplink to the BSs.

In order to limit the amount of feedback information which needs to reported by each UE, 3GPP Long Lerm Evolution (LTE) considers quantization of CSI by using specific weight vectors from a given codebook [3GP07b, and subsequent versions].

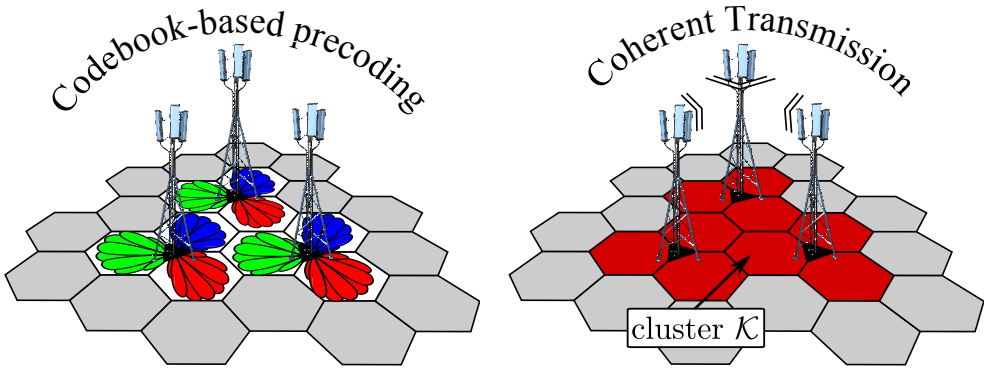

(a) Transmission according PMI feedback. (b) CoMP transmission.

Figure 1.1: From codebook based, decentralized transmission to coherent, joint transmission of collaborative base stations.

These codebooks contain multiple so-called precoding matrices which are known to both the transmitters and receivers in the system. Following a certain metric, each UE is selecting its preferred entry from that codebook, denoted as precoding matrix indicator (PMI), refer to Figure 1.1(a). In order to enable single-cell, channel-aware scheduling, UEs also provide feedback on their signal-to-interference-and-noise ratios (SINRs) in the form of so-called channel quality indicator (CQI) values for sub-groups of sub-carriers denoted as physical resource blocks (PRBs). These CQIs correspond to a specific PMI and a spatial transmission mode, which is indicated by the rank indicator (RI). When multiple users are served on the same PRB, the spatial multiplexing (SMUX) transmission mode [ZT03] is generalized from single-user MIMO (SU-MIMO) to multi-user MIMO (MU-MIMO) transmission. The achievable spectral efficiency may be enhanced by enabling MU-MIMO into system design and thus turning the focus to multi-user links [GKH$^+$07]. As a first extension towards multi-cell processing, adjacent base stations shall be synchronized and multi-cell reference signal (RS) can be introduced. They enable interference-aware equalization at the UE and improve the SINR estimation accuracy, leading to a more precise link adaptation at the BS side [TSWJ09].

The system performance can further be improved, by introducing multi-cell CSI feedback from the UE to the serving BS. Thus, BSs can determine the optimal beamforming weights for the set of users multiplexed on the same PRB in adjacent cells. Early concepts considered a huge centralized wireless distributed network (WDN), where all BS antenna are connected via a fast backhaul link to a central unit (CU) [BMWT00,SZ01,WMS$^+$02,GJJV03]. This setting corresponds to the MIMO broadcast channel (BC). Non-linear signal pre-processing, known as dirty paper precoding [Cos83], was shown to achieve the BC capacity [CS03, VT03, JVG04]. By allowing full coordination among the whole network, multi-cell interference can be removed to a certain degree, which depends on the selected precoding strategy

as well as on the channel knowledge. Due to additional beamforming gains, the system throughput can exceed the one known from an isolated cell [HV04]. In theory, this yields a block diagonal receive covariance matrix. Of course, this requires additional feedback overhead, since each UE has to convey the full multi-cell MIMO channel coefficients measured at the antenna ports of the serving cells in addition to the CQI. An extension of the block diagonalization concept called multi-user eigenmode transmission (MET) is proposed in [BH07b]. It assumes a linear transmission strategy based on zero-forcing beamforming in combination with eigenmode feedback from each UE. In [BH07b], multi-user eigenmode transmission (MET) was introduced as a linear transceiver optimization method, which was shown to approach the BC capacity in an isolated cluster. The eigenmode concept was shown to reduce the peak-to-average power ratio (PAPR) for linear precoding [JHJvH02] as well as for non-linear Tomlinson-Harashima precoding (THP) [NMK$^+$07]. In general, by limiting each user to report its strongest eigenmodes only, feedback may be reduced.

Considering practical aspects like degraded channel knowledge [JCUC12], linear precoding strategies without a strict zero-forcing (ZF) constraint might show a beneficial behavior. However, high complexity, growing data rates on the backhaul and the additional overhead remain serious challenges for the introduction of CoMP in next generation mobile networks. Especially backhaul requirements increase linearly with the number of BSs performing a coordinated transmission [HS09]. Therefore, BSs are merged into certain groups serving a specific set of users. These groups of BSs are referred as *clusters*, where only BSs belonging to the same cluster are allowed to perform CoMP transmission [PGH08, WGS$^+$11, MF11, LSB$^+$11, BSC$^+$11, IDM$^+$11]. As a result, costs can be scaled down with the size of the cooperation cluster. Furthermore, a distributed implementation of CoMP is desirable where the serving BS cooperates with a small subset of BSs in its direct vicinity [ZSK$^+$06, MF07, JTS$^+$08, NEHA08, PHG09, ZMS$^+$09, TWH$^+$09], refer to Figure 1.1(b). Recently, we have reported on a first real-time implementation [JTW$^+$09, JFJ$^+$10] of downlink CoMP demonstrating its feasibility. In [WBBJ11, WB11] authors relaxed the constraint of full data and CSI exchange for the case of static and arbitrarily varying interference. They focused on the case of two BSs, exchanging only partial information about their messages. By employing the Willems' conferencing protocol [Wil83], authors proved that the single-user sum capacity can already be achieved without full information exchange. This study clearly motivates the development of CoMP schemes involving partial CSI and data sharing among cooperating BSs as e.g. discussed for coordinated scheduling and beamforming concepts [GKGi07, KG08, CMIH08, HTH$^+$09, GA10, DUD11] as well as interference alignment techniques [CJ08, ST08, SW12, ABW12].

Recent results applying generalized MIMO techniques in wireless networks show huge gains [FHK$^+$05, KFV06]. In addition, [ZD04] proposes a common framework to study multi-user CoMP downlink transmission, considers practical signal processing issues and emphasizes the advantage of power gain, enhanced channel rank and

macro diversity. In [JJT+09], the authors confirm these findings based on channel measurements from a real cellular urban-macro deployment. The work in [VHLV09] promises significant gains obtained from a simulator including realistic operational conditions valid for an Worldwide Interoperability for Microwave Access (WiMAX) system operated in an indoor scenario.

1.2 Contribution and Organization of this Thesis

In order to evaluate various system concepts for spatial interference management on a multi-cell basis, we developed a system-level simulation tool chain. This tool chain covers state-of-the-art channel modeling as well as physical (PHY) and medium access control (MAC) layer emulations. As a main contribution of this thesis, direct and quantitative comparison is valid for most of the transceiver schemes in Chapters 3-6. Although, some results do not follow this target, we felt them worth for inclusion into this document.

Chapter 2 introduces the cellular OFDM system model. The general notation for transmit and receive beamforming is subsequently given for the MIMO downlink direction.

In **Chapter 3** we consider the downlink of a multi-user MIMO OFDM system in a cellular environment under limited feedback constraints. In particular, users are scheduled to the transmission resources in time, frequency and space. Targeting a practical solution, we assume to use fixed DFT-based precoding streams at the base stations and linear receivers at the multi-antenna terminals. After having received feedback on the frequency-selective interference conditions from all terminals, each base station schedules the terminals to their resources of highest quality while following a fair scheduling policy. It is shown that this rather simple practical concept enables spatial multiplexing transmission for most of the users in the system, in particular even for users at cell-edge. This results in a scaling of the throughput which is similar to the one known for the capacities of isolated point-to-point links. Furthermore, fair resource assignment is mandatory in cellular networks in order to guarantee radio access for all users. The multi-path structure of signal and interference channels may be used beneficially in this interference-aware scheduling process. Supplemental to the time-domain scheduling already used in todays radio systems, groups of frequency resources may be assigned to the users according to frequency-selective SINR conditions. In this case users may beneficially be assigned to their best resources. Chapter 3 concludes with system and user throughput results for various antenna configurations obtained from the system-level simulator.

In **Chapter 4** we study two major challenges which are connected to the limited feedback assumption. First, we focus on channel estimation and modeling of corresponding errors. Therefore, Section 4.1 starts from an additive white Gaussian noise (AWGN) assumption, over received covariance estimation based on transmitted data, towards pilot sequence-based estimation of multiple BSs. Multi-cell

channel estimation is achieved by a so-called *virtual pilot* scheme [TSSJ08]. It enables mobile terminals to distinguish the more of the strong interference channels the slower they are moving in the service area. Hence, without increasing the pilot overhead, low-mobility terminals can take most benefit of advanced interference mitigation schemes. Second, in Section 4.2 we reduce the amount of feedback, which is given by each UE according to 3GPP suggestions for the FDD downlink. Finally, this chapter concludes with a comparison of certain key performance indicators (KPIs) such as propagation parameters and data rates for a variety of channel modeling assumptions. Over the last decades, state-of-the-art channel models developed further from a Rayleigh fading assumption, over geometry-based stochastic channel model (GSCM) towards quasi-deterministic models, being capable to precisely track user movements and to model multiple links coherently.

In **Chapter 5** we focus on downlink CoMP using *centralized joint transmission*. Therefore, we assume an ideal, user-centric clustering method and study the effect on the achievable data rate from a growing cluster size. Furthermore, we introduce a two-step transceiver optimization concept and a unified CSI feedback framework to cope with different user-specific types of channel feedback. Initially, channel estimation and CSI feedback is assumed to be ideal, i.e. all data is known to all BSs in the cluster. This chapter concludes with a system-level simulation study for full CSIT as a function of an additional error drawn from a zero mean i.i.d. Gaussian distributed process with a certain variance.

In **Chapter 6** we start from the weighted sum-rate maximization problem by evaluating the capacity of the BC. In Section 6.1, we employ non-linear dirty paper coding (DPC) on a cluster basis with and without additional CCI. We reveal the scaling behavior of the capacity under the aspect of CoMP transmission. These results serve as a performance bound for results obtained with specific and non-ideal clustering and user grouping strategies, which are introduced in Sections 6.2 and 6.3. These methods are used to assess the required amount of feedback as a function of the cluster size and thus, in dependency of the achievable system and user throughput. The challenge of CSI feedback and out-dating of this information due to processing delays is carefully modeled and evaluated in Section 6.4. Furthermore, we study the effect of multiple antennas at the receiver and transmitter side as well as simple linear 1-dimensional channel prediction in frequency domain.

Chapter 7 finally concludes the thesis and highlights possible future research directions.

2

System Model for Cellular MIMO Transmission

2.1 Framing Structure of an OFDM System

orthogonal frequency division multiplex (OFDM) is a frequency division multiplex (FDM) scheme where the available bandwidth is divided into smaller partitions, carrying orthogonal data streams. Each data stream is carried by closely spaced and orthogonal sub-carriers, while each sub-carrier can use an individual modulation and coding scheme (MCS) depending on the current narrow-band channel quality. Therefore, Long Lerm Evolution (LTE) uses quadrature phase shift keying (QPSK), 16-quadrature amplitude modulation (QAM) and 64-QAM as possible modulation schemes combined with efficient forward error correction (FEC). Each time domain OFDM symbol contains a linear superposition of the instantaneous signals from all sub-carriers in frequency domain.

The protection against multi-path delay spread is one huge advantage of OFDM systems. Another important reason is comparatively simple equalization of frequency and phase distortions caused by transmitter impairments or radio-channel imperfections. This ability originates from the signal representation in the frequency domain by phase and amplitude for each sub-carrier. Additional advantages are high spectral efficiency, efficient implementation via fast Fourier transform (FFT), inherent bandwidth scalability and a high degree of freedom for resource allocation by the flexibility of many narrow-band sub-carriers for transmissions.

However, OFDM suffers from its high sensitivity to carrier frequency offsets which will cause inter-carrier interference (ICI). The main sources for these carrier frequency errors are Doppler shifts originating from the mobility of the user equipments (UEs) as well as local oscillator limitations. Therefore, each base station (BS) periodically sends a synchronization signal to align the oscillators at the transmitter

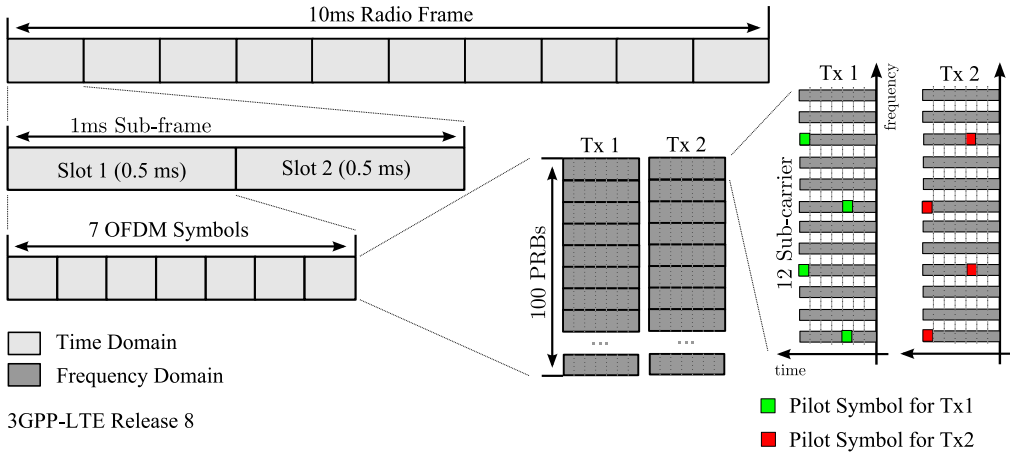

Figure 2.1: Framing structure of an OFDM system, here we used LTE Release 8 [3GP07b] as an example.

and receiver side. However, the Doppler shift and oscillator phase noise remains as an impairment in the system.

Due to multi-path propagation, a transmitted OFDM symbol arrives multiple times at the receiver side. This phenomenon is known as time-spreading and causes inter-symbol interference (ISI). In order to keep ISI as low as possible, each OFDM symbol consists of two parts in the time domain, a guard interval named cyclic prefix (CP) and the FFT period[1] carrying the payload information. The length of the CP is chosen according to the highest allowed delay spread due to multiple reflections in the propagation path. In a cellular LTE system the standard, i.e. short CP length is 4.69 µs in time domain. This corresponds to a path lengths difference of approximately 1.4 km[2] for all multi-path components arriving at the receiver. Note, depending on the cell size or desired application, a long CP length of 16.67 µs is available. This provides a protection against a time spreading which is equivalent to path length of 5 km.

The LTE framing structure is given in [3GP07b, Chapter 4] and is summarized as follows: One radio frame is divided into ten sub-frames, each having a duration of 1 ms. Sub-frames are equally divided into two slots of 0.5 ms, refer to Figure 2.1. According to the CP length, each slot includes six or seven OFDM symbols. For short CP, seven symbols with $7 \cdot (4.69 + 66.67)\,\mu s = 0.5$ ms result into the duration of a slot. Directly related to the time domain one resource element (RE) covers a bandwidth of 15 kHz. Note, individually assigned RE would cause a tremendous signalization overhead. Hence, multiple REs are grouped into a physical resource block (PRB), consisting of 7×12 RE in time and frequency dimensions, respectively.

[1] A FFT period in LTE is 66.67 µs, which is the inverse of 15 kHz carrier spacing.
[2] Here we assume that radio waves propagate with the speed of light.

This results in a bandwidth of 180 kHz and a duration of 0.5 ms.

Throughout this thesis, we do not consider ISI as well as ICI as sources for performance degradation. In contrast, we limit our studies on co-channel interference (CCI) caused by all BSs in the considered deployment.

2.2 Downlink Transmission Schemes

Let us consider a cellular OFDM downlink where a central site is surrounded by multiple tiers of sites. We assume each site to be partitioned into three 120° sectors, i.e. the system model covers a set $\mathcal{M}$ consisting of $M = |\mathcal{M}|$ sectors in total. Each sector constitutes a cell transmitting its own id. $\mathcal{M}_c \subset \mathcal{M}$ represents the set of cells included in a given cluster and $M_c = |\mathcal{M}_c|$ denotes its size. In general, joint processing will only be possible between BSs belonging to the same cluster, where BSs outside the cluster are not coordinated and thus cause residual inter-cluster interference. Furthermore, we consider a interference limited setup, such that frequency resources are fully reused in all M cells, i.e. frequency reuse of $\eta = 1$.

In particular, we focus on the broadband multi-user (MU) multiple-input multiple-output (MIMO)-OFDM downlink direction, where each BS and each UE are equipped with multiple transmit antennas N_t and multiple receive antennas N_r, respectively. A set $\mathcal{K}$ of UEs is uniformly placed into the region covered by all M cells. Thus, the compound downlink MIMO-OFDM transmission system for all BSs and UEs is described on a per sub-carrier basis

$$\mathbf{y} = \mathbf{H}\mathbf{S} + \mathbf{n} \,, \tag{2.1}$$

where $\mathbf{H}$ is the $KN_r \times MN_t$ channel matrix, $\mathbf{S}$ is the $MN_t \times |\mathcal{T}_s|$ matrix containing precoded user data and the set of active spatial data streams is combined in $\mathcal{T}_s$. The relation between transmit antennas and data symbols might be linear as e.g. in case of codebook based precoding and zero-forcing (ZF) beamforming; or more general non-linear as e.g. in case of Tomlinson-Harashima precoding (THP) and dirty paper coding (DPC). For simplicity, let us consider a linear combination of transmit antennas and data, i.e. $\mathbf{S} = \mathbf{B}\,\mathbf{P}^{1/2}\mathbf{x}$, where $\mathbf{B}$ is the $MN_t \times MN_t$ precoding matrix and matrix $\mathbf{P}$ is carrying the corresponding power allocation. The $MN_t \times 1$ vector of transmitted symbols is denoted as $\mathbf{x}$; $\mathbf{y}$ and $\mathbf{n}$ provide the $KN_r \times 1$ vectors of the received signals and of the additive white Gaussian noise (AWGN) samples, respectively, with covariance $\mathbb{E}\left\{\mathbf{n}\mathbf{n}^H\right\} = \sigma_n^2\mathbf{I}$. $\mathbb{E}\{\}$ is the expectation operator. The transmit covariance matrix is given by $\mathbf{\Phi} = \mathbb{E}\left\{\mathbf{S}(\mathbf{S})^H\right\}$, where the appropriate selection of the precoding entries is typically subject to a *sum*, *per-BS* or *per-antenna* power constraint. The structure of the precoding matrix can vary from block-diagonal with sub-matrices of dimension $N_t \times N_t$, in case of non-coordinated

BSs, up to a fully populated matrix where all transmit antennas contribute to all data streams in case of a network-wide joint signal processing.

As a next step, let us focus on certain cluster c of BSs.[3] As a consequence, we denote the corresponding user set as $\mathcal{K}_c \subset \mathcal{K}$. It combines the users following a certain metric. A scheduling algorithm selects a subset of UEs out of $\mathcal{K}_c$ to be simultaneously served on the same resources in time and frequency using spatial multiplexing (SMUX) transmission. The received downlink signal $\mathbf{y}_k$ at UE k is given by

$$\mathbf{y}_k = \underbrace{\mathbf{H}_{c,k}\mathbf{s}_{c,k}}_{\substack{\text{Desired signal}\\ \overline{\mathbf{h}}_k}} + \underbrace{\sum_{j\in\{\mathcal{K}_c\setminus k\}} \mathbf{H}_{c,k}\mathbf{s}_{c,j}}_{\substack{\text{Intra-cluster interference}\\ \boldsymbol{\vartheta}_k}} + \underbrace{\sum_{l\in\{\mathcal{M}\setminus\mathcal{M}_c\}}\sum_{j\in\{\mathcal{K}\setminus\mathcal{K}_c\}} \mathbf{H}_{l,k}\mathbf{s}_{l,j} + \mathbf{n}}_{\substack{\text{Inter-cluster interference}\\ \mathbf{z}_k}} \quad (2.2)$$

where $\mathbf{s}_{c,k} \in \mathbb{C}^{[M_c N_t \times 1]}$ denotes the precoded signals targeted towards UE k and to be transmitted from all BS antennas connected to cluster c. We emphasize that the rank 1 transmission assumption is only made to simplify the notation. This assumption can easily be extended to the more general case of sending multiple independent streams to a subset of scheduled users. The desired data stream x_k is distorted by intra-cluster and inter-cluster interference plus noise aggregated in $\boldsymbol{\vartheta}_k$ and $\mathbf{z}_k$, respectively. Note, $\mathbf{H}_{c,k}$ spans the $N_r \times M_c N_t$ channel matrix between all BSs in cluster c and UE k.

2.3 Downlink Reception Schemes

Assuming that $N_r > 1$ and a linear equalizer $\mathbf{w}_{k,t}$ is employed to extract the useful signal from $\mathbf{y}_{k,t}$ connected to stream t, this yields a post-equalization signal-to-interference-and-noise ratio (SINR) given by

$$\mathrm{SINR}_{k,t} = \frac{\mathbf{w}_{k,t}^H \overline{\mathbf{h}}_{k,t} \overline{\mathbf{h}}_{k,t}^H \mathbf{w}_{k,t}}{\mathbf{w}_{k,t}^H \mathbf{Z}_{k,t} \mathbf{w}_{k,t}}, \quad (2.3)$$

where $\mathbf{Z}_{k,t}$ is the received covariance matrix of interfering signals. In particular, it combines intra- as well as inter-cell interference $\mathbf{Z}_{k,t} = \boldsymbol{\Theta}_{k,t} + \mathbf{Z}_k$, where $\boldsymbol{\Theta}_{k,t}$ and $\mathbf{Z}_k$ are the received covariance matrices of the interfering signals aggregated in $\boldsymbol{\vartheta}_{k,t}$ and $\mathbf{z}_k$, i.e. $\boldsymbol{\Theta}_{k,t} = \boldsymbol{\vartheta}_{k,t}\boldsymbol{\vartheta}_{k,t}^H$ and $\mathbf{Z}_k = \mathbf{z}_k \mathbf{z}_k^H$.

There are different spatial receive filtering strategies, involving different degree of channel knowledge. The scheme with lowest requirements is known as maximum ratio combining (MRC). Receiver weights are given as

$$\mathbf{w}_{k,t}^{\mathrm{MRC}} = \overline{\mathbf{h}}_{k,t} \quad (2.4)$$

[3] Note, the special case of single-cell cluster, i.e. $|\mathcal{M}_c| = 1$ covers the typical Third Generation Partnership Project (3GPP) LTE application.

Corresponding post-equalization SINRs are given by

$$\mathrm{SINR}_{k,t}^{\mathrm{MRC}} = \frac{\left|\overline{\mathbf{h}}_{k,t}^{H}\overline{\mathbf{h}}_{k,t}\right|^{2}}{\overline{\mathbf{h}}_{k,t}^{H}\mathbf{Z}_{k,t}\overline{\mathbf{h}}_{k,t}}. \tag{2.5}$$

In particular, in applications where a BS is transmitting multiple spatial data streams, each UE is able to estimate intra-cell interference $\boldsymbol{\vartheta}_{k,t}$ besides the desired channel $\overline{\mathbf{h}}_{k,t}$. Therefore, BSs usually transmit pilot tones known as common reference signals (CRS), refer to Figure 2.1. On these resources, users can estimate the channel coefficients in $\mathbf{H}_{m,k}$ to a certain degree, where m corresponds to a specific BS. Section 4.1 covers the topic of channel estimation and highlights potential losses connected to that estimation process. For sake of simplicity, we introduce error free receiver models at this stage. As a consequence, we introduce the minimum mean square error (MMSE) receiver, which utilizes explicit channel knowledge for $\overline{\mathbf{h}}_{k,t}$ and $\boldsymbol{\vartheta}_{k,t}$, and only a total received power estimate for residual inter-cell interference and AWGN in $\mathbf{z}_k$. The receiver weights are given by

$$\mathbf{w}_{k,t}^{\mathrm{MMSE}} = \left[\overline{\mathbf{h}}_{k,t}\overline{\mathbf{h}}_{k,t}^{H} + \boldsymbol{\Theta}_{k,t} + \mathrm{diag}\left(\mathbf{Z}_k\right)\right]^{-1}\overline{\mathbf{h}}_{k,t} \tag{2.6}$$

where $\mathrm{diag}\left(\mathbf{Z}_k\right)$ is a diagonal matrix with the diagonal elements from covariance matrix $\mathbf{Z}_k$. The SINR is determined by Equation (2.3).

For optimum combining (OC) [Win84], the interference-aware MMSE receiver is used

$$\mathbf{w}_{k,t}^{\mathrm{OC}} = \mathbf{R}_{yy}^{-1}\overline{\mathbf{h}}_{k,t} \tag{2.7}$$

where $\mathbf{R}_{yy}$ denotes the covariance matrix of all received signals in $\mathbf{y}_{k,t}$, i.e.

$$\mathbf{R}_{yy} = \mathbf{Z}_{k,t} + \overline{\mathbf{h}}_{k,t}\overline{\mathbf{h}}_{k,t}^{H} \tag{2.8}$$

The corresponding SINR after equalization simplifies from Equation (2.3) to

$$\mathrm{SINR}_{k,t}^{\mathrm{OC}} = \overline{\mathbf{h}}_{k,t}^{H}\mathbf{Z}_{k,t}^{-1}\overline{\mathbf{h}}_{k,t} \tag{2.9}$$

Using these SINRs as inputs for a so-called link-2-system interface, we obtain the achievable spectral efficiency for the orthogonal frequency division multiple access (OFDMA) downlink in our multi-cellular simulation environment.

2.4 Link-2-System Interface

For the sake of completeness, we summarize the two major methods to obtain data rates within system-level simulations. Starting from a theoretic point of view, SINRs from receiver processing can be directly mapped into data rates by employing the famous Shannon formula, i.e. $R = \sum_{\forall PRBs} B_{PRB} \log_2 (1 + \mathrm{SINR}_{PRB})$, where B_{PRB} corresponds to the bandwidth of a PRB. In particular, when focusing on practical system constraints, these so-called Shannon information rates are typically replaced by another simple mapping function. Therefore, input SINRs are mapped to a desired operational range, e.g. $\lfloor -10, 25 \rceil$ dB, taking into account that practical modulations cannot be applied below or above a certain threshold. Due to additional channel coding, e.g. low density parity check (LDPC) or turbo codes, a specific modulation can be applied on a broader range of SINRs. Although, gross bit rate remain constant, net bits per sub-carrier are reduced by the current code rate. Due to these limitations it is reasonable to introduce an additional offset for input SINRs in order to take the effects of non-ideal resource loading into account.

Figure 2.2 is showing both Shannon mapping schemes in addition to a 4 bit quantized MCS as given in [3GP12, Table 7.2.3-1]. Due to the extraordinary computational complexity of FEC, data transmission is usually abstracted using a state-of-the-art link-2-system interface. These mapping curves are the result of extensive link-level simulations and are not part of this thesis.

Most of our performance results are based on SINRs obtained on a per PRB basis instead of simulating 1200 sub-carriers at 20 MHz bandwidth. In Section 4.2, we introduce a grouping of multiple PRBs into a small number of sub-bands, according to suggestions in 3GPP [3GP12, Table 7.2.2-2]. In order to determine the resulting channel quality indicators (CQIs) per sub-band using the SINRs per PRB as an input, we employ the well-known exponential effective SINR mapping (EESM). The EESM is also part of the link-2-system interface, which maps a set of SINR values into data rates without directly employing FEC in system-level simulations. A comparison of different mapping functions is given in [AAB+05]. Thereby, the link-2-system interface uses a vector of SINR values as well as a desired target block error rate (BLER) as inputs and determines an effective scalar SINR which corresponds to a single-input single-output (SISO) AWGN link-level performance curve.

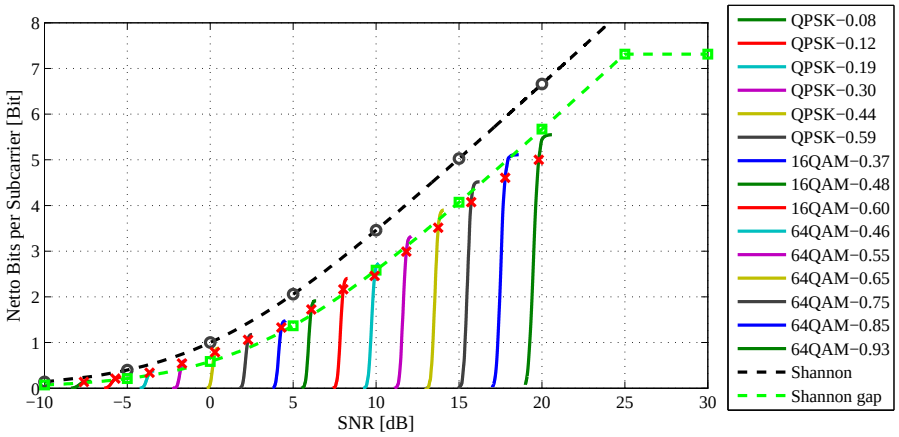

Figure 2.2: Mapping interface from SNRs or SINRs into data rates. Here we include Shannon information rates and a mapping using a 3 dB Shannon gap approach including a mapping of input SINRs to the range of $\lfloor -10, 25 \rceil$ dB. Curves with specific modulation format and corresponding code rate are part of the MCS in LTE [3GP12, Table 7.2.3-1], transport block size of 630 Bits and target BLER of 0.1.

3

Decentralized Interference Management with Limited Feedback

Transmission with multiple antennas both at the transmitting and receiving ends of a wireless link has become increasingly mature in recent years. From theory, the fundamental capacity gain in the MIMO radio link, being proportional to the minimum of the number of transmit and receive antennas, is well understood for an isolated point-to-point link. A fundamental trade-off between different transmission modes has been pointed out in [ZT03], which are SMUX and spatial diversity (SDIV), revealing that the mode maximizing the capacity depends on the actual channel state.[1] This fact motivated the development of an adaptive transmission system, selecting the transmission mode depending on the actual channel quality in order to improve the error rate performance for fixed data rate transmission [HP05] or to increase the spectral efficiency [CLH$^+$04].

To enable ubiquitous broadband wireless access, MIMO transmission must be made robust against multi-cell interference. However, it has not been fully evident yet how the potential capacity gains of MIMO can be realized under these conditions. In fact, early results, obtained for a small set of linear transceiver setups indicate only small gains for SMUX over SDIV systems [CDG00]. The achievable spectral efficiency may be enhanced by enabling multi-user MIMO (MU-MIMO) into system design and thus turning the focus to multi-user links [GKH$^+$07]. However, BSs would require coherent channel state information to optimally serve their users in MU-MIMO, which is difficult to obtain in frequency division duplex (FDD) systems, as a high rate feedback link would be required. In particular, joint DPC enables

[1] Note, that the achievable data rate also depends on the knowledge on channel state information (CSI) at both, receiver and transmitter side.

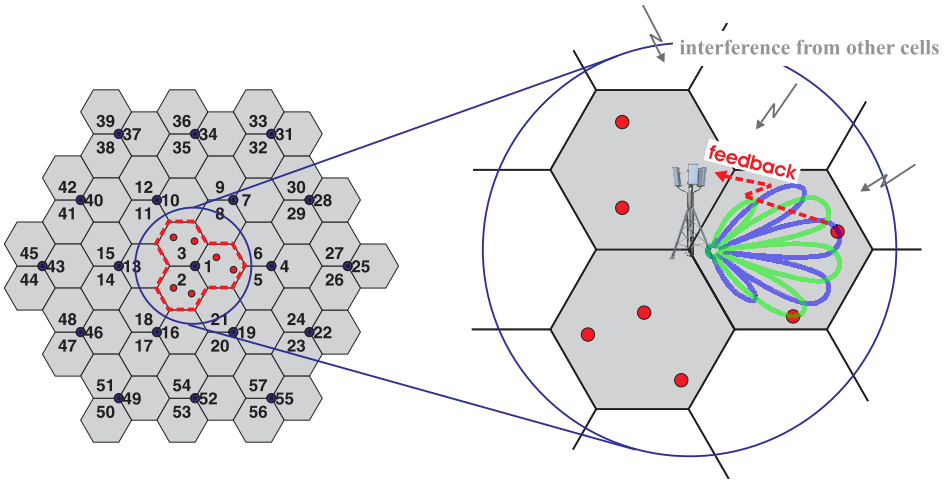

Figure 3.1: System concept assuming multiple antennas at the base station for the purpose of unitary fixed DFT-based precoded beamforming. SINR feedback is provided by the terminal for possible transmission modes using a narrow band feedback channel.

the capacity of the broadcast channel and is considered as an upper bound for multi-user transmission [VT03, CS03, JVG04]. Section 6.1 summarizes the non-linear precoding concept and evaluates the resulting data rate if jointly applied onto a certain set of BSs. For multi-cell applications, however, the base station would need coherent intra-cell channel state information, and also the inter-cell interference must be known in advance. A distant mobile terminal, measuring these quantities at vehicular velocities in the downlink, may have limited power, and hence a limited uplink capacity, to feed back such complex information instantaneously to the base station. Consequently, in this chapter, MIMO equalization is placed at the terminal side and feedback is provided for post-equalization SINRs. This approach reduces bandwidth and latency requirements for the control channels. An estimation of required feedback and a summary on achievable data rates are given in Section 4.2.

In this chapter[2], we focus on a *non-cooperative* downlink transmission scheme, i.e. where no explicit cooperation takes place between BSs, but where interference-aware transmission and reception is performed within cells. The BSs perform intra-cell precoding based on limited feedback from the UEs, in conjunction with interference-aware scheduling and advanced receivers at the terminal side. Targeting a practical solution for decentralized interference management, we consider downlink transmission using a fixed grid of beams (GoB) as depicted in Figure 3.1. In particular, terminals are assumed to report their preferred precoding indices out of a known

[2]This chapter is based in parts on [TSWJ09].

codebook in combination with corresponding post-equalization SINRs via a low-rate feedback channel. The key to success is a predictable interference scenario at the receiver side, which also helps to improve the link adaptation process. As a side effect, codebook based precoding can help to provide such a quasi-static interference scenario. An inherit delay between the feedback from a user k and the time instant where neighboring BSs may have changed their scheduling decisions, can cause a major discrepancy in CCI [OL05] which is experienced at a user terminal k. This so-called *flashlight effect* [VRH09] can be alleviated by allowing a certain degree of coordination among BSs. Once the selection of neighboring precoders is coordinated, interference conditions are mainly influenced by the fast-fading properties of the observed users.

Near-optimum equalization requires the UEs to collect precise multi-cell channel knowledge from their direct vicinity, which may be obtained by multi-cell channel estimation based on pilot symbols [TSSJ08, JMT$^+$09]. Therefore, downlink transmission has to be synchronized [JWS$^+$08]. With this approach we demonstrate substantial throughput gains for MIMO systems in multi-cell environments, similar to those known for point-to-point links. Section 4.1 further indicates the potential performance under the influence of imperfect channel estimation in systems with non-synchronized and synchronized BSs.

In order to determine the maximum system performance we may assume SINR frequency-selective feedback per PRB for all possible single- and multi-stream transmission modes as indicated in Figure 3.2. The mode itself is always selected at the base station, using a score-based scheduling algorithm. This heuristic approach may easily be implemented and reaches the performance of the proportional fair scheduler asymptotically [Bon04]. The original algorithm has been extended to support multiple transmission modes, see also [STJH07]. At the terminal the most appropriate receiver algorithm is used.

Our results clearly illustrate the gain of frequency-selective scheduling in cellular environments. However, we point out that proportional fair scheduling policies are rather costly in a cellular network, compared to the throughput-maximizing approach. We illustrate the benefit of multi-antenna receiver algorithms that are aware of the interference (refer to optimum combining (OC) or interference rejection combining (IRC) [Win84, BZ71, TJ08]) and extend these algorithms to the case of multi-stream transmission. While the single-stream transmission mode is valuable for cell-edge users as well as for users with singular channels, the gains, compared to a SISO system, vanish in this case for SMUX if multiple streams are assigned to a single user, as reported in [CDG01]. Nonetheless, multi-stream detection is valuable at the terminal side. It enables a new class of multi-user transmission schemes where parallel streams are transmitted from the base station and separated at each terminal. These streams may be scheduled to distinct users, based on their feedback information. This mode is called MU-MIMO [SJSC06]. It is selected frequently by the scheduler, even close to the cell-edge, and it can be identified as one of the major driving forces enabling the multi-antenna throughput gain also for

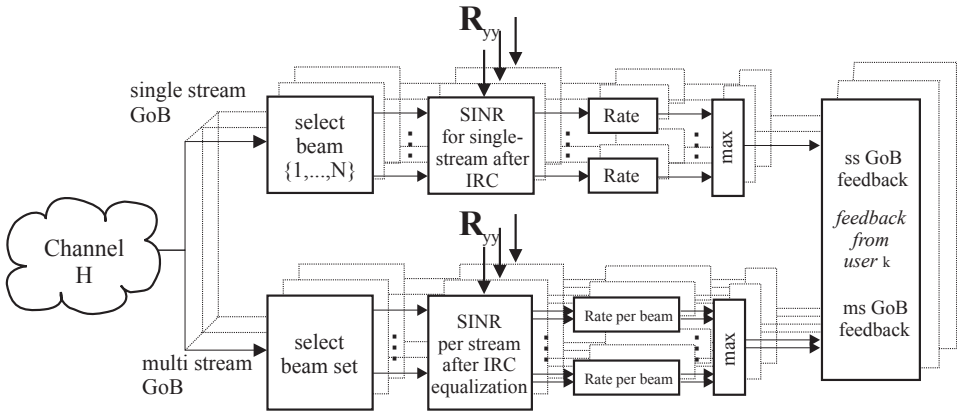

Figure 3.2: Block diagram for the adaptive transmission strategy. The terminals need to determine the achievable SINRs for single-stream and multi-stream transmission.

cellular networks. Highest gains and lowest outage are achieved when the switching between all modes is allowed. In this way, the fundamental MIMO throughput scaling law, proportional to the minimum number of receive and transmit antennas, can be realized in a proportional fair sense for all users within a cell. Of course, there will be a small penalty attributed to the limited feedback assumption.

3.1 System Model for Limited-Feedback Precoding

In the following paragraph, we extend the multi-antenna OFDMA downlink model from Equation (2.1) towards cell-independent, linear precoded transmission using predefined *codebook* entries according to LTE specifications. This implies that each BS may transmit up to N_t *data streams* simultaneously on the same time and frequency resources, while each UE may receive up to N_r streams simultaneously. Clearly, there is a degree of freedom in the number of active data streams per BS to serve the UEs. This concept is later introduced as *transmission mode switching*.

We are observing *non-cooperative* downlink transmission, this means that each stream may only be transmitted from a single BS. Consequently, the overall precoding matrix $\mathbf{B} \in \mathbb{C}^{MN_t \times MN_t}$ as introduced in (2.1) is sparse, as each column connected to one UE and one stream may only have non-zero entries connected to the antennas of one BS.

In the sequel, let us observe one UE k which is served by the m-th BS. The set $\mathcal{K}_m$ captures all UEs which can be served by BS m within a certain time duration. Each BS can offer a set of spatial layers $\mathcal{T}$. The number of UEs which are simultaneously served on the same frequency resource are mapped onto active data streams, also called active spatial layers $\mathcal{T}_s \subset \mathcal{T}$. Obviously the number of active

layers is limited by transmit antennas, i.e. $|\mathcal{T}_s| \leq N_t$ in case of linear precoding techniques. Therefore, let us assume a scheduling algorithm which selects a subset of active users per PRB according to a specific metric. Thus, the received downlink signal $\mathbf{y}_{k,t}$ for $t \in \mathcal{T}_{s,k} \subset \mathcal{T}_s$ at user k in the cellular environment is given by

$$\begin{aligned}\mathbf{y}_{k,t} = \; & \underbrace{\mathbf{H}_{m,k}\left[\mathbf{B}_m\right]_{:,t}\sqrt{p_{m,t}}x_{m,t}}_{\overline{\mathbf{h}}_{k,t}} + \underbrace{\sum_{j\in\mathcal{T}_s\setminus\{t\}}\mathbf{H}_{m,k}\left[\mathbf{B}_m\right]_{:,j}\sqrt{p_{m,j}}x_{m,j}}_{\substack{\text{Intra-cell interference}\\ \boldsymbol{\vartheta}_{k,t}}} \\ & + \underbrace{\sum_{l\in\mathcal{M}\setminus\{m\}}\sum_{j=1}^{N_t}\mathbf{H}_{l,k}\left[\mathbf{B}_l\right]_{:,j}\sqrt{p_{l,j}}x_{l,j} + \mathbf{n}}_{\substack{\text{Inter-cell interference}\\ \mathbf{z}_k}}\end{aligned} \tag{3.1}$$

where $\mathbf{H}_{m,k}$ is the channel between UE k and the m-th BSs, $\mathbf{B}_m \in \mathbb{C}^{N_t\times N_t}$ is the compound precoding matrix used at the m-th BS, and $[\mathbf{B}_m]_{:,t}$ is the t-th column vector intended for user k, i.e. the t-th data stream. We write as $\overline{\mathbf{H}}_k$ the *effective* channel between UE k and its serving BS after precoding, which consists of multiple, i.e. $|\mathcal{T}_{s,k}|$, column vectors $\overline{\mathbf{h}}_{k,t}$. The corresponding potential data streams are stacked into $\mathbf{x}_k$ and $\mathbf{x} \sim \mathbb{C}\mathcal{N}(\mathbf{0}, \mathbf{I})$. Downlink transmission is distorted by the intra-cell and inter-cell interference aggregated in $\boldsymbol{\vartheta}_{k,t}$ and $\mathbf{z}_k$, respectively. Each BS m may select a limited number $|\mathcal{T}_s| \leq N_t$ of active streams to serve one user with multiple streams or multiple users simultaneously.

In case of LTE transmission concepts, each BS chooses its desired precoding matrix $\mathbf{B}_m$ from a certain set of precoding matrices combined in a codebook $\mathcal{B}$. In particular, this set may consist of two elements with $\mathcal{B} = \{\boldsymbol{\beta}_1, \boldsymbol{\beta}_2\}$ in the case of $N_t = 2$, codebook size of $|\mathcal{B}| = 2$ and discrete Fourier transform (DFT)-based precoding. Thus, the different precoding matrices $\boldsymbol{\beta}_i$ are given by

$$\boldsymbol{\beta}_1 = \frac{1}{\sqrt{2}}\begin{bmatrix} 1 & 1 \\ i & -i \end{bmatrix} \text{ or } \boldsymbol{\beta}_2 = \frac{1}{\sqrt{2}}\begin{bmatrix} 1 & 1 \\ 1 & -1 \end{bmatrix}. \tag{3.2}$$

Columns in $\mathbf{B}_m$ which represent non-active data streams can conveniently be filled with zeros. In order to maintain full transmission power P_m per BS, $\mathbf{B}_m$ can be scaled depending on the choice of $|\mathcal{T}_s|$ such that $\mathrm{tr}\{\mathbf{B}_m(\mathbf{B}_m)^H\} = 1$. If only one stream is active, i.e. $|\mathcal{T}_s| = 1$, we name it single-stream transmission mode, while for $|\mathcal{T}_s| > 1$, we refer to it as multi-stream transmission mode.

3.2 Codebooks for Multi-User Cellular Systems

In general, perfect channel knowledge at the BS side is usually infeasible, especially in FDD systems. Thus, UEs are allowed to report limited or partial CSI. There are two main categories of limited feedback assumptions [LHL+08]. As first concept, users are assumed to quantize their downlink channel $\mathbf{H}_{m,k}$. This is usually done by random vector quantization (RVQ) techniques with sub-sequent ZF beamforming [Jin06, YL05, RHV09]. Authors in [HAH09] denote this scheme as ZF-SDMA with prior RVQ. The second concept is denoted as opportunistic SDMA (OSDMA). In this approach, the precoders $\mathbf{B}_m$ are usually chosen from a random codebook set $\mathcal{B}$ [SH05]. Each user is assumed to provide feedback for either its best stream index only or for all combinations. The authors in [LHL+08] provide a very good literature overview on this topic. The main drawback is a quite poor performance in the regime of small amount of users in $\mathcal{K}_m$, due significant intra-cell interference originating from the random spatial structure of data streams. Standardization activities developed an improved version denoted as per user unitary and rate control (PU2RC). Instead of randomly generated spatial beams, precoders are derived from a fixed codebook of multiple orthogonal bases, aggregated in the set $\mathcal{B}$. [HAH09] compares the difference for all three concepts at different SNR regimes. In particular, authors highlight the superior performance of PU2RC over ZF-SDMA in case of a large user set $\mathcal{K}_m$.

Authors in [LH03a] introduce the term of equal gain transmission (EGT), where the MIMO transmission is performed by using beamformers chosen from a unitary set. Therefore, authors used a DFT matrix where all column vectors are naturally following this EGT concept. Furthermore, [LH03a] proposes a quantized version of EGT in combination with a codebook design, proving full guarantee of full diversity order. Later [KPLK07] reused this concept to derive the codebook entries from a huge DFT matrix, selecting multiple column vectors as active streams. They developed a scheme choosing and combining those column indices having a maximum chordal distance, into a precoding matrix $\boldsymbol{\beta}_i$. By use of computer simulations, authors demonstrated under Rayleigh fading assumptions, that inter-stream interference can be significantly reduced when the amount of available codewords in $\mathcal{B}$ increases.

Figure 3.3 depicts the resulting precoding characteristic for $N_t = 4$ transmit antennas at the BS using a typical co-polarized sector antenna. The precoders are generated following the scheme from Equation (3.2). Current LTE specification [3GP10] suggests using Householder precoders instead. Note, LTE mainly targets single-user transmission. In case of $N_t = 2$, the set of precoding vectors $\mathcal{B}$ consists of $\boldsymbol{\beta}_1$, $\boldsymbol{\beta}_2$ and a matrix corresponding to antenna selection, i.e. in total 2 bit resolution. In contrast, for $N_t = 4$, Householder reflections form a set $\mathcal{B}$ with resolution of 4 bit, i.e. a total number of 16 precoding matrices $\boldsymbol{\beta}_i$. Figure 3.4 shows all combinations for the case of full multi-stream transmission, i.e. $|\mathcal{T}_s| = N_t = 4$. In particular,

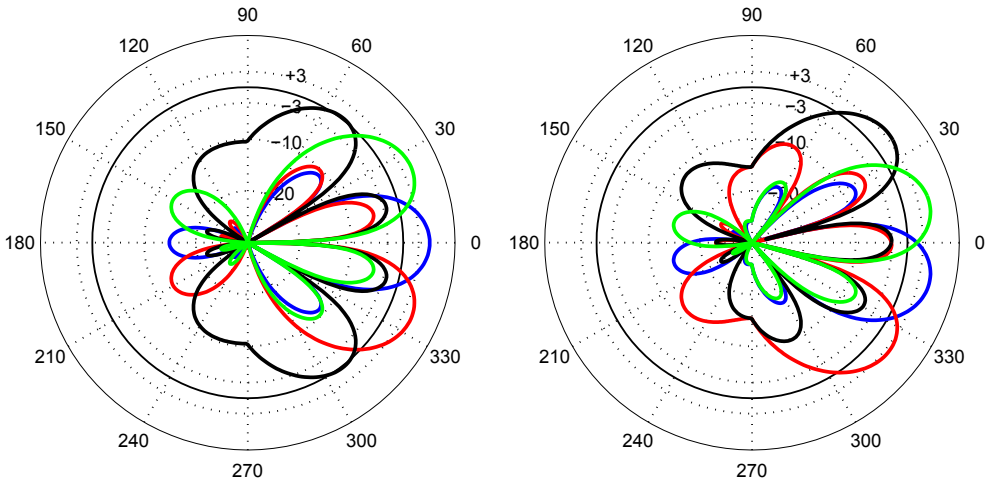

(a) First DFT matrix $\boldsymbol{\beta}_1$.

(b) Second DFT matrix $\boldsymbol{\beta}_2$.

Figure 3.3: Precoding characteristic for $N_t = 4$ transmit antennas and $\lambda/2$ antenna spacing. Figures from left to right show first and second DFT set, similar to Equation (3.2). Sector antenna characteristic is already included into the diagram.

precoding sets $\boldsymbol{\beta}_1$, $\boldsymbol{\beta}_3$, $\boldsymbol{\beta}_9$ and $\boldsymbol{\beta}_{11}$ show a similar spatial structure in the azimuth direction, refer to Figure 3.4(a). However, each of these sets is deactivating its spatial layers in a different order for $|\mathcal{T}_s| < N_t$, i.e. for three, two and a single active data stream. Thus, the matrix index in combination with the number of active layers in $\mathcal{T}_s$ inherently defines the spatial stream structure on a given time and frequency resource. Furthermore, it turns out, that also some kind of antenna selection radiation characteristic is available, refer to Figure 3.4(e).

Precoders derived from DFT matrices have a number of beneficial properties for multi-user MIMO systems:

- Uniform spatial radiation characteristic if all spatial layers are active, and thus, a robust CCI for all users in all cells.
- Spatial layers enable a kind of sub-sectorization in azimuth direction, with a maximum chordal distance. Thus, inter-stream interference is kept to a minimum.
- Transmission mode switching, i.e. a concept for rank-adaptive transmission, can conveniently be included into the scheduling process.
- Naturally given equal gain per stream.

In practice, there are a couple of issues which need to be addressed. Let us assume $N_t = 4$, $|\mathcal{B}| = 1$ and $|\mathcal{T}_s| = 2$, then there exist $\binom{4}{2} = 6$ combinations to

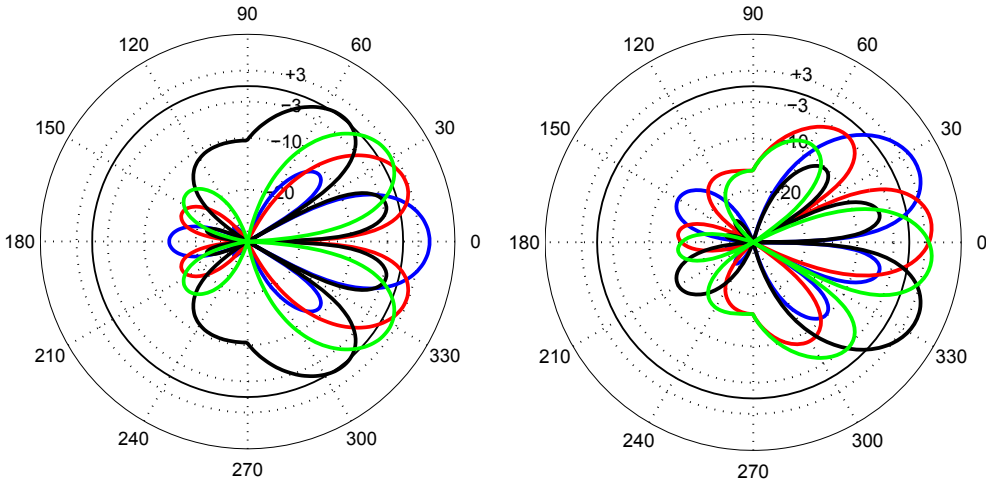

(a) 1st, 3rd, 9th, 11th Householder set.

(b) 2nd, 4th, 10th, 12th Householder set.

(c) 5th, 7th Householder set.

(d) 6th, 8th Householder set.

(e) 13th, 14th, 15th, 16th Householder set. Each line corresponds to two streams.

Figure 3.4: Precoding characteristic for $N_t = 4$ transmit antennas and $\lambda/2$ antenna spacing. Figures depict the different sets derived from Householder precoders, refer to LTE specification [3GP10]. Sector antenna characteristic is already included.

activate 2 spatial layers. Further, consider that a UE has to estimate SINR values for all combinations and PRBs. This not only exceeds the desired amount of data in limited feedback assumptions but also poses an extensive computational burden to the user. However, we will concentrate on the ideal performance within the current chapter, while Section 4.2 introduces practical constraints of sub-band and wide-band feedback. In the following section, we develop a heuristic metric to combine the user scheduling and adaptive spatial layer assignment, while maintaining fairness among the users.

3.3 Resource Allocation and Fair User Selection

3.3.1 Overview

Let us consider a set of users $\mathcal{K}_m$ UEs assigned to BS m. To decide for the used transmission mode and the particular radio resource assignment, the BS evaluates the feedback reported by the UEs. This may be done using different scheduling algorithms.

The round-robin metric is a simple algorithm to serve the users by assigning time and/or frequency resources one after another to a different user. After K_m resources, the same user is served again. This is a simple way to ensure fairness but it is known to be suboptimal in terms of data throughput since channel conditions are not taken into account. As time and frequency resources of different users may show independent fading, a channel-dependent resource assignment will be beneficial.

The maximum throughput metric is assigning the resources to the users with highest CQIs. At this stage spatial mode adaptation can be included as well. This adds a spatial dimension to the already available resources defined in time and frequency. In case that an additional spatial layer can improve the system throughput, the BS is loading another spatial layer using a specific precoding strategy. On the other hand, maximizing the throughput cannot meet *fairness* requirements. In a multi-cell environment, there is a certain spread of the effective SINRs at the different UEs. Since fairness is a soft term, it is important that the scheduling algorithms can cover different degrees of fairness.

The max-min metric targets at maximizing the throughput of the worst users. The fairness is achieved in terms of an equivalent data rate for each user. [RC00] describes a simple algorithm which establishes this performance metric.

The score-based metric is a heuristic scheduling algorithm tending to assign distinct users to their best PRBs or groups of PRBs, while simultaneously ensuring instantaneous fairness within each time slot. Each user independently ranks all its

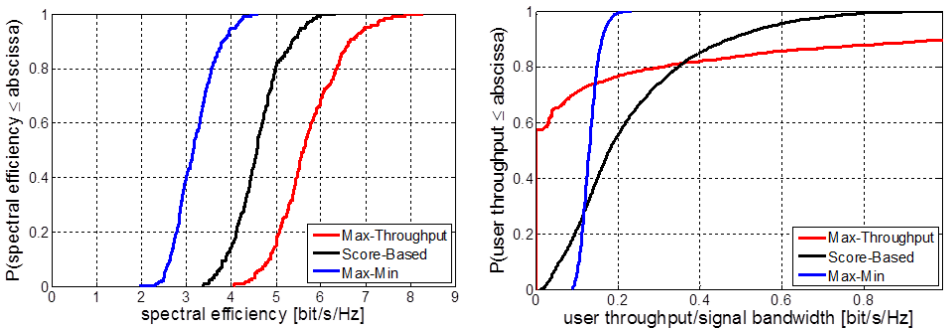

Figure 3.5: High-level overview on achievable system (left) and user data rates (right) using different scheduling strategies.

PRBs by the achievable throughput, in a descending manner, based on the post-equalization SINRs for all physical layer modes. Corresponding scores chosen from a unique set are assigned. The fairness is achieved in terms of an equivalent amount of resources for all active users. Thus each user may realize an equivalent fraction of his total achievable data rate. The score-based scheduling metric asymptotically realizes a performance similar to the proportional fair scheduler [VTL02], see [Bon04].

3.3.2 Score-Based Scheduling and Spatial Mode Adaptation

Resource allocation and selection of the proper spatial transmission modes, i.e. either single-stream transmission or multi-stream transmission, can be conveniently carried out by a score-based scheduling process developed in [Bon04,STJH07], which is briefly described as follows: In a first step, the user terminals evaluate the current channel conditions per PRB in terms of their achievable SINR conditions. By using equations (2.9) and (2.5) and a suitable SINR-to-rate mapping function from Section 2.4, they can determine the expected data rate per supported stream for each transmission mode. This information is conveyed as CQIs to the base station, where a score-based resource scheduling algorithm is carried out.

Spatial mode adaptation requires a direct comparison of the data rates per-stream from different spatial modes. The different data rates need to be weighted according to the number of active spatial layers. This accounts for the higher power allocated to the single-stream transmission compared to multi-stream transmission mode. In particular, let $\mathcal{T}_s$ be the set of active spatial layers for downlink service at the BS of interest. The general rationale behind the weighting factors is as follows: As we aim for a high-user throughput, spatial mode selection should favor transmission modes with $|\mathcal{T}_s| < N_t$ whenever the user rate can be expected to be larger than the rate expected in full multi-stream transmission mode, i.e. $|\mathcal{T}_s| = N_t$. In contrast, the set of available resources is increased if the BS decides

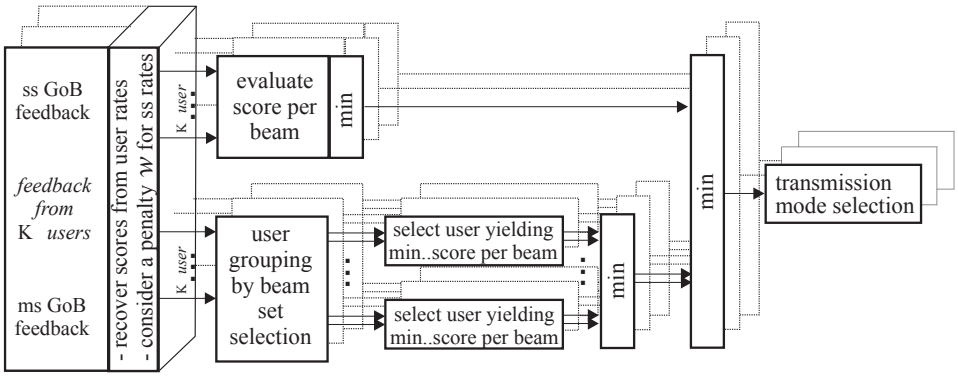

Figure 3.6: Block diagram of the score-based scheduling metric which covers spatial mode adaptation.

for multi-stream transmission mode. Assuming the scheduler can combine multiple users on these streams, without significantly reducing the per-user SINRs compared to the single-stream mode, will increase both system and user throughput linearly with amount of data streams in $\mathcal{T}_s$. Hence, from a single-user point of view, we can conclude that decisions in favor of certain spatial transmission modes at user k should be taken according to

$$\mathcal{T}_{s,k} = \underset{\mathcal{T}_s \subset \mathcal{T}}{\arg\max} \left(|\mathcal{T}_s| \max_{t \in \mathcal{T}_s} \left(rate \left(\mathrm{SINR}_{k,t} \right) \right) \right) \tag{3.3}$$

The rationale clearly prefers MU-MIMO transmission with a single data stream per user. However, the selection scheme can be easily adapted to favor multi-stream transmission per UE by taking the sum-rate over the t strongest data streams for user k into account. Depending on the desired amount of feedback, each UE could perform a selection of CQI values for feedback provisioning using (3.3). This rationale can be employed to choose between multiple precoding matrices $\boldsymbol{\beta}_i \in \mathcal{B}$ with the same and/or different amount of spatial layers. Note, there is a trade-off between the amount of feedback and the gains from MU-MIMO, especially if the feedback is reduced to a minimum.

For each user, the (weighted) data rates per stream from all modes over all PRBs are ranked by their quality, and corresponding scores are assigned. Mode selection and resource assignment is then done for each PRB individually: Initially, each stream available per transmission mode is assigned to the user providing minimum, i.e. best score for that stream. Thereafter, the mode is selected which corresponds to the minimum overall user scores.

The objective of this score-based resource allocation process is to assign each user to his best resources, and the decision on the spatial mode is taken under the premise of achieving a high throughput for each user. Clearly, the process is of heuristic nature, and hence the global scheduling target of assigning each user an

equal amount of resources is achieved on average only or if the number of available resources tends to infinity. However, its convenient property for practical applications is its flexible utilization, as the set of resources can be defined over arbitrary dimensions (time/frequency/space). Thus, fairness with respect to an equal amount of resources for all active users can be established on a small time scale, e.g. even for the scheduling of resources contained within a single OFDM symbol.

Mode selection probabilities clearly demonstrate spatial multiplexing transmission for all users in the system, in particular for users at cell edge. Initial performance evaluation is carried out for a system setting in an isolated cell [Sch09, STHJ10, TSWJ09] ($\mathbf{z}_k = \mathbf{n}_k$), where K UEs, each equipped with $N_r = 2$ receive antennas, communicate with a dual-antenna BS ($N_t = 2$). The evaluation environment is based on the spatial channel model extended (SCME) [3GP11], and full channel state information at the receiver (CSIR) is assumed. We investigate the probabilities of mode selection depending on the mean SNR conditions, which are depicted in Figures 3.7(a) and 3.7(b) for $K = 2$ and $K = 10$ users, respectively. Note, that resources where a rate cannot be supported by any user are not assigned by the scheduler. For that reason, the selection probability of the single-stream transmission mode drops down to 75% at SNR $= -5$ dB in Figure 3.7(a). Two different configurations of the adaptive mode switching system are considered here:

1. *Adaptive MU-MIMO* system with the first precoding matrix $\boldsymbol{\beta}_1$ from (3.2) being available. Simultaneously active streams can be assigned independently to different users. The mode per user is selected per PRB, i.e. a user may be served in different modes simultaneously.

2. *Adaptive SU-MIMO* system, where the multi-stream transmission mode is assigned to a single user. Now only one user is served per PRB either in diversity or single-user MIMO (SU-MIMO) mode.

The crossing point of the curves for single-stream transmission and multi-stream transmission mode in Figure 3.7 highlights the point in the SNR region where the multi-stream transmission mode becomes the dominantly selected one. From both figures, we observe that going from SU-MIMO to MU-MIMO promotes selection of the multi-stream transmission mode substantially, as the crossing point is shifted by 5 dB in case of 2 users and by more than 10 dB in case of 10 users down towards the low SNR regime. For 10 users, the crossing point falls below an SNR of 0 dB. The support for MU-MIMO mode also results in significant gains in the spectral efficiencies in multi-cell deployments, refer to Section 3.4. These results strongly emphasize that MU-MIMO is the key for the efficient use of spatial multiplexing transmission even at low SNR. Further, it can be observed that the shape of the probability curves approach that of a step function, highlighting that the system behavior tends towards a hard mode switching at a fixed SNR value.

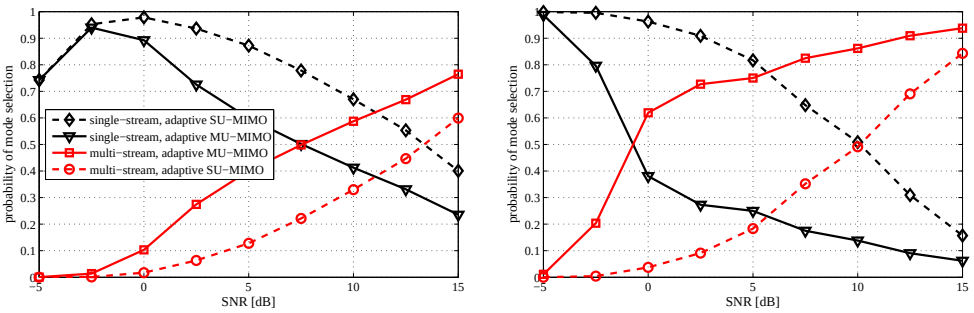

(a) $K = 2$ users (b) $K = 10$ users

Figure 3.7: Probability of mode selection vs. SNR $= P_m/\sigma_n^2$. Black: single-stream transmission mode, red: multi-stream transmission mode. [TSWJ09, Sch09]

Rate region histograms illustrate the performance achievable by the score-based scheduler as given in Figure 3.8. It depicts the histogram of normalized achievable user rates in the rate region plane for two users which may be scheduled in each PRB. In particular, we assume two spatial layers to be available in each PRB (i.e. $N_t = 2$), allowing two users to be served simultaneously in MU-MIMO mode. The rate allocated to each of these two users is normalized to the rate it would achieve if the PRB was assigned exclusively to it. Figure 3.8(a) shows the distribution of normalized rates if the total set of users to select from is limited to $K = 2$, while Figure 3.8(b) refers to the case of $K = 20$. From both figures, it is clearly seen that the achievable rates lie beyond the Time Division Multiple Access (TDMA) rate region (indicated by the dashed red line in the rate region plane). For increasing number of users K, the histogram is more and more concentrated in the upper right corner of the rate region. This illustration indicates that the heuristic score-based scheduling approach significantly outperforms TDMA scheduling and conveniently achieves high user rates by properly utilizing MU-MIMO.

3.4 System Performance under Idealistic Assumptions

Turning the focus to a multi-cell system, the performance is investigated in a triple-sectored hexagonal cellular network with $M = 57$ BSs in total, i.e. a center site surrounded by two tiers of interfering sites, as indicated in Figure 3.1. Simulation parameters are given in Table 3.1. Initial results are based on the assumption of full and perfect CSIR and are reported in [TSZJ07, TWS+11] based on SCME [3GP07a]. For the sake of comparability with results in Section 6.4, the following results are based on the latest implementation of our quasi-deterministic radio channel generator (QuaDRiGa) with urban-macro scenario parameters.

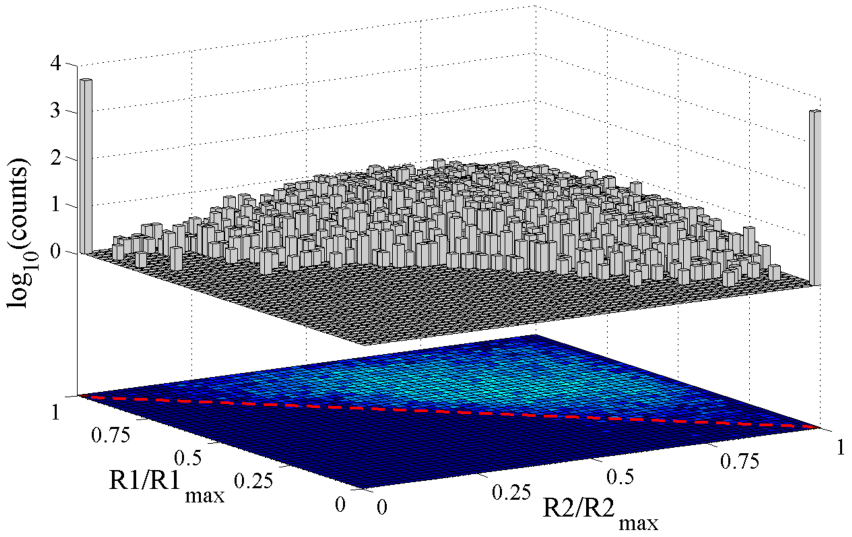

(a) $K = 2$ users

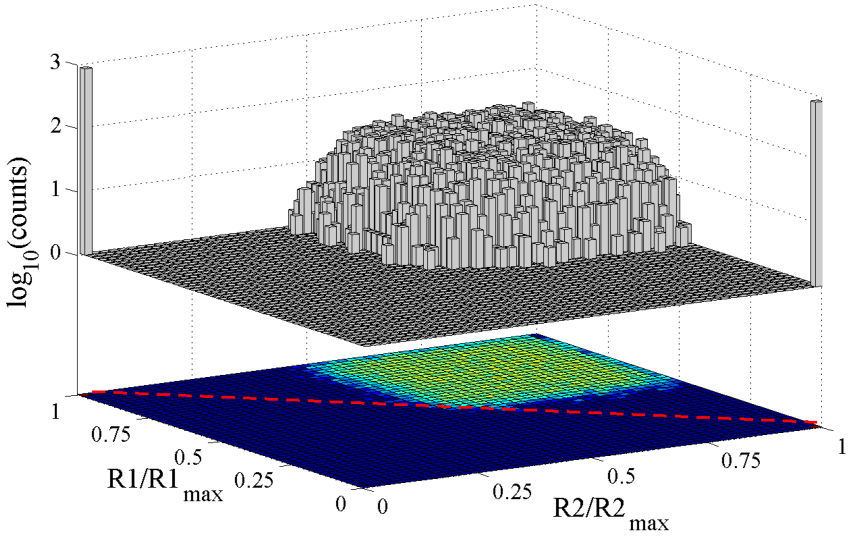

(b) $K = 20$ users

Figure 3.8: Rate allocation across two data streams

Table 3.1: Simulation assumptions.

Parameter	Value
Channel model	QUADRIGA
Simulation type	Monte Carlo
Drops	500
Scenario	Urban-macro
Propagation	NLOS
Large-scale fading	Geo-correlated parameters maps
Traffic model	Full buffer
Carrier frequency	2.6 GHz
Frequency reuse	1
Signal bandwidth	18 MHz, 100 RBs
Inter-site distance	500m
Number of BSs	19 having 3 sectors each
N_t ; spacing	1,2,4 ; co-pol 4λ
Transmit power	46 dBm
Transmit antenna	Azimuth: FWHM of 58°
	Elevation: FWHM of 6.2°
	10° electrical downtilt
BS height	32m
Number of active UEs	K=20 per sector
N_r ; spacing	1,2,4 ; co-pol $\lambda/2$
UE height	2m
Channel estimation error	perfect
CQI and precoding matrix indicator (PMI)	per 1 PRB
feedback delay	0ms
traffic model	full buffer

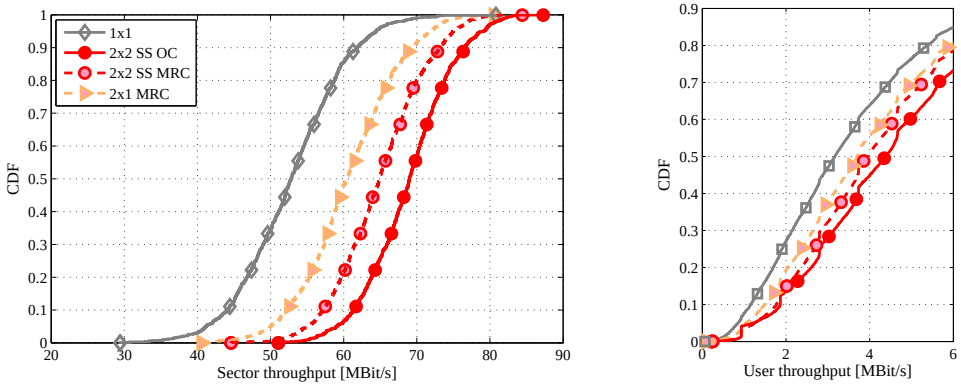

(a) System throughput (b) User throughput

Figure 3.9: Both system and per user performance for $N_t \leq 2$, $N_r \leq 2$ and $K = 20$ UEs per sector, under full buffer assumptions and ideal CQI & PMI feedback. The system may only utilize single-stream transmission mode. Note, steps in user rates are attributed to fixed MCS; time averaged data rates will not show such a behavior.

The UEs are always served by the BS whose signal is received with highest average power over the entire frequency band and a certain time interval. For capacity evaluation, only UEs placed inside of the center cell are evaluated. In this way, BS signals transmitted from the 1st and 2nd tier model the inter-cell interference [TSZJ07]. Performance is evaluated for both the sum throughput in a sector and the throughput for individual users. The achievable rates are determined from the SINRs after equalization according to expressions (2.5) or (2.9). These post-equalization SINRs are mapped into data rates using a quantized rate mapping function [IST07], representing achievable rates in a practical system, refer to Section 2.4. From these results, cumulative distribution function (CDF) plots are obtained.

Effect of different transmission modes In Figure 3.9 we study the effect of introducing additional antennas at the receiver and at the transmitter side, i.e. $N_r = 2$ and $N_t = 2$, respectively. For the asymmetric case of $N_r = 2$ and $N_t = 1$, we employ MRC and thus show a relative gain over the SISO system of approximately 14% and 22% for the median throughput per sector and at the cell-edge, i.e. 5%-ile user rate. Subsequently introducing an addional transmit antenna per BS, i.e. $N_t = 2$, enables the spatial precoding. Where we use a precoding matrix derived from the codebook $\mathcal{B}$ according to Equation (3.2). Figure 3.9 therefore assumes a set with a single matrix entry, i.e. $\boldsymbol{\beta}_1$. The chosen transmission mode is fixed to single-stream transmission, i.e. selection of either the first or the second column vector from $\boldsymbol{\beta}_1$. Note, the whole transmit power is allocated into the active spatial

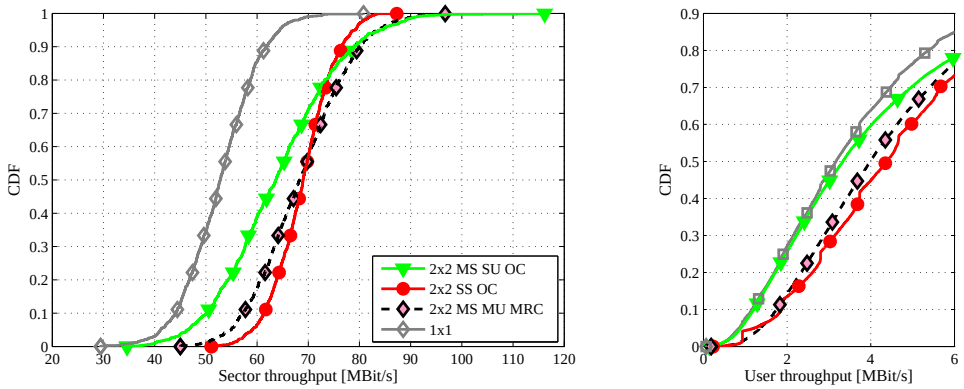

(a) System throughput (b) User throughput

Figure 3.10: Both system and per user performance for $N_t = 2$, $N_r = 2$ and $K = 20$ UEs per sector. The system may only utilize multi-stream transmission mode.

layer. The median sector throughput is increased by 22%, while the cell-edge user rates can be improved by 40%. By introducing OC at the terminal side, the SINR and thus the sector throughput is further increased by 30% with respect to our SISO baseline. The 5%-ile of the user rate is almost equivalent to MRC performance. Note that the covariance matrix of interference plus noise needs to be estimated at the OC. This knowledge may be gained by using a multi-cell channel estimation based on orthogonal pilots or by averaging the covariance of the received signal $\mathbf{y}_{k,t}$ over a sufficiently large number of consecutive transmitted data symbols. Section 4.1 investigates the performance having non-ideal channel knowledge at the receiver side.

For Figure 3.10, we configure the BSs to transmit with $|\mathcal{T}_s| = N_t = 2$ spatial layers, i.e. full multi-stream transmission. However, scheduling only permits transmission of both layers towards the same user, i.e. *single-user* SMUX, where each user is allowed to use OC for receive processing. We abbreviate this transmission mode as *2x2 MS SU OC*. As already observed in [CDG01], SMUX can hardly show any gain over single-stream transmission also referred as spatial diversity transmission. Gains compared to the single-stream transmission can only be achieved for peak data rates from both system and user perspective. At cell-edge, users experience the same conditions as in SISO communication systems.

However, this should not lead to the conclusion that the multi-stream transmission mode is not applicable in cellular systems. Rather, it opens the field for a transmission scheme called *multi-user* SMUX [SJSC06]. It can be regarded as a generalization of the multi-user diversity concept where we use parallel data streams in a given sector. Note, that the resources on these parallel streams may be assigned

to different users, owing to the above described score-based scheduling algorithm. This can be very efficient in terms of both sector throughput and individual user rates. Hence, we characterize the system performance for multi-stream transmission, where the scheduler can assign both active spatial layers in $\mathcal{T}_s$ to two different users. At this stage, we limit the receive processing to MRC. Figure 3.10, *2x2 MS MU MRC* shows superior performance compared to the single-user SMUX mode. Only for peak user rates, the single user transmission mode can exceed the multi-user rate achievable with MRC. Note, the slope of the resulting CDF is slightly smaller compared to the one for single-stream transmission.

Finally, we investigate multi-stream transmission in terms of the resulting system and user data rates under the assumption of ideal linear receive combining. The *2x2 MS MU OC* shows an impressive performance for both system as well as user perspective. Note, with $|\mathcal{T}_s| = 2$ available resources are doubled with respect to the single-stream transmission. By efficient interference rejection, terminals are no longer suffering from a second active spatial layer, although the transmission power needs to be shared among all active data streams per BS. The mode of multi-user SMUX with subsequent OC improves the multi-user SMUX with MRC by approximately 26% and 15% both for median sector and cell-edge user throughput. The adaptive transmission mode switching conecpt, described in Section 3.3, is able to improve the cell-edge user throughput by additional 6.5% compared to the fixed multi-stream mode. However, the median system data rate is reduced by approximately 1.8%. Offering a second precoding matrix in $\mathcal{B}$, i.e. $\boldsymbol{\beta}_1$ and $\boldsymbol{\beta}_2$ from Equation (3.2), provides an additional gain in the order of 9.3% and 8.4% for median sector and cell-edge user rate.

Figure 3.12 summarizes these findings by combining the median system throughput and the cell-edge user rate in terms of a 2 dimensional plot: Single-user SMUX transmission significantly reduces the cell-edge user data rates without improving the median system throughput, compare the green shapes. The single-stream transmission indicates the huge operational range, depending on the employed receive beamforming technique, i.e. MRC, MMSE or OC. It can be seen that MMSE can only slightly improve data rates. In all studies we assumed, that all BSs perform the same transmission mode according to our cell of interest, i.e. for single-stream all BSs transmit with a single data stream. At this point, we also evaluate the performance of BS m in single-stream transmission mode, while all other BSs $\mathcal{M} \setminus \{m\}$ are using $|\mathcal{T}_s| = 2$ spatial layers. The red dot, denoted as *SS OC rank 2 CCI* shows a significant loss in cell-edge user performance, while the median system throughput is maintained at roughly 65 Mbit/s. Compared to the *SS OC*, where all other cells behave equivalent to the m-th sector, system rates drop by 7% and cell-edge user rates lose 22%. All black shapes depict the multi-user SMUX performance, while blue symbols indicate the data rates of the adaptive spatial mode swichting concept. Note, in case of multi-stream transmission, all neighboring cells in $\mathcal{M} \setminus \{m\}$ use multiple layers as well.

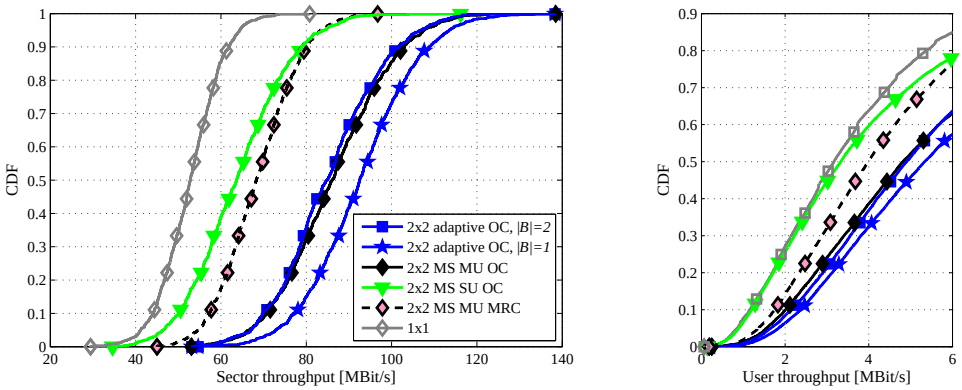

(a) System throughput. (b) User throughput.

Figure 3.11: Both system and per user performance for $N_t = 2$, $N_r = 2$ and $K = 20$ UEs per sector. Application of efficient multi-user SMUX and adaptive transmission mode switching is shown for $|\mathcal{B}| = 1$ and $|\mathcal{B}| = 2$.

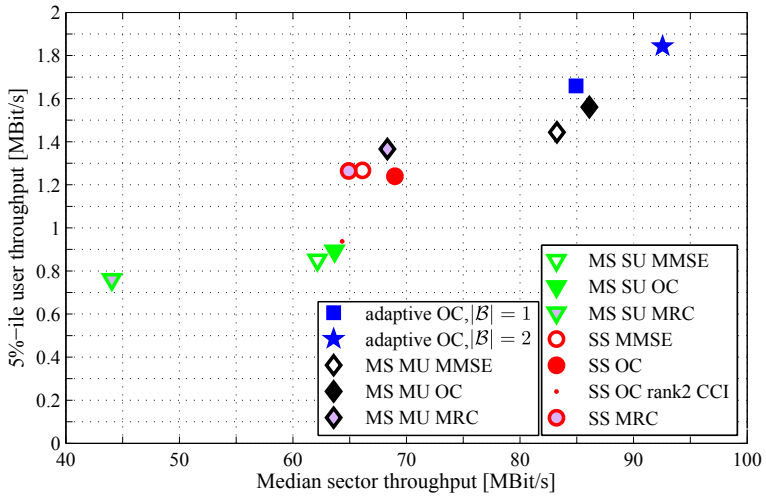

Figure 3.12: Summary plot for different spatial transmission strategies in a 2×2 setup.

Spatial transmission mode switching for higher order MIMO setups In Figure 3.13 we compare the performance of adaptive transmission mode switching for $1 \leq N_t \leq 4$ and $1 \leq N_r \leq 4$. In general, we assume OC at the receiver side, if not stated differently. For $N_t = 4$ and $N_r = 2$, which will be the desired setup for current LTE deployments (and also its advanced candidates), we study the impact of increasing the user set in the range of $5 \leq |\mathcal{K}_m| \leq 40$. We observe, that the median system throughput is increasing with a larger user set. In particular, gains with respect to $K_m = 5$ attribute to 15%, 29% and 39% for 10, 20 and 40 user terminals in $\mathcal{K}_m$, respecively. In Section 6.3, Figure 6.10, we study the scaling of data rates when performing spatial division multiple access (SDMA) under ZF constraint combined with a greedy user selection under equivalent channel conditions for the cellular setup.

Concluding we summarize the achievable gains for median sector throughput with respect to the SISO setup: 23% for 2×1, 60% and 75% for 2×2 with $|\mathcal{B}| = 1$ and $|\mathcal{B}| = 2$, 87% for 2×4, 120% for 4×2, and finally 180%, 196%, 202% for 4×4 with $|\mathcal{B}| = \{1, 2, 4\}$. We can observe only small additional capacity gains for systems with $N_t > N_r$ compared to a system with $N_t = N_r$. This is mainly caused by the constraint of DFT-based precoding, where the total transmit power is distributed evenly over all transmit antennas. In contrast, the system with $N_t < N_r$ benefits from advanced capabilities for interference suppression, as well as higher receive diversity. This enables the system to achieve larger improvements for MIMO 4×2.

Overall, we highlight that with limited feedback assumptions, where the users report all constellations of CQI and PMI, it is possible to triple the data rates in the system when receive and transmit antennas are quadrupled. Cell-edge user rates show a slightly better scaling, i.e. with 36% for 2×1; 94% and 115% for 2×2; 137% for 2×4; 176% for 4×2; 268% , 304% and 313% for 4×4.

For the sake of completeness, Figures 3.14(a) and 3.14(b) depict the selection probabilities for different spatial transmission modes in case of $N_t = 2$ and $N_t = 4$ transmit antennas, respectively. As a degree of freedom, we vary the size of the codebook set $\mathcal{B}$ equivalent to the simulation studies in Figure 3.13, where we use the same colors to ease comparability. We observe, that with a larger set $\mathcal{B}$, the system tends to select higher transmission ranks more frequently for both $N_t = 2$ and $N_t = 4$: E.g. rank 2 transmission is chosen with a probability of 85% in case of 2×2 setup with $|\mathcal{B}| = 1$, while with $|\mathcal{B}| = 2$ this already strongly preferred rank 2 mode is selected with 97%. This can easily be explained by an improved quantization of dominant channel directions due to the larger codebook set.

Furthermore, we study the effect of multi-user diversity on the behavior of mode selection probabilities. Therefore, we fix our analysis to 2×4 setup with $|\mathcal{B}| = 1$ but with $5 \leq K_m \leq 40$. Figure 3.14(b) shows the same tendency, which we already learned from a larger set of precoding matrices: With an increasing user set size, the scheduler predominantly selects rank 3, i.e. $|\mathcal{T}_s| = 3$, transmission mode. However, with a smaller user set the system mainly suffers from the scheduler not finding

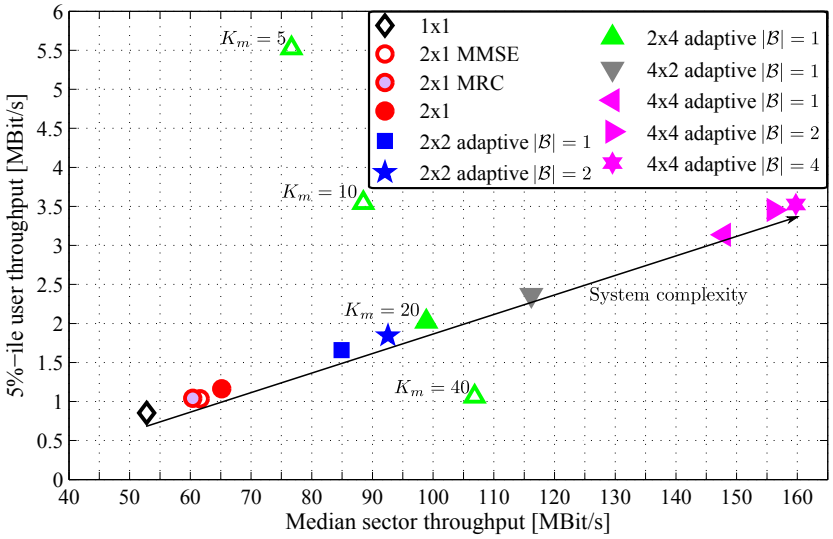

Figure 3.13: Ideal system performance for the SISO, MIMO 2×2 ($N_r \times N_t$), 2×4, 4×2 and 4×4 system for $K_m = 20$ users dropped into the sector m.

suitable users for grouping. Hence, from an originally intended rank 3 transmission, the system falls back to rank 2.

Our studies also demonstrated, that in case of $|\mathcal{T}_s| = 2$, the scheduler often chooses the precoding matrix that maximizes the chordal distance between the remaining precoding columns in $\boldsymbol{\beta}_i$. This observation was already highlighted by authors in [KPLK07], where the design of DFT based precoding matrices for multi-user transmission was initially discussed.

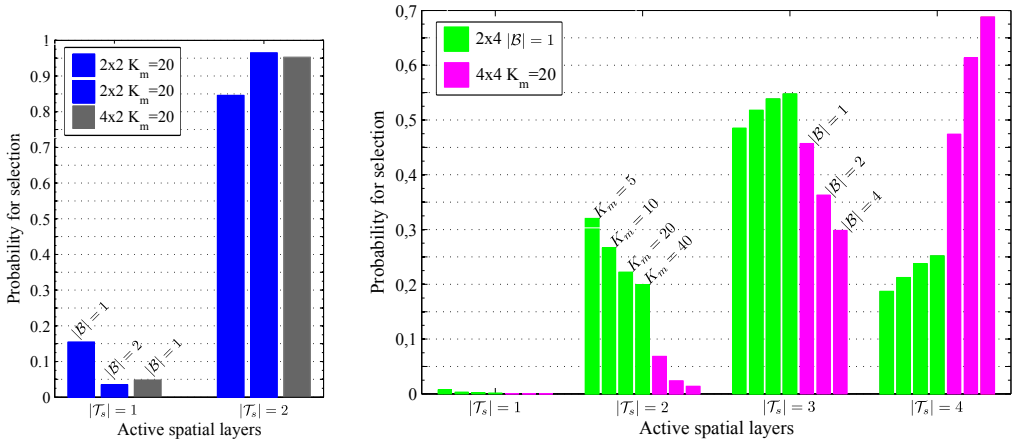

(a) System with $N_t = 2$.

(b) System with $N_t = 4$.

Figure 3.14: Transmission mode selection probabilities for different transceiver settings, for different size of codebook sets $\mathcal{B}$ and user sets $\mathcal{K}_m$.

4

Challenges in Limited Feedback

Multi-cell interference is undoubtedly the major limiting factor in full-coverage broadband wireless access networks [LHZ09,ZSSD11,SHC+10]. Mitigating it's effect onto the downlink data transmission is one of the key challenges in future wireless communication systems. The better the knowledge about the interference channels, the better is also the basis for any interference mitigation. Multi-cell channel knowledge can be exploited by simple, receiver-based schemes as optimal interference rejection combining [BZ71, TSZJ07] or advanced schemes based on cooperative base stations such as joint transmission [WMS+02, HV04].

In general, the concept of the arbitrarily varying channel (AVC) is commonly used to address the impact from unknown varying CCI [WB12b, and references there in] in coexisting wireless systems. These concepts perfectly match with the problem of pilot sequence design for channel estimation. In [WBB10, WB12b] authors showed that uncoordinated transmission of codewords (or pilot sequences), results into the problem that a UE may receive multiple valid codewords from multiple BSs. As a consequence, reliable data transmission would be impossible if the desired signal power is less or equal to the interference power. With regard to channel estimation this would mean: If two BSs are using the same pilot sequences at the same time and frequency resources, a UE would estimate the sum-channel of both BSs, where the channel coefficients superimpose weighted by their received power. In case of this very strong interference assumption, these channel estimates would result into decoding weights $\mathbf{w}_{k,t}$ which have a poor match with the desired channel. However, introducing transmitter coordination based on common randomness ensures that the non-Gaussian unknown interference affects the achievable data rate equivalent to Gaussian noise of same power [WB12b]. With regard to channel estimation this means, that pilot sequences need to fulfill at least the common randomness criteria. More desirable, cell planning and pilot sequence design should target at good separation of desired and interfering channel coefficients. For LTE deployments,

pilot sequences are introduced on orthogonal time and frequency resources for the purpose of intra-cell channel estimation. Dependent on the current cell-id, pilot positions from other sites are cyclic shifted in time and frequency. However, there is only a limited number of shift operations allowed. Therefore, pilots sequences are chosen from a huge Gold sequence with a cell-dependent initial point. In essence, this pilot scheme leads to the fact that channel estimation can be carried out on a sub-frame basis, where other cell's data and pilot symbols behave like additive white Gaussian noise. Note, this rather pragmatic system design is not applicable for the generic case of spectrum sharing from either multiple operators, heterogeneous cell overlays or introduction of primary and secondary services, e.g. operation of sensor systems in the cellular spectrum.

This chapter studies two major challenges for limited feedback in cellular systems: First we focus on channel estimation and corresponding receive processing for the case of multi-antenna UEs. In order to obtain the achievable data rate in a practical system, we introduce different channel estimation models: AWGN for asynchronous BSs and pilot symbol aided channel estimation for synchronous BSs. In order to estimate the channels of interferers, the BSs must transmit training sequences being orthogonal among the antennas of different sectors and sites. On the other hand, quite a lot of these channels must be estimated to combat the interference until the noise floor is reached. The more interferer channels are distinguishable, the more orthogonal pilots must be transmitted. This would consume a large fraction of the potential capacity gain. Second we will reduce the amount of feedback from the UE according to 3GPP suggestions for the FDD downlink and study the loss in sector and per-user data rates. Especially, the application of the MU-MIMO mode allows to operate the system in SMUX, while each user is providing feedback for a single data stream. This chapter concludes with a comparison of certain key performance indicators (KPIs) such as propagation parameters and data rates for a variety of channel modeling assumptions. Over the last decades, state-of-the-art channel models developed further from a Rayleigh fading assumption, over geometry-based stochastic channel model (GSCM) towards quasi-deterministic models, being capable to precisely track user movements.

4.1 Channel Estimation and Error Models

In [TSWJ08], OC was shown to be highly sensitive to estimation errors, since the spatial structure of the interference covariance matrix is utilized for equalization. In the following we assume quasi-static channel conditions over the observation interval. For evaluation, we assume perfect synchronization between UEs and their serving BSs [MKP07] and a sufficiently large cyclic prefix, which alleviates the effect of ISI. Feedback delay will not be considered at this stage, since a continuous link-adaptation can alleviate the out-dating of reported MCS levels at low mobilities. These so called *channel aging effects* will become more severe when applying

channel-aware precoding, as used in coordinated multi-point (CoMP) transmission, refer to Section 6.4.

In general, we may describe the mismatch between the ideal channel and its estimated version by evaluating the corresponding relative mean square error (rMSE) per sub-channel for user k. Therefore, we define $\mathbf{\Delta}_{c,k} = \mathbf{H}_{m,k} - \hat{\mathbf{H}}_{m,k}$ as the element-wise difference matrix between the ideal channel and its estimated version and normalize the resulting error by the average channel gain of $\mathbf{H}_{m,k}$.

$$\mathrm{rMSE}_k = \frac{\mathrm{tr}\Big(\mathbf{\Delta}_{c,k}\mathbf{\Delta}_{c,k}^H\Big)}{\mathrm{tr}\Big(\mathbf{H}_{m,k}\mathbf{H}_{m,k}^H\Big)} \tag{4.1}$$

The average rMSE defined as μ is obtained over multiple Monte-Carlo drops and users k

$$\mu = 1/(K \cdot Drops) \sum_{\forall k, drop} \mathrm{rMSE}_{k,drop} \tag{4.2}$$

As a starting point, we introduce a simple approach to model channel estimation errors with an additive error term drawn from a zero mean independent identically distributed (i.i.d.) Gaussian distributed process with variance μ per sub-channel. The noisy channel coefficient is used at the receiver side for equalization purpose and is given by $\widehat{\overline{\mathbf{h}}}_{k,t} = \overline{\mathbf{h}}_{k,t} + \delta_k$. The term $\widehat{\overline{\mathbf{h}}}_{k,u}$ denotes the biased estimate of variable $\overline{\mathbf{h}}_{k,t}$, and δ_k denotes the zero-mean Gaussian distributed error with variance μ.

Post-Equalization SINRs For signal detection, we may define linear equalizers. Dependent on the available channel knowledge, MRC or OC may be applicable. In addition to the rMSE, post-equalization SINRs are of major importance, also refer to Section 2.3, in particular to equations (2.3), (2.5) and (2.9).

Ideal SINRs
The achievable spectral efficiency with perfectly known variables, i.e. equalization vector $\mathbf{w}_{k,t}$, desired and interfering signals $\overline{\mathbf{h}}_{k,t}$, $\boldsymbol{\vartheta}_{k,t}$ and $\mathbf{z}_k$, respectively.

$$\mathrm{SINR}_{k,t} = \frac{\mathbf{w}_{k,t}^H \overline{\mathbf{h}}_k \overline{\mathbf{h}}_k^H \mathbf{w}_{k,t}}{\mathbf{w}_{k,t}^H \mathbf{Z}_{k,t} \mathbf{w}_{k,t}} \tag{4.3}$$

Achievable SINRs
The resulting spectral efficiency utilizing the estimated equalization vectors $\widehat{\mathbf{w}}_{k,t}$, i.e. the rate which may be achieved in maximum using an erroneous estimated receiver.

$$\widetilde{\mathrm{SINR}}_{k,t} = \frac{\widehat{\mathbf{w}}_{k,t}^H \overline{\mathbf{h}}_k \overline{\mathbf{h}}_k^H \widehat{\mathbf{w}}_{k,t}}{\widehat{\mathbf{w}}_{k,t}^H \mathbf{Z}_{k,t} \widehat{\mathbf{w}}_{k,t}} \tag{4.4}$$

Estimated SINRs
Where the UE utilizes the estimates $\widehat{\mathbf{w}}_{k,t}$, $\widehat{\overline{\mathbf{h}}}_{k,t}$ and $\widehat{\mathbf{Z}}_{k,t}$.

$$\widehat{\mathrm{SINR}}_{k,t} = \frac{\widehat{\mathbf{w}}_{k,t}^H \widehat{\overline{\mathbf{h}}}_k \widehat{\overline{\mathbf{h}}}_k^H \widehat{\mathbf{w}}_{k,t}}{\widehat{\mathbf{w}}_{k,t}^H \widehat{\mathbf{Z}}_{k,t} \widehat{\mathbf{w}}_{k,t}} \tag{4.5}$$

SINR estimation error
The difference $\Delta_{\mathrm{SINR}_{k,t}}$ between the estimated and achievable SINR at the UE.

$$\Delta_{\mathrm{SINR}_{k,t}} = \widehat{\mathrm{SINR}}_{k,t} / \widetilde{\mathrm{SINR}}_{k,t} \tag{4.6}$$

In order to obtain the different SINRs from (4.3), (4.4), (4.5) and (4.6), we need to determine the channel coefficients from the serving cell and optionally interfering cells. In particular, the multi-cell interference needs to be known as a received covariance matrix $\mathbf{Z}_{k,t}$ or $\mathbf{Z}_k$. In the following, f and n denote the discrete frequency and time index, respectively. Initially, we consider two options, which are based on the received interference power only:

Frequency-flat i.i.d. interference power $\sigma^2_{\mathbf{IF}}$

$$\widehat{\mathbf{Z}}_{k,t} = \mathbf{I} \left(\mathbb{E}_f \left\{ \left(\sum_{\forall l,j} |\overline{\mathbf{h}}_{l,j}(f)|^2 \right) - |\widehat{\overline{\mathbf{h}}}_{k,t}(f)|^2 \right\} + \sigma_n^2 \right) \tag{4.7}$$

Frequency-selective i.i.d. interference power $\sigma^2_{\mathbf{IF}}$

$$\widehat{\mathbf{Z}}_{k,t}(f) = \mathbf{I} \left(\left(\sum_{\forall l,j} |\overline{\mathbf{h}}_{l,j}(f)|^2 \right) - |\widehat{\overline{\mathbf{h}}}_{k,t}(f)|^2 + \sigma_n^2 \right) \tag{4.8}$$

4.1.1 Covariance Estimation - Subsequent Data Transmission

Knowledge on interference conditions may also be obtained by estimating the covariance matrix $\mathbb{E}_n \left\{ \mathbf{y}_{k,t}(f,n) \mathbf{y}_{k,t}(f,n)^H \right\}$ of the received signal vector $\mathbf{y}_{k,t}(f,n)$ across several subsequently received data symbols n. Therefore, asynchronous downlink transmission from all BSs in the system may be sufficient. By assuming data transmission of i.i.d. symbols x_k across channel k and averaging over n symbols the estimation error in $\widehat{\mathbf{R}}_{yy}$ decreases with n [SFFM99, JHJ+01]. Let the total number of transmitted data symbols across a quasi-static channel be given by N.

$$\begin{aligned} \widehat{\mathbf{R}}_{yy}(f) = \frac{1}{N} \sum_{\forall n} \mathbb{E}_n \Bigg\{ & \left(\sum_{\forall l,j} \overline{\mathbf{h}}_{l,j}(f,n) x_{k,l}(f,n) + \mathbf{n} \right) \\ & \left(\sum_{\forall l,j} \overline{\mathbf{h}}_{l,j}(f,n) x_{k,l}(f,n) + \mathbf{n} \right)^H \Bigg\} \end{aligned} \tag{4.9}$$

The estimation error between $\mathbf{R}_{yy}$ and the estimated covariance matrix $\widehat{\mathbf{R}}_{yy}$ is shown in Figure 4.2.

Frequency-selective interference covariance $\mathbf{Z}_{k,t}$ is given by

$$\widehat{\mathbf{Z}}_{k,t}(f) = \mathbb{E}_n \left\{ \mathbf{y}_{k,t}(f,n) \mathbf{y}_{k,t}(f,n)^{\mathrm{H}} \right\} - \widehat{\overline{\mathbf{h}}}_{k,t}(f) \widehat{\overline{\mathbf{h}}}_{k,t}(f)^{\mathrm{H}} \tag{4.10}$$

4.1.2 Correlation-Based Estimator - Virtual Pilots

In order to improve the channel estimation at the UE side, we propose a trade-off between the ability to track the interference channels and the mobility of the user. Therefore, we introduce a time-sequence based concept known as virtual pilots [TSSJ08]. In fact, our virtual pilot scheme does not consume additional pilot tones compared to the current LTE system. It enables mobile terminals to distinguish the more of the strong interference channels the slower they are moving in the service area. Hence, without increasing the pilot overhead, low-mobility terminals can take most benefit of advanced interference mitigation schemes.
The proposal is based on a LTE draft 8 specification where orthogonal pilot signals between different sectors are assumed while different sites are non-orthogonal but marked with a pseudo-random scrambling sequence (PRS) defined by the network operator. We propose to use not random but deterministic sequences denoted as virtual pilots and provide a pilot reuse scheme based on the partial correlation principle. In this way, channels of nearby base stations can be separated using a short correlation window, e.g. over a few sub-frames, while estimating the channels of more distant stations requires a longer correlation window and hence allows for a reduced user mobility.

At the UE, a correlation-based estimator is used to separate the channels $\mathbf{h}_{k,l}$ for the n distinct groups. The main reason to use the correlation-based estimator is its moderate computational complexity. The correlation-based estimator is given by

$$\widetilde{\mathbf{h}}_{\nu}(f) = \frac{1}{N} \sum_{n=0}^{N-1} c_{\nu}^{*}(n) \mathbf{y}_{k,t}(f,n) \ , \ \text{with } \nu = \{0, ..., N-1\} \tag{4.11}$$

where $c_{\nu}(n)$ and $\mathbf{y}_{k,t}(f,n)$ denote the code symbol and the received signal at the given discrete time index n, respectively.

Hence, we can determine the received interference covariance matrix $\widehat{\mathbf{Z}}_{k,t}$ by evaluating

$$\widehat{\mathbf{Z}}_{k,t}(f) \ = \ \sum_{\forall l,j} \widehat{\overline{\mathbf{h}}}_{l,j}(f) \widehat{\overline{\mathbf{h}}}_{l,j}^{\mathrm{H}}(f) - \widehat{\overline{\mathbf{h}}}_{k,t}(f) \widehat{\overline{\mathbf{h}}}_{k,t}^{H}(f) \ , \tag{4.12}$$

where index l and j correspond to a group of BSs and data streams which may be estimated at user k.

Here we suggest to apply Hadamard sequences spread over the time domain from slot to slot with a maximum sequence length of 16. Figure 4.1 visualizes the suggested pilot grid, where the number (hex-base) indicates the code $\mathbf{c}_\nu$ chosen from the sequence matrix $\mathbf{C}$, i.e. the row of the Hadamard matrix of maximum length $N = 16$. The decimal numbers indicate the sequence length over the time domain. Note, that the suggested scheme covers different sequence length $n = \{1, 2, 4, 8, 16\}$, since the sequence pattern repeats itself every n rows. Thus the system may benefit from a more precise channel estimation for increasing sequence length n.

Definition: Block-Orthogonal Sequence Each row of a block-orthogonal sequence matrix is orthogonal to all other rows of the same matrix with full correlation length, i.e. $\mathbf{C}\mathbf{C}^H = \mathbf{I}$. Reducing the correlation length to n yields to a matrix with block wise orthogonal properties, where each block is of size $n \times n$. Furthermore, each n-th row should be identical for a given correlation length n.

The suggested scheme assigning virtual pilot sequences to the multi-cell system is translational invariant with respect to the estimation error. Its block-orthogonality is sustained even after a cyclic shift. Note that the suggested scheme can be easily extended to the case of larger correlation length. Furthermore, each block-orthogonal sequence may be applied instead of Hadamard sequences yielding the same performance. E.g. resorting the columns and rows of the DFT matrix such that block-orthogonality is given, leads to sequences having the same properties required by the correlation-based estimator. In this way, the virtual pilots can be interpreted as discrete frequency shifts by a fraction of a sub-carrier spacing and partial correlation is a filtering process with limited spectral resolution.

Properties of the Scheme: The scheme in Figure 4.1 maximizes the distance between cells using the same Hadamard sequence. After 4 cells in a row the same sequence is assigned. That applies to the horizontal and both diagonal alignments. All cells in a radius of 4 have orthogonal sequences to the cell in the middle of the scheme. The assignment of the Hadamard sequences to cells is completely defined by an arbitrary rhombus containing 16 cells, each one using another pilot sequence. The rhombus is repeated to fill an infinity plane. One possible rhombus in Figure 4.1 is enclosed by the cells E,0,1,7. Note that each permutation of the assignment would effect the channel estimation rMSE. In our suggested scheme it is guaranteed that the mean channel estimation error of a UE is independent of the cell where it is placed. That means it is sufficient to consider only cell 0, refer Figure 4.1, for the simulation.

Proof of scheme properties: For the cells a, b we write $a \equiv b$, if each base station a_1 has a correspondent base station b_1, whereas a UE placed in a measuring a_1 can expect the same channel estimation error like a UE placed in b measuring b_1. The error depends on the distances and pilot sequences of all BSs. More precisely,

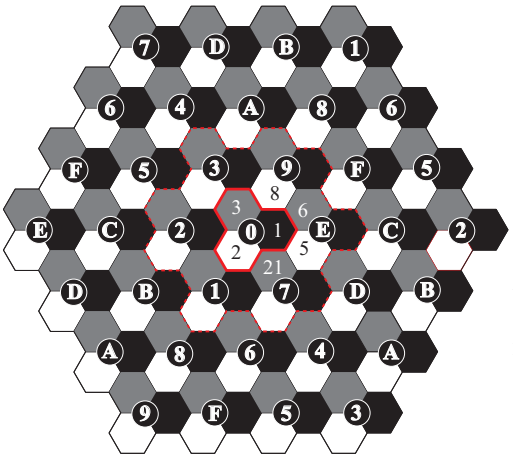

	1	2	3	4	5	6	7	8	9	10	11	12	13	14	15	16
0	1	1	1	1	1	1	1	1	1	1	1	1	1	1	1	1
1	1	-1	1	-1	1	-1	1	-1	1	-1	1	-1	1	-1	1	-1
2	1	1	-1	-1	1	1	-1	-1	1	1	-1	-1	1	1	-1	-1
3	1	-1	-1	1	1	-1	-1	1	1	-1	-1	1	1	-1	-1	1
4	1	1	1	1	-1	-1	-1	-1	1	1	1	1	-1	-1	-1	-1
5	1	-1	1	-1	-1	1	-1	1	1	-1	1	-1	-1	1	-1	1
6	1	1	-1	-1	-1	-1	1	1	1	1	-1	-1	-1	-1	1	1
7	1	-1	-1	1	-1	1	1	-1	1	-1	-1	1	-1	1	1	-1
8	1	1	1	1	1	1	1	1	-1	-1	-1	-1	-1	-1	-1	-1
9	1	-1	1	-1	1	-1	1	-1	-1	1	-1	1	-1	1	-1	1
A	1	1	-1	-1	1	1	-1	-1	-1	-1	1	1	-1	-1	1	1
B	1	-1	-1	1	1	-1	-1	1	-1	1	1	-1	-1	1	1	-1
C	1	1	1	1	-1	-1	-1	-1	-1	-1	-1	-1	1	1	1	1
D	1	-1	1	-1	-1	1	-1	1	-1	1	-1	1	1	-1	1	-1
E	1	1	-1	-1	-1	-1	1	1	-1	-1	1	1	1	1	-1	-1
F	1	-1	-1	1	-1	1	1	-1	-1	1	1	-1	1	-1	-1	1

Figure 4.1: Left: Pilot reuse pattern based on orthogonal code sequence, e.g. Hadamard, in a 3-fold sectorized cellular system. Decimal numbers indicate the sector index. Right: Hadamard sequences spread over space (rows) and time (columns) domain. Hex-base numbers indicate sites with the same virtual pilot sequence.

we write $a \equiv b$, if exists an bijective map $f_{ab} : C \times C \longrightarrow C \times C$, where C is the infinite set of cells. For arbitrary a_1, a_2 with $f_{ab}(a_1, a_2) = (b_1, b_2)$ the map must have the following properties: The distance between a, a_1 is equal to b, b_1. The same holds for a, a_2 and b, b_2. Also both pairs of pilot sequences assigned to a_1, a_2 and b_1, b_2 must have the same orthogonality property (true/false) after a correlation length of 2,4,8 and 16. In other words, each pair a_1, a_2 has a correspondent pair b_1, b_2 with the same distance and sequence (orthogonality) property. Regarding to our suggested scheme we define the following bijective map for any $a, b \in C$:

$$f_{ab}(a \oplus (r_1, d_1), a \oplus (r_2, d_2)) = (b \oplus (r_1, d_1), b \oplus (r_2, d_2)),$$

where r_1, d_1, r_2, d_2 are arbitrary integer numbers, $c \oplus (r, d)$ defines a new cell going r steps right and d steps down right along the hexagonal grid. The above mentioned distance property is fulfilled. To show the orthogonality property we checked only 16×15 pairs of sequences with a simulation program, because of the assignment repetition in the suggested scheme.

The rMSE in Static Channels Results for the covariance estimation are shown in Figure 4.2. It compares the mean rMSE for the covariance and correlation-based estimators, applicable over all OFDM data symbols or using virtual pilots, respectively. Note that the correlation-based estimator requires at least a number of 7 OFDM symbols to be transmitted, i.e. one correlation length, where as the covariance estimator is capable to start the estimation with the first transmitted

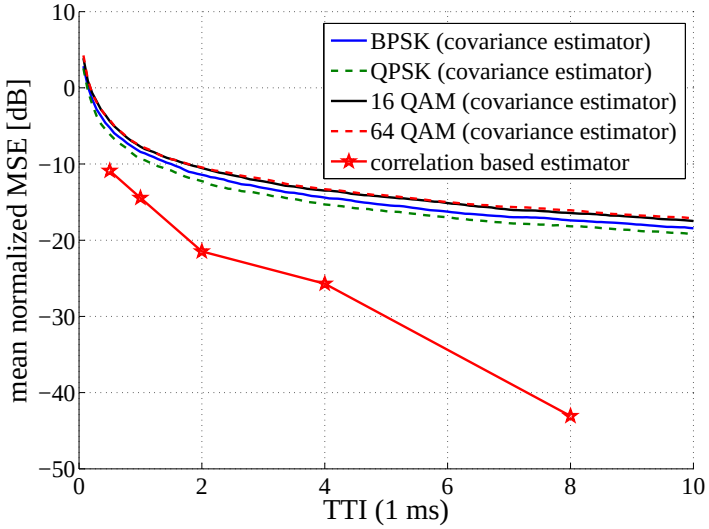

Figure 4.2: Estimation of interference covariance matrix $\mathbf{Z}_{k,t}$, performance shown as mean rMSE for both estimation techniques, i.e. received signal covariance estimation and multi-cell channel estimation.

data symbol. It turns out that the correlation-based estimator outperforms the covariance estimator already for correlation length of one slot.

Figure 4.3 shows the rMSE, normalized by the receive power of the associated sector. It compares the different performance in the channel estimation process using virtual pilots based on pseudo-random (Figure 4.3(a)), randomly arranged Hadamard (Figure 4.3(b)) and Hadamard sequences (Figure 4.3(c)) arranged in the specific pattern shown in Figure 4.1. In these figures, the achievable rMSE is given for top-N strongest sectors showing instantaneously the five highest receive powers at the UE. It turns out that using virtual pilots based on randomly arranged orthogonal sequences, e.g. Hadamard (Figure 4.3(b)), cannot reduce the rMSE compared to the case of using pseudo-random sequences. However, the suggested sequence reuse pattern assigning Hadamard sequences to the BSs does clearly show a superior performance compared to the random arrangement of sequences. Within that scheme BSs being closely located to each other are assigned to orthogonal sequences requiring smaller correlation lengths to be separable.

Figure 4.3(c) and 4.3(d) indicate the achievable rMSE for the top-N strongest sectors as well as for a fixed set of sectors. For the latter, we can observe that the error of the multi-cell channel estimation is less than -10 dB for sequence length larger than 4, i.e. 2 transmission time intervals (TTIs), for all sectors with index $= \{1, 2, 3, 8, 21\}$; index is indicated in Figure 4.1. After full correlation length, the channel estimation of adjacent BSs is almost perfect, i.e. with a rMSE $>$ 40dB.

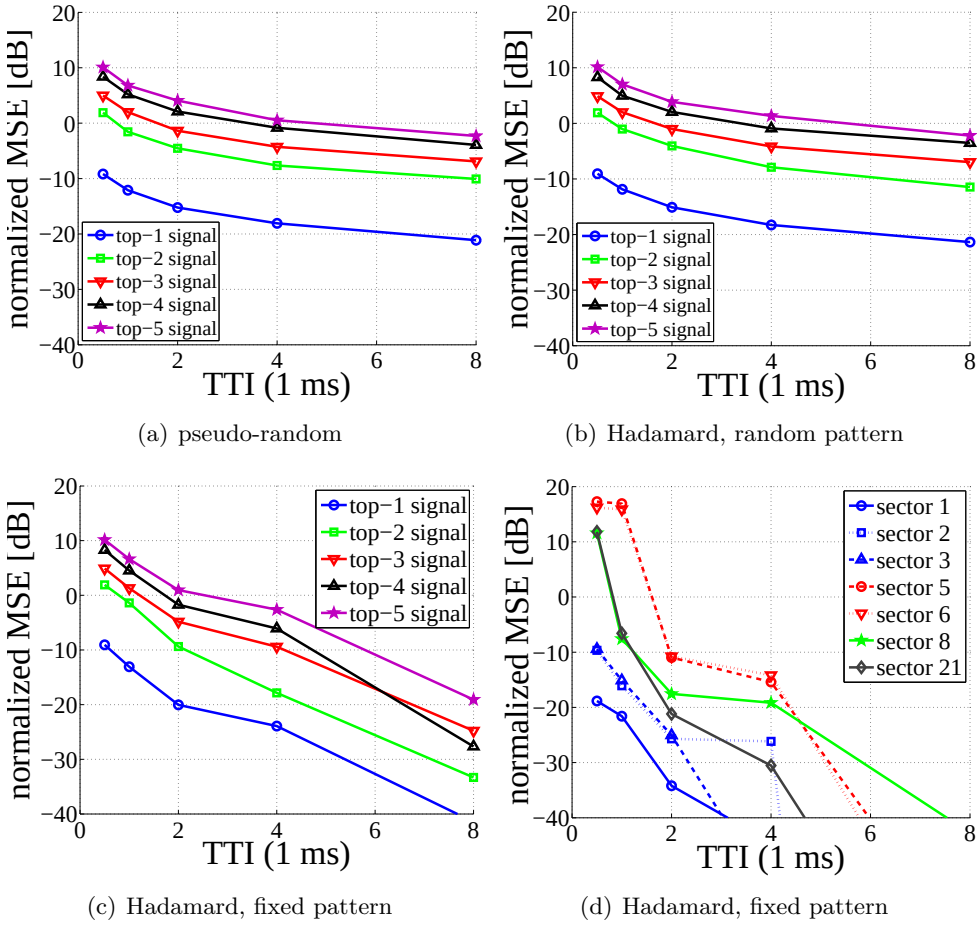

(a) pseudo-random

(b) Hadamard, random pattern

(c) Hadamard, fixed pattern

(d) Hadamard, fixed pattern

Figure 4.3: The rMSE is obtained for the correlation estimator, in case of a static channel, for the five strongest (a,b,c) and inner sectors (d).

However, estimating the top-N strongest channels may cause higher errors. This is due to the fact that the top-N strongest channels may not belong to the adjacent BSs. Nevertheless, by using a more orthogonal grid for larger correlation length it is possible to reduce the rMSE as indicated in Figure 4.3(c). Note that the reduction of the rMSE for the strongest signals is significant. For correlation length of 16, i.e. 8 TTIs, the rMSE is below -19 dB for the top-5 strongest channels.
For quasi-static channels, the suggested multi-cell channel estimation approach may be implemented easily. On the other hand, sites must be synchronized, e.g. by using global positioning system (GPS). Furthermore, phase noise must be reduced compared to present cellular systems.

The rMSE in Time-Selective Channels The following part evaluates the performance degradation in the estimation process due to time varying channels, e.g. caused by a certain velocity of the UE or simply phase noise. Introducing a constant phase rotation to a static channel would result in the simplest form of a time varying channel [BS03].

$$\begin{aligned}\mathbf{y}_k(f,n) = \overline{\mathbf{h}}_{k,t}\mathrm{e}^{\frac{jn\phi_{k,t}}{N}}x_{k,t} \\ + \sum_{\substack{j=1\\ j\neq t}}^{N_T}\overline{\mathbf{h}}_{k,j}\mathrm{e}^{\frac{jn\phi_{k,j}}{N}}x_{k,j} + \sum_{\substack{\forall l,j\\ l\neq k}}\overline{\mathbf{h}}_{l,j}\mathrm{e}^{\frac{jn\phi_{l,j}}{N}}x_{l,j} + \mathbf{n}\ ,\end{aligned} \tag{4.13}$$

where n is the discrete time index $n \in \{0, ..., N-1\}$. The random phase terms $\phi_{k,t}$, $\phi_{k,j}$ and $\phi_{l,j}$ are defined in the range $0 \leq \phi \leq 2\pi/9$ having i.i.d. properties for all BSs and transmit elements in the environment. Limiting the phase rotation to a maximum value of $2\pi/9$ within a time period covering the maximum seqeuence length of $N = 16$ results in a rather low speed user profile.[1]
With these parameters, the evaluation for the achievable rMSE is conducted again resulting in the performance given below. Figure 4.4(a) indicates the achievable rMSE in case of time variant channel conditions. It turns out that all estimation errors converge to almost the same value, i.e. ≈ -20 dB, for the maximum correlation length $N = 16$. Note that the estimation error of the strongest signal even increases from correlation length $N = 8$ to $N = 16$. In this case, the error caused by the phase rotation prevails the estimator gain. The loss in the rMSE compared to static channel conditions is given in Figure 4.4(b). Again it turns out, that the estimation error basically increases for those channels with lowest rMSE from the static case.

Conclusion The scheme uses a specific cell planning for the sequences by which pilots of different sites are scrambled. It is shown that multi-cell estimation clearly outperforms the covariance estimator required for interference rejection combining at the terminal. Also it is shown that the suggested scheme achieves a rMSE below -19 dB for the five strongest downlink signals received by a terminal. This is a good basis for advanced interference mitigation schemes using cooperative transmission. The next section will consider the loss in data throughput by such schemes based on realistic channel knowledge.

[1] The approximation of the speed is given by $v = c\frac{\phi}{2\pi\Delta t f_c} \approx 2$ m/s, $\Delta t = 8$ ms is the time period.

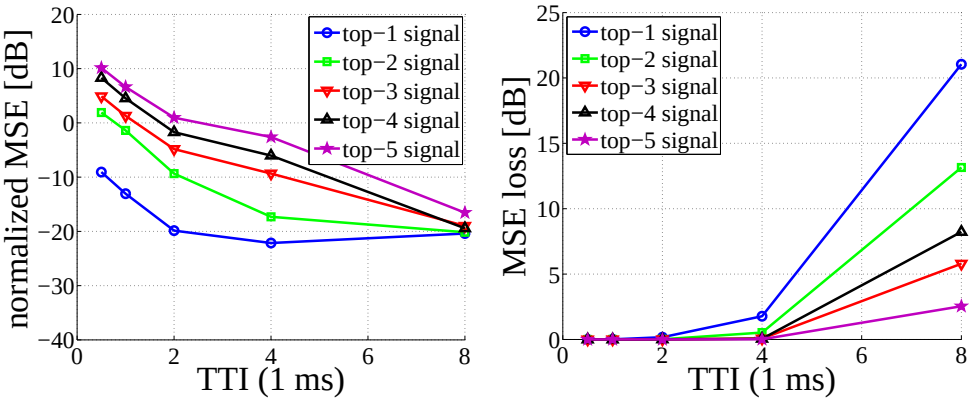

(a) Hadamard, fixed pattern (b) Hadamard, fixed pattern

Figure 4.4: The rMSE is obtained for the correlation estimator using the suggested virtual pilot pattern, in case of a dynamic channel, for the five strongest sectors (a) and the loss in the rMSE compared to static channel conditions (b).

4.1.3 Affecting Linear Receivers and System Performance

Basically, radio systems may be operated by utilizing asynchronous or synchronous downlink transmission from all base stations in the system, where synchronization between terminals and their serving base station is mandatory in both concepts. We provide a comparison between the theoretical achievable spectral efficiency in an OFDMA systems using different linear equalizers and their resulting performance taking estimation errors into account. It is shown, that the choice of the appropriate receiver depends on the degree of synchronization in the system. We demonstrate that a Long Lerm Evolution radio system may achieve higher spectral efficiency thanks to interference suppression if fully synchronized data transmission from all base stations is introduced.

While the MRC receiver (2.5) only requires knowledge on its own channel vector, the OC approach (2.9) additionally requires the received covariance matrix including the most prominent interfering signals. The latter is shown to be highly sensitive to estimation errors while the first is quite robust against it. For interference suppression, we consider two different techniques in order to obtain this mandatory knowledge:

- Asynchronous downlink data transmission from all BSs in the observation area is assumed. Here, the received covariance may be estimated, i.e. averaged over i.i.d. data symbols according to (4.9) with a decreasing rMSE for increasing number N of data symbols [SFFM99, JHJ+01].

- Fully synchronized BSs and application of multi-cell channel estimation based on partially orthogonal virtual pilot sequences, as described in Section 4.1.2 and [TSSJ08]. We demonstrate, that interference suppression techniques increase the spectral efficiency in LTE radio system, if fully synchronized data and pilot transmission from all BSs is introduced.

Asynchronous transmission assumes that BSs are not synchronized to each other with respect to carrier frequencies and frame start. For sake of simplicity, we model the channel estimation errors with AWGN properties, refer to Section 4.1. Note, channel estimation in LTE behaves similar. LTE Release 8 specification [3GP07b] defines common pilot symbols on orthogonal time and frequency resources for the purpose of intra-cell channel estimation. Dependent on the current cell-id, pilot positions from other sites are cyclic shifted in time and frequency. However, there is only a limited number of shift operations allowed. Therefore, pilots sequences are chosen from a huge Gold sequence with a cell-dependent initial point. In essence, this pilot scheme leads to the fact that channel estimation can be carried out on a sub-frame basis, where other cell's data and pilot symbols behave like additive white Gaussian noise.
For SINR estimation, we consider knowledge on frequency-flat and frequency-selective i.i.d. interference powers σ^2_{IF} according to (4.7) and (4.8), respectively. Further, we

consider the case of full frequency-selective covariance knowledge based on received data signals in $\mathbf{y}_{k,t}$.

From [PNJvH05] we assume the estimation error to be modeled by a Gaussian distribution with a variance equal to an average rMSE with $\mu \in \{0, -10, -20, -30\}$ dB. Figure 4.5(a) compares the sector spectral efficiencies using a TDMA round-robin scheduler for the SISO and MIMO 2×2 and perfectly known SINRs (4.3). Furthermore, it may be observed that the achievable SINR knowledge from (4.4) with $\mu = -10$ dB may be sufficient to approach 99% of the ideal MRC performance with perfect channel estimates. Thus, the lower bound for the SINRs, which is determined by the estimate in (4.14), is quite close to the resulting performance from our simulations.

$$
\begin{aligned}
\widehat{\mathrm{SINR}}_{k,t}^{\mathrm{MRC}} &= \frac{\widehat{\overline{\mathbf{h}}}_{k,t}^{H} \overline{\mathbf{h}}_{k,t} \overline{\mathbf{h}}_{k,t}^{H} \widehat{\overline{\mathbf{h}}}_{k,t}}{\widehat{\overline{\mathbf{h}}}_{k,t}^{H} \mathbf{Z}_{k,t} \widehat{\overline{\mathbf{h}}}_{k,t}} \\
&= \frac{\left(\overline{\mathbf{h}}_{k,t} + \delta_{k,t}\right)^{H} \overline{\mathbf{h}}_{k,t} \overline{\mathbf{h}}_{k,t}^{H} \left(\overline{\mathbf{h}}_{k,t} + \delta_{k,t}\right)}{\left(\overline{\mathbf{h}}_{k,t} + \delta_{k,t}\right)^{H} \mathbf{Z}_{k,t} \left(\overline{\mathbf{h}}_{k,t} + \delta_{k,t}\right)} \\
&\overset{A \ll 1}{\approx} \frac{\left\| \overline{\mathbf{h}}_{k,t}^{H} \overline{\mathbf{h}}_{k,t} \right\|^2}{\overline{\mathbf{h}}_{k,t}^{H} \mathbf{Z}_{k,t} \overline{\mathbf{h}}_{k,t}} \Bigg(1 + \frac{2\mathrm{Re}\left\{ \delta_{k,t} \overline{\mathbf{h}}_{k,t} \overline{\mathbf{h}}_{k,t}^{H} \overline{\mathbf{h}}_{k,t} \right\}}{\left\| \overline{\mathbf{h}}_{k,t}^{H} \overline{\mathbf{h}}_{k,t} \right\|^2} + \frac{\delta_{k,t}^{H} \overline{\mathbf{h}}_{k,t} \overline{\mathbf{h}}_{k,t}^{H} \delta_{k,t}}{\left\| \overline{\mathbf{h}}_{k,t}^{H} \overline{\mathbf{h}}_{k,t} \right\|^2} \\
&\quad \underbrace{- \frac{2\mathrm{Re}\left\{ \overline{\mathbf{h}}_{k,t}^{H} \mathbf{Z}_{k,t} \delta_{k,t} \right\}}{\overline{\mathbf{h}}_{k,t}^{H} \mathbf{Z}_{k,t} \overline{\mathbf{h}}_{k,t}} - \frac{\delta_{k,t}^{H} \mathbf{Z}_{k,t} \delta_{k,t}}{\overline{\mathbf{h}}_{k,t}^{H} \mathbf{Z}_{k,t} \overline{\mathbf{h}}_{k,t}}}_{A} \Bigg) \\
&\geq \underbrace{\frac{\left\| \overline{\mathbf{h}}_{k,t}^{H} \overline{\mathbf{h}}_{k,t} \right\|^2}{\overline{\mathbf{h}}_{k,t}^{H} \mathbf{Z}_{k,t} \overline{\mathbf{h}}_{k,t}}}_{\mathrm{SINR}_{k,t}^{\mathrm{MRC}}} \left(1 - \underbrace{\mu \left(1 - \frac{1}{N_r} \right)}_{\text{loss}} \right)
\end{aligned}
\tag{4.14}
$$

For Figure 4.5(b) the covariance estimator from (4.10) is employed across 1 and 2 sub-frames, i.e. 7 and 14 OFDM data symbols, yielding an estimate $\widehat{\mathbf{R}}_{yy}$. In combination with the channel estimation error model, which was already introduced for MRC, it is possible to determine $\widehat{\mathbf{w}}_{k,t}^{\mathrm{OC}} = \widehat{\mathbf{R}}_{yy}^{-1} \widehat{\overline{\mathbf{h}}}_{k,t}$. Comparing both figures it may be observed that the achievable performance of the OC receiver highly depends on the estimate $\widehat{\overline{\mathbf{h}}}_{k,t}$ showing hardly any gain for a $\mu = -20$ dB compared to the MRC approach. In case of an assumed $\mu = -30$ dB and a covariance estimation over 2 sub-frames, the system outperforms the simple MRC receiver in 60% of all cases. However, these assumptions are not feasible in a system under realistic conditions. Thus, it is doubtable whether these OC gains are still present.

For synchronized BSs, we assume to use multi-cell channel estimation based on

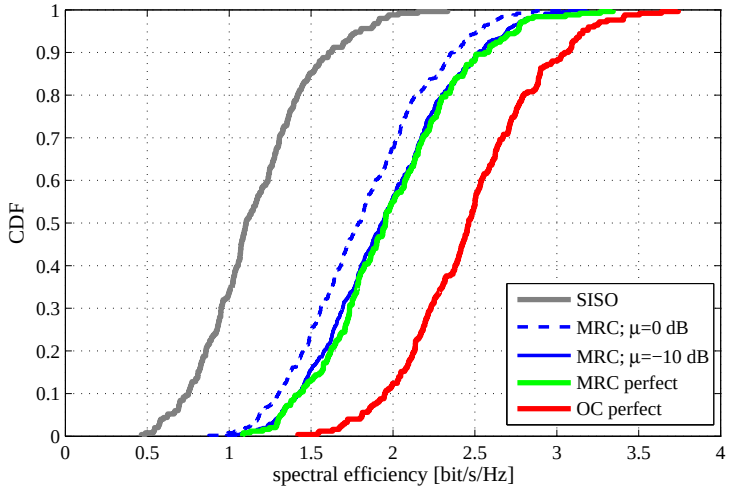

(a) MRC

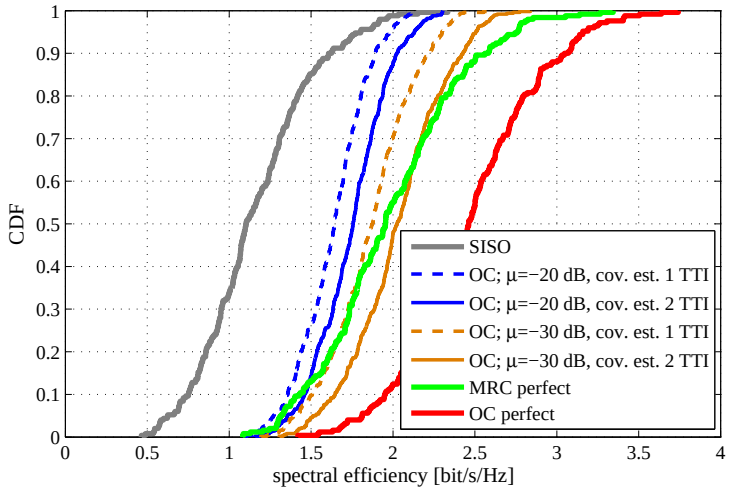

(b) OC

Figure 4.5: System's spectral efficiency based on perfect (4.3) and achievable (4.4) SINRs for MRC and OC receivers in non-synchronized downlink transmission systems. $\widehat{\widetilde{\mathbf{h}}}_{k,t}$ is generated using the AWGN estimation loss model [PNJvH05] with a given error variance chosen according to μ, refer to Section 4.1; the covariance is estimated over 1 and 2 sub-frames using (4.10).

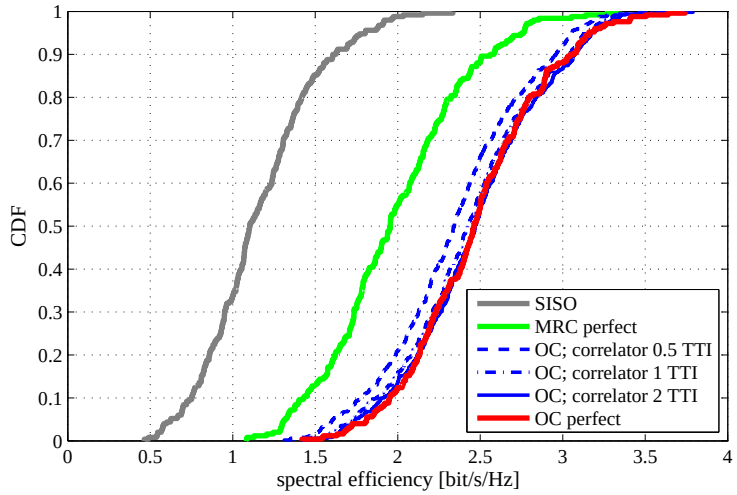

Figure 4.6: Performance comparison of ideal systems (case A) and IRC using the correlation based estimator (case B). As correlation intervals we selected 0.5, 1 and 2 TTIs.

virtual pilot sequences [TSSJ08] from Section 4.1.2. These sequences are block-orthogonal and are defined over time-domain. For channel estimation, the receiver is based on a simple correlator.

Figure 4.6 compares the system spectral efficiency using perfect (4.3) and achievable (4.4) SINRs for OC based on the correlation-based estimator. Assuming a multi-cell channel estimation over 0.5 sub-frames, i.e. only one LTE time slot, clearly outperforms the MRC receiver. Thus, LTE systems may already profit from higher spectral efficiencies when employing interference suppression using OC based on the correlation-based estimator. Therefore, no additional scrambling for common pilots symbols of different sites has to be introduced, but downlink transmission from all BSs has to be synchronized. In this case the achievable median spectral efficiency reaches 94.7% of the perfect performance. If the estimation is done over 1 subframes the median performance reaches 98.4% . Finally, after 2 subframes there is hardly any difference between the performance based on estimates from (4.3) and (4.4). Furthermore, it can be observed that estimation errors caused by the correlation-based estimator only result in a constant shift of the original CDF with perfect channel knowledge and OC (Figure 4.6). In contrast, the estimation errors caused by the covariance estimator dramatically change the shape of the distribution, removing high spectral efficiencies of the system which indicates the highly error limited behavior (Figure 4.5(b)).

Figure 4.7 depicts the estimation error of the single-stream transmission SINR at the terminal. We compare the ratio of the estimated $\widehat{\text{SINR}}_{k,t}$ to the achievable $\widetilde{\text{SINR}}_{k,t}$ under perfect CSIR and estimated equalization weights. Employing

either MRC in an asynchronous network or OC in a synchronized system, leads to significantly different estimation error distributions.
For MRC, based on (4.8), the estimation suffers in two ways: There is a median shift of -1.9 dB, i.e. $\widehat{\mathrm{SINR}}_{k,t}$ is systematically to low. In addition, the estimation error has a considerable variance. With overestimated SINR conditions, the channel may be overloaded, resulting in substantial performance degradation. Assuming that strong channel codes as well as hybrid automatic repeat request (HARQ) mechanisms are able to correct errors if 10% of the resources are overloaded, we have to ensure that the 90-percentile of $\widehat{\mathrm{SINR}}_{k,t}/\widetilde{\mathrm{SINR}}_{k,t}$ is below 0 dB. This can be achieved by introducing an outer link adaptation control loop, which shifts the MCS switching points by a certain on-level ε correspondingly.
For MRC based on (4.8), we can estimate $\varepsilon = 2.3$ dB from Figure 4.7. Focusing on the median value, there is an overall on-level offset of approx. $\varepsilon = 4.2$ dB at the medium access control (MAC) compared to achievable $\widetilde{\mathrm{SINR}}_{k,t}$. Averaging the interference power σ^2_{IF} over the entire frequency band, i.e. using (4.7), reduces the offset to $\varepsilon = 3.7$ dB. Covariance estimation, i.e. (4.10), leads to unbiased estimates $\widehat{\mathrm{SINR}}_{k,t}$, but the on-level offset is significantly higher due to the larger variance, resulting in $\varepsilon = 6.3$ dB. Concentrating on asynchronous downlink transmission, we conclude, that frequency-flat i.i.d. σ^2_{IF} results in highest performance.
The offset values ε can further be reduced, if the interference is estimated more precisely, e.g. in a synchronous system using OC receiver and the correlation approach as given in (4.12). For a correlation window spanning $N = 3$ pilot symbols, we assume to be able to distinguish between the channels belonging to 3 out of 57 sectors. Hence, interference cannot be separated sufficiently, and thus SINRs are systematically overestimated. However, already with a correlation window spanning $N = 12$ pilot symbols, 12 sectors and thus more interferers can be identified, and the SINR is determined more precisely [TSWJ08]. The on-level offset factor is then $\varepsilon = 0.9$ dB, and the median shift becomes negligible.

Figure 4.8 shows the achievable sum rates in the multi-cell system including the specific ε. As lower bounds, we use the performance in SISO case including the effects of estimation errors for the desired channel $\widehat{\mathbf{h}}_{k,t}$. The upper bound is given by the adaptive transmission system from Section 3.4 assuming perfect CSIR. Assuming the UE is able to estimate its dedicated channel with an average rMSE $\mu = 0.1$ and $\mathbf{Z}_{k,t}$ according to (4.8) and the system is forced to SU-MIMO mode only, results in an inferior performance compared to the single-stream transmission mode using MRC. The reason is that the estimation error leads to inter-stream interference in the SU-MIMO case, which is not present with single-stream transmission.
The next three CDF curves are all based on the correlation estimates from (4.12). Although the use of the OC receiver can exploit the knowledge of interference, the single-stream transmission mode using the OC receiver outperforms the SU-MIMO transmission. Allowing the fully adaptive transmission yields a significant gain in system's spectral efficiency. This gain is mostly related to the MU-MIMO schedul-

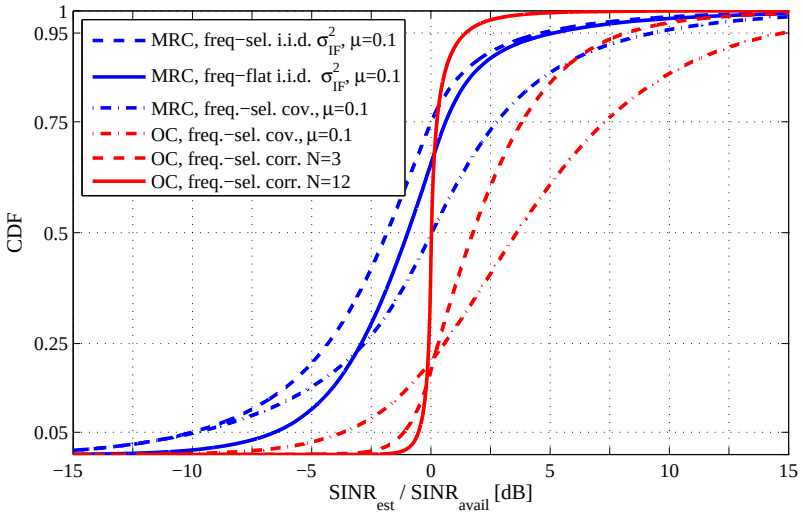

Figure 4.7: Maximum Δ_{SINR_u} (case C) of both available beams for single-stream transmission, while assuming asynchronous and synchronous transmission from all BSs and using appropriate receivers.

ing, also compare with Figure 3.7. Note, that the gap to the adaptive system with perfect CSIR amounts to 8% only, indicating the robustness of the proposed scheme. Thus, synchronized downlink transmission from all BSs in combination with the OC receiver based multi-cell correlator estimates outperforms the asynchronous case. However, if the system design would be constrained to non-sychronized BSs, single-stream transmission in combination with the MRC receiver would be a suitable choice. The difference in the average spectral efficiency between both cases is significant and amounts to 76% in our results. Thus, the overall gain achievable with synchronized base stations is still significant even under practical considerations.

Note, that considering independent adaptation of beam sets for all BSs does not influence the received interference covariance matrix $\mathbf{Z}_{k,t}$, since the Wishart product $\mathbf{B}_m\mathbf{B}_m^H$ equals the scaled identity matrix if we assume $\mathbf{B}_m$ to be unitary. However, changing the power allocation for different MIMO transmission modes results in a multi-cell system where $\mathbf{Z}_{k,t}$ cannot be predicted at the receiver side. In order to support cell-edge terminals, we suggest to arrange e.g. single-stream transmission with full base station power in a coordinated access scheme known to the users.

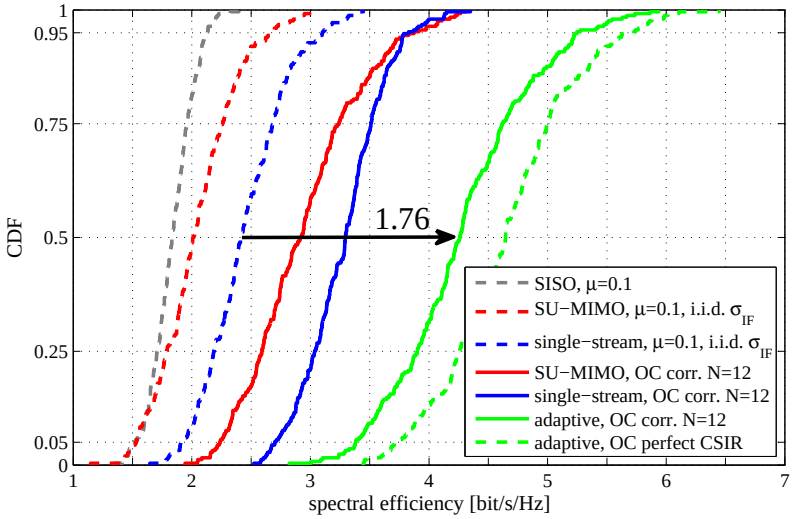

Figure 4.8: Spectral efficiency of various transmission schemes including estimation errors.

4.1.4 Conclusion

This work evaluates the gains from using interference-aware, frequency-selective MU-MIMO scheduling in a cellular network with synchronized BSs. UEs are assumed to be able to estimate their dedicated and interfering channel coefficients. With the suggested scheduling approach, we can conclude with two important observations: Efficient MU-MIMO transmission can be achieved by using fixed DFT-based unitary pre-coding, i.e. without the requirement of full channel state information at the transmitter. Further, proper application of the MU-MIMO mode enables to conveniently serve users in the multi-stream transmission mode who experience relatively poor SNR conditions. Thus, the MU-MIMO mode establishes a win/win situation for low- and high-rate users competing for a resource: Low-rate user can be served without blocking a given resource for any high-rate users, who can support a rate on any of the available beams. We further studied the suggested concept in an interference-limited environment and observed that knowledge of the interference channels yields a more precise estimation of the achievable SINR compared to the traditional approach, where interference is assumed white.

We implemented essential functions of this scheme in an experimental urban macro scenario, i.e. in the Berlin LTE-Advanced Testbed, and confirmed the significantly increased probability to select the multi-stream transmission mode also for realistic propagation conditions [STW+09, JST+09]. The experimental proof of MU-MIMO gains in the interference-limited scenario is subject of ongoing research.

4.2 Sub-Band vs. Wide-Band Feedback Information

In the following section we study the limited feedback concept from Chapter 3, where we successively reduce the amount of provided feedback. We start from a theoretic point of view, revealing results from Section 3.4: Each user provides full channel feedback but in a quantized manner, i.e. by using quantized SINRs in combination with precoding matrices $\boldsymbol{\beta}$ derived from a given codebook set $\mathcal{B}$ for feedback of channel direction. These feedback mechanisms are known as channel quality indicator (CQI) and precoding matrix indicator (PMI) feedback in 3GPP LTE.

Feedback for groups of multiple PRBs: As an initial step, 3GPP reduces feedback from a per PRB down to a sub-band basis. Therefore, [3GP12, Table 7.2.2-2] suggests to combine a number of 6 or 8 consecutive PRBs at 10 MHz and 20 MHz bandwidth, respectively. The UEs are allowed to report only a single CQI value per sub-band. Note, the average coherence bandwidth for an urban-macro channel is in the same range, i.e. $\overline{B}_C \approx 1$ MHz. However, the 5% -ile outage value is well below that range, refer to Section 4.3.2. In order to determine the resulting CQIs per sub-band using the SINRs per PRB as an input, we employ the well-known exponential effective SINR mapping (EESM). The EESM is part of a link-2-system interface, mapping a set of SINR values into data rates without directly employing FEC in system-level simulations.[2] Thereby, the link-2-system interface uses a vector of SINR values as well as a desired target BLER as inputs and determines an effective scalar SINR which corresponds to a SISO AWGN link-level performance curve.

Figures 4.9(a) and 4.9(b) depict the median sector and 5% -ile user throughput. The set of bars, denoted with the label $|\mathcal{B}_{mask}| = max$, summarize the results for full feedback from Section 3.4 and the same transmission concepts but with sub-band CQI and PMI feedback. The loss for sub-band reporting with a sub-band size of 6 PRBs attributes to 9% and 33% for median sector and cell-edge user throughput. Note, $\mathcal{B}_{mask}$ is a set of matrices which we introduce to account for the selection of specific data streams in case of $|\mathcal{T}_s| < N_t$. Its definition will be discussed later in this section.

As a next step, we assume a wide-band selection of PMI, while we increase the quantization of channel direction by enlarging the set of precoders in $\mathcal{B}$. As a main results, we cannot observe any additional loss from wide-band PMI and sub-band CQI for $|\mathcal{B}| = 1$. Hence, it is sufficient to adjust the precoder for each user on a wide-band basis. In essence, a frequency-selective selection of the quantized dominant channel directions[3] does not improve the system nor the user performance. Note, this conclusion is not applicable in systems using full CSI, as e.g. CoMP transmission

[2] Due to the extraordinary computational complexity of FEC, data transmission is usually abstracted using a state-of-the-art link-2-system interface. A comparison of different mapping functions is given in [AAB+05].

[3] Which is the main methodology in the PMI selection process.

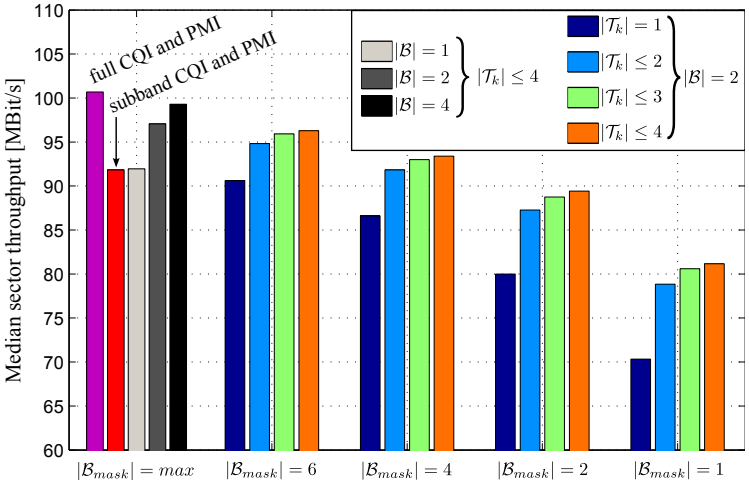

(a) Median system throughput.

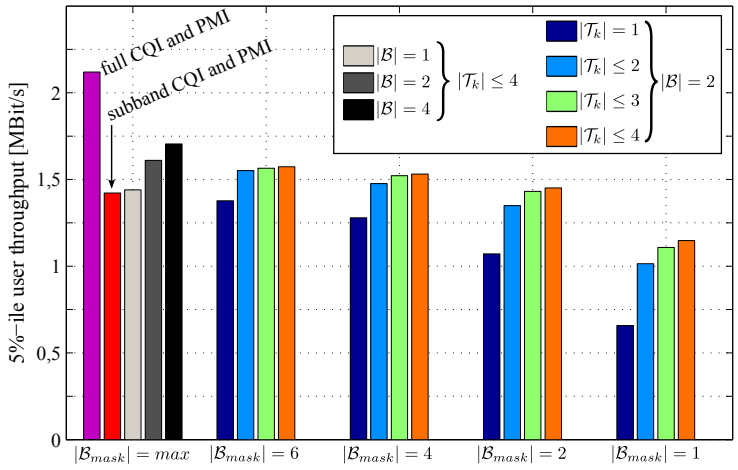

(b) 5% -ile user throughput.

Figure 4.9: Impact on system and user throughput due to limited feedback assumptions. Degrees of freedom are: reported data streams $|\mathcal{T}_k|$ per precoding matrix $\boldsymbol{\beta}_i$ in the codebook $\mathcal{B}$. $\mathcal{B}_{mask}$ is a set of matrices accounting for selection of data streams in case of $|\mathcal{T}_s| < N_t$.

using joint ZF precoding. As already found for full CQI and PMI feedback, there is a significant gain for $|\mathcal{B}| \geq 2$.

Transmission with $\mathcal{T}_s < N_t$: Let us assume, the serving BS is using rank 3, i.e. $|\mathcal{T}_s| = 3$ transmission. Hence, users are informed via the downlink signalization channel which combinations of data streams are available for the next time slot. In order to account for this selection procedure, we introduce a set of matrices $\mathcal{B}_{mask}$ masking certain data streams in a specific precoding matrix $\boldsymbol{\beta}_i$, e.g.

$$\begin{aligned}
\mathbf{B}_m &= \frac{1}{2\sqrt{3}} \underbrace{\begin{bmatrix} 1 & 1 & 1 & 1 \\ 1 & -i & -1 & i \\ 1 & -1 & 1 & -1 \\ 1 & i & -1 & -i \end{bmatrix}}_{\boldsymbol{\beta}_1} \underbrace{\begin{bmatrix} 0 & 0 & 0 & 0 \\ 0 & 1 & 0 & 0 \\ 0 & 0 & 1 & 0 \\ 0 & 0 & 0 & 1 \end{bmatrix}}_{\boldsymbol{\beta}_{mask,i}} \\
\mathbf{B}_m &= \frac{1}{2\sqrt{3}} \begin{bmatrix} 0 & 1 & 1 & 1 \\ 0 & -i & -1 & i \\ 0 & -1 & 1 & -1 \\ 0 & i & -1 & -i \end{bmatrix}
\end{aligned} \tag{4.15}$$

By changing the masking matrix $\boldsymbol{\beta}_{mask}$, users need to determine which constellation of possible active streams is desirable. In general, there exist $\binom{N_t}{|\mathcal{T}s|}$ options to combine the spatial layers defined in a precoding matrix. Figure 4.10 depicts the paradigm for the case of $|\mathcal{T}_s| = 3$, i.e. rank 3, data transmission. The users have to choose their desired precoding matrix based on a combination of $\boldsymbol{\beta}_i$ and corresponding selection of data streams following a specific metric, according to Equation (4.15). In our application, we determine the desired masking index i on a wide-band basis maximizing the channel gain for one single candidate data stream in $\boldsymbol{\beta}_1\, \boldsymbol{\beta}_{mask,i}$. As a side constraint, it would be beneficial to introduce the condition of smallest received sum power from all other active data streams in $\boldsymbol{\beta}_{mask,i}$. However, this would increase the complexity in the codebook selection procedure.

Results in Figure 4.9 summarize the median sector and cell-edge user throughput for $|\mathcal{B}| = 2$ and feedback reporting for a certain number of data stream combinations for transmission modes involving less data streams than possible. We start the analysis from $|\mathcal{B}_{mask}| = 6$ down to 1, referring to the x-axis from left to right. Note, for $|\mathcal{B}| = 2$ there exist a maximum number of 12 choices, i.e. $2\binom{4}{2} = 12$ with rank 2 transmission. Thus, the condition of $|\mathcal{B}_{mask}| = 6$ allows only 50% of reporting in case of $|\mathcal{T}_s| = 2$ and 75% reporting for $|\mathcal{T}_s| = \{3, 1\}$. Focusing on the orange bars on left of each set in Figure 4.9, we observe a significant increase in data rates from $|\mathcal{B}_{mask}| = 1 \rightarrow 2$.[4] In detail, compared to the ideal reference case, i.e. $|\mathcal{B}| = 2$ and $|\mathcal{B}_{mask}| = max$, the system and cell-edge user rates are losing 16% , 8% , 4% , 1% and 29% , 10% , 5% , 2% for $|\mathcal{B}_{mask}| = 1 \rightarrow 2 \rightarrow 4 \rightarrow 6$, respectively.

[4] Note, here we assume each user is reporting CQI values for all entries in a the selected precoding matrix $\boldsymbol{\beta}_i\, \boldsymbol{\beta}_{mask,i}$.

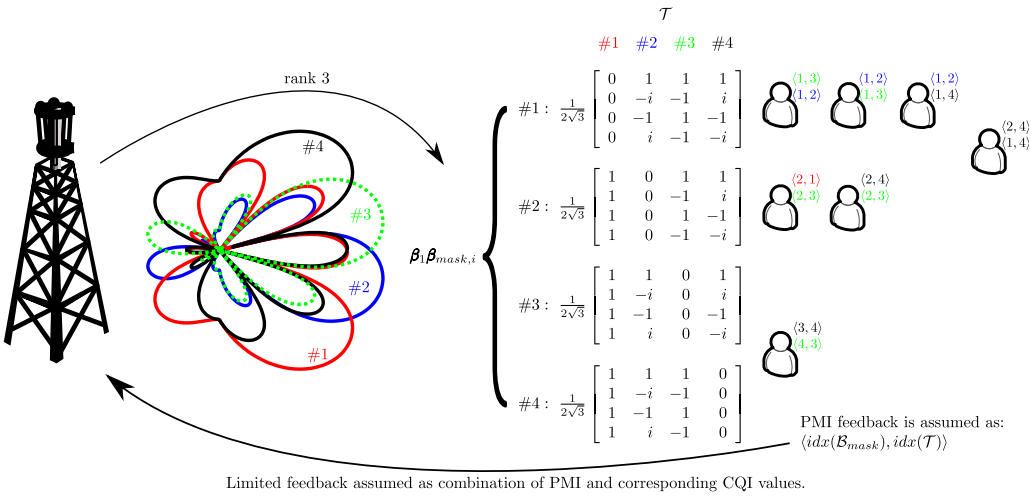

Figure 4.10: Overview on the precoding matrix selection procedure in case of $|\mathcal{T}_s| < N_t$, i.e. non-full data stream transmission.

Reducing CQI feedback values per precoding matrix: As a final step, we further reduce the feedback by limiting the users to report less CQI values per active precoding matrix $\mathbf{B}_m$. In our study, each user has only $N_r = 2$ receive antennas. Thus, it is not possible to transmit 4 data streams to a single user. In general, as shown in Section 3.4 it will be more efficient to serve each user with a single data stream, but multiple users at the same time in a multi-user MIMO (MU-MIMO) mode. Therefore, let us assume that we allow each user to report 2 CQI values. As given in Figure 4.10 we further assume each UE to report its PMIs as a collection of indices following the rationale $\langle idx(\mathcal{B}_{mask}), idx(\mathcal{T})\rangle$. Now, each user can decide to provide feedback for either 2 CQIs per sub-band and for a single precoding matrix $\boldsymbol{\beta}_1\boldsymbol{\beta}_{mask,i}$, or 2 values per sub-band for different precoding matrix selection $\boldsymbol{\beta}_1\boldsymbol{\beta}_{mask,i}$ and $\boldsymbol{\beta}_1\boldsymbol{\beta}_{mask,j}$. This is depicted as superscripts for each user in Figure 4.10. Top to bottom is indicating the order of choices, starting with the best from top.

The loss in median sector and cell-edge user throughput attributes to 28% and 59% , respectively, for the constraint of a single CQI value per sub-band ($|\mathcal{B}_{mask}| = 1$). This loss can be alleviated to 19% and 37% for $|\mathcal{T}_k| = 2$ and $|\mathcal{B}_{mask}| = 1$, and for $|\mathcal{T}_k| = 1$ and $|\mathcal{B}_{mask}| = 2$ the loss reduces further to 18% and 34% . Another significant step in system and per-user performance is reached for $|\mathcal{T}_k| = 2$ and $|\mathcal{B}_{mask}| = 2$, where the loss is in the order of 10% and 16% for median sector and cell-edge user data rates compared to ideal, full sub-band CQI and wide-band PMI assumption.

Green and light blue bars in Figure 4.9 represent the case where each user is allowed to feedback $|\mathcal{T}_s| = 3 \rightarrow 2$ CQIs per sub-band and codebook matrix $\boldsymbol{\beta}_{mask}$. Since there is only a marginal gain in providing additional CQIs for more than 2 data streams per precoding matrix, we conclude it is not worth spending the feedback.

4.3 Evolution of Channel Models

Current progress in wireless communications demand for increasingly sophisticated channel models, which are capable to capture most of the relevant effects from real world propagation conditions. Over the last decades, information theory was considering different effects of single- and multi-user fading channels even with time-varying fading properties [TH98, HT98]. In most applications, co-channel interference was modeled under the assumption of AWGN. The Wyner model [Wyn94] introduces an idealized, symmetric linear 1-dimensional model for inter-cell interference. This model was adopted in [SW97a] to assess different multiple-access techniques, where [SW97b] extends the model for multi-cell site processing.

The guidelines of the 3GPP spatial channel model (SCM) [3GP03, 3GP11] introduce a ray-based double-directional multi-link model. The model was continuously improved within a European project denoted as Wireless World Initiative New Radio (WINNER)[5] [KMH+07, MKH+10], to cover emerging requirements for 3GPP standardization of future cellular air interfaces such as LTE or Long Term Evolution - Advanced (LTE-A). The fundamental idea of those channel models is to emulate the wireless channel with a set of rays, having a direct connection or being scattered at obstacles in the surrounding environment denoted as line-of-sight (LOS) and non line-of-sight (NLOS), respectively. Each ray arrives at the receiver with a certain delay and power under a deterministic angle for the LOS connection. For the NLOS or multi-path components (MPC), this angle is following a certain geometry, yielding the multi-tap channel profile. The WINNER model, which is the evolution of the SCM, is a GSCM, where multiple rays are combined into a group of scatterers for a given multi-antenna configuration, as depicted in Figure 4.11. The spatial distribution of the scatterer groups, which specify the direction of the scattered rays, are stochastically generated following a specific distribution of angular spreads at the receiver as well as at the transmitter side. Thereby, GSCM supports specific antenna configurations and spatial beam patterns. The parameters for generating the MIMO channels are extracted from measurements as recently summarized in [MKH+10]. Such GSCM as well as the COST 2100 model [OCD+12][6] have been proven as reliable tools for the system-wide evaluations of wireless transceiver algorithms.

In particular, system-level simulations often require two important features: multi-link capabilities and time evolution of the channel impulse response. First, multi-link features are mandatory to evaluate cooperative techniques where multiple UEs simultaneously communicate with multiple BSs. Another application are heterogeneous networks or dense deployments, where pico- and/or femto-cells are placed

[5] There were three consecutive phases of the WINNER project covering a period from 2004 until 2010, WINNER I, WINNER II and WINNER+, http://www.celtic-initiative.org/Projects/Celtic-projects/Call5/Winner+/Project-default.asp

[6] Note, the COST 2100 model follows a more deterministic approach, since it first defines the scatterer group locations and then determines angular distributions and the K-Factor.

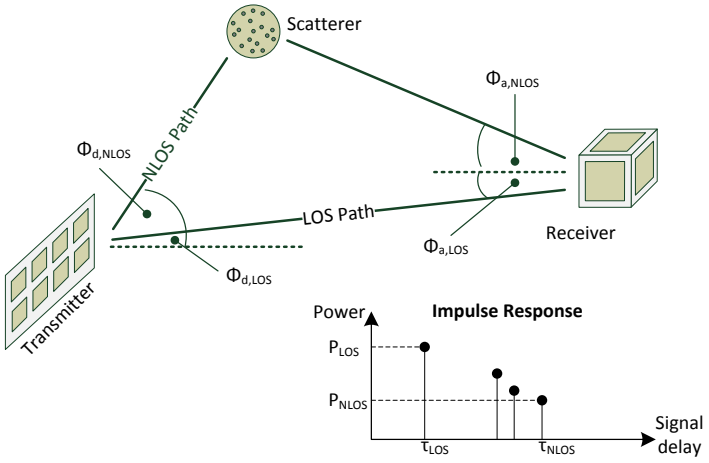

Figure 4.11: Typical structure of geometry-based stochastic channel model, depicting a direct LOS component and for simplicity a single cluster of scatter points. In general, a typical urban channel consists of up to 20 clusters.

into the standard homogeneous macro cellular grid. Currently, these concepts are of major interest since the system capacity can be further improved due to an increased reuse of spatial resources. Thus, it is important to capture the multi-user channel towards several transmitters simultaneously. Second, deterministic time evolution is important in all applications where the UEs are moving fast enough to observe changes in small- or even large-scale channel parameters within the observation time. This time duration can range from a few milliseconds for fast feedback control loops, covering scheduling or precoding decisions, up to several seconds for rather slowly changing control mechanisms such as handover or cell activation for energy efficient transmission concepts [Gre]. Currently, the COST 2100 [OCD+12] is the only channel model supporting time evolution. It characterizes the channel on the level of individual groups of scatterers and thus, it intrinsically includes the correlation between multiple links [CO08]. Unfortunately, available parameterization is rather limited compared to the widely used WINNER model. In contrast, WINNER lacks in a time evolution beyond the scope of a few milliseconds and a validation for multi-link setups.

The contribution of this section is to provide an overview on desired components for a future multi-cell channel model. The model needs to address the issues from above without the tremendous computational complexity and effort for parameterization of much more precise ray-tracing solutions. Subsequent paragraphs introduce main components of our channel model and provide a comparison with the different

evolutionary steps in channel modeling.

4.3.1 Components of QUADRIGA

We present a new model based on the WINNER method, which allows to calculate channel traces with a temporal evolution. The so-called quasi-deterministic radio channel generator (QuaDRiGa)[7] supports configurable network layouts with multiple transmitters and receivers and is scalable from single-user single-antenna systems to heterogeneous multi-user MIMO scenarios. By updating the delays, the departure- and arrival angels, the polarization, the shadow fading and the K-Factor based on the position of the terminal, we achieve a time evolution of both small- and large-scale components.

A more precise description of the different components, the corresponding implementation guidelines as well as the verification with measurement data are summarized in our work in [JBT12, BDJT12].

3-Dimensional polarimetric antenna models: Over the last decade, channel modeling considered 2-dimensional propagation environments along with antenna characteristics valid in the azimuth plane only. Models like SCM and WINNER Phase II model (WIM2) followed this principle. In [TWB+09], we introduced 3-dimensional antenna characteristics and proved its impact by channel measurements. We included precise modeling of directional base station antennas with remote electrical tilt (RET) units according to latest prototypes such as the Kathrein 80010541 antenna[8]. Finally, the WINNER+ model (WIM+) included the additional elevation component. The RET limits the effective cell size according to the desired setup. Figure 4.12 depicts the received power under the assumption of 2D and 3D antenna diagrams, respectively. The highly directive elevation pattern of real-world BS antennas significantly influences the propagation behavior in cellular systems. At the particular distance where the main lobe touches the ground, we observe a clear change in the propagation conditions. This distance determines the desired effective cell radius. While the received power is almost constant inside of the effective cell[9], outside the cell the path loss exponent is significantly increased compared to standard urban path loss assumptions. These effects have been observed in an experimental setup and are described in more detail in [JJJ+09, TWB+09, JTB+09]. In particular, co-channel interference (CCI) from neighboring BSs is becoming a rather local phenomenon, i.e. the origin of strong interference is close to the user's location [TWB+09].

[7] The model is available at http://www.hhi.fraunhofer.de/quadriga. Funding was provided by German Ministry of Economics (BMWi) in the national collaborative project IntelliSpektrum under contract 01ME11024 and by the ESA/ESTEC contract AO/1-5985/09/08/NL/LvH (Acronym: MIMOSA).

[8] http://www.kathrein-scala.com/catalog/80010541.pdf

[9] This is attributed to a very careful antenna design, where the elevation pattern is manipulated to constitute several side lobes underneath the main lobe.

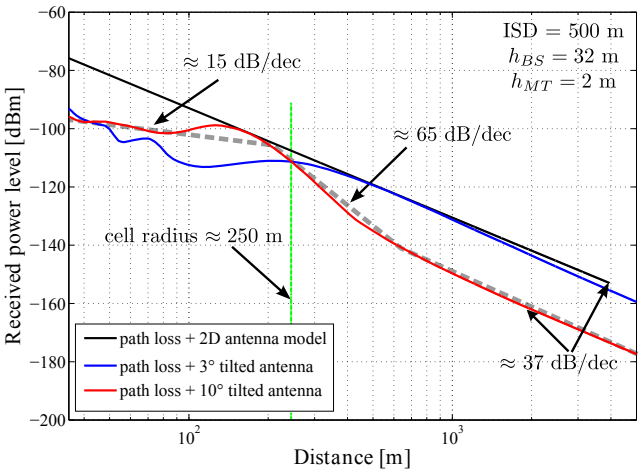

Figure 4.12: Received power taking into account a common path-loss model [ETS98] and a 2D or 3D antenna model.

Another important issue is the modeling of polarization effects along a given user trajectory. SCM was lacking in providing this feature, where the WIM2 partially introduced this effect in a stochastic manner. In [JBTJ12], we describe a deterministic approach to model 3-dimensional polarimetric wavefronts based on the Jones calculus [Jon41]. In addition, we proposed a method to calculate the channel cross-polar ratio (XPR) inspired by Jones. The new method was validated by outdoor measurements in downtown Berlin, Germany.

Large-scale parameters with 2-dimensional auto-correlation: In QuaDRiGa each environment type is characterized by seven scenario-dependent so-called large-scale parameters (LSPs):

1. RMS delay spread (DS)
2. Ricean K-Factor (KF)
3. Shadow fading (SF)
4. Azimuth spread of departure (AsD)
5. Azimuth spread of arrival (AsA)
6. Elevation spread of departure (EsD)
7. Elevation spread of arrival (EsA)

The LSPs are taken from 2-dimensional maps. Each of these maps has certain auto-correlation, inter-parameter and inter-site cross-correlation properties according to [Gud91, MKH+10, KM99]. Based on these findings, we derive 2-dimensional

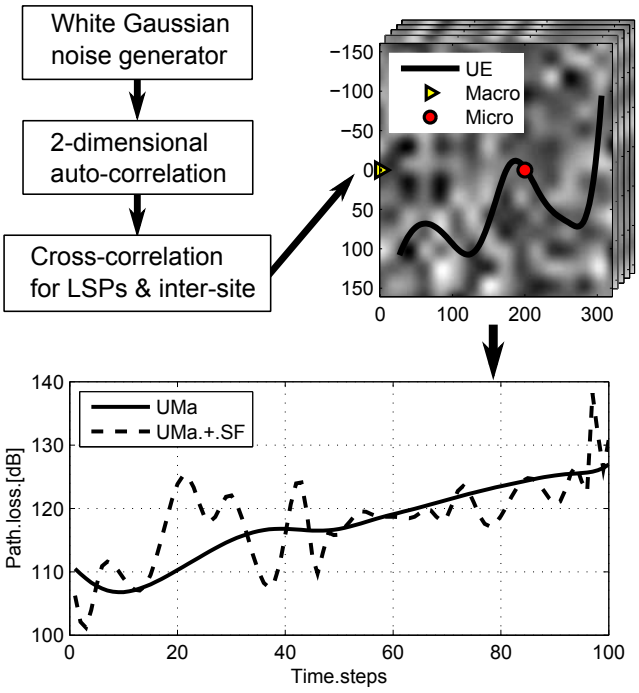

Figure 4.13: Methodology to generate multiple correlated LSPs maps.

maps as shown in Figure 4.13. As an initial step, random values following a Gaussian distribution are filtered to obtain the desired spatial correlation. Subsequent to the auto-correlation of the parameters, cross-correlation properties between different LSPs and between different transmitters have to be taken into account [SYT10, Cla05, KM99].

In particular, each of these LSPs follows a normal distribution which is being described by multiple values with a desired cross-correlation behavior: The median, its variance and an exponential decaying factor corresponding to the de-correlation distance. Thus, the exponential decaying function represents the spatial, i.e. 2-dimensional auto-correlation of each LSP. In general, all these values are determined by extensive measurements as reported in [MKH$^+$10, JBT12].

Time evolution: In order to explain the methodology behind the time evolution, both on small- as well as on large-scale channel parameters, let us assume an UE moves along a pre-defined trajectory, refer to Figure 4.14. By updating the delays and various angles we can emulate a deterministic drifting of phases for the different MPCs, while tap locations are not kept fixed [BHS05, JBT12], refer to Figure 4.14. The time evolution on a larger scale requires an update of path loss, shadow fading (SF), K-factor and received power due to the antenna characteristics.

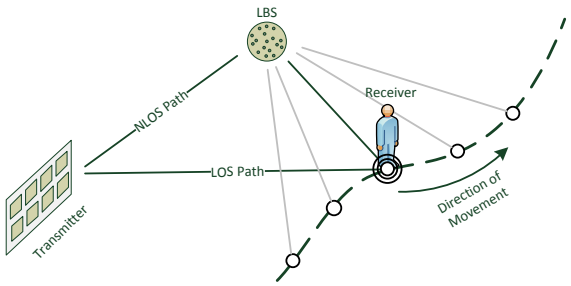

Figure 4.14: Along with the knowledge of transmitter and receiver position, delays and angles the NLOS and LOS path length can be determined.

Calculation of channel coefficients: The following part is intended to briefly summarize how the different components are merged such that the resulting channel coefficients follow the desired properties. Each component of the channel impulse response is given as $g_{l,s}$ and is calculated for a specific receive and transmit antenna pair, as well as for a given MPC, i.e. tap l and for a specific time sample n. Following the notation of our work in [JBT12], each coefficient is given by

$$g_{l,n} = P_{LSP} \cdot P_{l,K} \cdot P_{l,norm} \sum_{m=1}^{M} g_{l,m,n}^{[pol]} \, \mathrm{e}^{j\psi_{l,m,n}^{+}} \tag{4.16}$$

where P_{LSP} contains the power scaling values derived from path-loss and shadow fading. $P_{l,K}$ and $P_{l,norm}$ ensure a correct normalization of received power in terms of the K-Factor as well as the desired power value for the set of MPCs. As stated in [JBT12], a set of $M = 20$ multi-path componentss is combined into a group of so-called LBS. A set of L different groups of those last bounce scatterers (LBSs) result into the physical taps of the impulse response. The polarimetric part of the channel coefficient is condensed into $g_{l,m,n}^{[pol]}$ per sub-path. In [JBTJ12], we carefully derived a method to deterministically adapt the change in polarization while the electromagnetic wave is propagating along a given path. With a reasonable setting for XPR and inclusion of realistic antenna patterns from both receiver and transmitter side, QuaDRiGa can realistically model polarimetric propagation conditions. Finally, $\exp\left(j\psi_{l,m,n}^{+}\right)$ represents the phase per sub-path.

4.3.2 Comparison of Channel Modeling Evolution

The following section evaluates the different steps in the evolution of spatial channel models. Thus, it demonstrates which steps are of major importance, since these changes significantly impact the system performance. We configure our QuaDRiGa

channel model for $N_t = N_r = 2$ such that we obtain the different evolutionary steps. All LSPs are configured according to WIM+, urban-macro scenario (UMa C2) for $f_c = 2.6$ GHz carrier frequency, refer to [MKH+10].

1. QuaDRiGa with co-polarized antennas, inter-site cross-correlation set to 0.5
2. QuaDRiGa with cross-polarized antennas, i.e. polarization with $\pm 45°$
3. QuaDRiGa with co-polarized antennas and an adaptive and distance-based inter-site cross-correlation following [KM99]
4. Co-polarized antennas without XPR, i.e. there is no loss in received power due to rotation of polarization, residual settings are based on typical QuaDRiGa settings
5. Co-polarized antennas without XPR and without inter-site cross-correlation
6. WIM+ with 3D Kathrein BS antenna, i.e. without polarization effects and without a fixed inter-site cross-correlation
7. WIM+ with 2D Kathrein BS antenna, same as above but without the elevation transmit pattern
8. WIM+ with 2D 3GPP BS antenna, similar to above, but using a typical antenna model from [3GP03][10]

The evaluation process is using several KPIs on the channel layer such as the median channel condition number, the median RMS delay spread (DS), its standard deviation value, the corresponding 5% -ile coherence bandwidth B_C, the median user geometry and the mean cluster distance. The 5% -ile of B_C serves as a measure to assess the frequency selectivity of the channel frequency response, i.e. it provides an estimate of the bandwidth fraction for which the channel frequency response can be considered as quasi flat. The median user geometry [HVKS03] characterizes the deployment parameters such as path loss, shadow fading, antenna broadsides and radiation characteristics. It can be considered as a long-term and wide-band average SINR. Finally, the mean cluster[11] distance is a metric where we initially determine the set of BSs which can be received within a given range, e.g. $T = 15$ dB below the strongest signal. Then we determine for each of the cell-ids the corresponding distance to the specific UE. The median cluster distance is a simple metric value indicating the spatial distribution for inter-cell interference. Note, the corresponding BSs would be a desired choice for CoMP transmission to jointly serve the users, refer to Section 6.2.

[10] Also comparable to SCME, but LSPs such as delay and angular spreads are configured slightly different.

[11] The term cluster means a group of BSs which may be used for CoMP transmission.

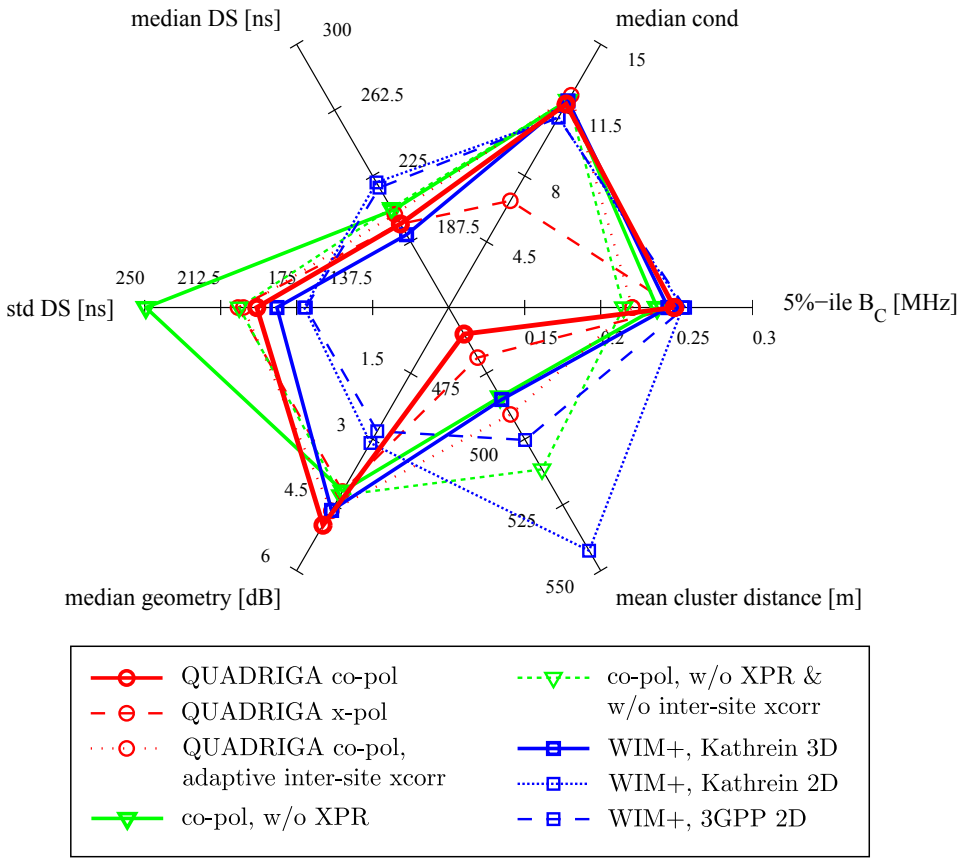

Figure 4.15: Channel-layer specific KPIs for different evolutionary steps in channel modeling for $N_t = N_r = 2$.

Based on Figure 4.15, we observe a significant improvement in channel condition for the setup using dual-polarized arrays. This is not very surprising and its effect for larger arrays is studied in [JBTJ12]. On the other hand, polarization has hardly any impact on other channel-specific KPIs. The effect of 2D auto-correlation and inter-site cross-correlation is getting prominent for the mean cluster distance, where we can observe larger distances for less correlation properties. The worst case mean cluster distance appears for the 2D antenna radiation characteristics, while the most optimistic assumption is found with a fixed inter-site cross-correlation value of 0.5. The deactivation of XPR, i.e. ignoring the effect of the polarization rotation while the electromagnetic wave is propagating along a given path, leads to a significantly increased standard deviation of the RMS DS.

In addition to the channel layer specific KPIs, we use the median per-sector and 5% -ile per-user throughput to compare the different evolutionary steps. Figures 4.16 and 4.17 show the corresponding data rates from score-based scheduling

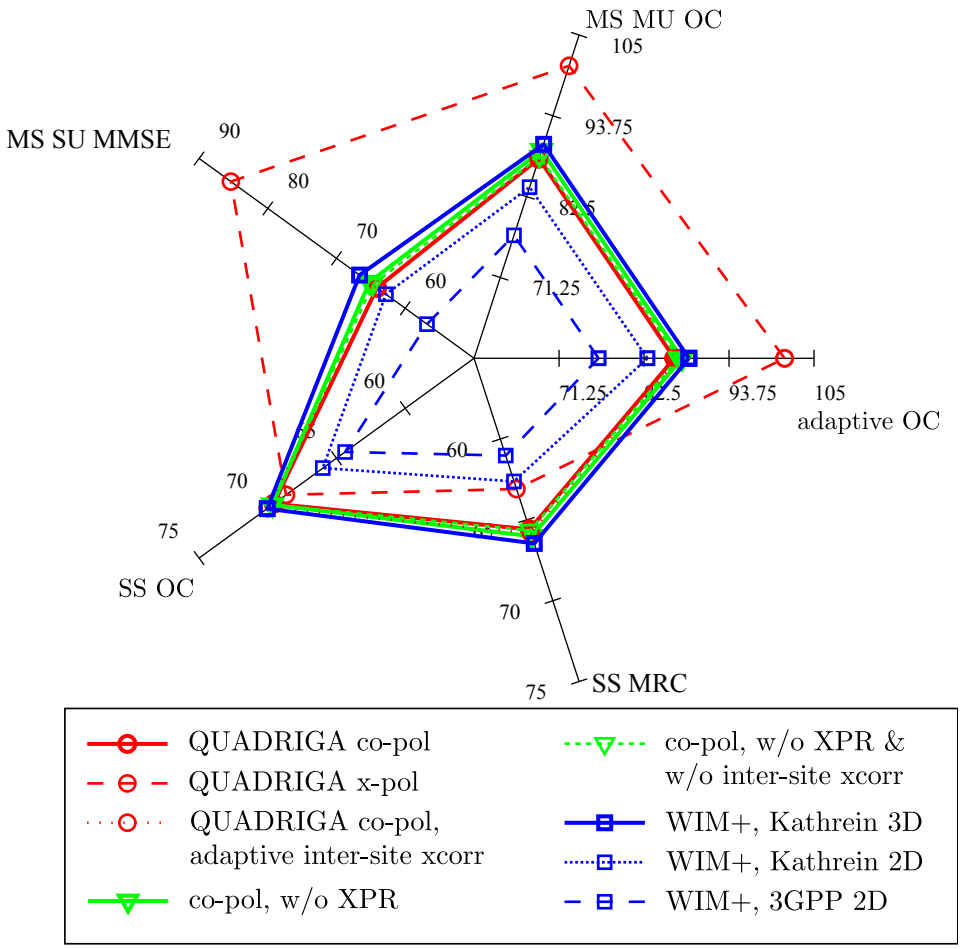

Figure 4.16: Median per-sector throughput at 20 MHz bandwidth using $N_t = N_r = 2$ and score-based scheduling.

and for a variety of transmission modes introduced in Section 3.4: multi-stream (MS) transmission to multiple users (MU) or to a single-user (SU) using MMSE or OC receivers. In addition, we include single-stream data rates for OC and MRC filters. For dual-polarized antennas, we observe that the all multi-stream transmission modes improve in sum throughput thanks to a better channel condition. 2D antenna radiation characteristics yield a worse system throughput due to an increased interference floor, also refer to the user geometries in Figure 4.15. All other configurations of QuaDRiGa result in rather equivalent data rates. Conclusions from cell-edge user performance are manifold. The direction-based inter-site cross-correlation of LSPs is improving the cell-edge user performance (compare red solid and dotted lines), where gains from multi-stream modes are disproportionately high. Again, dual-polarized antennas can also improve data rates at cell-edge. All

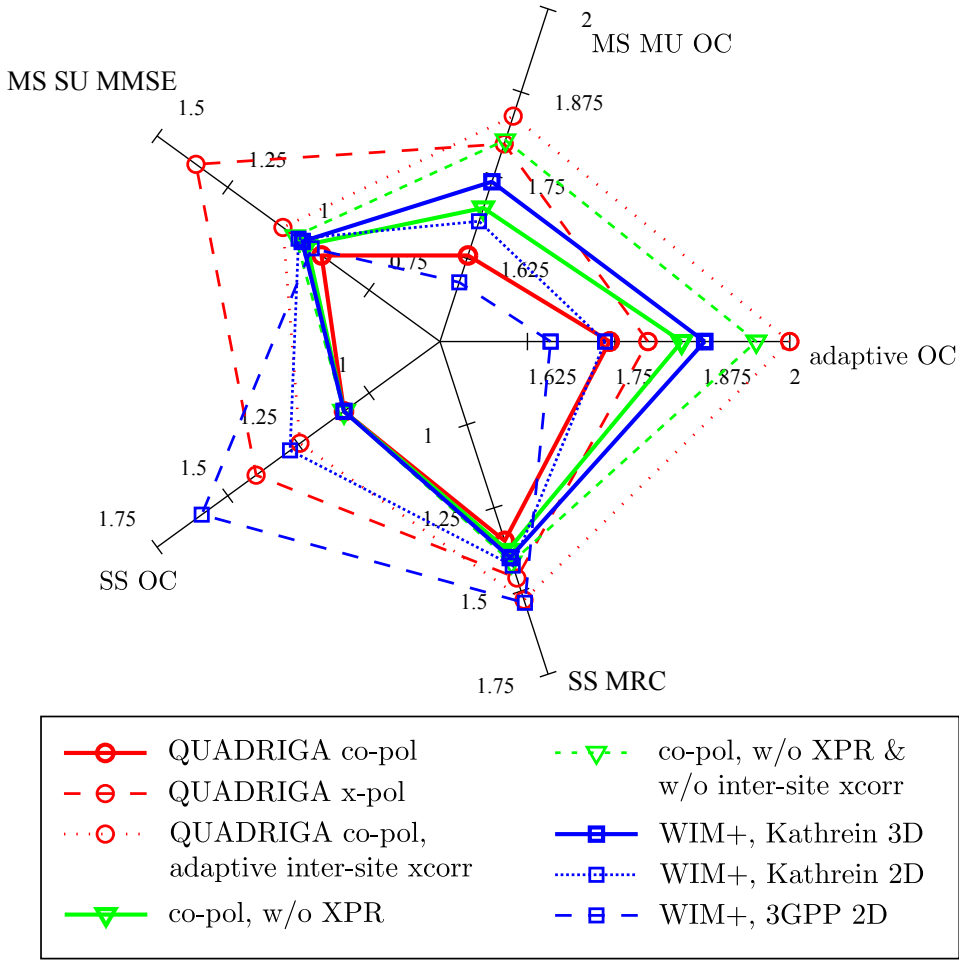

Figure 4.17: 5% -ile per-user throughput at 20 MHz bandwidth using $N_t = N_r = 2$ and score-based scheduling.

WIM+ assumptions seem to overestimate the 5% -ile user performance, where the largest discrepancy can be found for single-stream OC. In general, the result for single-stream OC is very surprising, since in most cases its performance is inferior to MRC. However, in theory SINRs obtained from OC should be larger or equal to those obtained by MRC. The reason may be found in a combination of different scheduling decisions for both receiver types and the very rough 4 Bit quantization for CQI, especially in the very low SINR regime.

5

Distributed CoMP approaching Centralized Joint Transmission

First of all, let us clarify the usage of the three different terms: *decentralized*, *centralized* and *distributed*. In case of a *decentralized* system concept, each BS is assumed to have no feedback information, in particular no CSI, from other BS's users. In contrast, the *centralized* system concept assumes full channel state information at the transmitter (CSIT) as well as scheduled user data shared among all BSs in the cluster. And finally, the term *distributed* indicates that a specific system concept can be implemented in a distributed manner, i.e. without a central unit (CU).

In this chapter, we focus on downlink MIMO transmission while observing *centralized joint transmission*. Here, multiple BSs cooperate in jointly transmitting precoded data symbols to multiple UEs such that desired signals overlap coherently and the interference is partially canceled out. First, CoMP transmission requires knowledge on the compound channel matrix, i.e. multi-cell CSIT, between all UEs and BSs involved in the coherent downlink transmission, in order to obtain the spatial precoding weights. Second, we initially assume that both the multi-cell CSIT as well as the scheduled data bits to be transmitted to the UEs are distributed to all involved BSs, refer to Figure 5.1. The assumption of sharing scheduled user data will be alleviated in Section 6.2.3.

We derive a solution to efficiently merge linear receive antenna combining and distributed MIMO signal processing. Therefore, we propose a practical unified feedback scheme for the required CSIT. The effective multi-cell channel seen after linear receiver processing is fed back and distributed within the cluster. Thus, each terminal can be treated as a single-antenna receiver. The user-specific CSI feedback can be based on an eigenmode-aware receive combining (ERC) or eigenmode-aware optimum combining (EOC), in order to strengthen the desired signal from the cluster or even suppress non-coordinated CCI. This allows distributed MIMO pre-processing

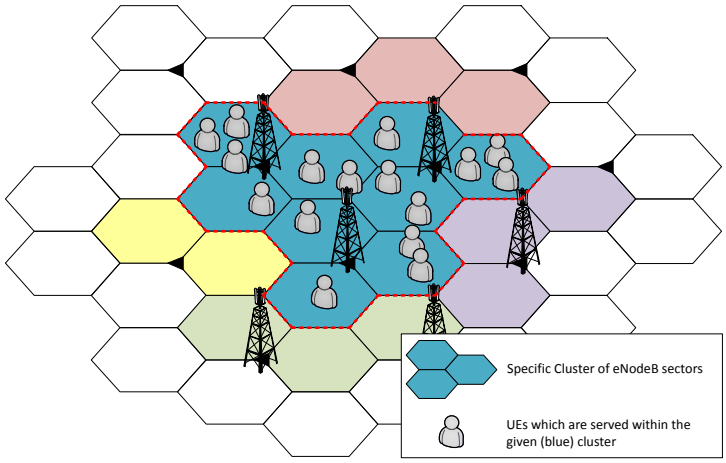

Figure 5.1: Coherent transmission in a cluster of collaborative base stations.

at each base station belonging to a specific cluster and makes the implementation of downlink coordinated multi-point transmission feasible. Subsequent application of advanced receivers such as OC [Win84] helps to reduce effects of system impairments, refer to Section 6.4. The overlap of multiple clusters can be treated in frequency domain. In this work, we consider coherent ZF beamforming and demonstrate the achievable system gains as a function of the cluster size and the accuracy of CSI. Furthermore, we show that significant gains can already be realized within a small cluster. The different concepts are evaluated in a cellular scenario, taking realistic multi-cell channel modeling into account.

The subsequent chapter is organized as follows: In Section 5.1, we introduce an extended system model which covers the algorithms described in this work. As a consecutive step, we introduce concepts to alleviate the major drawbacks related to joint transmission e.g., its higher complexity, increased backhaul and signaling overhead. Those concepts cover linear precoding techniques and a greedy *user selection* process, where details are given in Section 6.3 and *clustering* solutions from Section 6.2. The clustering can be carried out statically or dynamically and restrict joint processing techniques to a limited number of base stations. Moreover, the cluster formation may be performed and optimized by a central entity (*network-centric*), or in a per-user way (*user-centric*). In particular, Section 5.2 introduces a concept for a two-step transceiver optimization and a unified CSI feedback framework to cope with different user-specific types of channel feedback. Finally, we summarize a system concept where each terminal provides channel feedback to its serving base station only; the base stations in the same cluster exchange the channel feedback and payload data in order to determine the precoding weights and perform the spatial precoding, both in a distributed manner.

5.1 System Model for Coordinated Multi-Point

For the use of joint transmission (JT) CoMP in practice the overhead for pilots, feedback and backhaul has to be kept within reasonable limits. The most efficient way to reduce overhead is to limit the cooperation area. Hence, we focus on a realistic size of the clusters ranging from 3 up to 10 BS sectors, Figure 5.1, where joint processing is only allowed between BSs belonging to the same cluster. BSs outside the cluster are not coordinated and thus cause residual inter-cluster interference. Furthermore, dynamic clustering allows a more efficient power allocation. Mobile users experiencing a weak channel to a given cluster are assigned to another BS cluster.

The general system model from (2.2) can be easily extended to the case of linear precoding, in which the transmitted signal is a spatially multiplexed, linear combination of the users' data signals. Thus, we write $\mathbf{s}_{c,k} = \mathbf{b}_{c,k}\sqrt{p_{c,k}}\, x_{c,k}$, where $\mathbf{b}_{c,k} \in \mathbb{C}^{[M_c N_t \times 1]}$ is the involved precoding vector. We consider a cellular OFDM downlink where a central site is surrounded by multiple tiers of sites. We assume each site to be partitioned into three 120° sectors, i.e. a set $\mathcal{M}$ consisting of $M = |\mathcal{M}|$ sectors in total. Each sector constitutes a cell, and frequency resources are fully reused in all M cells. $\mathcal{M}_c$ represents the set of cells included in a given cluster and $M_c = |\mathcal{M}_c|$ denotes its size. At this stage, we assume disjoint clusters, i.e. a given BS cannot belong to more than one cluster operated at the same time/frequency resource. For OFDM systems, the overlap of multiple clusters can be achieved conveniently in the frequency domain.

Each cluster selects a set of active users $\mathcal{K}_c$ following a specific scheduling metric. In the c-th cluster, there are M_c BSs, each one equipped with N_t transmit antennas, while the $K_c = |\mathcal{K}_c|$ users are equipped each with N_r receive antennas. The users inside the cluster are served by signals jointly emitted from $M_c N_t$ transmit antennas, where $M_c \cdot N_t \geq K_c \cdot N_r$. The $M_c N_t \times M_c N_t$ precoding matrix $\mathbf{B}_c = [\mathbf{B}_{c,1} \cdots \mathbf{B}_{c,K_c}]$ contains the precoders $\mathbf{B}_{c,k}$ designed for each of the users. Note, each UE might receive multiple spatial layers at the same time, i.e. $\mathbf{B}_{c,k}$ is of dimension $M_c N_t \times |\mathcal{T}_{s,k}|$, where $\mathcal{T}_{s,k}$ denotes the set of spatial layers selected for instantaneous downlink service at user k. The maximum number of entries in this set is limited by the number of receive antennas, i.e. $|\mathcal{T}_{s,k}| \leq N_r$. The set $\mathcal{T}_s$ combines all selected spatial layers for SDMA service of the UEs in $\mathcal{K}_c$.

For further analysis, we assume the c-th cluster is surrounded by $M - M_c$ BSs evoking non-coordinated CCI. Thus, the received downlink signal $\mathbf{y}_{k,t}$ for $t \in \mathcal{T}_{s,k} \subset \mathcal{T}_s$ at user k in the cellular environment is given by

$$\mathbf{y}_{k,t} = \underbrace{\mathbf{H}_{c,k}\left[\mathbf{B}_{c,k}\right]_{:,t}\sqrt{p_{c,t}}x_{c,t}}_{\overline{\mathbf{h}}_{k,t}} + \underbrace{\sum_{j\in\mathcal{T}_s\setminus\{t\}}\mathbf{H}_{c,k}\left[\mathbf{B}_{c}\right]_{:,j}\sqrt{p_{c,j}}x_{c,j}}_{\boldsymbol{\vartheta}_{k,t}} + \underbrace{\sum_{m\in\mathcal{M}\setminus\mathcal{M}_c}\sum_{j=1}^{N_t}\mathbf{H}_{m,k}\left[\mathbf{B}_{m}\right]_{:,j}\sqrt{p_{m,j}}x_{m,j}+\mathbf{n}}_{\mathbf{z}_k} \tag{5.1}$$

$[\mathbf{B}_{c,k}]_{:,t}$ denotes the t-th column element in the global precoding matrix $\mathbf{B}_c$, where $\mathbf{B}_{c,k}$ correspond to the column elements designed for user k. The desired t-th data stream is distorted by the intra-cluster and inter-cluster interference plus noise aggregated in $\boldsymbol{\vartheta}_{k,t}$ and $\mathbf{z}_k$, respectively. $\mathbf{H}_{c,k}$ spans the $N_r \times M_c N_t$ channel matrix for user k formed by the c-th cluster and $p_{c,t}$ is its power allocation valid for the t-th data stream. Thus, $\boldsymbol{\vartheta}_{k,t}$ denotes the interference generated within the cluster.[1] The $N_r \times 1$ vector $\mathbf{n}$ denotes the AWGN samples with covariance $\mathbb{E}\left\{\mathbf{n}\mathbf{n}^H\right\} = \mathbf{I}\sigma_n^2$. The noise power consists of the receiver noise figure and the thermal noise power.
The achievable SINR is estimated at each UE, according to

$$\mathrm{SINR}_{k,t} = \frac{\left|\mathbf{w}_{k,t}^H\mathbf{H}_{c,k}\left[\mathbf{B}_{c,k}\right]_{:,t}\sqrt{p_{c,t}}\right|^2}{\sum\limits_{j\in\mathcal{T}_s\setminus\{t\}}\left|\mathbf{w}_{k,t}^H\mathbf{H}_{c,k}\left[\mathbf{B}_{c}\right]_{:,j}\sqrt{p_{c,j}}\right|^2 + \mathbf{w}_{k,t}^H\left[\mathbf{z}_k\mathbf{z}_k^H\right]\mathbf{w}_{k,t}}, \tag{5.2}$$

with $\mathbf{w}_{k,t}$ being the combining weights at the k-th receiver and for data stream t.

5.2 Two-Step Transceiver Optimization

In the following, we describe a CoMP scheme using joint transmission (JT) of user data, which uses a centralized architecture.[2] However, optimization of receive and transmit beamforming is carried out in two consecutive steps. Once CSI feedback is available at all BSs in $\mathcal{M}_c$, algorithms can easily be implemented in a distributed manner, which reduces the computational burden per BS. For cellular deployments, the joint precoding algorithm has to be independent from the signal processing strategies at each user equipment. In particular, receive antenna processing for $N_r > 1$, enables us to combine single- as well as multi-antenna terminals in the CoMP downlink. Therefore, we introduce an unified CSI reporting, which is based on the

[1] Note, under ideal conditions and a ZF precoding constraint $\left|\mathbf{w}_{k,t}^H\boldsymbol{\vartheta}_{k,t}\right| = 0$.
[2] The whole CSI data is available in all BSs within the cluster.

effective multiple-input single-output (MISO) channel principle [BH07b, TBH08b, TWH+09].

According to Figure 5.2, the process is split into three phases:

1. *Phase I: User-Assisted Feedback Generation (Sections 5.2.1-5.2.2).*
   Each user performs a cluster-wide channel estimation using appropriate pilot tones. According to Section 5.2.2, each UE generates MISO-CSI (5.8) and feeds back this information in conjunction with the expected post-equalization SINR (5.2). Therefore, terminals will not consider any intra-cluster interference since this interference will be removed by the joint precoder. In particular, the achievable SINR (5.4) together with the CSI (5.8) is then conveyed to the serving BS.

2. *Phase II: Distributed precoder calculation (Sections 5.2.3-5.2.4).*
   A scheduling instance in the cluster combines a total number of $M_c N_t \leq |\mathcal{T}_s|$ MISO channels to a compound MIMO channel matrix.[3] A proper user selection plays an important role to prevent grouping UEs with strongly correlated MIMO channels. Different user grouping strategies will be addressed in Section 6.3. In the following, each BS is responsible for a specific sub-band of the overall bandwidth where CoMP JT is employed. Therefore, BSs partially exchange their collected CSI and determine the linear precoder for their specified sub-bands but for all $M_c N_t$ antennas of the cluster. Afterwards, BSs exchange their precoding weights $\mathbf{B}_c$ and power allocation $\mathbf{P}_c$, both obtained per sub-band, as well as the complete user (payload) data. Therefore, BSs use logical interconnections, e.g. the X2 interface in LTE-A. Finally, all BSs in the c-th cluster perform the coherently precoded downlink transmission, where each BS is using the weights corresponding to its own transmit antennas.

3. *Phase III: "Intra-cluster-interference-free" data reception at the terminal side.*
   In this step, each UE performs its own preferred spatial equalization strategy $\mathbf{w}_{k,t}$. Therefore, each user may select the same weights as used in *Phase I* or may perform the equalization using the optimal linear receive combining given in (2.6) and known as OC [Win84]. The post-equalization SINR is determined by (5.2) and is used as inputs for the link adaptation. In this work, we simply map the SINRs to Shannon information rates with a certain gap and cut-off rate.

5.2.1 Phase I: CQI Feedback

In *Phase I*, each UE selects its desired receive processing weights $\mathbf{\Upsilon}_k = \left[\boldsymbol{\upsilon}_{k,1} \ldots \boldsymbol{\upsilon}_{k,|\mathcal{T}_k|}\right]$ in order to decompose the MIMO channel into a set of $\mathcal{T}_k$ MISO channels. For fur-

[3] With a proper user selection, the mandatory full rank condition of the compound channel matrix can be frequently met in the multi-point-to-multi-point channel with independent links [ZD04, JJT+09].

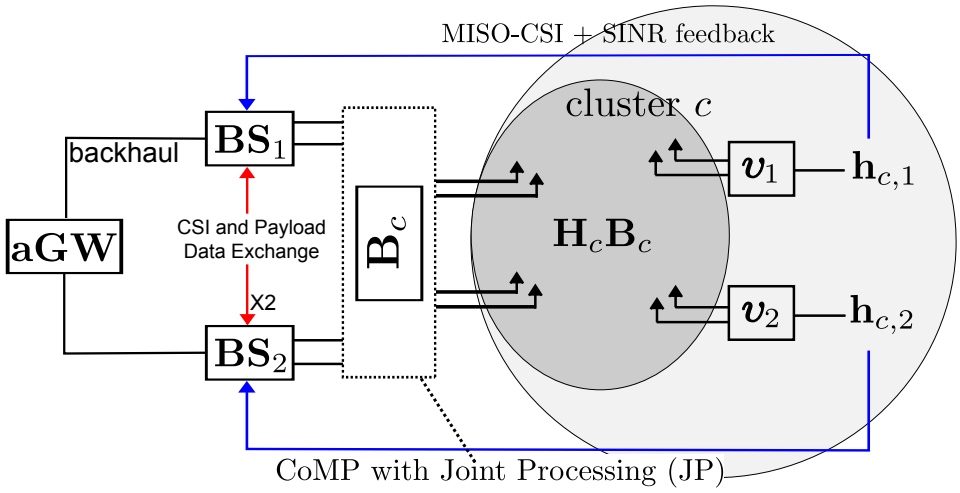

Figure 5.2: True and effective multi-cell channel. The precoder $\mathbf{B}_c = \left[\left([\mathbf{B}_c]_{1:N_t,:}\right)^T \left([\mathbf{B}_c]_{1+N_t:2N_t,:}\right)^T\right]^T$ for coherent joint transmission can be calculated distributively, while each BS uses the rows corresponding to its own antennas.

ther details refer to Section 5.2.2 and (5.8). The selected receive strategy also affects the achievable SINR per data stream after equalization. According to Section 2.3, the post-equalizaion SINR is mainly influenced by the receive strategy, where each strategy assumes a certain degree of channel and interference knowledge.

Starting from (5.2), each UE k has to initially assume a couple of variables, which are unknown at this stage. These variables are:

1. The precoder for user k and data stream t, i.e. $[\mathbf{B}_{c,k}]_{:,t}$.
2. Its power allocation $\sqrt{p_{c,t}}$.
3. The precoders for all other data streams $[\mathbf{B}_c]_{:,j}$ inside the cluster c, i.e. $j \in \mathcal{T}_{s,k} \setminus \{t\}$ and the corresponding power allocation $\sqrt{p_{c,j}}$.
4. The received inter-cluster interference covariance matrix.

In general, if we assume that the UEs provide CSI feedback using a specific decomposition strategy $\boldsymbol{\Upsilon}_k$, then this leads to intra-cluster interference free transmission under a ZF precoding constraint as long as the transceiver chain remains static. This can be ensured if the UEs utilize the same decomposition weights for equalization, i.e. SINR estimation. In particular, let us assume that the decomposed channel is given by $\hat{\mathbf{H}}_k = \boldsymbol{\Upsilon}_k^H \mathbf{H}_{c,k}$, details are given in Section 5.2.2.[4]

[4]Note, at this stage we drop the influence of any kind of impairments.

Hence, the k-th terminal uses the same weights for SINR estimation in *Phase I*. Furthermore, it has to assume an initial power allocation $\widehat{p}_{c,t}$, a precoder according to

$$\left[\widehat{\mathbf{B}}_{c,k}\right]_{:,t} = \left[\left[\hat{\mathbf{H}}_k\right]_{t,:}\right]^H / \left\|\left[\hat{\mathbf{H}}_k\right]_{t,:}\right\|_2 \tag{5.3}$$

and no intra-cluster interference.
Thus, the SINR from (5.2) simplifies to

$$\begin{aligned}
\mathrm{SINR}_{k,t}^{(I)} &= \frac{\hat{p}_{c,t}\left|\boldsymbol{\upsilon}_{k,t}^H \mathbf{H}_{c,k}\left[\hat{\mathbf{B}}_{c,k}\right]_{:,t}\right|^2}{\boldsymbol{\upsilon}_{k,t}^H\Bigg[\underbrace{\sum_{j\in\mathcal{T}_s\setminus\{t\}}\left(p_{c,j}\mathbf{H}_{c,k}\left[\mathbf{B}_c\right]_{:,j}\left(\mathbf{H}_{c,k}\left[\mathbf{B}_c\right]_{:,j}\right)^H\right)}_{\boldsymbol{\vartheta}_{k,t},\text{ where }\boldsymbol{\upsilon}_{k,t}^H\boldsymbol{\vartheta}_{k,t}\boldsymbol{\upsilon}_{k,t}=0} + \left[\mathbf{z}_k\mathbf{z}_k^H\right]\Bigg]\boldsymbol{\upsilon}_{k,t}} \\
&= \frac{\hat{p}_{c,t}\left|\left[\hat{\mathbf{H}}_k\right]_{t,:}\left[\hat{\mathbf{B}}_{c,k}\right]_{:,t}\right|^2}{\boldsymbol{\upsilon}_{k,t}^H\mathbf{Z}_k\boldsymbol{\upsilon}_{k,t}} \\
&= \frac{\hat{p}_{c,t}}{\left\|\left[\hat{\mathbf{H}}_k\right]_{t,:}\right\|_2^2}\cdot\frac{\left|\left[\hat{\mathbf{H}}_k\right]_{t,:}\left[\left[\hat{\mathbf{H}}_k\right]_{t,:}\right]^H\right|^2}{\boldsymbol{\upsilon}_{k,t}^H\mathbf{Z}_k\boldsymbol{\upsilon}_{k,t}}
\end{aligned} \tag{5.4}$$

As long as the terminal does not change its receiver weights for *Phase III*, the $\mathrm{SINR}_{k,t}^{(I)}$ provides a relatively robust expectation value of $\mathrm{SINR}_{k,t}^{(III)}$. Assuming further, that the received covariance matrix of the inter-cluster interference remains constant[5], both SINRs differ by a simple scaling factor taking into account the correct power allocation $p_{c,t}$ and the correct precoder $[\mathbf{B}_{c,k}]_{:,t}$. Note, the BSs can simply rescale SINRs in order to perform the correct link adaptation, user selection and final power allocation. This issue will be addressed in Section 5.2.5.

In *Phase III*, each UE may use its stored equalization weights from *Phase I*, i.e. $\boldsymbol{\upsilon}_{k,t}$. However, it may be beneficial to deviate from these weights and to utilize new weights which are obtained by the OC technique [Win84]. In theory, this will maximize the achievable post-equalization SINR at the UE. In practice, we know that the performance of OC significantly depends on the available degree of interference knowledge, refer to Section 4.1. Nevertheless, a time and frequency selective fading channel will always cause channel aging effects within a certain time duration. Assuming a continuous channel estimation leads to refreshed cluster-wide CSI at the receiver. Utilizing this knowledge in the equalization phase enables each UE to follow the aged channel condition and thus maintains the ZF precoding constraint to a certain degree, refer to Section 6.4.

[5] Which is the case, if other cells use LTE codebooks without changing the precoding matrices from *Phase I* to *Phase III*.

Note, impairments such as channel estimation errors, feedback delays and mobility are user-specific properties. Let us define a matrix $\boldsymbol{\Delta}_k$ which destroys the orthogonality of the precoded channel $\boldsymbol{\upsilon}_{k,t}^H \mathbf{H}_{c,k} \boldsymbol{\Delta}_k \left[\mathbf{B}_{c,k}\right]_{:,t}$ for the k-th UE, and does not effect other users. In case of rather small impairments, we may assume $\boldsymbol{\Delta}_k \approx \mathbf{I}$. Section 6.4 provides an in-depth study of these effects in cellular CoMP transmission systems using computer simulations.

For notational reasons, $\mathbf{w}_{k,t}$ denotes the equalizer in *Phase III*. The OC is a generalized version of the well-known MMSE receiver with perfect knowledge of the co-channel interference (CCI)[6], induced by the surrounding BSs in the system operating with full frequency reuse factor. The interference-aware OC receiver is given by

$$\mathbf{w}_{k,t}^{\mathrm{OC}} = p_{c,t} \mathbf{R}_{yy}^{-1} \mathbf{H}_{c,k} \left[\mathbf{B}_{c,k}\right]_{:,t} \tag{5.5}$$

where $\mathbf{R}_{yy}$ denotes the received covariance matrix of the received signal $\mathbf{y}_{k,t}$, i.e.

$$\mathbf{R}_{yy} = \mathbb{E}\left\{\mathbf{y}^m \left(\mathbf{y}^m\right)^H\right\} = \mathbf{Z}_{k,t} + \mathbf{H}_{c,k} \left[\mathbf{B}_{c,k}\right]_{:,t} \left[\mathbf{B}_{c,k}\right]_{:,t}^H \mathbf{H}_{c,k}^H \tag{5.6}$$

and $\mathbf{Z}_{k,t} = \boldsymbol{\Theta}_{k,t} + \mathbf{Z}_k$, where $\boldsymbol{\Theta}_{k,t}$ and $\mathbf{Z}_k$ are the received covariance matrices of the interfering signals aggregated in $\boldsymbol{\vartheta}_{k,t}$ and $\mathbf{z}_k$, i.e. $\boldsymbol{\Theta}_{k,t} = \boldsymbol{\vartheta}_{k,t} \boldsymbol{\vartheta}_{k,t}^H$ and $\mathbf{Z}_k = \mathbf{z}_k \mathbf{z}_k^H$.

As shown in [SB04], the OC receiver yields a post-equalization SINR

$$\mathrm{SINR}_{k,t}^{\mathrm{OC}} = p_{c,t} \left[\mathbf{B}_{c,k}\right]_{:,t}^H \mathbf{H}_{c,k}^H \mathbf{Z}_{k,t}^{-1} \mathbf{H}_{c,k} \left[\mathbf{B}_{c,k}\right]_{:,t}. \tag{5.7}$$

5.2.2 Phase I: CSI Feedback

From [YR06] we know that each UE is most likely to select a beamforming strategy which effectively reduces its receive antennas to a single-dimension. Thus, we consider each UE k to provide feedback for a set $\mathcal{T}_k$ MISO channels combined in the matrix $\hat{\mathbf{H}}_k$ effectively seen through an appropriate receive filters $\boldsymbol{\Upsilon}_k$ according to

$$\hat{\mathbf{H}}_k = \boldsymbol{\Upsilon}_k^H \mathbf{H}_{c,k} \tag{5.8}$$

where $\boldsymbol{\Upsilon}_k = \left[\boldsymbol{\upsilon}_{k,1} \ldots \boldsymbol{\upsilon}_{k,|\mathcal{T}_k|}\right]$ and the Euclidean norm per column equals $\|\boldsymbol{\upsilon}_{k,i}\|_2 = 1$. Note, at this stage we drop the cluster index c in $\hat{\mathbf{H}}_k$ for simplicity. Besides, we use $\boldsymbol{\upsilon}_k$ to denote the linear combining scheme to generate MISO CSI feedback.

According to Section 5.1, we will concentrate on linear precoding strategies. One class of linear precoding techniques for the case of a single-antenna receiver is based on zero-forcing [BTC06, YG06, DS05, PHS05], where each user receives only its desired signal free from any additional intra-cluster interference $\boldsymbol{\vartheta}_{k,t}$. Since the number of spatial channels which are formed using linear beamforming is limited by the number of transmit antennas, the transmitter selects a set of active users for receiving data. This user selection could be done optimally using a brute-force search over all

[6] Either full knowledge, i.e. spatial structure, or partial knowledge, i.e. power of the inter-cluster interference may be considered

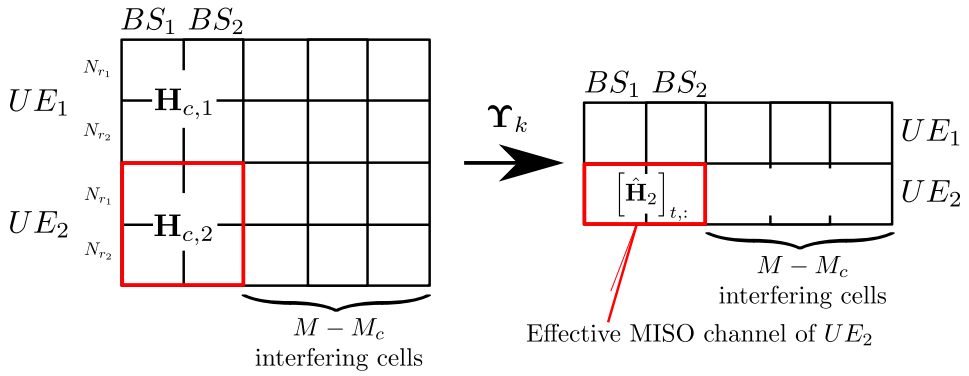

Figure 5.3: Transforming a MIMO channel into a set of effective MISO channels. This information is fed back and used as CSI at the BS side.

possible combinations of users, but due to the high complexity when the number of users is large, sub-optimal techniques based on a greedy algorithm has been shown to provide near-optimum performance [DS05, BH06]. This topic is studied in detail in Section 6.3. Extensions of the zero-forcing technique to the case of multiple receive antennas appear in [VVH03, CM04, SSH04], where multiple spatial streams (or eigenmodes) are transmitted to each user with no inter-user interference, resulting in a block-diagonal covariance matrix.

The Multi-User Eigenmode Principle

An extension of the block diagonalization (BD) concept, called multi-user eigenmode transmission (MET), was proposed in [BH07b, BHT07, TBH08a] and uses a linear transmission strategy based on zero-forcing beamforming for maximizing the weighted sum rate. On a frame-by-frame basis, MET distributes up to $M_c N_t$ spatially multiplexed streams for one or multiple users. MET was initially proposed for MU-MIMO transmission [BH07b] and was later utilized to cover the CoMP case [TWH+09]. According to the concept in [BH07b, NMK+07], the UEs are assumed to use linear receive filters $\boldsymbol{\upsilon}_k$ to transform their MIMO channel into an effective MISO channel. In essence, each user is assumed to multiply its channel matrix $\mathbf{H}_{c,k} = \mathbf{U}_{c,k}\boldsymbol{\Sigma}_{c,k}\mathbf{V}_{c,k}^H$ with a set $\mathcal{T}_k$ of Hermitian left dominant eigenvectors (5.9), i.e. the column vectors $[\mathbf{U}_{c,k}]_{:,t}$ included in $\mathbf{U}_{c,k}$ which correspond to the $|\mathcal{T}_k|$ strongest Eigenvalues in $\boldsymbol{\Sigma}_{c,k}$, i.e. $\boldsymbol{\Upsilon}_k = \left[[\mathbf{U}_{c,k}]_{:,1} \dots [\mathbf{U}_{c,k}]_{:,|\mathcal{T}_k|}\right]$.

$$\begin{aligned} \left[\hat{\mathbf{H}}_k\right]_{t,:} &= [\mathbf{U}_{c,k}]_{:,t}^H \mathbf{H}_{c,k} \\ &= [\mathbf{U}_{c,k}]_{:,t}^H \mathbf{U}_{c,k}\boldsymbol{\Sigma}_{c,k}\mathbf{V}_{c,k}^H = [\boldsymbol{\Sigma}_{c,k}]_{t,t}[\mathbf{V}_{c,k}]_{:,t}^H \end{aligned} \tag{5.9}$$

The scheme maximizes the signal power transfered from the collaborative BSs to the specific UE by using the dominant channel direction experienced by the receiver.

The maximum received power would be achieved, if the precoder and receive filters are selected according to the right and left hand side matrices containing the corresponding eigenvectors $[\mathbf{V}_{c,k}]_{:,t}$ and $[\mathbf{U}_{c,k}]_{:,t}^{H}$, respectively. However, the t-th precoder obtained from *Phase II* significantly depends on the selected set of active users $\mathcal{K}_c$. In practice, the performance for the k-th user will be inferior. Thus, multiple UEs should be grouped preferably so that their effective channels $\hat{\mathbf{H}}_k$ show highest orthogonality, refer to Section 6.3. In general, appropriate user grouping keeps the costs in terms of a reduced received power after channel aware precoding as small as possible [BHT07, TBT07, TSW+09]. The k-th user estimates the following SINR in terms of *Phase I*

$$\mathrm{SINR}_{k,t}^{(I,MET)} = \frac{\sigma_{c,t}^2 \widehat{p}_{c,t}}{[\mathbf{U}_{c,k}]_{:,t}^{H} \mathbf{Z}_k [\mathbf{U}_{c,k}]_{:,t}} \tag{5.10}$$

Figure 5.4 depicts the spatial structure for different receive beamformers as well as the post-equalization signal-to-interference ratios (SIRs) per user after ZF precoding. Let us consider 3 random UE positions in sector 1, while sectors 6 and 8 cause additional inter-cell interference. The UEs decompose the MIMO channel according to the MET principle into a MISO channel and convey this CSI feedback to the BS. In particular, Figures 5.4(a) and 5.4(b) depict the directivity patterns $\Omega(\xi)$ of receive beamformers taking the array response $\mathbf{a}(\xi)$ into account

$$\Omega(\xi) = \left| \boldsymbol{\upsilon}_k^H \mathbf{a}(\xi) \right|^2 = \left| \boldsymbol{\upsilon}_k^H \left[1 \; \mathrm{e}^{-j2\pi d \sin\xi} \; \ldots \; \mathrm{e}^{-j2\pi(N_r-1)d\sin\xi} \right]^T \right|^2 \tag{5.11}$$

where $\xi \in [-\pi, \pi]$ is the azimuth angle and d is the element spacing of the uniform linear array (ULA) in wavelength. In order to allow comparability of the directivity at different SNR regimes, we normalize all patterns to the isotropic radiator, i.e. $\sum_{\forall \xi} \Omega(\xi) = 1$. Note, this plot visualizes the gains in directivity for the different azimuth angles ξ. The area inside the beam shapes does not represent the cumulative received power. The black and grey directivity patterns for UEs 1, 2 and 3 depict the receive beamformer using MET, i.e. $[\mathbf{U}_{c,k}]_{:,t}$, while the green and red shapes show the receive beamformer with respect to the dominant eigenmode of interfering sectors with cell-ids 6 and 8. Hence, green and red beam shapes indicate the main direction of inter-cell interference.

Figure 5.4(c) shows the instantaneous post-equalization SIRs per UE taking the CCI from cells 6 and 8 into account. Cells with ids 3, 2, 21 and 5 are not active! Recall, each multi-antenna UE can use OC filters [Win84] to determine the optimal receive weights for signal equalization, i.e. $\mathbf{w}_{k,t}$ can be selected according to (5.5). A change in the equalization filter with respect to the combiner $\boldsymbol{\upsilon}_{k,t}$ chosen for the CSI generation in *Phase I*, causes a partially destroyed orthogonality between data streams within the cluster. However, the OC receiver determines the optimal linear receiver weights, while considering upcoming intra-cluster interference and suppression of inter-cluster interference.

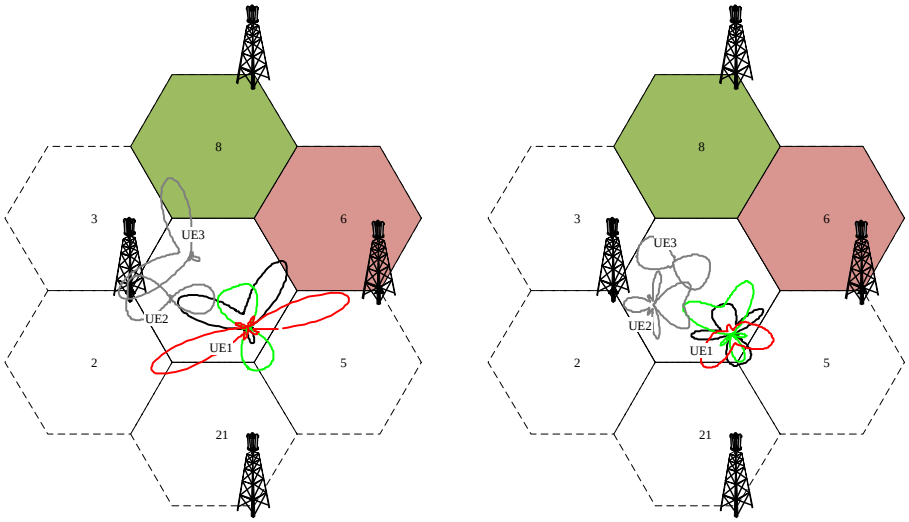

(a) Line-of-Sight, $k = 10$ dB.

(b) Line-of-Sight, $k = 0$ dB.

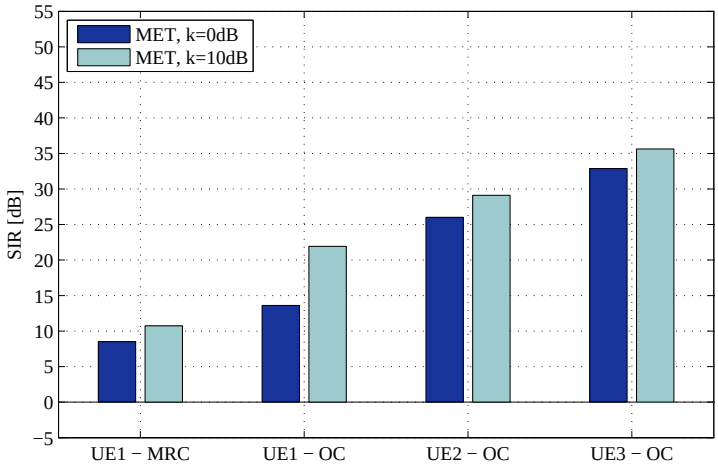

(c) Instantaneous user SIRs.

Figure 5.4: Top: Azimuth receive beamformer in LOS channel with different Ricean k-factor, $N_r = 4$ and an element spacing of $d = 0.5\lambda$. Bottom: Instantaneous post-equalization SIRs per UE taking the CCI from cells 6 and 8 into account.

Eigenmode-Aware Optimum Combining (EOC)

In general, if the receiver has sufficient knowledge on the inter-cluster interference, it will be possible to include this information already in the CSI. Hence, we can merge OC into the MET feedback [TBH08b, TWH+09]. We denote this type of CSI feedback provisioning as eigenmode-aware optimum combining (EOC). The details are discussed below.

Consider an isolated set of $M_c N_t$ coordinated antennas combined in a cluster of BSs. In this isolated scenario, the MET feedback concept is very promising. Each user will be served on a beam closest to its individual dominant eigenmode providing maximum received power for the specific user, while forcing the inter-user interference to be zero. However, in a cellular network this cluster is always surrounded by non-coordinated BSs causing inter-cluster interference. Thus, the main target is slightly different: Assuming the UE is aware of the spatial structure of the received inter-cluster interference covariance matrix $\mathbf{Z}_k$, it is beneficial to use the spatial degrees of freedom at the UEs to combat CCI while selecting a channel direction which provides high received power for the desired signal. Thus, we suggest to extend the MET concept with an OC method. The effective channel is given by

$$\left[\hat{\mathbf{H}}_k\right]_{t,:} = \left[\boldsymbol{\upsilon}_{k,t}^{\mathrm{EOC}}\right]^H \mathbf{H}_{c,k}. \tag{5.12}$$

The UE reports the effective MISO channel $\left[\hat{\mathbf{H}}_k\right]_{t,:}$ observed after the linear EOC filter. Since the precoder in the cluster already mitigates the intra-cluster interference, there is no reason to include it into the OC. Thus, the transmitter is serving the users on orthogonal beams and each receiver is able to combat the residual CCI from the surrounding cells through

$$\boldsymbol{\upsilon}_{k,t}^{\mathrm{EOC}} = \gamma \, p_{c,t} \mathbf{Z}_k^{-1} \left[\mathbf{U}_{c,k}\right]_{:,t}. \tag{5.13}$$

Each user is assumed to be served on a precoded downlink channel with

$$\begin{aligned} \mathbf{H}_{c,k} \left[\mathbf{B}_{c,k}\right]_{:,t} &= \mathbf{H}_{c,k} \frac{\left[\hat{\mathbf{H}}_k\right]_{t,:}^H}{\left\| \left[\hat{\mathbf{H}}_k\right]_{t,:} \right\|_2} \\ &= \frac{1}{\left\| \left[\mathbf{U}_{c,k}\right]_{:,t}^H \mathbf{Z}_k^{-1} \mathbf{H}_{c,k} \right\|_2} \mathbf{H}_{c,k} \mathbf{H}_{c,k}^H \mathbf{Z}_k^{-1} \left[\mathbf{U}_{c,k}\right]_{:,t} \end{aligned} \tag{5.14}$$

Thus, the k-th user would estimate the following SINR in *Phase I*:

$$\begin{aligned}\mathrm{SINR}_{k,t}^{(I,EOC)} &= \frac{\widehat{p}_{c,t}}{\left\|\left(\boldsymbol{\upsilon}_{k,t}^{\mathrm{EOC}}\right)^H \mathbf{H}_{c,k}\right\|_2^2} \frac{\left|\left(\boldsymbol{\upsilon}_{k,t}^{\mathrm{EOC}}\right)^H \mathbf{H}_{c,k}\mathbf{H}_{c,k}^H \boldsymbol{\upsilon}_{k,t}^{\mathrm{EOC}}\right|^2}{\left(\boldsymbol{\upsilon}_{k,t}^{\mathrm{EOC}}\right)^H \mathbf{Z}_k \boldsymbol{\upsilon}_{k,t}^{\mathrm{EOC}}} \\ &= \frac{\widehat{p}_{c,t}\left|[\mathbf{U}_{c,k}]_{:,t}^H \mathbf{Z}_k^{-1}\mathbf{H}_{c,k}\mathbf{H}_{c,k}^H\mathbf{Z}_k^{-1}[\mathbf{U}_{c,k}]_{:,t}\right|^2}{\left\|[\mathbf{U}_{c,k}]_{:,t}^H \mathbf{Z}_k^{-1}\mathbf{H}_{c,k}\right\|_2^2 [\mathbf{U}_{c,k}]_{:,t}^H \mathbf{Z}_k^{-1}[\mathbf{U}_{c,k}]_{:,t}}. \end{aligned} \quad (5.15)$$

The main advantage is, that the projection of external interference into this spatial filter is known at the receiver and influences the selection of $\boldsymbol{\upsilon}_{k,t}^{EOC}$ such that the achievable SINR is maximized. Under ideal precoding conditions[7], the final SINR can be fully recovered at the BS based on the $\mathrm{SINR}_{k,t}^{(I,EOC)}$ from (5.15) which was reported from the UE while assuming an initial power allocation $\widehat{p}_{c,t}$. Section 5.2.5 describes the process of link adaptation at the BS which is based on the feedback of Phase I.

Figure 5.5 depicts the receive beamformers for EOC as well as the post-equalization SIRs per user after ZF precoding. In order to indicate the direction of received inter-cell interference, we include receive beamformer belonging to the dominant eigenmode of interfering sectors associated with cell-ids 6 and 8 as red and green beam shapes. In contrast to Figure 5.4(a), the diagrams clearly show a directional null which is aligned with the LOS connection to cell-id 6. The instantaneous SIRs in Figure 5.5(c) can significantly be improved for UEs 2 and 3 in strong LOS condition with a Ricean k-factor of $k = 10$ dB. In case of multi-path propagation the gain compared to MET decomposition is in the order of a couple dB. In the end of this section, we will provide a statistical comparison of post-equalization SIRs.

Receive Antenna Selection

As a next step, we consider a simple setup where UEs are equipped with a single receive antenna or in case of $N_r > 1$ terminals will use a simple receive antenna selection approach. Thus, the feedback information is given by

$$\left[\hat{\mathbf{H}}_k\right]_{t,:} = \left[\boldsymbol{\upsilon}_{k,t}^{\mathrm{Rx}}\right]^H \mathbf{H}_{c,k} \quad (5.16)$$

where $\boldsymbol{\upsilon}_{k,t}^{\mathrm{Rx}}$ is the t-th column element chosen from $\boldsymbol{\Upsilon}_k^{\mathrm{Rx}} = \mathbf{I}$ such that it maximizes the received power from $\mathbf{H}_{c,k}$

$$\boldsymbol{\upsilon}_{k,t}^{\mathrm{Rx}} = \underset{t=\{1\ldots N_r\}}{\arg\max} \left|\left[\hat{\mathbf{H}}_k\right]_{t,:}\right|^2. \quad (5.17)$$

[7] I.e. not considering any impairments such as channel estimation or channel aging.

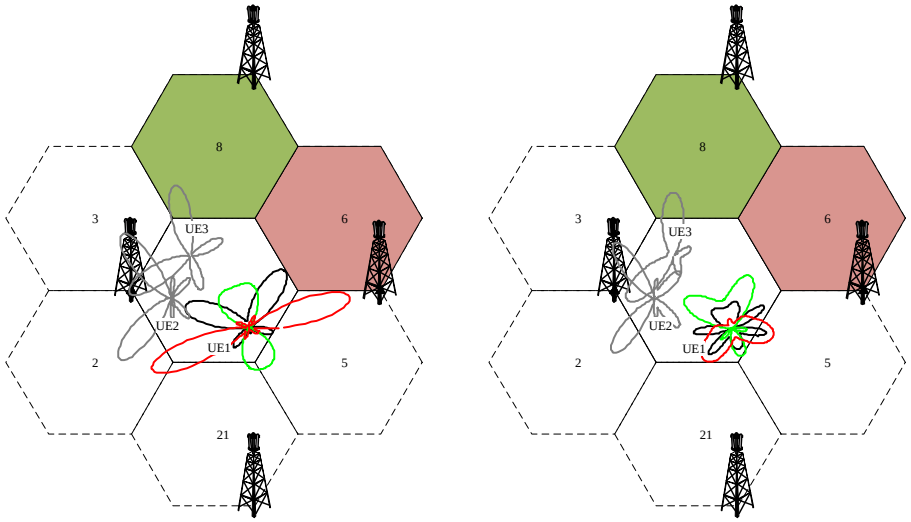

(a) Line-of-Sight, $k = 10$ dB.

(b) Line-of-Sight, $k = 0$ dB.

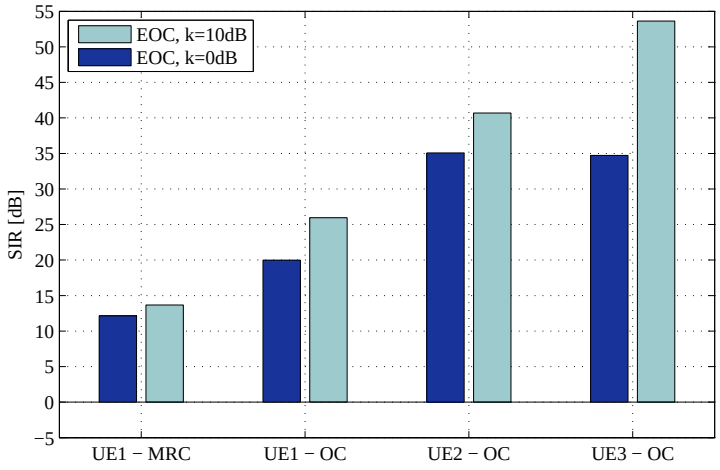

(c) Instantaneous user SIRs.

Figure 5.5: Top: Receive beamformer for EOC in LOS channel with different Ricean k-factor, $N_r = 4$ and an element spacing of $d = 0.5\lambda$. Bottom: Instantaneous post-equalization SIRs per UE taking the CCI from cells 6 and 8 into account.

In this case the receiver benefits from antenna selection diversity [WSG94]. However, UEs cannot utilize their degrees of freedom to enable any kind of receive beamforming gains in order to improve or even maximize their link SINR, as e.g. possible with MET or EOC.

$$\mathrm{SINR}_{k,t}^{(I,Rx)} = \frac{\widehat{p}_{c,t}\left|\left[\mathbf{H}_{c,k}\right]_{t,:}\right|^2}{\left[\boldsymbol{v}_{k,t}^{\mathrm{Rx}}\right]^H \mathbf{Z}_k \boldsymbol{v}_{k,t}^{\mathrm{Rx}}}. \tag{5.18}$$

Figure 5.6 depicts the receive beamformers for receive antenna selection as well as the post-equalization SIRs per user after ZF precoding. Again, we obtain the main direction of received interference by using the dominant eigenmode of interfering sectors with cell-ids 6 and 8, refer to red and green beam shapes. Due to the fact, that receive antenna selection results in an omni-directional antenna characteristic, we observe a rather poor performance when employing MRC reception after ZF precoding. Note, the user performance is not limited by the intra-cell interference, instead the user suffers from inter-cell interference caused by the red and green cells. In case of OC in *Phase III*, each user can use its receive antennas to improve its SIR by finding a trade-off between minimizing received inter-cell interference and keeping intra-cell interference low.

DFT-Based Receive Combiner (DRC)

Another solution providing similar selection diversity gains compared to receive antenna selection is to use fixed combining weights and select the one providing highest Euclidean norm, i.e. $\underset{\forall t \in \mathcal{T}_k}{\arg\max} \left\| \boldsymbol{v}_{k,t}^H \mathbf{H}_{c,k} \right\|_2$.
At the transmitter side, DFT-based beamforming is already suggested for LTE systems to reduce the complexity of the precoding. By selecting the best DFT beam out of a limited set which is scalable in size, the feedback is significantly reduced in downlink LTE. This concept was shown to approach a close-to-optimum performance [LH03b,LH05]. Here, we use the same concept but at the receiver side in order to generate MISO-CSI. The set of equalizers can conveniently be extended in order to improve the quantization granularity of the dominant channel direction [LH03b]. In particular, the weights are given by $\boldsymbol{\Upsilon}_k^{\mathrm{DRC}} = 1/\sqrt{N_r}\left[\mathrm{dft}\left(\mathbf{I}^{|\mathcal{T}_k|\times|\mathcal{T}_k|}\right)\right]_{1:N_r,:}$. The preferred set of column elements from matrix $\boldsymbol{\Upsilon}_k^{\mathrm{DRC}}$ can be obtained by subsequently choosing the t-th column which maximizes the received power, similar to (5.17)

$$\boldsymbol{v}_{k,t}^{\mathrm{DRC}} = \underset{t \in \mathcal{T}_k}{\arg\max} \left| \left[\left[\Upsilon_k^{\mathrm{DRC}} \right]_{:,t} \right]^H \mathbf{H}_{c,k} \right|^2 \tag{5.19}$$

The CSI feedback is given by

$$\left[\hat{\mathbf{H}}_k\right]_{t,:} = \left[\boldsymbol{v}_{k,t}^{\mathrm{DRC}}\right]^H \mathbf{H}_{c,k} \tag{5.20}$$

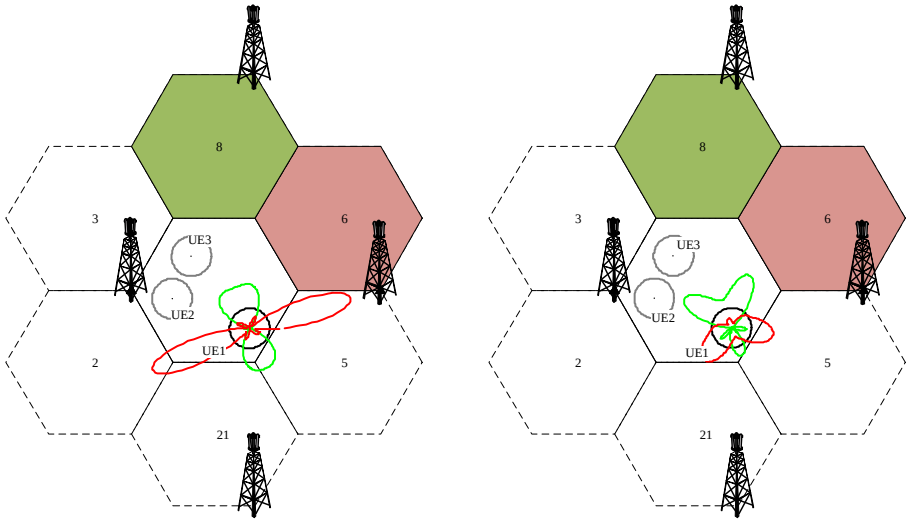

(a) Line-of-Sight, $k = 10$ dB.

(b) Line-of-Sight, $k = 0$ dB.

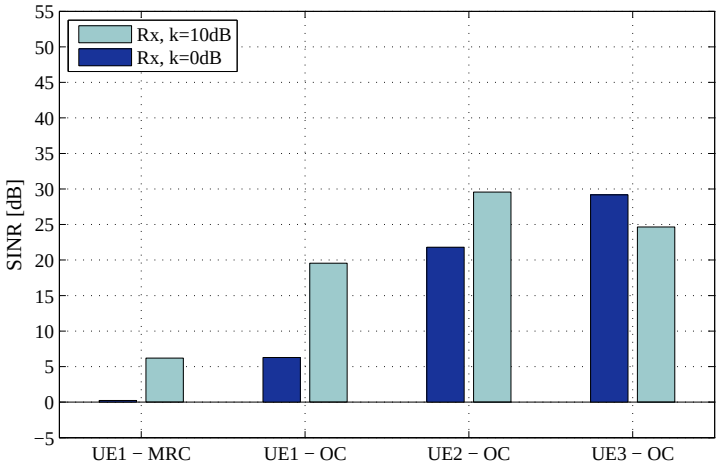

(c) Instantaneous user SIRs.

Figure 5.6: Top: Receive beamformer for receive antenna selection in a channel with different Ricean k-factor, $N_r = 4$ and an element spacing of $d = 0.5\lambda$. Bottom: Instantaneous post-equalization SIRs per UE taking the CCI from cells 6 and 8 into account.

and the SINR from Phase I can be obtained by evaluating (5.4)

$$\mathrm{SINR}_{k,t}^{(I,DRC)} = \frac{\widehat{p}_{c,t}}{\left\| \left[\boldsymbol{v}_{k,t}^{\mathrm{DRC}}\right]^H \mathbf{H}_{c,k} \right\|_2^2} \frac{\left| \left[\boldsymbol{v}_{k,t}^{\mathrm{DRC}}\right]^H \mathbf{H}_{c,k} \mathbf{H}_{c,k}^H \boldsymbol{v}_{k,t}^{\mathrm{DRC}} \right|^2}{\left[\boldsymbol{v}_{k,t}^{\mathrm{DRC}}\right]^H \mathbf{Z}_k \boldsymbol{v}_{k,t}^{\mathrm{DRC}}} \tag{5.21}$$

Figure 5.7 depicts the receive beamformers for discrete Fourier transform receive combining (DRC) as well as the user SIRs after ZF precoding. In case of strong LOS component, i.e. $k = 10$ dB, DFT decomposition of the MIMO channel is able to approach the performance of eigenmode decomposition when we allow the UE to use OC in *Phase III*. However, in presence of strong multi-path component, where the dominant signal as well as interference are not coming from a single direction, i.e. with relatively high spread in angel of arrivals (AoAs), channel-aware decomposition and reporting according to MET and EOC can improve the user experience.

Discussion

From paragraphs before, we already learned that the selected CSI decomposition method has significant influence on the user performance. However, the UE is not restricted to the same receive beamformer as used in *Phase I*. In particular, the optimum combining method provides the degrees of freedom to determine the specific receiver weights which maximize the post-equalization SINR after ZF precoding. Figure 5.8, depict the four different decomposition metrics as black lines. The dominant eigenmode received from the interfering cells 6 and 8 are shown as red and green lines. Their absolute gain value is scaled with respect to the ratio of the corresponding singular values, where the singular value from the desired signal (black line) is used as a reference. Hence, we maintain the relative received power levels of the different signals. Finally, we include the OC weights and observe that the resulting directivity pattern is significantly influenced by the original decomposition metric from *Phase I* and thus the final performance differs significantly. In particular, the local minimum at $\xi = 90°$ with respect to broadside of the ULA at the mobile in Figure 5.8(d) approaches a directivity value of $|\Omega_{Rx}(\xi = 90°)|^2 = -4.3$ dB while the same value in Figure 5.8(b) achieves a higher suppression with $|\Omega_{EOC}(\xi = 90°)|^2 = -8.8$ dB. The global maximum for receive antenna selection and EOC can be found at different azimuth angles with $|\Omega_{Rx}(\xi = \{25°, 155°\})|^2 = 5.9$ dB and $|\Omega_{EOC}(\xi = \{35°, 144°\})|^2 = 4.9$ dB. The serving base station can be found at the azimuth direction of $\xi = 138°$ with respect to UE broadside at $\xi = 0°$. Due to that reason, the MET pattern has its global maximum at the angle of $\xi = 138°$.

In the following paragraph, we will elaborate the behavior of the different CSI feedback methods in the same small scenario as described before, but in terms of a statistical analysis over a couple hundred different user distributions. The results shown in Figure 5.9 are twofold. First, the two very left CDFs depict the resulting

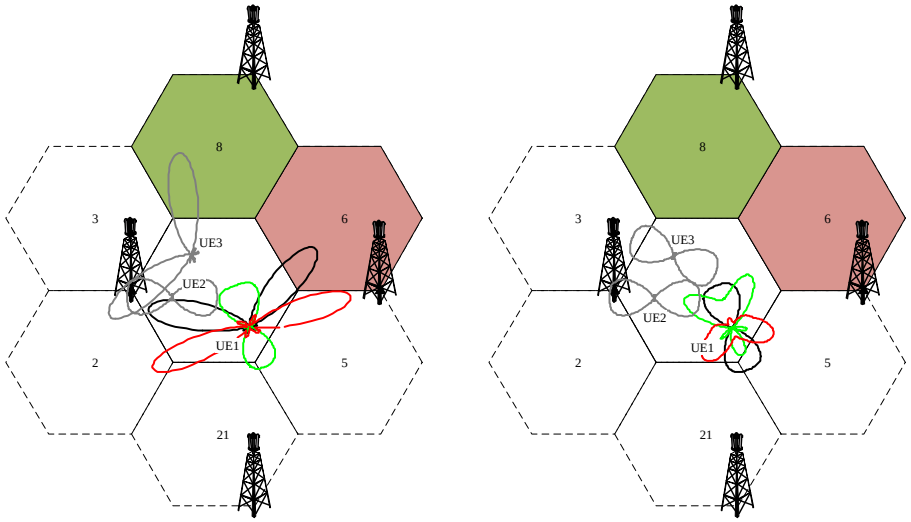

(a) Line-of-Sight, $k = 10$ dB.

(b) Line-of-Sight, $k = 0$ dB.

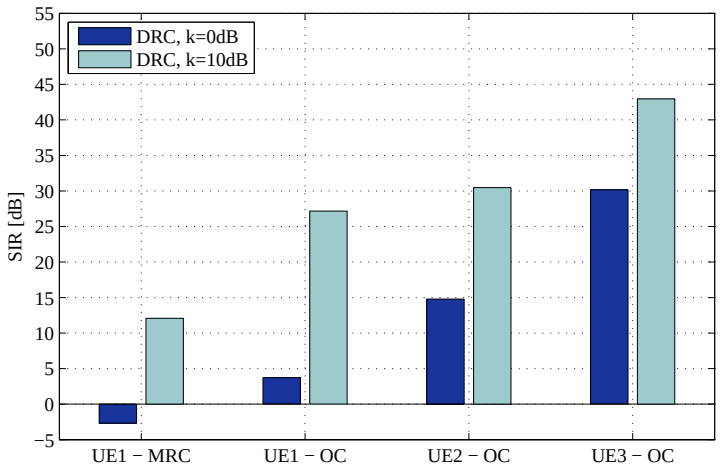

(c) Instantaneous user SIRs.

Figure 5.7: Top: Receive beamformer using DRC for different Ricean k-factor, $N_r = 4$ and an element spacing of $d = 0.5\lambda$. Bottom: Instantaneous post-equalization SIRs per UE taking the CCI from cells 6 and 8 into account.

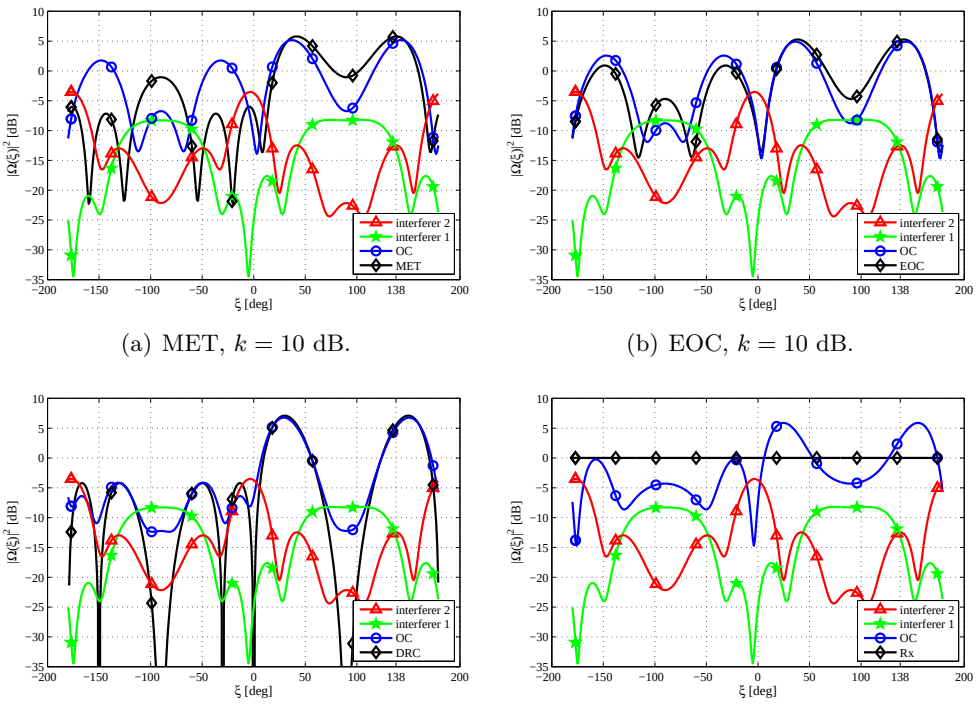

(a) MET, $k = 10$ dB.

(b) EOC, $k = 10$ dB.

(c) DRC, $k = 10$ dB.

(d) Rx, $k = 10$ dB.

Figure 5.8: Directivity diagram of specified receive beamformers which are used to decompose the MIMO in order to provide CSI feedback. In addition, we include the resulting OC filter which is used in *Phase III* after ZF precoding.

SIR when MRC is employed, i.e. no additional inter-cell interference suppression is used. Since EOC is based on interference suppression, results are provided for DRC and MET only. Receive antenna selection shows equivalent performance compared to DRC. Second, we have results with OC in the final phase. EOC shows superior performance compared to DRC and MET with approximately 2 dB and 1 dB gain, respectively. The significant gap between MRC and OC reception should not be overestimated, since in a fully deployed cellular grid multiple interfering BSs sum up to an interference floor which then limits the gain from interference suppression at the receiver side. Of course, inter-cell interference suppression will also be constrained by the lack of full knowledge on interfering channel coefficients.

5.2.3 Phase II: Distributed Precoder Calculation

Once users are grouped and assigned to a cluster, the precoder calculation and its power allocation have to be identical on all distributed processing units. Based on

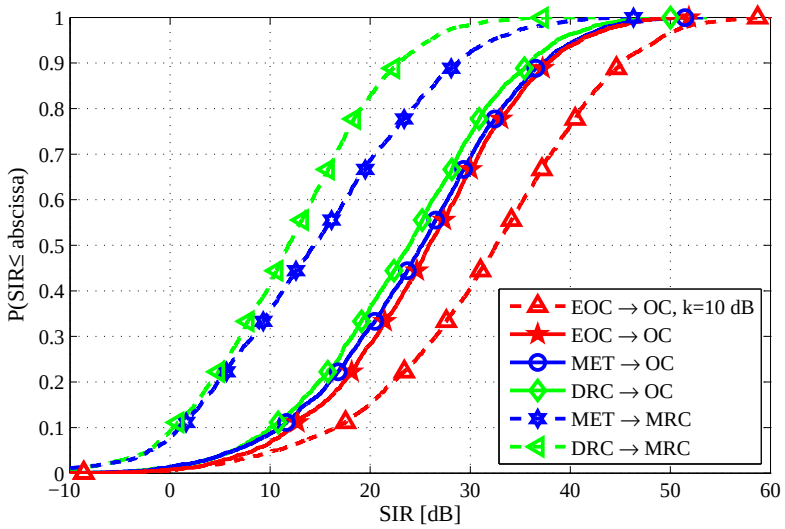

Figure 5.9: Statistical SIR analysis for the small scenario consisting of 3 sectors.

the CSI feedback of the UEs, the cluster combines the multi-cell, single-user CSI into a huge virtual multi-point-to-multi-point MIMO channel matrix $\mathbf{H}_{virt}$.

$$\mathbf{H}_{virt} = \left[\left[\hat{\mathbf{H}}_1 \right]^T \left[\hat{\mathbf{H}}_2 \right]^T \dots \left[\hat{\mathbf{H}}_{K_c} \right]^T \right]^T \tag{5.22}$$

Subsequently, we assume the clusters to generate the precoding filter by using a ZF constraint, i.e. forcing the inter-user interference to be zero. This can be either achieved by using the Moore-Penrose Pseudo inverse or more general by using BD transmission [SSH04]. Therefore, the scheduling entity in the BS has to select an appropriate set of users for instantaneous downlink service over multiple spatial layers, i.e. SDMA. For each UE, we define a signal space $\tilde{\mathbf{H}}_k$ of other users, i.e.

$$\tilde{\mathbf{H}}_k = \left[\left(\hat{\mathbf{H}}_1 \right)^T \dots \left(\hat{\mathbf{H}}_{k-1} \right)^T \left(\hat{\mathbf{H}}_{k+1} \right)^T \dots \left(\hat{\mathbf{H}}_{K_c} \right)^T \right]^T \tag{5.23}$$

The ZF constraint forces the signal space of user k to lie in the null space of all residual UEs $\mathcal{K}_c \backslash k$ combined in $\tilde{\mathbf{H}}_k$. Hence, we obtain the null space $\tilde{\mathbf{V}}_k^0$ by using the singular value decomposition (SVD) of $\tilde{\mathbf{H}}_k$

$$\tilde{\mathbf{H}}_k = \tilde{\mathbf{U}}_k \tilde{\mathbf{\Sigma}}_k \left[\tilde{\mathbf{V}}_k^1 \; \tilde{\mathbf{V}}_k^0 \right]^H \tag{5.24}$$

As long as the rank of $\tilde{\mathbf{H}}_k$ is less than or equal to $|\mathcal{T}_s| - |\mathcal{T}_{s,k}|$[8], $\tilde{\mathbf{V}}_k^0$ holds an orthogonal projection to the other users' signal space which may be used for downlink

[8] $\mathcal{T}_s$ and $\mathcal{T}_{s,k}$ are set of all selected spatial layers for users in $\mathcal{K}_c$ and selected spatial layers for user k, respectively.

transmission to user k. The dimension of $\tilde{\mathbf{V}}_k^0$ is $K_c N_t - \text{rank}(\tilde{\mathbf{H}}_k) \times K_c N_t$. For the special case of $K_c N_t - \text{rank}(\tilde{\mathbf{H}}_k) = 1$, $\tilde{\mathbf{V}}_k^0$ may directly be used as a precoder for user k. For the more general case of $K_c N_t - \text{rank}(\tilde{\mathbf{H}}_k) > 1$, we have to determine the most suitable projection of $\hat{\mathbf{H}}_k$ into this multi-dimensional null space by evaluating the SVD of user space and the null space

$$\hat{\mathbf{H}}_k \tilde{\mathbf{V}}_k^0 = \hat{\mathbf{U}}_k \hat{\mathbf{\Sigma}}_k \left[\hat{\mathbf{V}}_k^1 \; \hat{\mathbf{V}}_k^0\right]^H \tag{5.25}$$

Finally, we obtain the precoding matrix $\mathbf{B}_{c,k}$ for user k which maximizes the received power under ZF constraint,

$$\mathbf{B}_{c,k} = \tilde{\mathbf{V}}_k^0 \hat{\mathbf{V}}_k^1 \tag{5.26}$$

and the whole precoder for the c-th cluster including power allocation is given by

$$\mathbf{B}_c = \left[\tilde{\mathbf{V}}_1^0 \hat{\mathbf{V}}_1^1 \;\; \tilde{\mathbf{V}}_2^0 \hat{\mathbf{V}}_2^1 \;\; \ldots \tilde{\mathbf{V}}_1^0 \hat{\mathbf{V}}_1^1\right] \;\; . \tag{5.27}$$

5.2.4 Phase II: Power Allocation Strategies

In practice, a per-BS or an even more restrictive per antenna power constraint (PAPC) is a mandatory constraint if such algorithms are used in a cellular deployment, where multiple BSs belonging to the same cluster $\mathcal{M}_c$ have to meet their own power constraints while jointly serving the users in $\mathcal{K}_c$. Thus, the maximum available transmit power at each BS is restricted to a P_m value and in case of a very strict per-antenna power constraint, P_m can be equally divided to all antenna elements, i.e. $P_n = P_m / N_t$. In order to meet this constraint, we use the expression for matrix $\sqrt{\mathbf{P}_c}$ as given in [ZD04]:

$$\sqrt{\mathbf{P}_c} = \left\{ \min_{n=1,\ldots,N_t \cdot M_c} \sqrt{\frac{P_n}{\|\mathbf{B}_n\|_2}} \right\} \cdot \mathbf{I}_{[|\mathcal{T}_s| \times |\mathcal{T}_s|]}, \tag{5.28}$$

where $\mathbf{B}_n$ is a row of matrix $\mathbf{B}_c$ related to an antenna element in the cluster $\mathcal{M}_c$. Note that this power allocation is suboptimal and typically results in only one BS antenna transmitting with maximum power, and hence, the remaining $M_c N_t - 1$ antennas transmit with less than P_m / N_t. Note, the optimal power allocation can be determined by the water filling (WF) solution [ZHC00, PF05, JRV+05] under a certain power constraint.

In this work, we consider five different power allocation strategies:

1. Equal per beam power (EBP) with total power constraint (TPC)
2. Equal per beam power (EBP) with PAPC
3. Beam power, according to $\log_2(1 + \text{SINR})$ and PAPC
4. Beam power, according to SINR and PAPC
5. Beam power, according to channel inversion [GV97] and additional PAPC

5.2.5 Phase II: Link Adaptation based on User Feedback

Consider, each UE reports its CSI, i.e. $\hat{\mathbf{H}}_k$ (5.8), as well as its estimated post-equalization SINR per subband according to (5.4). Thus, the cluster may determine the expected post-equalization SINR per user, which will be realized in *Phase III* for the k-th terminal

$$\widehat{\mathrm{SINR}}_{k,t}^{(III)} \approx \psi \cdot \mathrm{SINR}_{k,t}^{(I)} \tag{5.29}$$

In order to obtain a correct power rescaling factor ψ, UEs would have to select identical equalization weights for *Phase I* and *Phase III*, i.e. $\boldsymbol{\upsilon}_{k,t} = \mathbf{w}_{k,t}$. In case of OC in *Phase III* with $\mathbf{w}_{k,t}^{\mathrm{OC}} \neq \boldsymbol{\upsilon}_{k,t}$, ψ would yield a lower bound of the post-equalization SINR[9], i.e. $\mathrm{SINR}_{k,t}^{(III)} \geq \widehat{\mathrm{SINR}}_{k,t}^{(III)}$. The power rescaling factor is given by (5.30)

$$\begin{aligned}
\psi_{k,t} &= \frac{p_{c,t} \cdot \boldsymbol{\upsilon}_{k,t}\mathbf{H}_{c,k}\left[\mathbf{B}_{c,k}\right]_{:,t}}{\widehat{p}_{c,t} \cdot \boldsymbol{\upsilon}_{k,t}\mathbf{H}_{c,k}\left[\widehat{\mathbf{B}}_{c,k}\right]_{:,t}} \\
&= \frac{p_{c,t} \cdot \left[\mathbf{H}_k\right]_{t,:}\left[\mathbf{B}_{c,k}\right]_{:,t}}{\widehat{p}_{c,t} \cdot \left[\mathbf{H}_k\right]_{t,:}\left[\widehat{\mathbf{B}}_{c,k}\right]_{:,t}} \\
&= \frac{p_{c,t} \cdot \left[\mathbf{H}_k\right]_{t,:}\left[\mathbf{B}_{c,k}\right]_{:,t}}{\widehat{p}_{c,t} \cdot \left[\mathbf{H}_k\right]_{t,:}\frac{\left(\left[\mathbf{H}_k\right]_{t,:}\right)^H}{\left\|\left[\mathbf{H}_k\right]_{t,:}\right\|_2}}
\end{aligned} \tag{5.30}$$

$$\begin{aligned}
\psi_{k,t}^{\mathrm{ERC}} &= \frac{p_{c,t} \cdot \left[\boldsymbol{\Sigma}_{c,k}\right]_{t,t}\left[\mathbf{V}_{c,k}\right]_{:,t}^H\left[\mathbf{B}_{c,k}\right]_{:,t}}{\widehat{p}_{c,t} \cdot \left[\boldsymbol{\Sigma}_{c,k}\right]_{t,t}\left[\mathbf{V}_{c,k}\right]_{:,t}^H\left[\mathbf{V}_{c,k}\right]_{:,t}} \\
&= \frac{p_{c,t}}{\widehat{p}_{c,t}}\left[\mathbf{V}_{c,k}\right]_{:,t}^H\left[\mathbf{B}_{c,k}\right]_{:,t}
\end{aligned} \tag{5.31}$$

In case of eigenmode-aware receive combining (ERC), ψ simplifies into two parts: The ratio of the valid power allocation $p_{c,t}$ over the assumed power allocation $\widehat{p}_{c,t}$ times the scalar product of the normalized effective channel at the receiver and the valid ZF beamformer for the k-th user.

In order to predict the final SINR after ZF precoding based on the application of the pre-chosen combining weights $\boldsymbol{\upsilon}_{k,t}$ from (5.8), equalization filters $\mathbf{w}_{k,t}$ have to be kept identical, i.e. $\mathbf{w}_{k,t} = \boldsymbol{\upsilon}_{k,t}$. In this case, the normalization factors $\psi_{k,t}$ obtained from the m-th column of the spatial precoder and therefore for the t-th data stream to k-th UE is calculated and then multiplied with the reported SINR. However, due to residual co-channel interference (CCI) the receiver may benefit from adapting its linear equalization weights according to $\mathbf{w}_{k,t} = \mathbf{w}_{k,t}^{\mathrm{OC}}$.
The rescaled SINRs may be mapped into certain MCS, which is part of standard link-to-system (L2S) interface. The achievable data rate and/or BLER can be obtained

[9] Only under ideal feedback conditions, i.e. without any impairments.

Table 5.1: Simulation parameters.

Parameter	Value
Channel model	3GPP SCME 3D
Large-scale fading maps	i.i.d. parameter statistics
Propagation conditions	mixture between LOS and NLOS
Scenario	urban-macro
Simulation methodology	Monte Carlo
Carrier frequency	2 GHz
Frequency reuse	1
Signal bandwidth	18 MHz, 100 RBs
Inter-site distance	500m
Number of BSs	19 having 3 sectors each
N_t ; spacing	2 ; co-pol 4λ
Transmit power	46 dBm
Sectorization	triple, with FWHM of 68°
Elevation pattern[10]	FWHM of 6.2°, elec. downtlit 10°
BS height	32m
Number of active UEs	N_t per sector
N_r ; spacing	2 ; co-pol $\lambda/2$
UE height	2m
Link-2-System	Shannon-gap, SINRs $\lfloor -8, 26 \rceil$ dB
Channel estimation error	i.i.d. Gaussian; variance $\mu \geq -40$ dB
BS clustering	ideal, user-centric
User grouping	received power based, round-robin

by using the final SINR from *Phase III*. In particular, SINRs from *Phase III* and the estimates from the BS may differ significantly if the delay between CQI feedback and downlink service increases.

5.2.6 Performance evaluation

The combined receiver-transmitter concepts described in the previous chapters are evaluated in a triple-sectored hexagonal cellular network with $M = 57$ BS sectors in total, refer to Figure 5.10. All sectors operate with full frequency reuse. We employ the wrap-around technique described in [TWS+09], which ensures that the interference scenario is complete and follows i.i.d. statistics for all users. The different channel matrices are generated by employing the widely used SCME with urban macro scenario parameters [BSM+05] listed in Table 5.1.

[10] Using a 3-dimensional measured radiation pattern, KATHREIN 80010541.

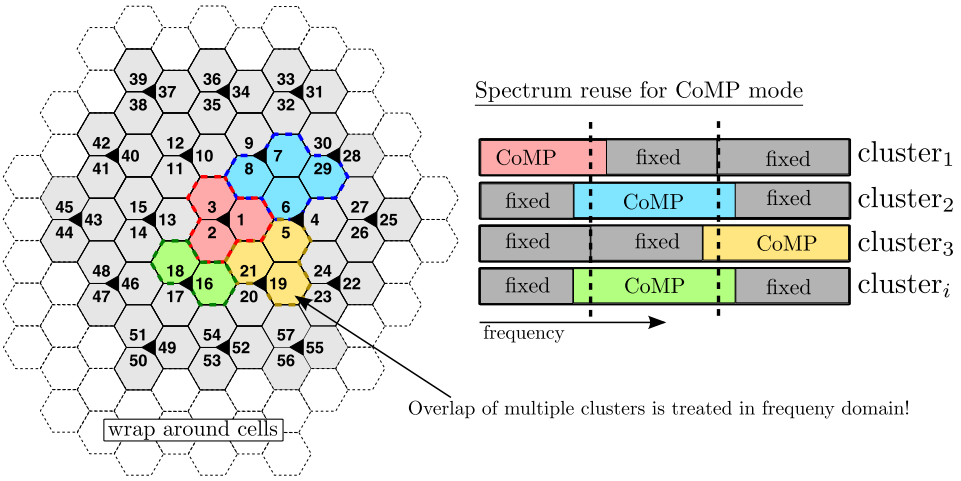

Figure 5.10: Framework for performance evaluation: A cluster island performing a CoMP transmission which is surrounded by predictable CCI assuming standard LTE codebooks.

According to Section 4.3, we extend the general spatial channel model by multiple features. As stated in Section 4.3, BS are usually equipped with highly directive ULAs, which especially holds for the elevation characteristics. Thus, 3-dimensional antenna models are a mandatory requirement which needs to be included to model the cellular propagation conditions for future standards such as LTE. In [TWB+09], we demonstrated that hereby co-channel interference (CCI) from neighboring BSs is becoming a rather localized phenomenon, i.e. the origin of strong interference is close to the user's position. This of course promotes the assumptions which are made for clustered CoMP transmission. Other additional features such as spatially correlated large-scale fading maps are dropped at this stage, since we simplify the clustering of BS and the grouping of users. These maps are then introduced in Sections 6.3 and 6.2, where we focus on algorithms for user grouping and cluster formation.

Let us assume that each user generates and conveys the CSI for its desired cluster of BSs, where any constellation of cell-ids is allowed. In Section 6.2 we will call this kind of clustering as *user-centric* and dynamic over frequency. The clusters contain disjoint sets of BSs and the overlap of clusters is achieved in frequency or time domain. In a large-scale network, we suggest to arrange the access to the radio channel using CoMP or standard LTE codebook based transmission in an alternating manner. E.g. this can be achieved by defining a kind of spatial reuse of the CoMP transmission mode in neighboring clusters, refer to Figure 5.10. Thus, potential overlap of multiple clusters can be orthogonalized in frequency domain. Each cluster is assigned to a specific frequency sub-band, where coherent channel-aware CoMP transmission is permitted, while the surrounding BSs are forced to

use a codebook-based precoding only. This ensures the CCI from other clusters to be predictable. Note, this non-cooperative ring of BSs should have a width of at least one BS sector, which directly results from the natural cell isolation caused by antenna tilting. Nevertheless, we have to reserve a significant part of the frequency band for those users, where CoMP transmission is not applicable: E.g. in case of highly mobile users, as well as cell-center users where CoMP cannot provide additional throughput gains, due to the limited MCS. The task of defining these network-centric clusters will be addressed in Section 6.2. Further, assume a set $\mathcal{K}_c$ of multi-antenna terminals being uniformly distributed in a specific c-th cluster of the cellular environment. The scheduling entity in this cluster splits the $\mathcal{K}_c$ UEs into $|\mathcal{M}_c|$ subsets, with $\mathcal{K}_{c,m} \subset \mathcal{K}_c$, according to the cell-id with highest received channel gain. Within the next step, the scheduler selects from each user group $\mathcal{K}_{c,m}$ a number of N_t UEs to be active, where it follows a round-robin metric. This ensures that each cell-id inside $\mathcal{K}_c$ acts as a master BS for an equivalent amount of users and hence CoMP transmission from all $\mathcal{M}_c N_t$ antennas to all active users becomes effective. Note, in this section we ensure each user in $\mathcal{K}_c$ is served on a single data stream, i.e. $|\mathcal{K}_c| = |\mathcal{M}_c| N_t$. Results are provided as a function of the cluster size, i.e. $M_c \in \{1, 2, 3, 4, 5, 10\}$.

Once we improved the SINR conditions for the users by use of ZF beamforming in a cluster, practical link adaptation can still limit the peak data rates of the UEs and the system. As provided in Section 2.4, LTE compliant MCS levels cover QPSK up to 64 QAM (64 QAM) with code rates from 78/1024 up to 948/1024. In theory, for large clusters we expect SINRs to exceed 20 dB. Hence, we employ a Shannon gap model according to Section 2.4 where post-equalization SINRs are first reduced by 3 dB, then cut into a range of $\lfloor -8, 26 \rceil$ dB and finally mapped into bit/s/Hz using Shannon's formula.

In this section, we consider the median sum-rate per cell as well as the 5% -ile and 95% -ile user throughputs for performance evaluations. All values are based on Shannon information rates using SINRs from *Phase III* according to (5.2). Since network-wide collaborative signal processing is hardly feasible, we start evaluating the potential gains from CoMP with JT by increasing the cluster size up to $M_c = 10$ sectors. We observe that multi-cell cooperation provides increasing gains with increasing cluster size, where already small cluster sizes provide significant gains.

Erroneous CSI estimation and feedback Despite the fact of using ZF beamforming, practical systems will always suffer from intra-cluster interference. There is a variety of reasons which destroy the inter-user orthogonality [MTO+11]: Channel estimation and quantization, channel aging effects and synchronization errors to multiple BSs. For sake of simplicity, we combine all sources of errors into a single process and thus include an AWGN error prior to ZF beamforming [PNJvH05]. In general, we may describe the mismatch between the ideal channel and its estimated

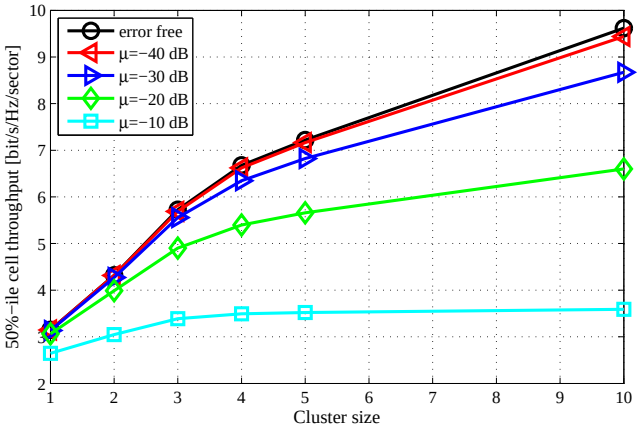

(a) 50% -ile cell throughput.

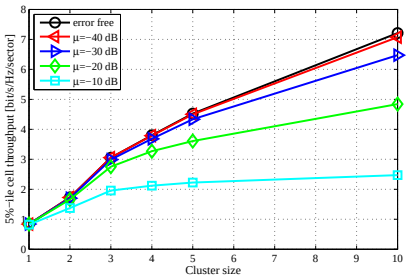

(b) 5% -ile cell throughput.

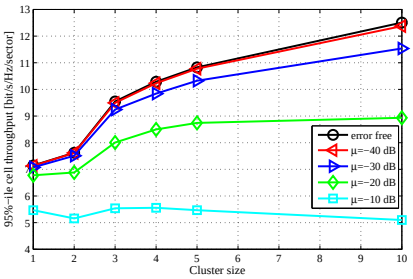

(c) 95% -ile cell throughput.

Figure 5.11: Erroneous CSI: Cell throughput obtained from SINR distributions based on ERC, L2S interface is based on Shannon-gap.

version by evaluating the corresponding rMSE per sub-channel for user k. Therefore, we define $\mathbf{\Delta}_{c,k} = \mathbf{H}_{c,k} - \hat{\mathbf{H}}_{c,k}$ as the element-wise difference matrix between the ideal channel and its estimated version and normalize the resulting error by the average channel gain of $\mathbf{H}_{c,k}$:

$$\mathrm{rMSE}_k = \frac{\mathrm{tr}\Big(\mathbf{\Delta}_{c,k}\mathbf{\Delta}_{c,k}^H\Big)}{\mathrm{tr}\Big(\mathbf{H}_{c,k}\mathbf{H}_{c,k}^H\Big)}. \tag{5.32}$$

The average rMSE defined as μ is obtained over multiple Monte-Carlo drops and users k

$$\mu = 1/(K \cdot Drops) \sum_{\forall k,drop} \mathrm{rMSE}_{k,drop} \tag{5.33}$$

The additional CSI error is drawn from a zero mean i.i.d. Gaussian distributed process with variance μ defined per sub-channel. The noisy CSI is used at the BSs to calculate the ZF precoding solution.

In the following, we evaluate the system level performance of CoMP transmission using MET [BH07b, NMK+07] and a dynamic cluster selection and a round-robin scheduling metric for active UEs [TJH10]. The erroneous feedback results in a more severe degradation with increasing cluster size. Finally, we increase the cluster size from $M_c = 1$ up to $M_c = 10$. Figures 5.11 and 5.12 depict the resulting Shannon information rates per sector and per user as a function of the cluster size M_c and accuracy of CSI feedback, i.e. in case of error free and erroneous channel feedback. These figures depict the cell-edge (5% -ile), median and peak (95% -ile) data rates for the system and its users. From the figure it is obvious that an rMSE with an average of $\mu = -10$ dB would restrict the useful cluster size to $M_c = 3$. Only the 5% -ile user throughput can further be improved with increasing M_c, refer to Figure 5.12(b). In essence, the CoMP gains as function of the cluster size show less saturation behavior for improved multi-cell channel knowledge. Concluding, we observe that the median sector spectral efficiencies are increased by 220% , 300% and 430% for coordinating 3, 5 and 10 cells for error free CSI feedback, respectively. These numbers are reduced to 190% , 230% and 300% in case of erroneous feedback with $\mu = -20$ dB.

Performance of reference cases For reference purpose, we provide performance results for a SISO as well as a MIMO 2×2 setup. For $N_t = 2$, two active fixed beams are sent to $K = 2$ different users in a round-robin manner as well as taking CQI feedback into account. The CQI-aware score-based solution outperforms both other reference cases with a relative throughput gain of $\varrho_{M_c=1} = 1.3$ and $\varrho_{M_c=1} = 2.3$ compared to round-robin and SISO at median sector throughput, respectively. At cell-edge, i.e. for 5% -ile user rate, differences are even more prominent. Note, with $K_c = N_t$, the MIMO setup benefits from an additional user in conjunction with an increase of antennas $N_t = N_r = 2$. All results in Figures 5.13 and 5.14 are based on an equal per beam power (EBP) with a PAPC according to LTE assumptions.

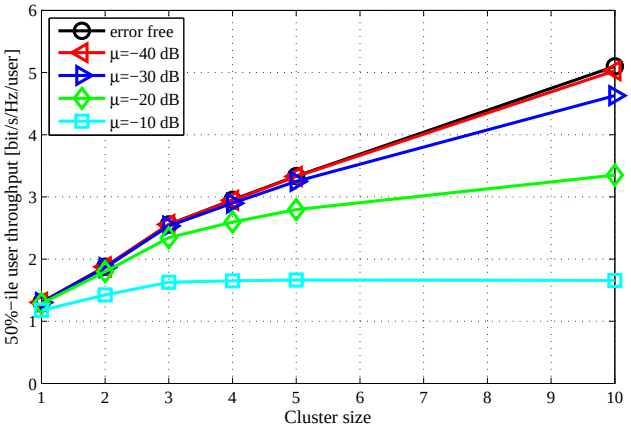

(a) 50% -ile user throughput.

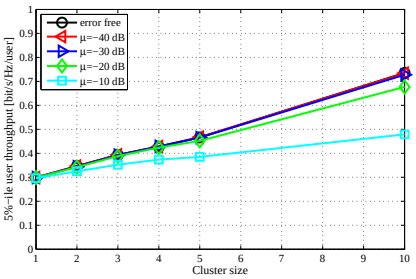

(b) 5% -ile user throughput.

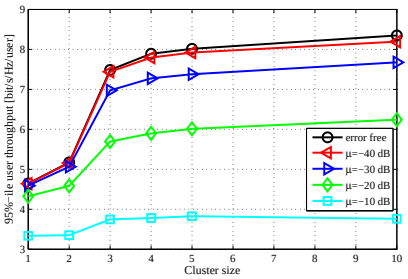

(c) 95% -ile user throughput.

Figure 5.12: Erroneous CSI: Per user throughput obtained from SINR distributions based on ERC, L2S interface is based on Shannon-gap.

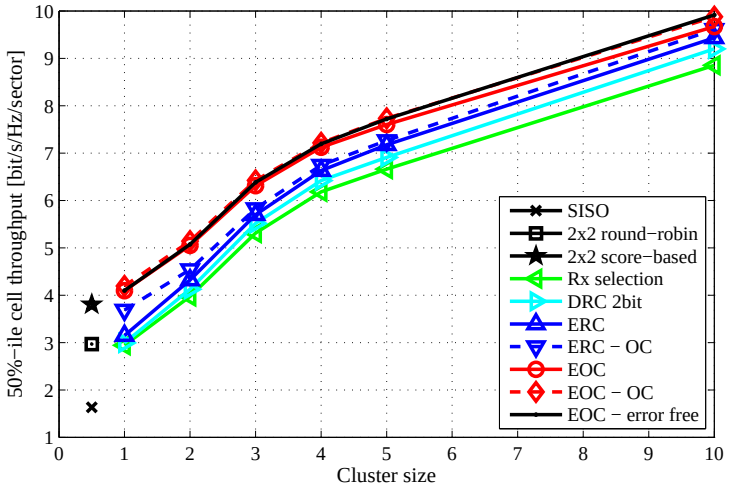

(a) 50% -ile cell throughput.

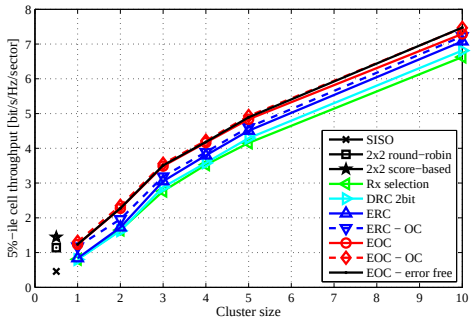

(b) 5% -ile cell throughput.

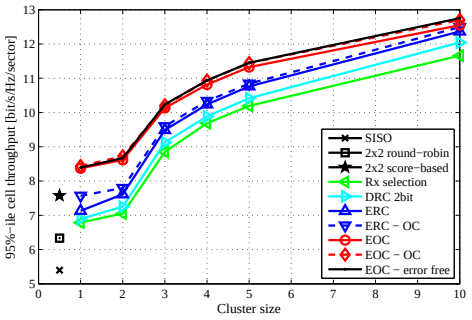

(c) 95% -ile cell throughput.

Figure 5.13: Cell throughput obtained from SINR distributions, where the L2S interface is abstracted using a Shannon gap model.

Gain from CSI feedback and CoMP transmission Figures 5.13 and 5.14 depict the achievable median sector and per user spectral efficiency in bit/s/Hz/sector as a function of M_c. The different CSI reporting strategies from Section 5.2.2 are evaluated and show equivalent scaling behavior for increasing M_c. For the eigenmode-aware receive combining (ERC) as well as the eigenmode-aware optimum combining (EOC) we additionally consider OC in *Phase III* in order to mitigate the effects of residual CCI caused by non-coordinated BSs and errors in CSI feedback. However, 5% -ile user rates in Figure 5.14(b) are rather low. This is caused by the limited number of users $K_c = N_t$ per cell, i.e. we cannot realize any multi-user selection diversity. In addition, peak user rates show a small increase from $M_c = 1$ to $M_c = 2$ and a much steeper gain switching to $M_c = 3$. This originates from the given cell geometry, where the main lobes of three different BS sectors are facing each other and therefore, a cluster size of $M_c = 3$ represents the smallest closed set.

In case of CSI feedback and ZF beamforming at a single BS, i.e. $M_c = 1$, EOC with subsequent OC provides a system gain of $\varrho_{M_c=1} = 2.6$ and $\varrho_{M_c=1} = 1.1$ compared to SISO and score-based beam assignment, respectively. The overall gain of CoMP with EOC attributes to $\varrho_{M_c=2} = 3.2$, $\varrho_{M_c=3} = 3.9$, $\varrho_{M_c=4} = 4.4$, $\varrho_{M_c=5} = 4.7$ and $\varrho_{M_c=10} = 6.1$ w.r.t the SISO case. The absolute gain from CoMP using EOC over simple receive antenna selection is almost constant over the whole evaluation range and attributes to ≈ 1.1 bit/s/Hz, where the relative gain reduces from 1.39 down to 1.12. Due to additional selection diversity gains, the DRC (2 bit) approach shows a superior performance w.r.t the simple receive antenna selection approach having only two degrees of freedom for selection, i.e. 1 bit quantization. As already described before, the gains for peak data rates attribute to $\varrho^{95}_{M_c=1} = 1.5$, $\varrho^{95}_{M_c=2} = 1.6$, $\varrho^{95}_{M_c=3} = 1.9$, $\varrho^{95}_{M_c=4} = 2.0$, $\varrho^{95}_{M_c=5} = 2.1$ and $\varrho^{95}_{M_c=10} = 2.4$, all for 95% -ile system data rates with respect to SISO case.

The 5% -ile and median user rates show an almost linear scaling behavior over the whole range of M_c.

Performance with different power allocation strategies In the following paragraph, we study the effect of different power allocation strategies on the system performance. In contrast to results from before, we decided to use Shannon information rates with full SINR range and without any gap. This methodology is chosen to ensure an idealistic comparison. Figure 5.15 depicts the achievable spectral efficiency per sector (right) as well as for the individual users (left). As reported in [GV97], channel inversion (green) leads to an inferior system performance caused by wasting transmit power for the user experiencing worst channel conditions. This behavior is often referred to as the price we have to pay for max-min fairness. In this case, the performance of the worst user is maximized, and in fact we can observe a very steep slope for user spectral efficiencies following the channel inversion method. Assigning the power budget proportional to the expected data rate per user (black) yields a significant increase in spectral efficiency per sector, i.e. factor

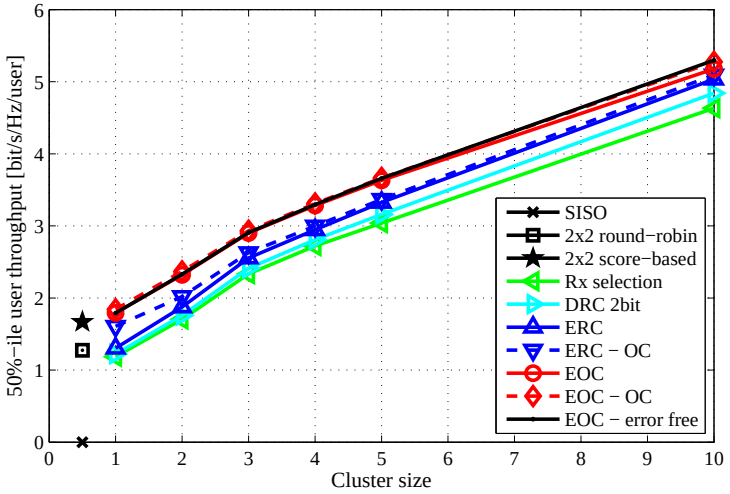

(a) 50% -ile user throughput.

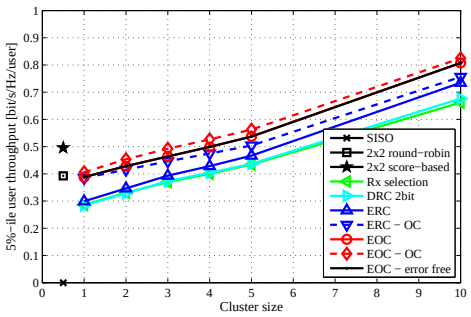

(b) 5% -ile user throughput.

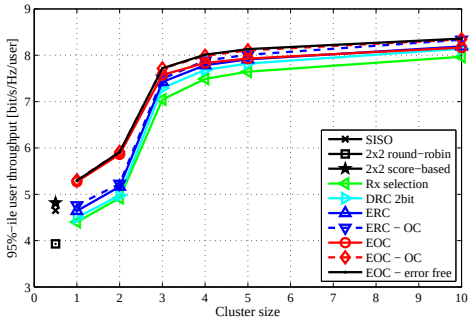

(c) 95% -ile user throughput.

Figure 5.14: Per user throughput obtained from SINR distributions, where the L2S interface is abstracted using a Shannon gap model.

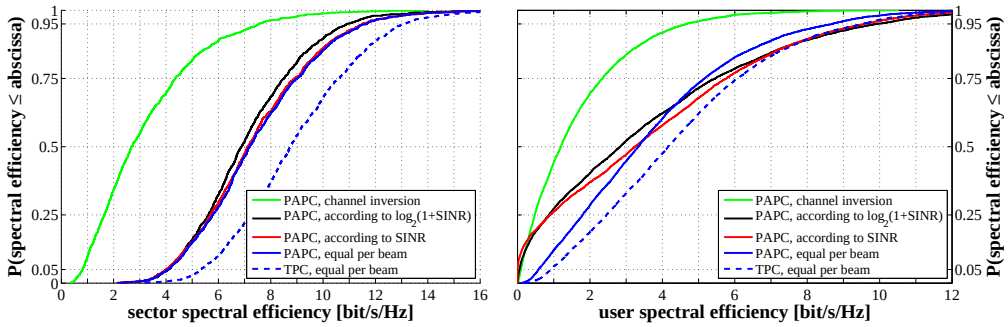

Figure 5.15: System as well as per user spectral efficiency for various power allocation strategies meeting the per antenna power constraint (PAPC). As reference, we provide results for equal per beam power with a total power constraint (TPC). Evaluation is carried out for $M_c = 3$ belonging to the cluster and the ERC was used.

of more than 2.5, as well as an improved user rate. Note, equivalent to the channel inversion, there is no user outage. The power allocation according to the expected SINR (red) achieves slightly higher median system and user spectral efficiencies, where users tend to show outage in the order of $\approx 8\%$. Assigning the per antenna power budget equally to the spatial beams achieves a per sector performance similar to the afore mentioned SINR-aware assignment. This originates from the fact, that each user is served on an effective channel, which yields improved per user SINRs. In addition, we determine precoding and power allocation weights in two subsequent steps in a single iteration. Hence, if no transmit power is allocated to a specific data stream, the system does not gain from refined precoders with additional transmit diversity. Extending the equal per beam power target to meet the TPC leads to an upper limit which cannot be realized in a distributed CoMP setup, since each BS has its own power limitation of P_m. The hypothetical gain would roughly attribute to 20% .

5.2.7 Conclusions

In this chapter, we investigated a centralized scheme for coordinated multi-point transmission in the downlink of next generation mobile networks. This scheme has the potential to be implemented in a distributed manner. Therefore, we consider coordinated transmission inside a limited cluster of cells forming an intra-cluster interference free island. This island is surrounded by multiple non-coordinated cells. For removing the interference inside the cluster, the common multi-user eigenmode transmission has been developed further. The gains from receive antenna combining have been included in the overall optimization as well and also for an innovative channel feedback scheme which allows for a two-step transceiver optimization for

multiple terminals using independent receiver algorithms. The performance has been studied in detail in a triple-sectored multi-cell scenario covering 57 cells. The effects of highly directive antenna elevation patterns have been included as well.

At first, we observed that CSI errors will have a significant impact on the CoMP performance, where rMSEs with $\mu \approx -10$ dB cause CoMP joint transmission being hardly beneficial. Second, the median sector spectral efficiencies are increased by 290% , 370% and 500% for coordinating 3, 5 and 10 cells, respectively, where the baseline is a SISO system. Peak user data rates can be increased by 60% assuming a cluster size of $M_c = 3$ compared to standard non coordinated systems already utilizing frequency-selective scheduling. However, backhaul requirements per feeder link will increase as well. The absolute gain of using the best eigenmode-aware optimum combining scheme at the receiver compared to the simplest receive antenna selection amounts to 1.1 bit/s/Hz, which is almost independent of the cluster size. Further, we demonstrate that subsequent optimum combining, in Phase III, can help to reduce errors made in the CSI feedback phase. Altogether, significant gains from coordination have already been realized by using small clusters.

6

Challenges Connected to CoMP

The methodology behind this chapter is the following: We start with the problem formalization in terms of a weighted sum-rate criteria. Then we split the combined user grouping and clustering problem into two parts. For this purpose, we first define the clusters of BSs and then determine the corresponding set of users $\mathcal{K}_c$ for a specific cluster $\mathcal{M}_c$. Note, we carefully select the specific cluster $\mathcal{M}_c$ in order to maintain a representative performance evaluation of clustered CoMP transmission in presence of inter-cluster interference. Finally, we conclude with an analysis of delayed channel feedback, also referred as channel aging, in combination with 1-D frequency domain channel prediction.

6.1 Weighted Sum-Rate Maximization

To study the limits of the cellular system under the premise of a downlink cooperation, we assume sum-rate maximized transmission for all transmit antennas which are combined in a certain cluster $\mathcal{M}_c$. The maximum sum-rate in $\mathcal{M}_c$ can be obtained under the assumption of a distributed antenna system, where a central unit calculates the optimal, non-linear transmission strategy for the corresponding BSs and users. Let us assume, that the set of users combined in $\mathcal{K}_c$ conveys their user-specific CSI feedback $\mathcal{T}_k \subset \mathcal{T}_K$ as potential receive space candidates for downlink transmission. The selected receive spaces are grouped into the set of active layers $\mathcal{T}_s$, while each user may receive multiple data streams combined in $\mathcal{T}_{s,k}$. The optimal transmission strategy, which achieves the capacity of the MIMO-broadcast channel (BC) [CS03, VT03, VJG03, JVG04], is the dirty paper coding (DPC) [Cos83] scheme. In [GUD09] authors proposed a simplified method to select users having highest gain compared to the standard single user service. In [SB04], the authors developed a framework for MU downlink beamforming with individual SINR constraints. These solutions are based on the assumption of perfect CSI at both UE

and BS side. Accordingly, let us define R_c as the maximum throughput in the c-th cluster with a common power constraint

$$R_c = \underset{\mathbf{\Phi}_k, k\in\mathcal{K}_c}{\arg\max} \log_2 \det\left(\mathbf{I} + \sum_{k=1}^{K_c} \alpha_k \mathbf{H}_{c,k}\mathbf{\Phi}_k\mathbf{H}_{c,k}^H\right) \tag{6.1}$$
$$\text{subject to} \begin{cases} \mathbf{\Phi}_k \succeq 0, k \in \mathcal{K}_c \\ \sum\limits_{m\in\mathcal{M}_c}\sum\limits_{t\in\mathcal{T}_s} E\left\{\text{tr}\{[\mathbf{\Phi}_t]_{:,m}\}\right\} \leq M_c P_m \end{cases}$$

where $\mathbf{\Phi}_k = \mathbb{E}\left\{\mathbf{S}_k(\mathbf{S}_k)^H\right\}$ with $\mathbf{S}_k$ being the precoded data intended for user k and P_m is the per-base station power budget. In case of linear precoding techniques $\mathbf{S}_k$ is simple combination of transmit antennas and data, i.e. $\mathbf{S}_k = \mathbf{B}_{c,k}\mathbf{P}_c^{1/2}\mathbf{x}_{c,k}$. We note that the original MIMO-BC capacity [CS03, JVG04], was calculated under a sum-power constraint. The problem of finding the sum-capacity region of a downlink system with per-antenna power constraint was considered in [YL07, BH06], where a generalized uplink-downlink duality was considered.

Simulation results for DPC with Sum-Power Constraint In the following, we consider the case where each BS is equipped with $N_t = 4$ transmit and each UE is equipped with $N_r = 2$ receive antennas. All $M_c \leq 21$ BS sectors are considered as a huge distributed antenna system (DAS) (i.e. one huge cluster), which jointly serves a set of users $\mathcal{K}_c$ [HWKS11]. Note, in contrast to the typical Rayleigh fading assumption, the MIMO channels in this evaluation do not have the same average SNR. This is caused by the different path-gain coefficients experienced from the distinct antenna arrays. The cellular channels are generated by the use of QuaDRiGa with a 3D antenna diagram, according to assumptions from Table 6.2. We are using an iterative WF algorithm with a sum-power constraint [JRV+05] to determine the maximum sum-rate of the system as a function of the size of the active set of users $\mathcal{K}_c$. However, in practice we would rather consider a per-BS or per-antenna power constraint than a sum-power constraint. These results should provide an overview on a well-known WF algorithm and its achievable sum-rates in a cellular system.

For the results shown in Figure 6.1, we consider the transmit power per PRB emitted by each BS which is set to $P_m = 40$W. As additive white Gaussian noise (AWGN), we assume thermal noise given at 20°C and an additional receiver noise figure of 9 dB. In particular, Figure 6.1(a) depicts the BC capacity as a function of the cluster size M_c in a deployment with total number of $M = 21$ sectors, i.e. the system performance converges towards noise limitation only. In contrast, results in Figure 6.1(b) clearly show that even with a cluster size of $Mc = 21$ in the $M = 57$ cell deployment, the sum capacity is still limited by surrounded out-of-cluster interference. The rationale for cluster formation is depicted in Figure 6.3. Note, results for single-cell processed DPC only show a marginal difference in sum capacity for the setup assuming $M = 21$ and $M = 57$ sectors.

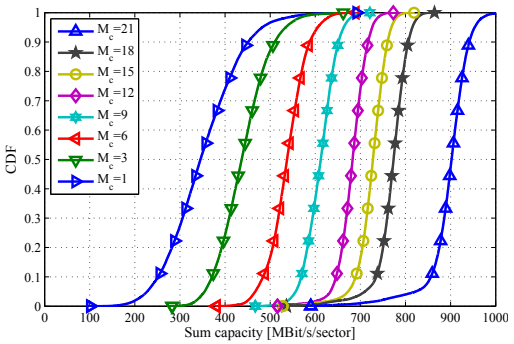

(a) Capacity for $K_m = 20$ and $M = 21$ as a function of M_c.

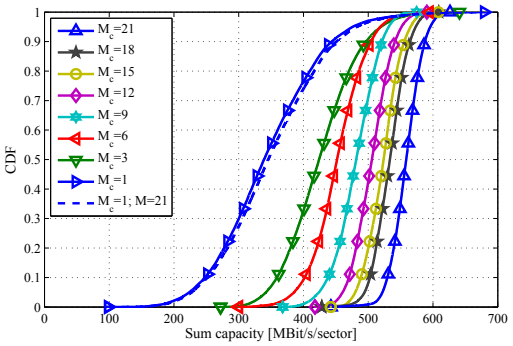

(b) Capacity for $K_m = 20$ and $M = 57$ as a function of M_c.

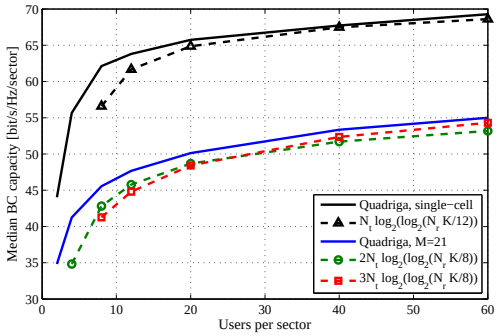

(c) Capacity for $M = M_c = 21$.

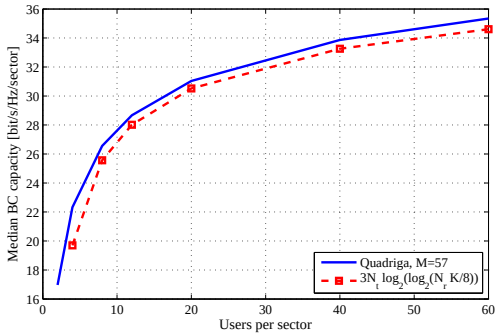

(d) Interference-limited capacity, $M > M_c = 21$.

Figure 6.1: Cluster-wide DPC using an iterative WF algorithm from [JRV+05] under a total power constraint. (a) and (c) depict results in a deployment with $M = 21$ sectors, as a function of the cluster size M_c and for fixed $M_c = 21$ as a function of the size of the user set $|\mathcal{K}_c| = 21\,K_m$. In contrast, (b) and (d) show the interference limited BC sum-rate as a function of the cluster size and for fixed $M_c = 21$ as a function of the user set in a deployment with $M = 57$ sectors.

Figure 6.1(c) focuses on inter-cluster interference free transmission, i.e. the system capacity is only limited by thermal noise. Therefore, we compare two extremes. First, an isolated cell assumption with $M = M_c = 1$ and second, a multi-cell assumption with $M = M_c = 21$ and cluster-wide DPC. The multi-cell system achieves a BC capacity of 79% of the isolated cell capacity. One reason for that observation is the fact, that in case of the multi-cell system the distinct BS antenna arrays have to bridge the significantly varying path gains to each user. This makes joint precoding less efficient compared to the case where all antennas are combined at a single spot. Second, we study the scaling behavior of system capacity with increasing amount of users per sector. By adding additional UEs per sector, the iterative WF algorithm utilize multi-user diversity to improve the BC capacity of the antenna system. Each sector contains a number of K_m terminals, while the cluster $\mathcal{M}_c$ has a total number of $K_c = 21\,K_m$. Based on the findings in [SH05], where the capacity of the BC grows with $N_t \log_2 \log_2(N_r K)$, we additionally add two lines representing a corresponding growth rate. We derive two main observations.
First, the isolated cell capacity scales differently compared to that in [SH05]. In general, the typical i.i.d. Rayleigh fading assumptions does not hold for the coefficients obtained from our channel model. The main difference is the fact that each antenna array undergoes its own channel gain to a specific UE. Since the number of transmit antennas N_t is fixed, the only degree of freedom to justify the scaling behavior is the number of users. In general, the user set contains a specific number of UEs but with significantly changing mean SNR.[1] The iterative WF solution, which targets at maximizing the sum-rate of the system, is selecting only users with highest channel gain. Thus, UEs experiencing relatively poor SNR conditions are not considered in the selection process. Due to that fact, it is reasonable to argue that the set of users per sector $\mathcal{K}_m$ has an effective size smaller than K_m. Our empirical observation is that the effective size amounts to $K_m/12$, i.e. roughly 8% of K_m. In essence, the BC capacity of the isolated cell scenario seems to scale with $N_t \log_2 \log_2(N_r K/12)$.[2] Second, the capacity for $M = M_c = 21$ sectors shows a slightly steeper scaling compared to the isolated cell. In the multi-cell setup, the paradigm of the effective user set is still valid. But on the other hand, we have more transmit antennas in the system. Since all transmit antennas from $M_c = 21$ sectors jointly perform DPC, it is reasonable to assume that the capacity may increase with ϵN_t. The empirical observation from Figure 6.1(c) is that $2 \leq \epsilon \leq 3$. In other words, a sub-cluster of $M_{c,k} = 2 \ldots 3$ sectors serves the set of users $\mathcal{K}_m$ per sector.

Finally, Figure 6.1(d) depicts the BC capacity for the deployment with a total number of $M = 57$ sectors, while the cluster consists of $M_c = 21$ cells. In this case, a significant amount of inter-cell interference remains between the cluster $\mathcal{M}_c$ and its surrounding cells. Since the WF solution distributes the total transmit power

[1] The SNR depends on the specific user distribution. To each position, we generate a specific path gain value which corresponds to a certain deterministic path loss, antenna gain and a stochastic realization of shadow fading.

[2] For $K_m = 60$ the user outage attributes to 92% .

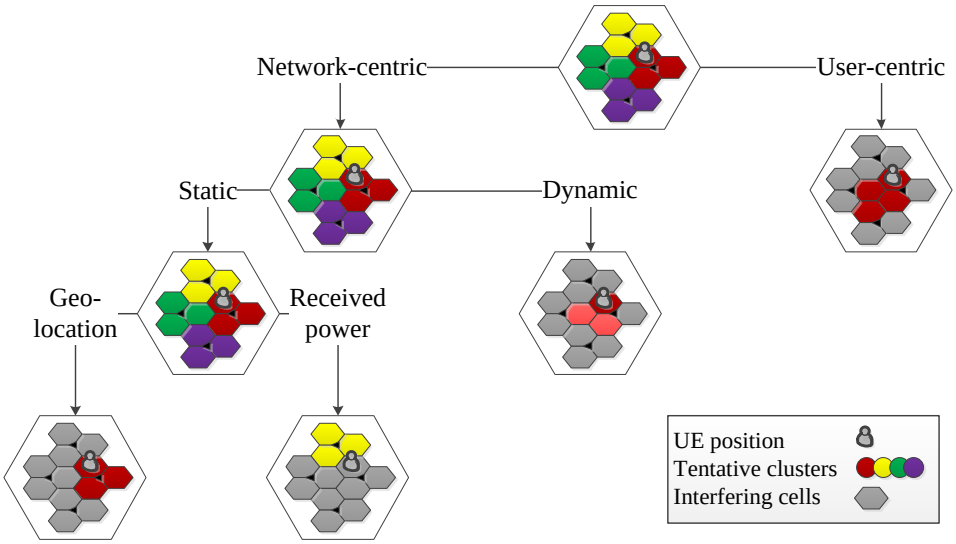

Figure 6.2: Different clustering concepts: from a totally static network towards a fully user-centric view. Therefore, we will consider the geo-location based, the received power based, the dynamic selection and finally the user-centric concept. In all cases, the selected cluster is highlighted in its specific color while the other cells are marked as interfering.

among data streams for the users, while considering the noise term only, power allocation and user grouping may not be optimal in the inter-cluster interference limited regime. As a consequence, the system capacity under inter-cluster interference limitation attributes to 51% of the isolated cell capacity.

6.2 Cluster Selection Methods

From a practical point of view, one of the major drawbacks related to joint processing is its higher complexity, i.e. increasing backhaul and signaling overhead. To reduce these complexity requirements, *clustering* solutions that restrict joint processing techniques to a limited number of BSs have been proposed. In these approaches, the network is statically or dynamically divided into clusters of cells [BH07a,PGH08, BHA08, TWH$^+$09, ZGN$^+$09, TBB$^+$10].

For the following investigation we will examine two fields of cluster selection approaches. The first one is done in a per-user way, i.e. *user-centric* clustering, where each users may choose its desired cluster topology. As a second approach, we consider a *network-centric* view, where a central entity is steering the clustering of base station into one or multiple clusters. This assumption is motivated by a given network backhauling topology, where certain cooperation between multiple sites may not be possible.

6.2.1 User-Centric Clustering

As practical limitation for cluster size M_c, it will be reasonable to combine as many sectors as can be received within a given received power threshold, measured with respect to the anchor cell. Intuitively, that may appear to be the optimal cluster selection scheme. However, in reality user grouping is hardly possible with the exhaustive number of possible clustering topologies.

The received power of different cells can be efficiently measured using cell-specific reference signal received power (RSRP) using primary synchronization signal (PSS). Note, these PSS are transmitted within a group of 6 resource block (RB) only. Hence, RSRP is obtained on narrow band basis but used as an indicator for cell assignment on the whole 20 MHz bandwidth.

6.2.2 Network-Centric Clustering

Within the network centric approach, we distinguish between *static* and *dynamic* clustering, refer to Figure 6.2:

Static clustering provides a set of clusters which remains fixed. Every sector exclusively belongs to one cluster. Static cluster selection can be either done geo-location based or received-power-based, i.e. user assisted. For the geo-location-based approach the UE is assigned to the cluster where it is located in. In contrast, user assisted static cluster selection offers the possibility to choose the best cluster based on a specific metric, e.g. received sum power connected with different clusters.

The cluster topology significantly affects the system performance using CoMP transmission. Therefore, we chose a given methodology to assess the system behavior as a function of the cluster size M_c. Thus, we subsequently merge additional sectors from the neighboring sites into the given cluster $\mathcal{M}_c$, refer to Figure 6.3. In each of the participating sectors, we will place a certain number of users, while the inter-cluster interference is generated by using codebook entries from LTE specification. The same cluster island concept is used in Chapter 5. Note, the used precoders for interfering cells ensure a spatially uniform transmission of data streams with an PAPC, while each antenna transmits with its maximum power level.

The cluster assignment is based on the UE measurements of the RSRP of the PSS according to [3GP]. The PSS are transmitted within the smallest OFDM bandwidth size of 1.08 MHz. Hence, these power values are determined on a narrow-band basis which can be obtained for a certain number of neighboring cell-ids. Then, the power values are sorted and the ordered list of BSs is conveyed to the cluster of interest. Here, we will distinguish between two selection conditions: First, only the strongest BS needs to be within the cluster and, second, the three strongest sectors must belong to the set $\mathcal{M}_c$. These two handover metrics are abbreviated as top-1

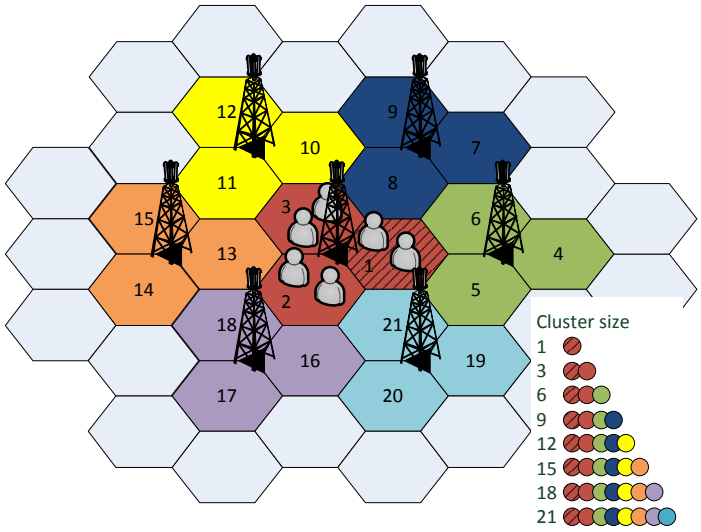

Figure 6.3: Cluster size growing by subsequently adding a 3-sectored site. Numbers in the sectors indicate their corresponding cell-ids.

and top-3. The assignment probability histogram for top-1 and top-3 handover and a cluster size of $\mathcal{M}_c = 3$ is depicted in Figures 6.4(a) and 6.4(b). The selected sector tuple, i.e. cluster, is $\mathcal{M}_c = \{\langle 1\rangle, \langle 2\rangle, \langle 3\rangle\}$, where $\langle x\rangle$ indicates the specific cell-id, refer to Figure 6.3. Note, in each of the three sectors we uniformly place a number of 60 UEs, i.e. a total number of $K_c = 180$ UEs.

In the case of top-1 handover, there are roughly 150 users connected. In contrast, for top-3 handover, we only have an average of 5 to 6 UEs connected to the three sectors within the cluster. If we further assume, each sector to be equipped with $N_t = 4$ transmit antennas, i.e. a total of 12 antennas per cluster, and each UE has $N_r = 2$ receive antennas, top-3 handover provides an average of 12 effective receive antennas, while top-1 allows to select a subset out of 300 tentative receiving points. Since data rates depend on both cluster formation and user grouping, we will compare the system performance when using an appropriate user grouping algorithm within Section 6.3.

The dynamic clustering approach requires the users to choose their desired cluster out of a limited set of overlapping defined clusters. The main difference to the static approach is, that each sector is not exclusively assigned to a single cluster. However, only users which report for the cluster $\mathcal{M}_c$ will be served on the same frequency and time partition. Figure 6.5 depicts the cluster selection sets used for dynamic cluster selection and for a cluster size $M_c = 3$. Here, the cluster selection for the cell of interest can be chosen from six different sets when considering

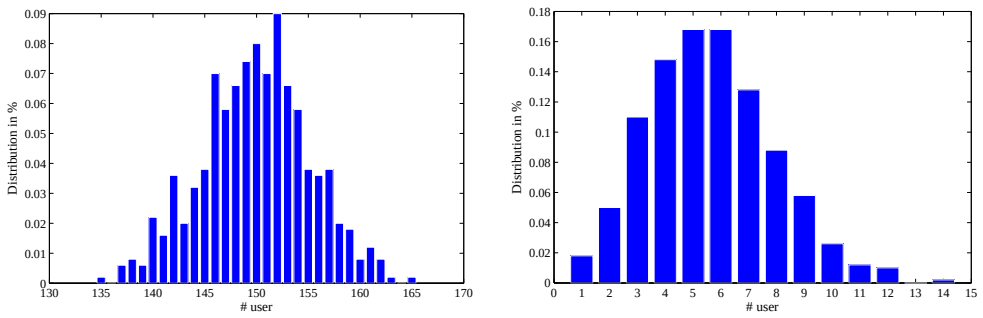

(a) Top-1 (b) Top-3

Figure 6.4: Probability histogram for both handover metrics.

only a cluster size of three for the anchor cell. The remaining clusters were chosen randomly with a uniform distribution for the cluster sizes ranging from one to four.

6.2.3 Sub-Clustering for Feedback Reduction

In Figure 6.2, we presented a hierarchical structure of possible clustering methods. Here, we extended the preferred network-centric clustering towards a user-driven selection of sub-clusters $\mathcal{M}_{c,k} \subset \mathcal{M}_c$. Each user can choose its desired subset e.g. based on the given received power. This results into an overlapping definition of sub-clusters within a static, network-centric cluster $\mathcal{M}_c$. Figure 6.6 depicts this concept, where $M_c = 21$ and the sub-clusters $\mathcal{M}_{c,k}$ with $M_{c,k} \leq M_c$ are chosen on a per-user basis. This is motivated by the assumption of a given network's backhaul topology, where the sub-clustering approach accounts for the specific user requirements in fixed set of BS sectors. In FDD system, where CSI needs to signalized via the precious uplink resources of the terminals, this sub-clustering concept potentially reduces the required feedback overhead. Therefore, we will consider three main direction for these subsets: *Full-sized* subsets, *network-defined* size of clusters and *threshold-based*, i.e. user-driven size of the corresponding sub-clusters. Note, the latter allows for a mode similar to the user-centric cluster selection, but which is restricted by the previously defined static cluster $\mathcal{M}_c$.

The effective cluster dimension A network-defined size for sub-clusters $\mathcal{M}_{c,k}$ allows each user to select e.g. its n-strongest cells out of $\mathcal{M}_c$. Instead to full-sized mode, CSI feedback only includes values for the cell-ids within $\mathcal{M}_{c,k}$ and all other entries $\mathcal{M}_c \backslash \mathcal{M}_{c,k}$ are set to zero entries in the feedback.
In the threshold-based mode, all BSs within a certain range T measured with respect to the anchor cell, are taken into account for the feedback. Therefore, the sub-cluster size is adapted dynamically to the user requirements and hence can differ from one

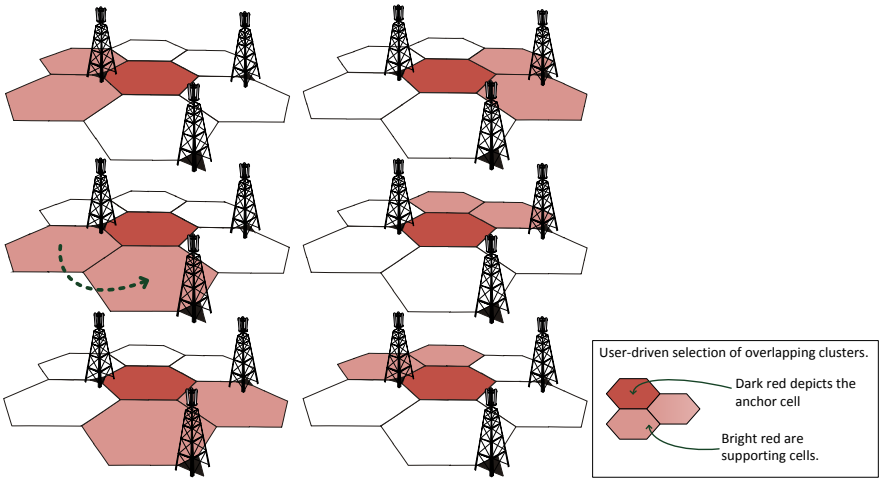

Figure 6.5: Concept of dynamic cluster selection. Each UE may select its desired set of cells out of predefined, network centric clusters; here depicted with cluster size $|\mathcal{M}_c| = 3$.

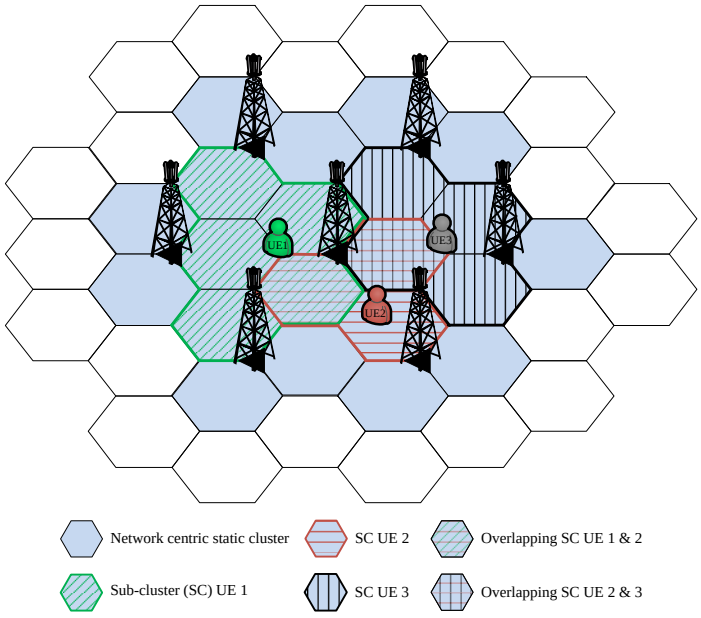

Figure 6.6: Sub-clustering in a huge static cluster with dimension $M_c = 21$.

Table 6.1: Probability for a given dimension of the sub-cluster $\mathcal{M}_{c,k}$.

$\lvert\mathcal{M}_{c,k}\rvert$	$T = 3$ dB	$T = 6$ dB	$T = 10$ dB	$T = 15$ dB	$T = 20$ dB
1	0.74	0.55	0.37	0.21	0.09
2	0.20	0.27	0.26	0.19	0.14
3	0.05	0.13	0.20	0.20	0.16
4	0.01	0.04	0.10	0.15	0.15
5	-	0.01	0.05	0.11	0.14
6	-	<0.01	0.02	0.07	0.11
7	-	-	<0.01	0.04	0.09
8	-	-	<0.01	0.02	0.06
9	-	-	-	0.01	0.04
10	-	-	-	<0.01	0.02
11	-	-	-	<0.01	0.01
12	-	-	-	-	<0.01
$\lvert\mathcal{M}_{c,k}\rvert_{eff}$	1.3	1.7	2.3	3.3	4.6

user to another. In order to determine a practical threshold value we investigate the number of BSs which are in a certain range $T = \{3, 6, 10, 15, 20\}$ [dB] compared to the maximum value. Since we want to avoid effects from the cluster border, we set the cluster size to $M_c = 21$, while only users being placed in the inner sectors $\langle 1, 2, 3\rangle$ are taken into account for evaluation. Results are given in Table 6.1. For this, an effective sub-cluster size can be derived by calculating the sum of the number of BSs multiplied with their corresponding probabilities, which is summarized at the end of the table. The advantage of the threshold-based clustering is that only BSs with a high channel gain are included into the subset. The minor drawback, of an adaptive feedback demand can be at least cut to a maximum amount of e.g. 6 cells within the sub-cluster.

6.2.4 Qualitative Comparison on a Per-User Basis

This section contains initial results for the cluster selection schemes which were introduced in Section 6.2. Results are valid for single user and are obtained on a wide-band received power basis. Network-centric clustering with and without sub-clustering in combination with user grouping algorithms will be reconsidered in Section 6.3. Figure 6.7(a) shows the results using an i.i.d. shadow fading (SF) with a standard deviation of 8 dB, while Figure 6.7(c) contains the results using a geo-correlated SF for a downtilt of 8 degrees. The cluster size was chosen to $M_c = 3$ accordingly. The median SINRs for the different approaches are in the range between 9 and 15 dB. It can be observed that assuming geo-correlated shadow fading the variance of the SINR distribution decreases especially for the user centric approach.

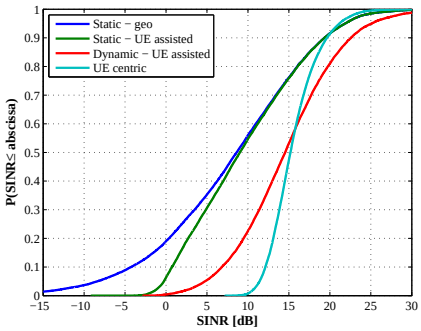

(a) 8° downtilt, i.i.d. SF.

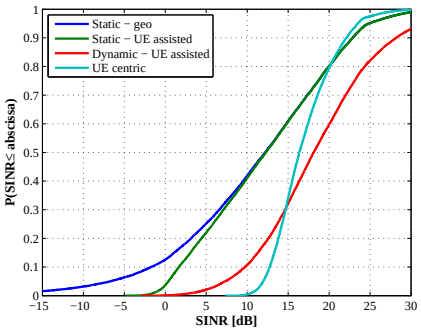

(b) 10° downtilt, i.i.d. SF.

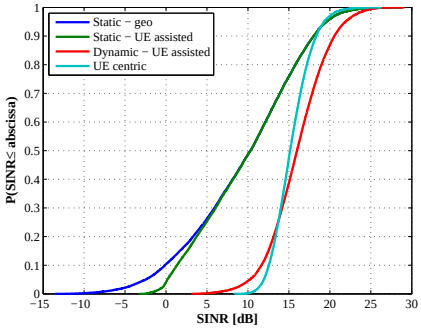

(c) 8° downtilt, geo-correlated SF.

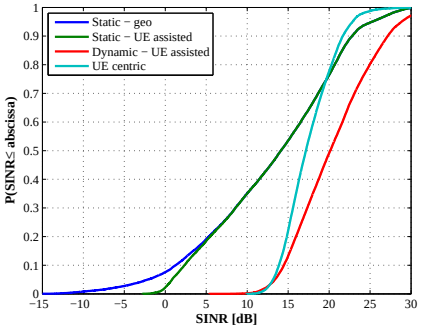

(d) 10° downtilt, geo-correlated SF.

Figure 6.7: Clustering methods: static vs. dynamic vs. user-centric clustering.

The network-centric and dynamic cluster formation performs worse in lower SINR compared to the user-centric cluster selection due to the fact that the user-centric cluster selection is not limited to cluster sizes of three. It simply selects all cells which may be received within a certain received power threshold. In contrast, for high SINR regions the user centric approach may only choose smaller cluster since fewer cooperation partners are within the received power threshold T, while all other methods always choose three cells. Figure 6.7(b) and Figure 6.7(d) show the same trend but using antenna downtilts of 10 degrees.

6.3 User Grouping Strategies

For SDMA service, in particular under a ZF constraint, user grouping methods are of major importance: Merging users, which experience correlated MIMO channels into the same user group will cause a significant reduction in channel norm after precoding [SSH04]. A brute-force user grouping in order to solve (6.1) is known to cause highest computational complexity since each user constellation significantly changes the precoding weights and thus the achievable SINRs at each UE.

Let us assume, that a set of $\mathcal{K}_c$ users reports a set $\mathcal{T}_K$ of tentative receive spaces, i.e. spatial layers, for a certain cluster set $\mathcal{M}_c$. For simplicity, further assume, that this cluster set is defined by the network and hence users can only choose between static defined clusters. The BSs inside the cluster $\mathcal{M}_c$ collect the information and select possible sets $\mathcal{T}_s \subset \mathcal{T}_K$ of receive spaces consisting of $1, 2, \ldots, M_c N_t$ users. Therefore, the scheduler at the BS has to consider up to $\sum_{t=1}^{\min(M_c N_t, |\mathcal{T}_K|)} \frac{|\mathcal{T}_K|!}{(|\mathcal{T}_K|-t)!t!}$ combinations. For $|\mathcal{T}_K| = 20$ and $M_c N_t = 3 \cdot 4 = 12$ transmit antennas we would have to solve the weighted sum rate maximization from (6.1) for $\approx 1 \times 10^6$ times. The authors in [BH06] describe generalization of a greedy user selection approach from [DS05]. This greedy approach significantly reduces the amount of potential candidate sets to $\sum_{t=1}^{\min(M_c N_t, |\mathcal{T}_K|)} |\mathcal{T}_K| - t$. Again, for $|\mathcal{T}_K| = 20$ and $M_c N_t = 12$, we would have to solve (6.1) only 162 times.

First, we will introduce a close to optimum selection algorithm, which combines a greedy user search [BH07b] with a rate approximation criteria described in [FGH06]. After studying the main effects, we will derive a very simple user grouping algorithm where the scheduling itself can be carried out on single-cell basis.

6.3.1 Greedy Rate Approximation

In [BH07b], the authors describe a greedy user selection method. The algorithm is clearly not sum-rate maximizing but has significantly less complexity compared to a brute-force user selection criteria. In general, a brute-force algorithm could be performed by considering all possible sets of users and their reported CSI.

The authors in [BH07b] define $\mathcal{T}_K$ to be the set of all K_c users' eigenmodes. Assuming $N_r < M_c N_t$, each user has at most N_r eigenmodes, and there are a total of $|\mathcal{K}_c| N_r$ eigenmodes in the set $\mathcal{T}_K$, refer to Algorithm 1. On the j-th iteration, they let t_j be the candidate eigenmode chosen among any of the available eigenmodes from any user. On the first iteration, the selected eigenmode t, will be the globally dominant eigenmode. In other words, its eigenvalue is the largest among all users' modes. However, the chosen set $\mathcal{T}_s$ will not necessarily contain the dominant eigenmodes of each user. Note also that not all eigenmodes will necessarily be active. While this greedy algorithm is sub-optimal, [BH07b] states that it achieves a good balance between performance and complexity. It is also totally flexible in that it can handle any combination of $M_c N_t$, K_c and N_r. However, the algorithm still requires the scheduling entity to calculate a considerable amount of SVD operations, since

Algorithm 1 Greedy user selection criteria [BH07b].

initialize $j = 1$, $\mathcal{T}_0 = \emptyset$, $R(\emptyset) = 0$, and $Done = false$
while $(j \leq \min(|\mathcal{K}_c|N_r, |\mathcal{M}_c|N_t))$ and $(!Done)$ **do**
  find $t_j = \underset{t \in \mathcal{T}_K \setminus \mathcal{T}_{j-1}}{\arg\max}\ R(\mathcal{T}_{j-1} \cup \{t\})$
  if $R(\mathcal{T}_{j-1} \cup \{t_j\}) < R(\mathcal{T}_{j-1})$ **then**
    $\mathcal{T}_s = \mathcal{T}_{j-1}$
    $Done = true$
  else
    $\mathcal{T}_s = \mathcal{T}_{j-1} \cup \{t_j\}$
    $j = j + 1$
  end if
end while

the achievable data rate highly depends on the user group.

In order to reduce the computational complexity at the BS side, [FGH06] describes a method to replace the SVD operations by an approximation using subsequent orthogonal projections into the separate users' null-spaces. Therefore, let us define a matrix $\tilde{\mathbf{\Psi}}_k$ which projects the channel matrix $\hat{\mathbf{H}}_k$ of user k into the null-space of $\tilde{\mathbf{H}}_k$. According to (5.23), $\tilde{\mathbf{H}}_k$ contains the others users' channel matrices and choosing any projection into its null-space $\tilde{\mathbf{V}}_k^0$ for downlink service of user k fulfills the ZF condition. The projector of user k is based on the CSI feedback of each user,

$$\mathbf{\Psi}_k = \mathbf{I} - \underbrace{\hat{\mathbf{H}}_k^H \left(\hat{\mathbf{H}}_k \hat{\mathbf{H}}_k^H\right) \hat{\mathbf{H}}_k}_{\substack{=\mathbf{V}_{c,k}\mathbf{V}_{c,k}^H \\ \text{in case of MET}}} \tag{6.2}$$

The projection matrix $\tilde{\mathbf{\Psi}}_k$, which combines all users' null-space except the k-th UE, can be approximated by repeatedly applying

$$\tilde{\mathbf{\Psi}}_k = [\mathbf{\Psi}_1 \cdot \ldots \cdot \mathbf{\Psi}_{k-1}\mathbf{\Psi}_{k+1} \cdot \ldots \cdot \mathbf{\Psi}_{K_c}]^n \text{, with } n \to \infty \text{ as the projection order.} \tag{6.3}$$

Authors in [FGH06] state, that for small projection order, i.e. $n \in \{1, ..., 4\}$ the user grouping performance is already sufficient. As stated in [FDGH07], we use

$$R_k = \log_2\left(1 + \frac{p_{c,k}}{\sigma_n^2} \|\hat{\mathbf{H}}_k \tilde{\mathbf{\Psi}}_k\|_F^2\right) \tag{6.4}$$

as an estimate to assess the link rate for the k-th UE. It may be considered as a lower bound for ZF capacity which may be obtained by using BD. The scheduling entity collects the projectors of already selected UEs and determines the tentative next user by evaluating (6.4) for all residual users or receive spaces. The UE with maximum link rate, i.e.

$$k : \underset{k \in \mathcal{K}_c \setminus \mathcal{T}_s}{\arg\max} \|\hat{\mathbf{H}}_k \tilde{\mathbf{\Psi}}_k\|_F^2 \tag{6.5}$$

Table 6.2: Simulation assumptions.

Parameter	Value
Channel model	According to QUADRIGA [3GP11]
Simulation type	Monte Carlo
Drops	500
Channel evolution	static channel
Scenario	Urban-macro
Propagation	NLOS
Large-scale fading	Geo-correlated parameters maps
Traffic model	Full buffer
f_c	2.6 GHz
Frequency reuse	1
Signal bandwidth	18 MHz, 100 RBs
Inter-site distance	500m
Number of BSs	19 having 3 sectors each
N_t ; spacing	4 ; 4λ
Transmit power	46 dBm
Transmit antenna	Azimuth: FWHM of 58°
	Elevation: FWHM of 6.2°
	10° electrical downtilt
BS height	32m
Beamforming	Cluster-wide MET, ZF constraint
Clustering	Network-centric, sub-clusters optional
User grouping	greedy rate approximation
N_r ; spacing	2 ; $\lambda/2$
UE height	2m
Link-2-System	Shannon, SINRs $\lfloor -\infty, \infty \rceil$ dB

is added to the group of already scheduled users' receive spaces $\mathcal{T}_s$. As an extension, we may change the metric from maximum rate to a metric which ensures some degree of fairness. By employing the score-based metric, we may ensure that each UE is assigned an equal amount of resources within a given time window.

In the following section, we provide performance results on the different clustering concept, described in Section 6.2 and the greedy rate approximation (GRA) user grouping strategy. The simulation assumptions are chosen according to the parameters given in Table 6.2.

Why should we spend the effort for user grouping? Let us consider a network-centric clustering with $M_c = 3$ sectors inside, according to Figure 6.3. In each sector we uniformly drop 60 UEs. Figure 6.8 shows the CDF of the achievable SINRs from active users in $\mathcal{K}_c$. In case of round-robin selection, the maximum number of 12 UEs is selected and served in parallel. While in case of GRA, we adaptively load the cluster with parallel data streams and select those users out of

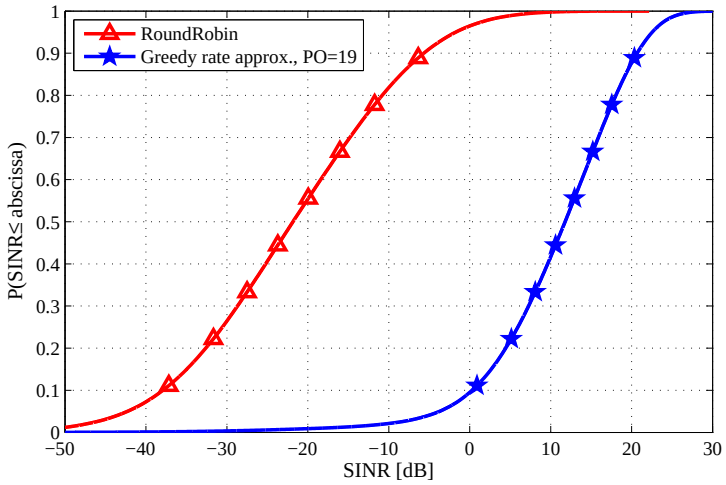

Figure 6.8: Motivation for adaptive user grouping.

$\mathcal{K}_c$ which improve the overall sum-rate. The significant difference in SINRs amounts to 32 dB.

Next, we study the variables of this GRA concept. Therefore, we vary the projection order PO in the range from 1 up to 23. Figures 6.9(a) and 6.9(b) show the resulting SINRs and corresponding Shannon information rates as a function of the projection order PO. It is obvious, that projection order $PO \in \{1, 2, 7\}$ shows a quite poor performance. From simulations we found $PO = 19$ to achieve highest system throughput while supporting good SINRs at the 5% -ile. Increasing the projection order further would improve the per-user SINRs further, but reduces the amount of active data streams, refer to Figure 6.9(c), to a degree where the sum-rate begins to drop.

One characteristic of this metric is an adaptive loading of spatial layers. It stops adding a new data streams when the approximated sum-rate decreases. Thus, it is clear that a sufficiently large set of users is required in order to exploit the multi-user diversity. Figure 6.9(c) depict the multi-user diversity gain as a function of the size of the user group $\mathcal{K}_c$, where $2 \leq K_c \leq 60$. The median sum throughput in 20 MHz bandwidth, increases from 85 Mbit/s/sector to 177 Mbit/s/sector for 2 and 20 users in $\mathcal{K}_c$. Thus, the throughput doubles thanks to the additional multi-user diversity. In contrast, choosing from a user set with $K_c = 60$ only enables additional 23 Mbit/s/sector, i.e. 13% . Note, the user grouping algorithm targets at maximizing the sum throughput and does not take into account any degree of fairness between multiple users.

Let us assume a static, network-centric and received power based clustering from Section 6.2.2 with a top-1 handover, compare Figure 6.4. Thus, Figure 6.11(a) depicts the behavior of the sum rate if we extend the size of cluster $\mathcal{M}_c$ following the

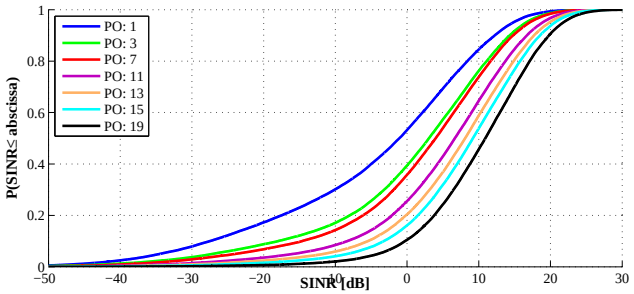

(a) User SINRs after ZF precoding.

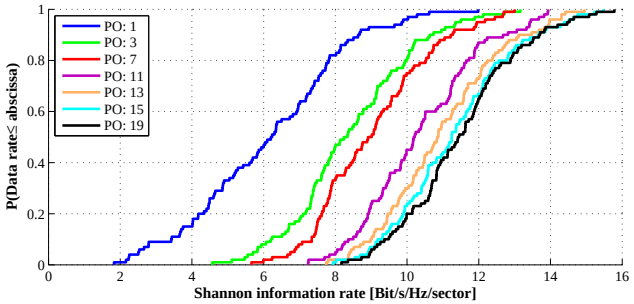

(b) Shannon information rates after ZF precoding.

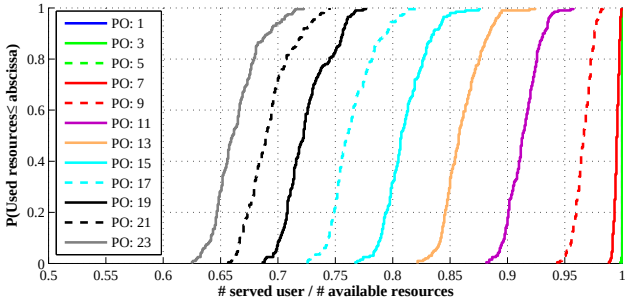

(c) Ratio of served UEs and available transmit antennas.

Figure 6.9: GRA metric as a function of the projection order PO. Cluster size is set to $M_c = 3$.

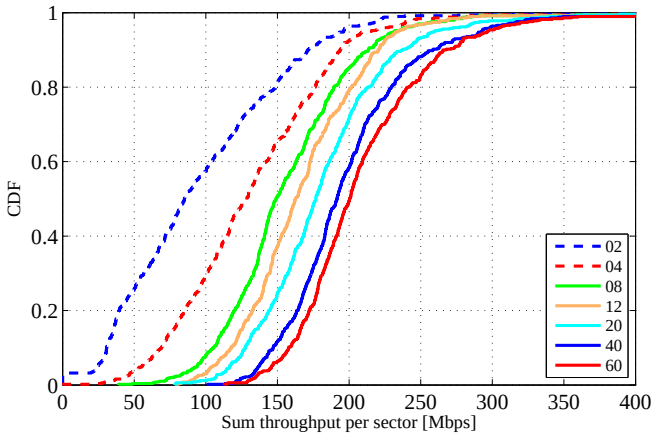

Figure 6.10: Gain from multi-user diversity in a system with $M_c = 1$.

rational from Figure 6.3. A so called *CoMP-gain* is visible, where the additional gains from increasing cluster size are getting smaller. The median throughput per sector improves by 30% from $M_c = 1$ to $M_c = 3$. Another tripling of transmit antennas to $M_c = 9$ yields an additional gain of 15% . Note, at this stage, we will consider full cluster-wide feedback. Feedback reduction using the sub-clustering concept will be considered later. As explained before, the data streams are adaptively loaded based on the cluster size and user feedback. Therefore, Figure 6.11(b) shows the amount of occupied resources as an average over 20 MHz bandwidth. Dividing these values by the overall transmit antennas in the cluster, i.e. $N_t M_c$, leads to a ratio of 0.74 for $M_c = 3$ and the value decreases to 0.62 for $M_c = 21$. This result, that in maximum 3/4 data streams are loaded, will be considered in Section 6.3.2.

For reference purpose, we include results from DPC and limited feedback assumptions, i.e. PMI feedback, according to Sections 6.1 and 3.4. We observe, that the system data rate of the GRA metric could be further increased by 69% with sum-rate maximizing non-linear DPC. Note, the gap is very large due to 2 reasons: First, in contrast to all other schemes, DPC is assuming sum-power constraint at the BS. Second, the user selection criterion leads to significantly different user outage values, i.e. 78% for DPC and 40% for GRA (compare Figure 6.17(a)). However, the limited feedback assumption using PMI feedback is only achieving 85% of the GRA metric and $M_c = 1$. Note, all results are obtained with a link-2-system interface using Shannon information rates.

The sub-clustering concept as described in Section 6.2.3 reduces the amount of feedback significantly. The users choose their desired sub-cluster $\mathcal{M}_{c,k} \subset \mathcal{M}_c$ with a fixed size $M_{c,k}$ out of the predefined network-centric and static cluster area $\mathcal{M}_c$. In Figure 6.12(a) a cluster size from $M_c = 1$ to $M_c = 12$ is given while considering

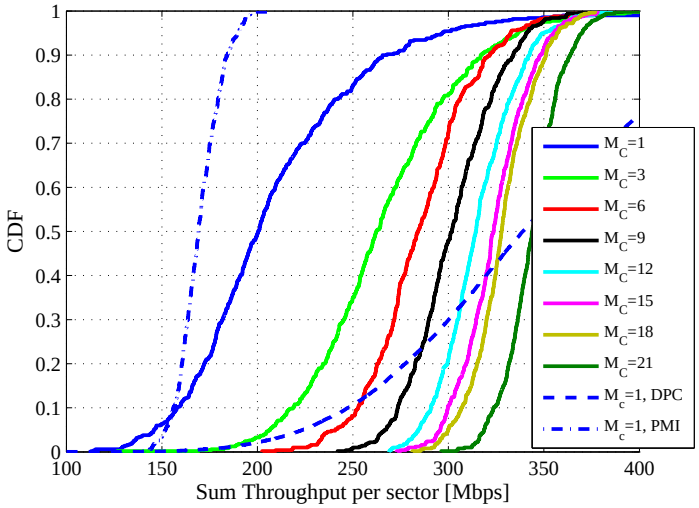

(a) Sum throughput.

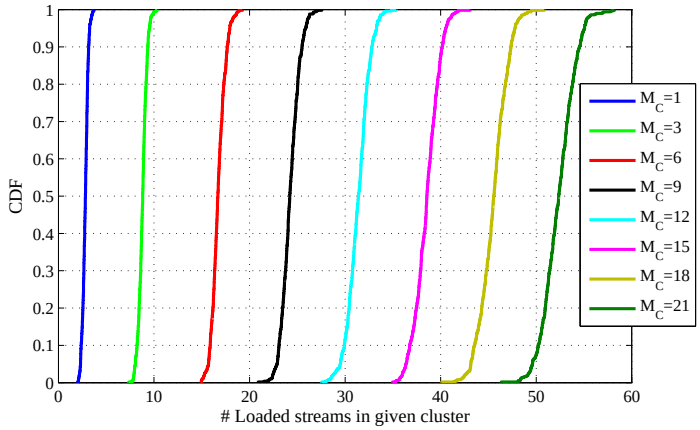

(b) Occupied resources.

Figure 6.11: Sum throughput and number of occupied resources for growing cluster size M_c and full cluster-wide feedback. In addition, we include the BC capacity obtained with DPC for single-cell operation, i.e. $M_c = 1$ in $M = 57$, refer to Section 6.1. Results with limited feedback assumptions from Section 3.4 are shown as $M_c = 1$ and PMI. All data rates are obtained with the same link-2-system interface according to Table 6.2.

$M_{c,k} = \{1, 3, 6\}$. In the left part of this figure, we can find the system configuration with $M_{c,k} = 1$ chosen out of $M_c = \{1, 3, 6\}$. All the median values are in the range of 200 Mbit/s/sector, only the slope of the CDF curves differs slightly due to different user selections. The curves are getting steeper with increasing cluster size which can be seen as an average over more sectors. Figure 6.12(b) focuses on the case of $M_{c,k} = 3$ where the cluster size continuously grows from $M_c = \{3, 6, 9, 12\}$, i.e. each user can select its desired sub-cluster out of a growing, static cluster. It is obvious, that with $M_c = 12$ there is significantly higher chance of finding the globally strongest three sectors compared to $M_c = 3$. For a specific pair of cluster size x and sub-cluster size y we will use the following short notation $\langle x, y \rangle$. From $\langle 3, 3 \rangle$ to $\langle 6, 3 \rangle$ a gain of 7% is shown due to selection diversity of the sub-cluster $\mathcal{M}_{c,k}$. This is confirmed by a further increase of 3% for $\langle 9, 3 \rangle$ and 1% for $\langle 12, 3 \rangle$. Figure 6.13 summarizes these findings for GRA as a function of the sub-cluster size $M_{c,k}$. The left y-axis depicts the median sum rate per sector, while the right y-axis provides rough estimates for the required feedback rate per user. The numbers are obtained based on the assumption, that feedback has to be provided once per 1 ms. The CSI is quantized with 12 bit for amplitude and phase, and independently for each sub-channel: As an example, let us consider $M_{c,k} = 3$. Thus, $\mathbf{H}_{c,k}$ has a number of $\mathcal{T}_k N_t M_{c,k} = 12$ sub-channels.[3] Considering the coherence bandwidth of urban-macro channels, it should be sufficient to report those sub-channels once per RB, i.e. the feedback rate $R_{fb,k}$ attributes to

$$R_{fb,k} = 12 \cdot \mathcal{T}_k N_t M_{c,k} \cdot 100/10^{-3} \text{ bit/s} = 13.7 \text{ Mbit/s}. \tag{6.6}$$

In Figure 6.12(c), it can be seen that $\langle 9, 3 \rangle$ and $\langle 12, 3 \rangle$ experiencing a slightly better performance than $\langle 6, 6 \rangle$ but requiring half of the feedback data because of the selection diversity gain based on the larger cluster size. Another result can be derived from the throughput difference between $\langle 6, 3 \rangle$ to $\langle 6, 6 \rangle$ and $\langle 9, 6 \rangle$ to $\langle 9, 9 \rangle$ which attributes to only 1.4% and 0.6% , respectively. The performance loss caused by inter-sub-cluster interference when excluding the three weakest BSs can be neglected for a cluster size greater than six.

Besides the feedback via the uplink, another important issue is the required traffic rate for the backhaul. Here, CSI feedback in conjunction with the user payload data has to be exchanged between all sectors within the cluster M_c, or at least within the sub-cluster $M_{c,k}$. Again for a rough estimate, let us assume that BSs exchange modulated and coded data, i.e. QAM symbols with e.g. a code rate of 0.5. This simplifies the data exchange, since BSs have to coherently transmit identical data. Thus, the required data rate on the backhaul interface at a certain BS $m \in \mathcal{M}_{c,k}$ is given by

$$R_{bh,m} = R_c(1 + \frac{M_{c,k} - 1}{coderate}) + |\mathcal{T}_s|/M_{c,k}(M_{c,k} - 1)R_{fb,k}. \tag{6.7}$$

[3] Assuming $\mathcal{T}_k = 1$, i.e. feedback for a single spatial layer per UE.

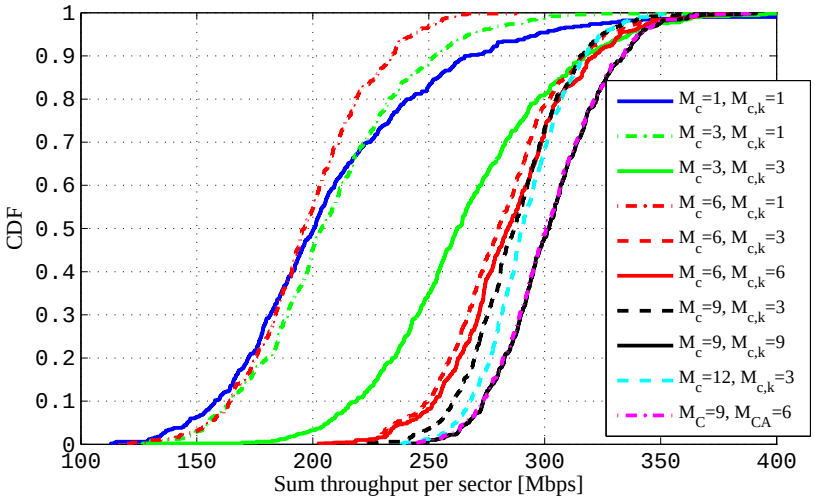

(a) Comparison

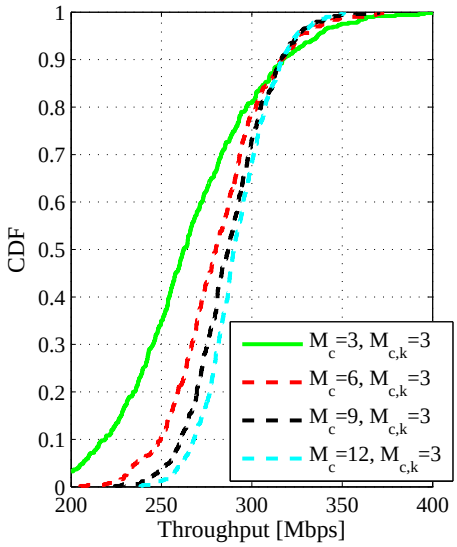

(b) $M_{c,k} = 3$

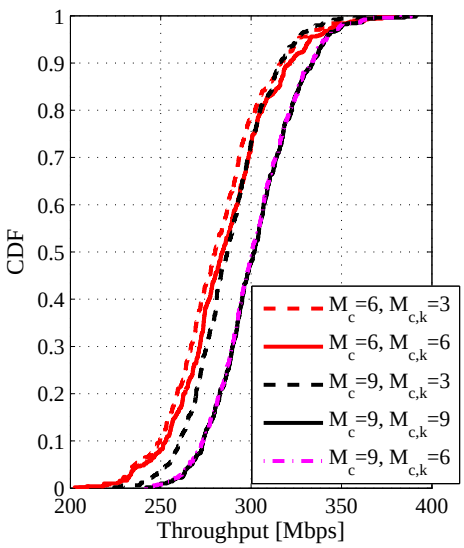

(c) $M_{c,k} = \{6, 9\}$

Figure 6.12: Results for the sub-clustering concept using the GRA metric.

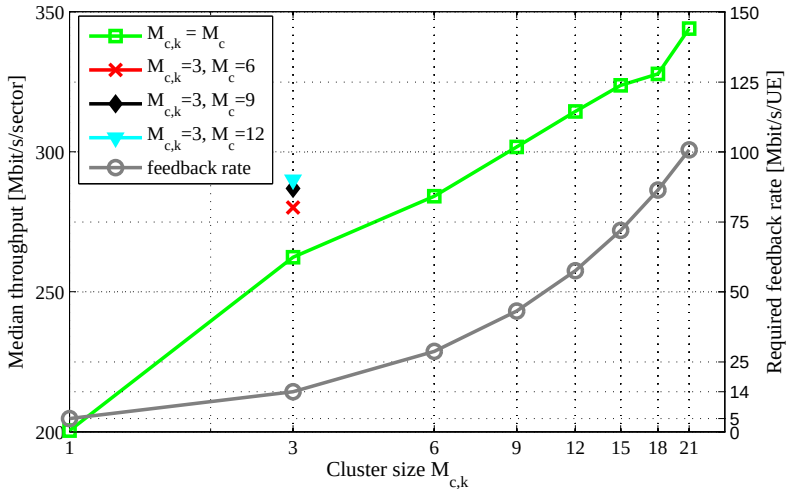

Figure 6.13: Median achievable system rate and required feedback rate as a function of sub-cluster size $M_{c,k}$. For CSI feedback we assume 12 Bit quantization of each complex-valued channel coefficient, for 100 PRBs and feedback interval of 1 ms.

The idea behind the first term is, that BS m has to receive the user data for its own UEs and the modulated data from $M_{c,k}-1$ other cells in the the cluster. The second term, indicates the feedback exchange data rate, while we consider that BS m has to receive feedback data from active users in $\mathcal{M}_{c,k} \setminus \{m\}$. With $M_c = M_{c,k} = 6$ the required backhaul rate is approximated with $R_{bh,m} = 3.05$ Gbit/s $+ 0.2$ Gbit/s. In contrast, with the sub-clustering concept, e.g. $M_c = 12$ and $M_{c,k} = 3$, the backhaul rate is significantly lower with $R_{bh,m} = 1.41$ Gbit/s $+ 0.08$ Gbit/s, while the data rate on the air interface is even slightly higher.

Let us summarize the steps so far. We characterize the data rate scaling behavior of clustered CoMP transmission. Since network backhaul topology will significantly influence the capability of setting up clusters for CoMP transmission, we assume network-centric clustering. In order to save precious uplink resources for CSI feedback, we suggest to enable user-driven sub-clustering. We show that moderate-sized static clusters with small sub-clusters of size $M_{c,k} = 3$ can outperform the symmetric $M_{c,k} = M_c = 3$ case by slightly increasing the feedback overhead, compare Figure 6.13. In contrast to the symmetric case, we have to add the feedback amount for signaling the cell-ids in conjunction with the standard CSI feedback. Since the connection status is changing rather on a slow-fading basis, we can assume this additional overhead in the order of a few kBit/s.

6.3.2 Received Power Based

As a next step, the main target is to simplify the selection criteria for the users which are assigned to a specific cluster $\mathcal{M}_c$ or $\mathcal{M}_{c,k}$. Based on the conveyed downlink user CSI, the cluster determines the sum received power per BS antenna array, which is included in the cluster $\mathcal{M}_c$. For each BS antenna array, the scheduler groups the users according to their individual highest channel gain, yielding $|\mathcal{M}_c|$ different user groups $\mathcal{K}_{c,m} \subset \mathcal{K}_c$. Within the next step, the scheduler selects from each user group $\mathcal{K}_{c,m}$ a certain number of active users. Choosing a subset of users can either be a simple round-robin mechanism, which ensures a certain degree of user fairness, or any other metric, e.g. maximum channel gain. This received power based approach is further divided into a fully and a partially loaded mode.

Fully Loaded System - FLS: In this mode each BS selects as many users out of its user group $\mathcal{K}_{c,m}$ as available transmit antennas. This mode exploits the maximum number of spatial dimensions for SDMA and is henceforth labeled as fully loaded system (FLS).

Partially Loaded System - PLS: Here, the cluster serves multiple users in SDMA, but with additional degrees of freedom for beamforming purpose. The difference to the fully loaded system from before is, that some degree of freedom are used to exploit channel hardening which means that the number of spatial layers is smaller than the maximum number of transmit antennas. The essence, with less constraints for ZF precoding, more transmit power can be directed to the active user set, which is well known as the trade-off between spatial multiplexing and diversity gain.

Simulation Results Again, the simulation assumptions for received power based user grouping are chosen according to the parameters given in Table 6.2. First, we focus on the FLS mode for $N_t = |\mathcal{T}_s| = 4$. Keep in mind that in this mode the maximum number of spatial layers per sector are active and utilized by the scheduling entity. Figure 6.14(a) provides the sum throughput per sector. A negative *CoMP-gain* appears, which attributes to -16% at the median value from $\langle 1,1 \rangle$ to $\langle 3,3 \rangle$. This performance loss further increases with a growing cluster size which can be derived from $\langle 1,1 \rangle$ to $\langle 6,6 \rangle$ where it attributes to -38% . This confirms earlier observations and is caused by the power loss due to the ZF constraint applied for a not appropriate user constellation. In contrast, loading the system only partially, i.e. PLS, trades certain degrees of freedom from multiplexing towards diversity transmission. In particular, these degrees of freedom improve the orthogonality between multiple users, which is also known in the context of channel hardening behavior or diversity transmission in single-link MIMO communications which is currently investigated under the term of *massive MIMO* [Mar10, HCPR11, HtBD11]. Considering the ratio of adaptively loaded streams from Figure 6.11(b), we choose a fixed

ratio of 75% , i.e. $|\mathcal{T}_s| = 3$ spatial layers per sector in $\mathcal{M}_c$ for $N_t = 4$. Figure 6.14(b) confirms our assumption that utilizing transmit diversity to a certain ratio will be better than maximizing the multiplexing degree in joint transmission under a ZF precoding constraint. The essential performance behavior for an increasing cluster size and a partially loaded system (PLS) is similar to the GRA approach. Curves for $M_{c,k} = 1$ are getting steeper with increasing cluster size. Note, for $M_{c,k} = 3$ the same selection gain is shown, for example from $\langle 3, 3\rangle$ to $\langle 9, 3\rangle$ with 11% at the median value.

Remark: The reader may ask himself about the performance loss from $\langle 1, 1\rangle$ to $\langle 3, 1\rangle$ despite the selection gain. This obvious contradiction is explained with the help of Figure 6.15. Yellow users illustrate the case $\langle 1, 1\rangle$. Here, only UEs inside of sector 1 are available in this case, i.e. cell-edge users from sectors 2 and 3, which might ask for service from sector 1 are not considered. Once we move to the case of $M_c = 3$, we uniformly drop the users in all three sectors and thus, it brings those cell-edge UEs into the game. These users are marked yellow but are located in sectors 2 and 3. Remember that in PLS all users are served, which means that these users, having poor channel conditions, will surely be considered over spatial and frequency domains.

Next, we focus on adaptive sub-clustering using certain threshold for received power to choose the corresponding subset $\mathcal{M}_{c,k}$. These thresholds T are evaluated in the range of 10 and 15 dB. As a result, the topology of the sub-clusters is tailored to the different user locations and thus to their needs. In essence, now we can combine users which report on different, tentatively overlapping sub-clusters with $1 \leq M_{c,k} \leq M_c$. Figure 6.16 shows the sum throughput per sector for $M_c = 3$ and $M_{c,k}$ based on a 10 dB power window. Reveal from Table 6.1, that the effective cluster size is given by $M_{c,k} = 2.3$. With this knowledge it is obvious that the system performance should be in the range of $\langle 3, 3\rangle$ and $\langle 3, 1\rangle$. Similar to the fixed sub-cluster size, a selection gain can be exploited from a larger cluster size.

Finally, as a last issue, Figure 6.17 compares the different user grouping strategies and their impact on the per-user rates, i.e. fairness in the scheduling step. In contrast to the sum rate, the user rates demonstrate a superior behavior of the received power based user grouping compared to the GRA. The GRA algorithm shows its typical sum-rate maximizing distribution: The dashed blue line has 37% outage from all connected users in the cluster. Beside the outage, 91% of all users experiencing less rate compared with to PLS in the $\langle 3, 3\rangle$ constellation. From the curve characteristics it is now clear that a significant fraction of system performance gain with GRA is exploited by only a few users but with extremely high data rates. Note, this is only possible by applying Shannon rates instead of a practical link-to-system interface using standard mapping curves. The key performance indicator, i.e. 5% user throughput highlights the advantage of the PLS strategy over the FLS and GRA.

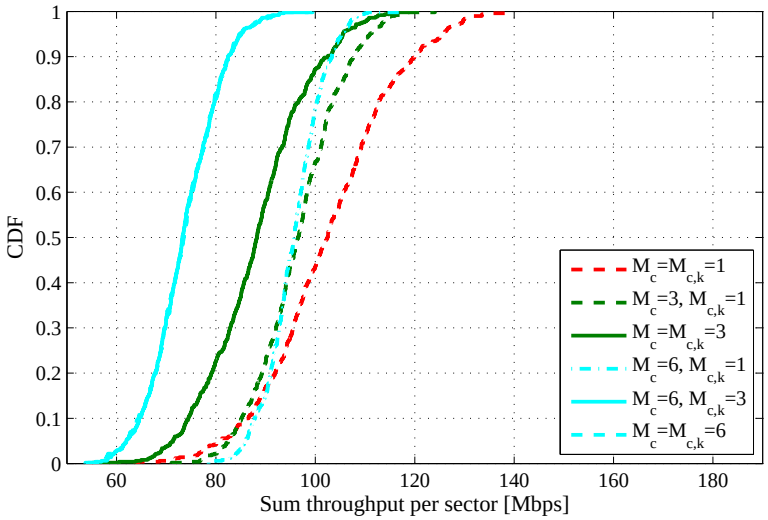

(a) Fully Loaded System - FLS

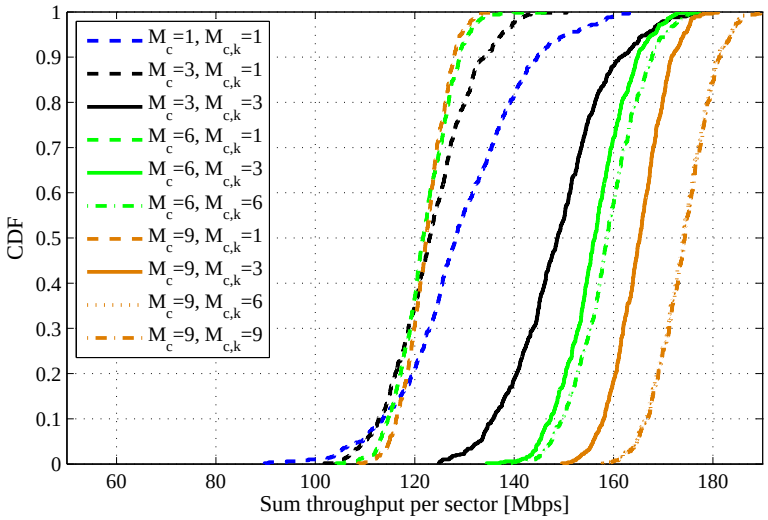

(b) Partially Loaded System - PLS

Figure 6.14: Fully loaded vs. partially loaded system with received power based grouping.

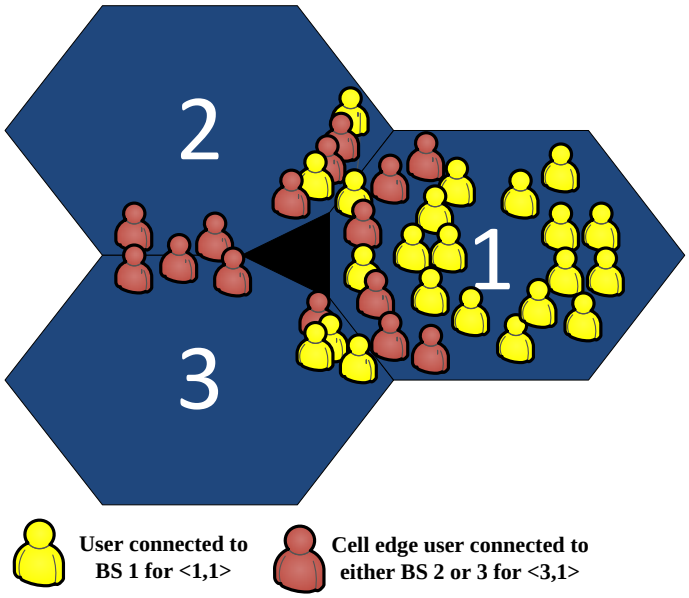

Figure 6.15: Cell-edge user problem shown for the case of sub-cluster size $M_{c,k} = 1$. Yellow users are connected to cell id 1.

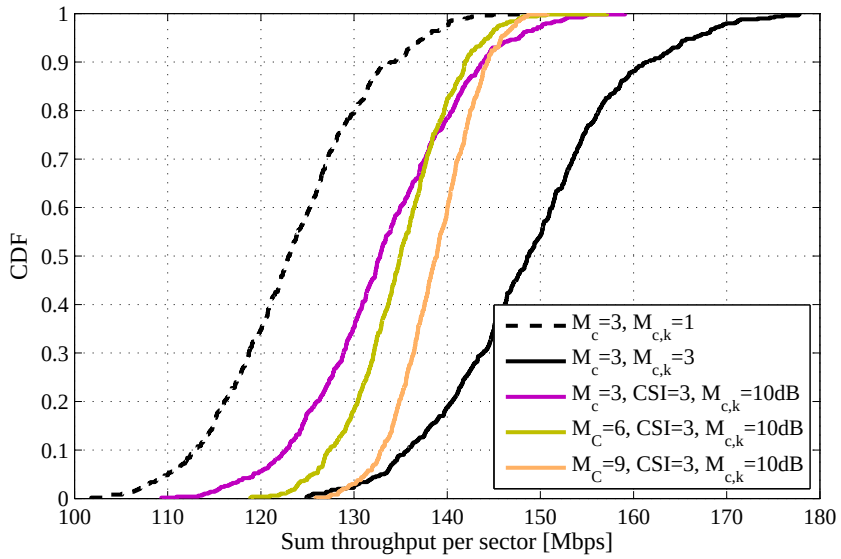

Figure 6.16: Threshold based sub-clustering using received power based user grouping with PLS.

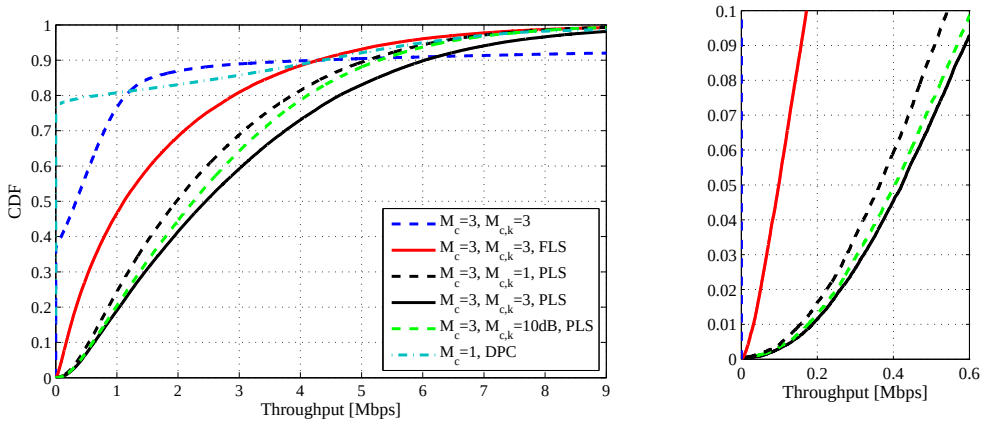

(a) Overall user throughput.

(b) Cell-edge.

Figure 6.17: User throughput indicating 40% outage for the GRA metric. Note, single-cell processed DPC leads to 78% outage.

6.4 Influence of Channel Aging in CoMP Transmission

By exploiting channel adaptive spatial precoding we can actively reduce the interference inside a cluster of cooperating BSs, denoted as CoMP transmission. Despite the fact of using ZF beamforming, practical systems will always suffer from intra-cluster interference. There is a variety of reasons which destroy the inter-user orthogonality: Channel estimation and quantization, channel aging effects and synchronization errors of multiple BSs. In practical systems, there is always a delay between the channel estimation at the mobile terminal, the feedback of CQI and CSI and the time instant when this estimate is used for composing the following downlink transmission, refer to Figure 6.18. The Rx delay is motivated by the fact, that CSI data cannot be transmitted instantaneously to the serving base station. Thus, data has to be split among several uplink symbols. Whereas the transmission delay is mainly influenced by the scheduling decisions. As the channel may change within this time duration, the channel observation may be outdated for precoding the next transmission. Reference [PNJvH03] provides a characterization of the channel evolution due to this aging process for point-to-point MIMO links. However, it assumes equal channel gain for all the links, which is not appropriate for JT CoMP. In addition, UEs may provide feedback information within a certain interval. [JCUC12] investigates a robust design of linear precoding under quantized channel feedback in combination with past channel information [CJCU08].

Let us consider a cellular OFDM downlink where a central site is surrounded by multiple tiers of sites. We assume each site to be partitioned into three 120° sectors, i.e. the system model covers a set $\mathcal{M}$ consisting of $M = |\mathcal{M}|$ sectors in total. Each sector constitutes a cell transmitting its own id. $\mathcal{M}_c$ represents the set of cells included in a given cluster and $M_c = |\mathcal{M}_c|$ denotes its size. Furthermore, we consider an interference limited setup, such that frequency resources are fully reused in all M cells. In order to limit the overhead for pilots and signalization data to a practical range, we focus on rather small clusters. We assume disjoint clusters, i.e. a given BS cannot belong to more than one cluster operated at the same time/frequency resource. For OFDM systems, the overlap of multiple clusters can be achieved conveniently in the frequency domain. Joint processing is only allowed between BSs belonging to the same cluster, where BSs outside the cluster are not coordinated and thus cause residual inter-cluster interference. Furthermore, dynamic clustering allows a more efficient power allocation. Mobile users experiencing a weak channel to a given cluster are assigned to another BS cluster [BHA08].

In [MTO+11], we focused on synchronization. The contribution of this work is to evaluate the effects caused by channel aging. Therefore, we carefully model the channel time evolution by modeling multiple Doppler components as required for multi-path propagation in a mobile user scenario. Thus, the channel behaves quasi-deterministic over time and frequency. In addition, we evaluate the discrepancy when simplifying the multiple Doppler components into a zero mean AWGN process at a given error variance. First, we will describe our system model in Sec-

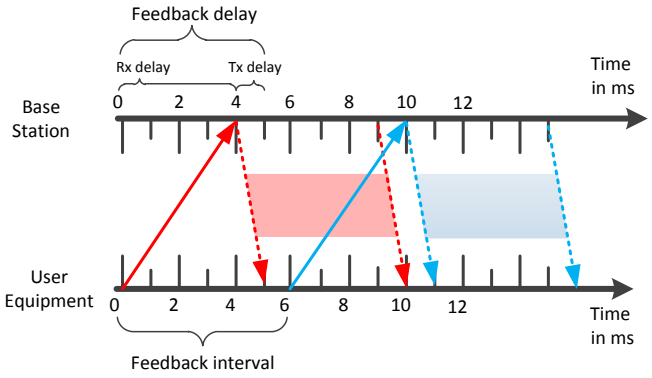

Figure 6.18: Definition of feedback delay and feedback interval according to 3GPP specifications.

tion 6.4.1. Second, we introduce a mismatch between the ideal channel and its estimated or delayed version by evaluating the corresponding rMSE and its average value. Section 6.4.2 therefore assumes a zero mean AWGN error distribution with different variances μ. In Section 6.4.3, we will study different liner frequency domain channel prediction methods and their performance in an isolated MIMO link. A study of the properties of such CSI errors as well as an overall performance evaluation, including precise modeling of channel time evolutions, is carried out in Sections 6.4.4 and 6.4.5.

6.4.1 Time-Variant System Model

In order to describe the effect of outdated channel knowledge, we extend the system model description from (5.1). We define $x_{c,t}(n)$ as the data symbol to be transmitted on the downlink and $\mathbf{H}_{c,k}(n)$ as the MIMO channel matrix at time instance n. $[\mathbf{B}_{c,k}]_{:,t}\,(n-\tau)$ denotes the precoding matrix used at time n but based on a τ-old estimate of the channel. Let us assume the precoder to follow a ZF constraint, which can be obtained using the Moore-Penrose pseudo inverse in case of MISO CSI feedback

$$[\mathbf{B}_{c,k}]_{:,t}\,(n-\tau) = \mathbf{H}_{virt}^{H}(n-\tau)\left[\mathbf{H}_{virt}(n-\tau)\mathbf{H}_{virt}^{H}(n-\tau)\right]^{-1}. \tag{6.8}$$

The total transmit power is equally distributed among all active data streams, while we maintain a PAPC by using a simplified solution from [ZD04]. The transmit power per antenna is chosen according to the row element in $\mathbf{B}_c$ with highest norm.

In addition, we may define a *difference matrix* $[\mathbf{\Delta}_k]_{:,t}\,(n,\tau)$ that relates the τ-old channel inverse with the current precoder as $[\mathbf{B}_{c,k}]_{:,t}\,(n) = [\mathbf{B}_{c,k}]_{:,t}\,(n-\tau) + [\mathbf{\Delta}_k]_{:,t}\,(n,\tau)$.

The received signal $\mathbf{y}_{k,t}(n)$ at the discrete time index n is given by,

$$\begin{aligned}
\mathbf{y}_{k,t}(n) &= \mathbf{H}_{c,k}(n)\left[\mathbf{B}_{c,k}\right]_{:,t}(n-\tau)\sqrt{p_{c,t}}x_{c,t}(n) \\
&\quad + \sum_{j\in\mathcal{T}_s\setminus\{t\}} \mathbf{H}_{c,k}(n)\left[\mathbf{B}_{c}\right]_{:,j}(n-\tau)\sqrt{p_{c,j}}x_{c,j}(n) + \mathbf{z}_k(n) \\
&= \mathbf{H}_{c,k}(n)\left[\left[\mathbf{B}_{c,k}\right]_{:,t}(n) - \left[\boldsymbol{\Delta}_k\right]_{:,t}(n,\tau)\right]\sqrt{p_{c,t}}x_{c,t}(n) \\
&\quad + \sum_{j\in\mathcal{T}_s\setminus\{t\}} \mathbf{H}_{c,k}(n)\left[\left[\mathbf{B}_{c}\right]_{:,j}(n) - \left[\boldsymbol{\Delta}_k\right]_{:,j}(n,\tau)\right]\sqrt{p_{c,j}}x_{c,j}(n) \\
&\quad + \mathbf{z}_k(n)
\end{aligned} \tag{6.9}$$

And the equalized signal after ZF precoding simplifies to

$$\begin{aligned}
\mathbf{w}_{k,t}^H(n)\mathbf{y}_{k,t}(n) &\overset{(5.27)}{=} \left(\beta_{c,t} - \mathbf{w}_{k,t}^H(n)\mathbf{H}_{c,k}(n)\left[\boldsymbol{\Delta}_k\right]_{:,t}(n,\tau)\right)\sqrt{p_{c,t}}x_{c,t}(n) \\
&\quad + \sum_{j\in\mathcal{T}_s\setminus\{t\}} \left(0 - \mathbf{w}_{k,t}^H(n)\mathbf{H}_{c,k}(n)\left[\boldsymbol{\Delta}_k\right]_{:,j}(n,\tau)\right)\sqrt{p_{c,j}}x_{c,j}(n) \\
&\quad + \mathbf{w}_{k,t}^H(n)\mathbf{z}_k(n) \\
&= \underbrace{\left(\beta_{c,t} - \mathbf{w}_{k,t}^H(n)\mathbf{H}_{c,k}(n)\left[\boldsymbol{\Delta}_k\right]_{:,t}(n,\tau)\right)\sqrt{p_{c,t}}x_{c,t}(n)}_{\overline{\mathbf{h}}_k} \\
&\quad \underbrace{- \sum_{j\in\mathcal{T}_s\setminus\{t\}} \mathbf{w}_{k,t}^H(n)\mathbf{H}_{c,k}(n)\left[\boldsymbol{\Delta}_k\right]_{:,j}(n,\tau)\sqrt{p_{c,j}}x_{c,j}(n)}_{\boldsymbol{\vartheta}_{k,t}} \\
&\quad + \mathbf{w}_{k,t}^H(n)\,\mathbf{z}_k(n)
\end{aligned} \tag{6.10}$$

From Equation (6.10) it becomes obvious that the feedback delay τ causes a time-variant change in the desired channel vector $\overline{\mathbf{h}}_k$ and causes intra-cluster, i.e. inter-user, interference $\boldsymbol{\vartheta}_{k,t}$ depending on the column vectors $\left[\boldsymbol{\Delta}_k\right]_{:,j}(n,\tau)$ from matrix $\boldsymbol{\Delta}_k(n,\tau)$, as it breaks the inverse relationship between the channel and the precoder.

6.4.2 Modeling Imperfect CSIT

For sake of completion, let us briefly summarize some results from Section 5.2.6. In general, we may describe the mismatch between the ideal channel and its estimated or delayed version by evaluating the corresponding rMSE per user k as well as the overall average μ, refer to Equations (5.32) and (5.33). In the following, we evaluate the system level performance of CoMP transmission using MET [BH07b, NMK+07] and a dynamic cluster selection and a round-robin scheduling metric for active UEs [TJH10]. We assume each UE to decompose its MIMO channel matrix into its dominant eigenspaces, where only the dominant one is used for feedback. In particular, we reveal results based on CSI feedback from UEs and an additional error drawn from a zero mean i.i.d. Gaussian distributed term with variance μ,

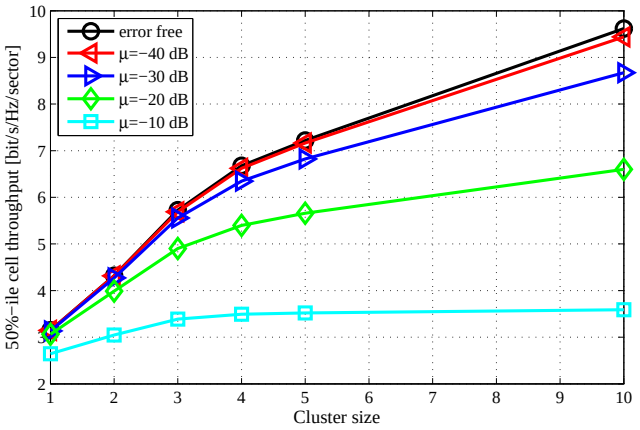

Figure 6.19: Performance results as a function of the cluster size M_c. The normalized MSE is per sub-channel, i.e. in case of $M_c = 10$ sectors in the cluster, each equipped with $N_t = 2$ antennas, the UE estimates up to $M_c \times N_t = 20$ sub-channels with a zero mean i.i.d. Gaussian distributed error with variance μ. Users are equipped with $N_r = 2$ receive antennas.

according to (5.33) per sub-channel. This non-perfect CSI is used at the BSs to calculated the ZF precoding solution.

The erroneous feedback results in a more severe degradation with increasing cluster size. Finally, we increase the cluster size from $M_c = 1$ up to $M_c = 10$. Figure 6.19 depicts the resulting Shannon information rate per sector as a function of the cluster size M_c and accuracy of CSI feedback, i.e. in case of error free and erroneous channel feedback. From this figure, it is obvious that an rMSE with an average of $\mu = -10$ dB would restrict the useful cluster size to $M_c = 3$. In essence, the CoMP gains as a function of the cluster size show less saturation behavior for improved multi-cell channel knowledge. Concluding, we observe that the median sector spectral efficiencies are increased by 220% , 300% and 430% for coordinating 3, 5 and 10 cells for error free CSI feedback, respectively. These numbers are reduced to 190% , 230% and 300% in case of erroneous feedback with an average rMSE of $\mu = -20$ dB.

6.4.3 Predicting the Channel's Time Evolution

In this section, we want to characterize the range of channel degradation using different linear channel prediction filters. This section briefly summarizes the state of the art as e.g. given in [Say08]. We first introduce the Wiener filter approach, indicating the main challenge of obtaining knowledge on the autocorrelation function (ACF) of the channel which needs to be predicted. Since this challenges is hardly feasible, adaptive filter algorithms such as normalized least-mean-squares (NLMS)

and recursive least squares (RLS) are put into the focus of research.

Let us define $h_{c,k}^{11}$ to be the 1st sub-channel coefficient of a MIMO channel matrix $\mathbf{H}_{c,k}$ on a given frequency block. Further assume, $\mathbf{h}_{c,k}^{11}(n)$ being a row vector with the last p observations of the channel frequency response, i.e.,

$$\mathbf{h}_{c,k}^{11}(n) = \left[h_{c,k}^{11}(n-p+1)\dots h_{c,k}^{11}(n)\right]. \tag{6.11}$$

Then the predicted channel response at time instant $n+\alpha$ is given as

$$\hat{\mathbf{h}}_{c,k}^{11}(n+\alpha) = \mathbf{h}_{c,k}^{11}(n)\,\boldsymbol{\omega}_n. \tag{6.12}$$

The optimal weight vector which minimizes the MSE follows from the solution of the normal equations [WFHE04], and is given as

$$\boldsymbol{\omega}_n = \left(\mathbf{R}_{h_{c,k}^{11}(n)} + \sigma_{est}^2\mathbf{I}\right)^{-1}\mathbf{r}_{n,\alpha}, \tag{6.13}$$

with σ_{est}^2 being the estimation error variance[4], and

$$\mathbf{r}_{n,\alpha} = \left[r_{h_{c,k}^{11}(n)}(\alpha+p-1) \quad \cdots \quad r_{h_{c,k}^{11}(n)}(\alpha)\right]^{\mathrm{T}}, \tag{6.14}$$

$$\boldsymbol{R}_{h_{i,m}^{11}(n)} = \begin{bmatrix} r_{h_{c,k}^{11}(n)}(0) & r_{h_{c,k}^{11}(n)}(1) & \dots & r_{h_{c,k}^{11}(n)}(p-1) \\ r^*_{h_{c,k}^{11}(n)}(1) & r_{h_{c,k}^{11}(n)}(0) & \dots & r_{h_{c,k}^{11}(n)}(p-2) \\ \vdots & \vdots & \dots & \vdots \\ r^*_{h_{c,k}^{11}(n)}(p-1) & r^*_{h_{c,k}^{11}(n)}(p-2) & \dots & r_{h_{c,k}^{11}(n)}(0) \end{bmatrix}, \tag{6.15}$$

and

$$\begin{aligned} r_{h_{c,k}^{11}(n)}(\tau) &= \mathbb{E}_n\left\{h_{c,k}^{11}(n+\tau)\left(h_{c,k}^{11}(n)\right)^*\right\} \\ &\approx \frac{1}{M}\sum_{n=0}^{M-1-\tau} h_{c,k}^{11}(n+\tau)\left(h_{c,k}^{11}(n)\right)^*. \end{aligned} \tag{6.16}$$

In (6.16), we use the sample ACF [Orf88, WFHE04] to estimate the ACF over the last $M \geq \alpha + p$ samples of the channel response. If not stated differently, we use $M = 100$ and $p = 20$ throughout this work, and solve Equation (6.13) at every time instant. Even though the linear system (6.13) may be solved with computational complexity $O(p^2)$ using the Levinson-Durbin recursion [GV96], this approach has comparable high computational complexity and memory requirements. Furthermore, we estimate the ACF over the whole channel, and use (6.13) to obtain

[4] We model the estimation error as AWGN with zero mean and variance $\sigma_{est}^2 = \frac{\mathrm{SNR}_{\mathrm{est}}}{\mathbb{E}\left\{\left|h_{c,k}^{11}\right|^2\right\}}$.

Table 6.3: Parameter assumption for channel prediction.

Default value	Description	Affected algorithm
$\lambda = 0.99$	Forgetting factor	RLS
$\epsilon = 0.01$	Regularization parameter	NLMS & RLS
$M = 100$	Memory length	Wiener
$p = 20$	Filter order	all
$\alpha = 5$ ms	Prediction horizon	all
$d = 1$ ms	Channel sample spacing	all

a nearly optimal predictor. This filter is denoted as Wiener$_{M\to\infty}$ and will be used to assess the performance of the considered prediction algorithms. Since this challenge is hardly feasible in practice, we draw our attention to adaptive filters.

Adaptive algorithms, e.g. the well-known NLMS and RLS filters [Say08], can be designed to converge towards the optimal solution of Wiener$_{M\to\infty}$. However, they need to be trained to adapt to the current channel statistics while a so-called forgetting factor λ steers the impact of τ-old channel estimates. An appropriate selection of λ is mandatory in order to optimize the trade-off between excess mean square error (EMSE) and convergence time. For the RLS filter, we chose the QR-decomposition (QRD) based implementation since it has superior numerical properties in finite precision. Note, that there exists fast RLS algorithms with only $O(p)$ operations per iteration [Say08, Ch. 37-43], as opposed to $O(p^2)$ in case of the classical implementation, which may be applied to this problem. Since those variants are more difficult to implement than QRD-RLS, and computational complexity is not an issue in our work, we do not consider them further.

Figures 6.20(a), 6.20(b) and 6.20(c) depict the tracking performance and the performance of ZF beamforming in a single 2×2 MIMO link. The blue solid line, denoted as perfect, depicts the MIMO link performance with noisy channel estimation but with instantaneous feedback. The blue dashed line, i.e. degraded, shows the effect from feedback out-dating, which becomes prominent from 10 dB SNR for channel estimation. Furthermore, we observe that in the low SNR regime time-domain filtering such as RLS not only improves the channel tracking performance but also has a de-noising character in the poor channel estimation regime, compare red and blue solid lines for $SNR \leq 15$ dB in Figure 6.20(c). Channel prediction parameters are summarized in Table 6.3.

It is shown that the RLS filter performs close to Wiener$_{M\to\infty}$ performance if the memory length is chosen large enough, i.e. in our case $\lambda = 0.99$ as forgetting factor. Figure 6.21 shows that our standard choice of $\lambda = 0.99$ is a fairly decent trade-off between convergence time and EMSE. As λ grows towards 1, the EMSE vanishes but the convergence time grows. We expect that the tracking performance in a non-stationary environment will suffer from a large λ. On the other hand, a small λ will

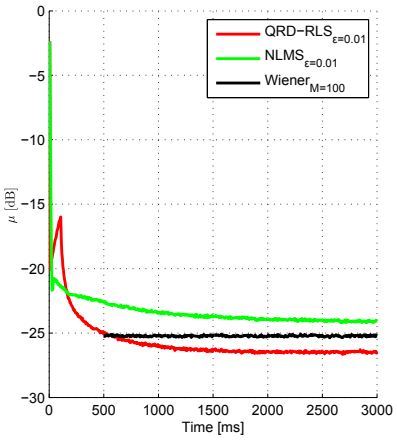

(a) Tracking perf. 3 km/h

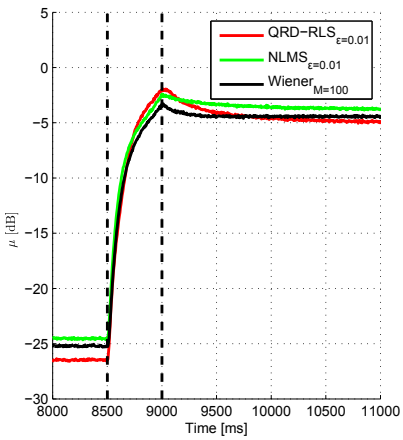

(b) Transition to 50 km/h

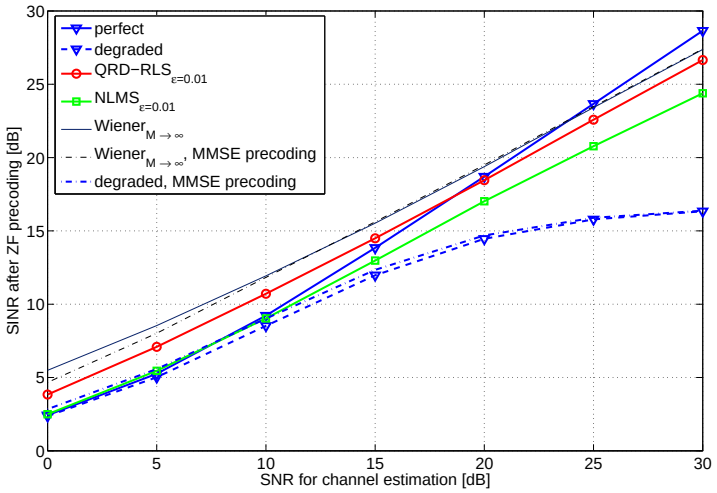

(c) ZF beamforming in 2×2 MIMO channel

Figure 6.20: Channel prediction performance with $p = 20$, both feedback delay τ and interval is set to 5 ms. The channel coefficients are generated using SCME with 3 km/h or 50 km/h mobility; observation duration is 18'000 ms. In (b), we linearly cross-fade the channels having 3 km/h into channels, where UEs move with 50 km/h, in order to estimate the tracking behavior when channel statistics are changing significantly.

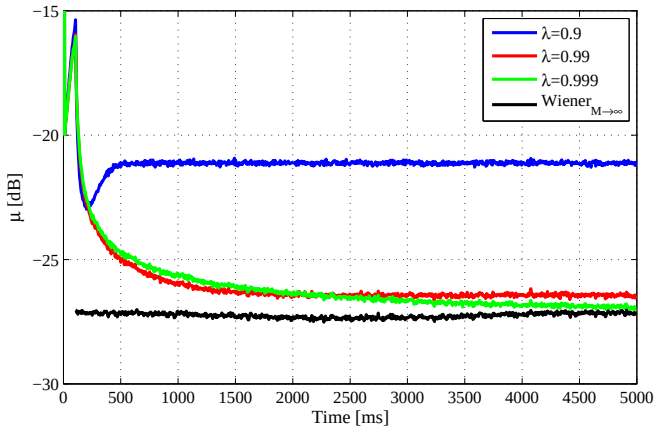

Figure 6.21: Impact of different memory lengths λ on the transient behavior of RLS, obtained from 10000 channel realizations and with a user mobility of 3 km/h.

result in a larger EMSE. We can conclude, that the memory length has to be chosen with great care, and dependent on the scenario. In a high mobility environment, for example, the time in which we can assume the channel to be stationary is very short. Therefore, the memory length has to be relatively small to improve tracking performance. We also evaluated the impact of different regularization parameter ϵ but did not observe any notable effects as long as we chose ϵ rationally.

6.4.4 Error Distribution Properties

In particular, Figure 6.22(a) depicts the median rMSE at different time instances, i.e. after certain settling times of the prediction filter. The error starts at a relatively low value, then rises until the RLS, at this stage, covered insufficient channel statistics while the probability for a changing channel is increasing. After a certain settling time, channel statistics get more sufficient and thus the error starts dropping and converges to a minimum value. Note, for the selected time window of 500 ms, cannot cover the entire transient response, and thus we cannot observe this convergence behavior.

Figure 6.22(b) depicts the error probability distribution function (PDF) for both an artificial AWGN error with an average rMSE of $\mu = -34$ dB and the resulting μ obtained from the system with continuous time evolution. The feedback delay is set to $\tau = 10$ ms and the performance observed after a settling time of 410 ms. In principle, both distributions are comparable. However, the error caused by channel aging is not of Gaussian shape, larger errors occur less frequent compared to the AWGN reference curve. Within the next section, we will derive the resulting system throughput by extensive computer simulations.

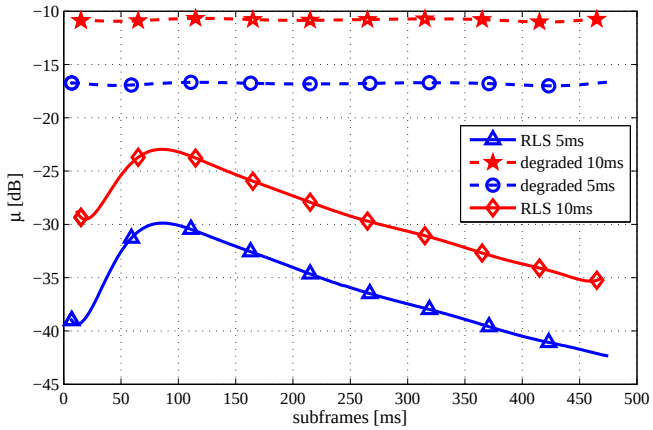

(a) rMSE

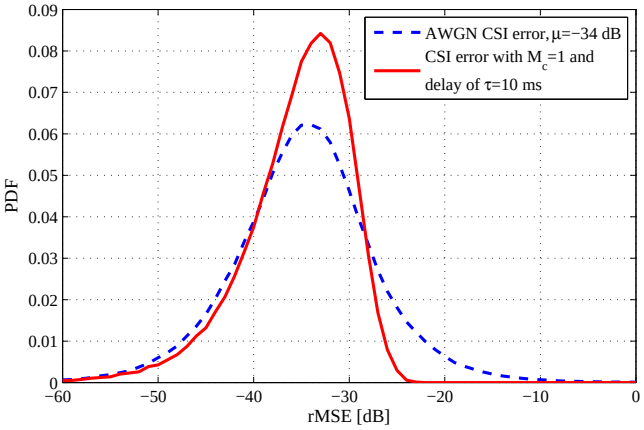

(b) Error probability density functions

Figure 6.22: CSI error properties due to delayed channel feedback for cluster size of $M_c = 1$. The lower figure shows the error PDF caused by a feedback delay of $\tau = 10$ ms and the settling time is set to 410 ms. For comparison we include an AWGN error for CSI feedback with $\mu = -34$ dB.

6.4.5 System Level Simulation including Channel's Time Evolution

In this section, we discuss the results we obtained from our system level simulations. Each UE is assumed to provide CSI and CQI feedback under the assumption of its own dominant eigenmode vector with respect to the cluster $\mathcal{M}_c$. Based on the conveyed downlink user CSI, the cluster determines the sum received power per BS antenna array. For each BS, the scheduler groups the users from $\mathcal{K}_c$ according to their individual highest channel gain, yielding M_c different user groups $\mathcal{K}_{c,m} \subset \mathcal{K}_c$. Within the next step, the round-robin[5] scheduler entity selects from each user group $\mathcal{K}_{c,m}$ a 3 different users for SDMA service, such that the number of active spatial layers $\mathcal{T}_s$ from the cluster $\mathcal{M}_c$ is given by $M_c(N_t - 1) = |\mathcal{T}_s|$. Hence, we reserve one antenna per BS for transmit diversity. A detailed list of the properties of the multi-cell channel and corresponding system-level simulation parameters are given in Table 6.4.

Figures 6.23(a), 6.23(b) and 6.23(c) show the performance results for a cluster size of $M_c = 1$, i.e. intra-cell interference nulling, for the 5% -ile, 95% -ile and 50% -ile system throughput. Note, system and per-user throughput will behave similarly, since we employ a round-robin user scheduling metric from Section 6.3.2 under the premises of a partially loaded system (PLS). This scheduling policy selects users independent from their CQI feedback. PLS simply ensures that each BS is transmitting less spatial layers than available transmit antennas, i.e. $T_s < N_t$.

In detail, Figure 6.23 depicts the loss due to channel aging, while the x-axis is scaled in intervals of the coherence time T_c. The y-axis is normalized to the maximum achievable data rate for $\tau = 0$ ms feedback delay, i.e. the scheme which performs best in the current study under ideal feedback conditions. In general, we assume CSI feedback based on the MET metric, while the UEs use different weights for receive processing. In case of the blue lines, we compare the system performance when both CSI feedback and final receive processing rely on the MET scheme. The red lines depict the system assuming MMSE receive processing in order to obtain the final data rate. All results are given for the case with and without linear channel prediction, shown as dashed and solid lines, respectively. For comparison, we also include the configuration of single-antenna receivers, i.e. $N_r = 1$. Finally, we can draw the following conclusions:

1. Updates for receive combining weights can help to mitigate cross-talk:
   Updating the receiver according to the current channel coefficients helps reducing the degradation due to channel out-dating to a certain degree, since receive antennas can be used to form a receive beamformer which follows the time evolution of the wireless channel. We emphasize, that in case of MMSE, the receiver is updated based on the current channel knowledge at the receiver, while in case of MET τ-old channel estimates of the receiver are utilized for receive processing.

[5]Note, this very simple scheme ensures a certain degree of fairness between the users.

Table 6.4: Simulation assumptions.

Parameter	Value
Channel model	QUADRIGA
Simulation type	Monte Carlo plus time evolution
Drops	500
Channel evolution	500 ms with 1 ms resolution
Scenario	Urban-macro
Propagation	NLOS
Large-scale fading	Geo-correlated parameters maps
Traffic model	Full buffer
f_c	2.6 GHz
Velocity, f_D, T_c	3 km/h, 7.5 Hz, 133 ms
Frequency reuse	1
Signal bandwidth	18 MHz, 100 PRBs
Inter-site distance	500m
Number of BSs	19 having 3 sectors each
N_t ; spacing	4 ; 4λ
Transmit power	46 dBm
Transmit antenna	Azimuth: FWHM of 58°
	Elevation: FWHM of 6.2°
	10° electrical downtilt
BS height	32m
Beamforming	Cluster-wide MET, ZF constraint
Clustering	Network-centric
User grouping	3 user per sector, round-robin
N_r ; spacing	2 ; $\lambda/2$
UE height	2m
Link-2-System	Shannon, SINRs $\lfloor -10, 40 \rceil$ dB
CSI delay	{0, 5, 10, 20, 40, 80, 120} ms
Channel prediction	RLS with $d = 1$ ms and α set
	to the considered feedback delay

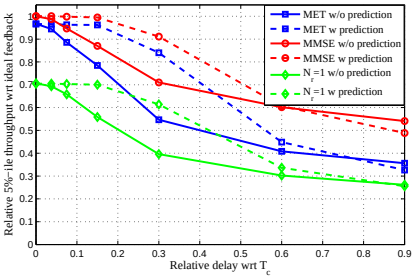

(a) 5% system throughput

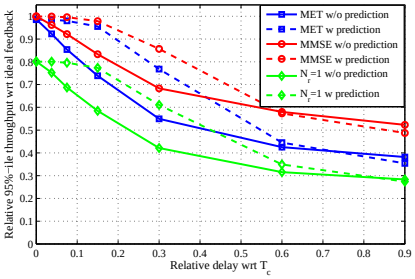

(b) 95% system throughput

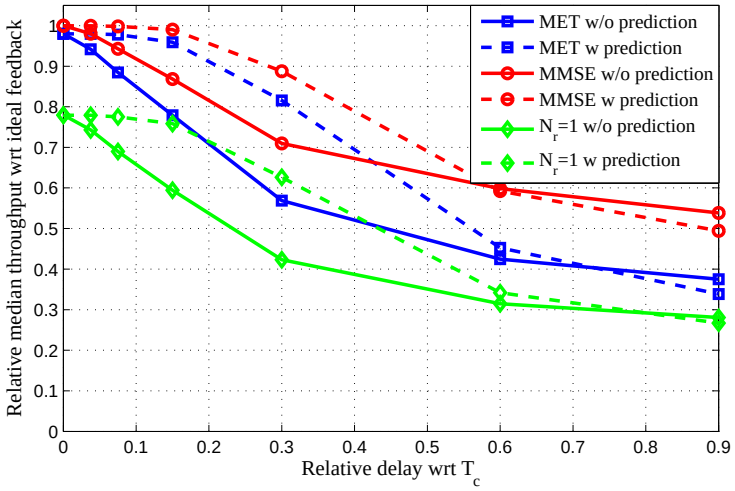

(c) 50% system throughput

Figure 6.23: Simulation results for $M_c = 1$, i.e. single-cell ZF precoding, taking precise channel evolution into account and specific channel feedback interval. Where the coherence time is set to the inverse of the maximal Doppler shift, i.e. $Tc = 1/f_D$.

2. Rather small throughput degradation at $0.3\,T_c$:
   90% of the ideal system throughput at $0.3\,T_c$ can be maintained by combining both linear channel prediction for CSI feedback provisioning and updated receiver weights (MMSE). At $0.6\,T_c$ the tracking performance degrades further to 60% of the ideal data rate, and for $0.9\,T_c$ it drops to 50% . In case of MET receive processing and single-antenna UEs, the situation is even worse, i.e. 38% and 35% of the ideal system throughput at $0.9\,T_c$ with respect to the ideal feedback case for both MET and $N_r = 1$.

3. Cross-over point for degraded and predicted channels:
   The cross-over point for the performance assuming linear channel prediction and the baseline without prediction is located in the range between $0.6\,T_c$ and $0.9\,T_c$ for all three methods. We emphasize, that for certain feedback delay e.g. $\tau \geq 0.3\,T_c$, linear channel prediction with filter properties according to Table 6.3 is no longer suitable. In order to cover a wide range of feedback delays, each user has to adaptively select the memory length λ of the RLS filter dependent on the current delay τ. Development of such a heuristic algorithm is of interest for future work.

It is very obvious, that the system throughput will further degrade with increasing cluster size M_c. Therefore, Figure 6.24 shows the effect of outdated CSI and cluster-wide ZF beamforming. For sake of simplicity, we concentrate onto the case of single receive antenna terminals without channel prediction filters (baseline) as well as improved multi-antenna terminals with MMSE receive processing and linear channel prediction in frequency domain (advanced). There is a significant gap between the performance of baseline and advanced receivers. As already shown in Section 6.3, there is a reasonable gain in throughput for $M_c = 3$ over $M_c = 1$. The rather minor gain from $M_c = 6$ can hardly be maintained if CSI feedback becomes outdated. However, we can conclude with roughly 112% gain in median system throughput for advanced receivers over baseline assumptions at $0.3\,T_c$ for the tested range of cluster size M_c.

Finally, let us compare the performance in Figure 6.24 with results in Figure 6.19. From Figure 6.22(a) the rMSE for $\tau = 10$ ms at time index $n = 410$ ms without and with channel prediction is in the order of $\mu(CSI_{n-\tau}) = -10$ dB and $\mu(CSI_{n-\tau+\alpha}) = -34$ dB, respectively. Taking precise channel's time evolution into account, the loss due to $\tau = 10$ ms feedback delay without prediction, i.e. $\alpha = 0$ ms[6], is in the order of 10% . If the UEs adapt their receive beamforming weights, i.e. MMSE receiver, the loss is even less. In contrast, the degradation from AWGN error modeling for CSI feedback results in significant higher ratios. In particular, the loss attributes to 11% , 21% and 31% for cluster size $1 \leq M_c \leq 3$. The reason for that discrepancy is manifold: The error's distribution properties are different, compare Section 6.4.4. In the time continuous simulations we use multiple antennas at trans-

[6] Where α is the prediction horizon.

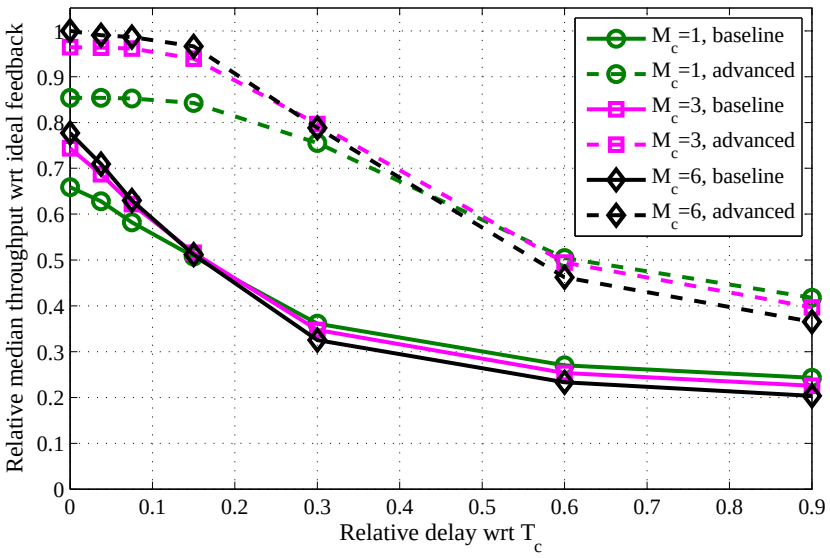

Figure 6.24: Simulation results for increasing cluster size M_c, i.e. CoMP joint transmission with ZF precoding. The x-axis is normalized to the coherence time $Tc = 1/f_D$. The y-axis is normalized to the median system throughput assuming $M_c = 6$ and ideal feedback. We compare baseline ($N_r = 1$ without prediction) and advanced ($N_r = 2$ with prediction) UEs, which employ MMSE receive beamforming weights based on current channel knowledge.

mit and receiver side. Each transmitter is using its $N_t = 4$ transmit antennas to serve 3 UEs is SDMA and the users are able to follow changes in channel's time evolution by means of MMSE receiver adaptation. Thus, AWGN modeling of CSI feedback errors is a simple tool to determine lower bounds for channel aging effects in CoMP transmission but with rather moderate accuracy. Furthermore, de-noising effects of time-domain filtering and time evolution of those CSI errors cannot be modeled with AWGN assumptions.

7

Conclusion and Outlook

In this work, we focused on the downlink direction of cellular multi-user multiple-input multiple-output (MIMO) systems based on orthogonal frequency division multiplex (OFDM) waveforms. Our target system is operated in the frequency division duplex (FDD) mode, while all base stations (BSs) use the same frequency spectrum for downlink transmission. State-of-the-art literature proved that the system performance is mainly limited by the existing co-channel interference. Hence, mitigating these effects would improve the achievable system throughput beyond current benchmarks of cellular systems. Very recently, operators started deploying Long Lerm Evolution (LTE) systems targeting peak data rates with up to 100 MBit/s per sector.

We developed transmission concepts for spatial interference management in the range of limited feedback assumptions, which are closely related to future Third Generation Partnership Project (3GPP) standards. Furthermore, we dealt with concepts for transceiver optimization strategies in the field of coordinated multi-point (CoMP) systems, where the requirements are still to demanding for a direct application into current systems.

Limited Feedback assumption: In Chapters 3 and 4 we introduced an efficient method to combine opportunistic precoding and scheduling with spatial division multiple access (SDMA) service of users. At a first step, we concentrated on the achievable system and user data rates assuming quantized but full feedback according to channel quality indicator (CQI), precoding matrix indicator (PMI) and rank indicator (RI). Based on a heuristic, fair scheduling strategy, we characterized the scaling behavior of the data rates depending on the amount of transmit and receive antennas as well as number of active users per sector. Overall, we highlighted that with limited feedback assumptions, where the users report all constellations of CQI and PMI, it is possible to triple the data rates in the system when receive and

transmit antennas are quadrupled. Cell-edge user rates improve linearly, i.e. data rates are quadrupled with $N_t = N_r = 4$. As a next step, we introduced feedback reduction methods on top of the limited, i.e. quantized feedback scheme.
In Chapter 4.2, we demonstrated that feedback can significantly be reduced at rather low costs in data rates. In particular, for $N_t = 4$ and a single precoding matrix in the given codebook $\mathcal{B}$, there exist a total number of 12 combinations of data streams at different spatial transmission ranks. In total, each user equipment (UE) would have to calculate and report 29 CQIs per physical resource block (PRB). Introducing sub-band and wide-band feedback we observed a loss of 9% in sum-rate compared to feedback per PRB. By further limiting each user to report only 4 CQIs per sub-band valid for two different combinations of precoding vectors chosen on a wide-band basis, we observed an additional loss in the order of 10%, while the required feedback is reduced to less than 3% in terms of CQI feedback and less than 1% for precoding matrices and corresponding combinations of data streams. Finally, Chapter 4.1 concludes with the observation that efficient multi-user MIMO (MU-MIMO) transmission can be realized without ideal channel estimation. In order to enable an interference-aware scheduling process, we introduced a virtual pilot scheme concept for channel estimation of most prominent interfering base stations. Finally, Chapter 4 provides a comparison of current geometry-based stochastic channel model (GSCM) commonly used for system-level simulations.

Full Channel Feedback in CoMP Transmission: Chapters 5 and 6 introduced the concept of cooperative transmission from multiple BSs. Therefore, we developed a unified multiple-input single-output (MISO) feedback scheme for multi-antenna receivers. This two-step transceiver optimization process is studied on a multi-cell basis under ideal feedback and backhauling conditions. Chapters 6.2 and 6.3 introduced practical concepts for clustering of BSs and grouping of instantaneously served users. We showed, that our greedy rate approximation (GRA) metric adaptively loads up to $0.75N_t$ data streams per sector in the cluster and thereby performs close to the capacity of the broadcast channel (BC). As a main results, the achievable system throughput is improved by 50% by combining the greedy user selection with a sub-clustering approach, while the required channel state information (CSI) feedback increases only linearly with the sub-cluster size.
Chapter 6 concludes with a detailed study on non-ideal channel state information at the transmitter (CSIT) caused by channel aging and a certain feedback delay. We demonstrated that MIMO processing at both ends of the link can improve system as well as user performance in presence of outdated CSI feedback. Finally, we conclude with the observation of a rather small loss in data rate at a feedback delay of 1/3 of the coherence time of the channel. In essence, by using simple 1-dimensional, adaptive channel prediction we can allow CSI feedback once per 40 ms in the quasi-static user regime of 3 km/h velocity. This reduces our estimate of

required channel feedback down to 350 kBit/s assuming 12 Bit quantized amplitude and phase information per PRB on 18 MHz bandwidth.

In order to compare the different system concepts for spatial interference management on a multi-cell basis, we developed a system-level simulation tool chain. This tool chain covers state-of-the-art channel modeling as well as physical (PHY) and medium access control (MAC) layer emulations. As a main contribution of this thesis, we targeted a direct and quantitative comparison for most of the transceiver schemes. In particular, results in Chapters 3 and 6, as well as results in Section 4.2 allow this comparison.

Future Work: There are a number of open issues, which are of interest for ongoing studies:

- Transmission concepts for interference coordination, i.e. using local CSI only. Performance comparison with current interference-alignment strategies.
- User-grouping strategies taking into account the current interference condition as well as the possible range for standard link-adaptation capabilities.
- Interference management schemes for heterogeneous networks covering the following topics:
  - Different, heterogeneous transmit power constraints.
  - Transmission concepts allowing inter-cell interference to a certain degree (interference acceptance).
  - Adaptive and robust precoding techniques covering the full range from strict interference nulling, over interference coordination towards interference acceptance.
- Application for Cloud-RAN with centralized and distributed deployment of antenna elements. In particular, what are the limits for *Massive MIMO* deployments in practice?
- Methods for 3-dimensional beamforming.
- Adaptive and self-configurable channel prediction methods.
- Trade-off between spectral and energy efficiency.
- Physical layer security, inherently enabling confidentiality at the lowest layer of wireless systems.

In particular, the issue of confidentiality at the physical layer gained significant interest recently. Besides spectral and energy efficiency, future wireless standards need to integrate services supporting transmission/reception of private, common as well as confidential messages. [WB12c] studied this so-called physical layer service

integration for bidirectional relay networks. The authors characterized the secrecy capacity regions for discrete memoryless and MIMO Gaussian channels under perfect channel knowledge. Channel uncertainty, as a ubiquitous phenomenon in practical applications, is addressed in [WB12d] for multi-user systems. Strong secrecy[1] and corresponding capacity results for the arbitrary varying wiretap channel are introduced in [BBS12]. The authors proved that secrecy is still maintained in presence of active jamming by eavesdroppers by introducing keys derived from a source of common randomness. In [WB12a], the authors showed that the secrecy capacity can be improved disproportionately by the introduction of CoMP concepts.

[1]Note, the strong secrecy criterion ensures an average error probability tending to one for all decoding strategies of the eavesdroppers [BBS12].

A

Published Papers

Parts of this thesis have been published in the following papers.

Book chapters

1. L. Thiele, T. Wirth, M. Schellmann, T. Haustein and V. Jungnickel, "Downlink Multi-User Beamforming with Interference Rejection Combining", *Coordinated Multi-Point in Mobile Communications, Cambridge University Press*, July 2011, ch. 5.1.

2. L. Thiele, T. Haustein, V. Jungnickel, W. Zirwas and F. Boccardi, "Downlink Distributed CoMP approaching Centralized Joint Transmission", *Coordinated Multi-Point in Mobile Communications, Cambridge University Press*, July 2011, ch. 6.3.

3. W. Zirwas, L. Thiele, T. Weber, N. Palleit and V. Jungnickel, "Channel Estimation for CoMP", *Coordinated Multi-Point in Mobile Communications, Cambridge University Press*, July 2011, ch. 9.1.

4. V. Jungnickel, A. Forck, S. Jaeckel, S. Wahls, L. Thiele, T. Haustein, W. Zirwas, H. Droste and G. Kadel, "Realtime Implementation and Field Trials for Downlink CoMP", *Coordinated Multi-Point in Mobile Communications, Cambridge University Press*, July 2011, ch. 13.3.

5. M. Boldi, F. Boccardi, E. Hardouin, V. Jungnickel, M. Olsson, T. Svensson, L. Thiele and A. Tölli, "Coordinated MultiPoint (CoMP) Systems", *Mobile and Wireless Communications for IMT-A & Beyond*, Wiley, 2011, ch. 6.

6. M. Schellmann, L. Thiele, T. Wirth, T. Haustein and V. Jungnickel, "Resource Management in MIMO-OFDM systems", *Orthogonal Frequency Division Mul-*

tiple Access: Fundamentals and Applications, Auerbach Publications, CRC Press, Taylor&Francis Group, 2010.

7. W. Zirwas, W. Mennerich, M. Schubert, L. Thiele, V. Jungnickel and E. Schulz, "Cooperative Transmission Schemes", *Long Term Evolution: 3GPP LTE Radio and Cellular Technology*, Auerbach Publications, CRC Press, Taylor&Francis Group, 2009, ch. 7.

Journal papers

1. L. Thiele, M. Kurras, M. Olbrich and T. Haustein, "Boosting 4G Networks with Spatial Interference Management under Feedback Constraints," *IEEE Vehicular Technology Magazine, Special Issue*, submitted 2012.

2. S. Jaeckel, K. Börner, L. Thiele and V. Jungnickel, "A Geometric Polarization Rotation Model for the 3D Spatial Channel Model," *IEEE Transactions on Antennas and Propagation*, pp. 1-11, 2012, accepted.

3. R. Irmer, H. Droste, P. Marsch, M. Grieger, G. Fettweis, S. Brueck, H.-P. Mayer, L. Thiele, V. Jungnickel, "Coordinated multipoint: Concepts, performance and field trial results", *IEEE Communications Magazine*, vol. 49, no. 2, pp. 102-111, February 2011.

4. L. Thiele, V. Jungnickel and T. Haustein, "Interference Management for Future Cellular OFDMA Systems Using Coordinated Multi-Point Transmission", *IEICE Transactions on Wireless Distributed Networks*, Dec. 2010, invited.

5. V. Jungnickel, M. Schellmann, L. Thiele, T. Wirth, T. Haustein, O. Koch, W. Zirwas and E. Schulz, "Interference Aware Scheduling in the Multiuser MIMO-OFDM Downlink", *IEEE Communications Magazine*, vol. 47, no. 6, pp. 56-66, June 2009.

6. M. Schellmann, L. Thiele, T. Haustein and V. Jungnickel, "Spatial transmission mode switching in multi-user MIMO-OFDM systems with user fairness", *IEEE Transactions on Vehicular Technology*, 2009.

7. V. Jungnickel, S. Jaeckel, L. Thiele, L. Jiang, U. Krüger, A. Brylka and C. v. Helmolt, "Capacity Measurements in a Cooperative MIMO Network", *IEEE Transactions on Vehicular Technologies*, 2008.

Conference papers

1. L. Thiele, M. Kurras, M. Olbrich and K. Börner, "On Feedback Requirements for CoMP Joint Transmission in the Quasi-Static User Regime," *IEEE 77th Vehicular Technology Conference VTC2013-Spring*, Jun. 2013, submitted.

2. L. Thiele, M. Kurras, K. Börner and T. Haustein, "User-Aided Sub-Clustering for CoMP Transmission: Feedback Overhead vs. Data Rate Trade-off", *IEEE 46th Annual Asilomar Conference on Signals, Systems and Computers*, Monterey, USA, Nov. 2012.

3. L. Thiele, M. Kurras, M. Olbrich and B. Matthiesen, "Channel Aging Effects in CoMP Transmission: Gains from Linear Channel Prediction", *IEEE 45th Annual Asilomar Conference on Signals, Systems and Computers*, Monterey, USA, Nov. 2011.

4. K. Manolakis, L. Thiele, C. Oberli, T. Haustein and V. Jungnickel, "Impairment Modeling for Joint Transmission CoMP", *IEEE 2nd International Conference on Wireless Communications, Vehicular Technology, Information Theory and Aerospace & Electronic System Technology (Wireless VITAE)*, Chennai, India, Mar. 2011, invited.

5. S. Jaeckel, L. Thiele and V. Jungnickel, "Interference Limited MIMO Measurements", *IEEE 71st Vehicular Technology Conference VTC2010-Spring*, Taipei, Apr. 2010.

6. V. Jungnickel, A. Forck, S. Jaeckel, F. Bauermeister, S. Schiffermueller, S. Schubert, S. Wahls, L. Thiele, T. Haustein, W. Kreher, J. Mueller, H. Droste and G. Kadel, "Field Trials using Coordinated Multi-Point Transmission in the Downlink", *3rd International Workshop on Wireless Distributed Networks (WDN), held in conjunction with IEEE PIMRC 2010*, Sept. 2010.

7. L. Thiele, F. Boccardi, C. Botella, T. Svensson and M. Boldi, "Scheduling-Assisted Joint Processing for CoMP in the Framework of the WINNER+ Project", *Future Network Mobile Summit*, Florence, Italy, June 2010.

8. Y. Hadisusanto, L. Thiele and V. Jungnickel, "Distributed Uplink Base Station Cooperation for Optimal SIR Assignment", *IEEE Wireless Communications and Networking Conference (WCNC)*, Sydney, Australia, Apr. 2010.

9. Y. Hadisusanto, L. Thiele and V. Jungnickel, "Joint Power Control, Beamforming and BS Assignment for Optimal SIR Assignment", *IEEE 43rd Annual Asilomar Conference on Signals, Systems and Computers*, Monterey, USA, Nov. 2009.

10. M. Schellmann, L. Thiele, T. Wirth, V. Jungnickel and T. Haustein, "Spatial mode switching in multi-user MIMO-OFDM systems: Performance in a real-world scenario", *13th International OFDM-Workshop (InOWo)*, Hamburg, Germany, Aug. 2009.

11. S. Jaeckel, L. Thiele, A. Brylka, L. Jiang, V. Jungnickel, C. Jandura and J. Heft, "Intercell Interference Measured in Urban Areas", *IEEE International Conference on Communications (ICC)*, Dresden, Germany, June 2009.

12. L. Thiele, T. Wirth, T. Haustein, V. Jungnickel, E. Schulz and W. Zirwas, "A Unified Feedback Scheme for Distributed Interference Management in Cellular Systems: Benefits and Challenges for Real-Time Implementation", *17th Euopean Signal Processing Conference (EUSIPCO2009), Glasgow, Scotland*, Aug. 2009, invited.

13. S. Jaeckel, L. Jiang, V. Jungnickel, L. Thiele, C. Jandura, G. Sommerkorn and C. Schneider, "Correlation properties of large and small-scale parameters from multicell channel measurements", *European Conference on Antennas and Propagation (EuCAP 2009)*, Berlin, Germany, 2009, invited.

14. V. Jungnickel, K. Manolakis, L. Thiele, T. Wirth and T. Haustein, "Handover Sequences for Interference-Aware Transmission in Multicell MIMO Networks", *International ITG Workshop on Smart Antennas (WSA 2009)*, Berlin, Germany, Feb. 2009.

15. L. Thiele, T. Wirth, K. Börner, M. Olbrich, V. Jungnickel, J. Rumold and S. Fritze, "Modeling of 3D Field Patterns of Downtilted Antennas and Their Impact on Cellular Systems", *International ITG Workshop on Smart Antennas (WSA 2009)*, Berlin, Germany, Feb. 2009.

16. L. Thiele, M. Schellmann, T. Wirth, V. Jungnickel, F. Boccardi and H. Huang, "DFT-based vs. Cooperative MET-based MU-MIMO in the Downlink of Cellular OFDM Systems", *International ITG Workshop on Smart Antennas (WSA 2009)*, Berlin, Germany, Feb. 2009.

17. L. Thiele, T. Wirth, M. Schellmann, Y. Hadisusanto and V. Jungnickel, "MU-MIMO with Localized Downlink Base Station Cooperation and Downtilted Antennas", *IEEE International Workshop on LTE Evolution*, Dresden, Germany, June 2009.

18. V. Jungnickel, L. Thiele, T. Wirth, T. Haustein, S. Schiffermüller, A. Forck, S. Wahls, S. Jaeckel, S. Schubert, C. Juchems, F. Luhn, R. Zavrtak, H. Droste, G. Kadel, W. Kreher, J. Mueller, W. Stoermer and G. Wannemacher, "Coordinated Multipoint Trials in the Downlink", *IEEE 5th Broadband Wireless Access Workshop (BWAWS), co-located with IEEE GLOBECOM 2009*, Honolulu, Hawai, Nov. 2009.

19. L. Thiele, M. Schellmann, T. Wirth and V. Jungnickel, "Interference-Aware Scheduling in the Synchronous Cellular Multi-Antenna Downlink", *IEEE 69th Vehicular Technology Conference VTC2009-Spring*, Barcelona, Spain, Apr. 2009, invited.

20. L. Thiele and V. Jungnickel, "Adaptive Transmission in a Realistic Multicell Scenario", *IEEE Radio and Wireless Symposium (RWS 2008)*, Jan. 2008.

21. L. Jiang, L. Thiele and V. Jungnickel, "Modeling and Measurement of MIMO Relay Channels", *IEEE 67th Vehicular Technology Conference VTC2008-Spring*, Singapore, May 2008.

22. L. Thiele, M. Schellmann, S. Schiffermüller, V. Jungnickel and W. Zirwas, "Multi-Cell Channel Estimation using Virtual Pilots", *IEEE 67th Vehicular Technology Conference VTC2008-Spring*, Singapore, May 2008.

23. L. Jiang, L. Thiele, A. Brylka, S. Jaeckel and V. Jungnickel, "Polarization Characteristics of Multiple-Input Multiple-Output Channels", *IEEE 19th Intern. Symp. on Personal, Indoor and Mobile Radio Communications (PIMRC 2008)*, Cannes, France, Sept. 2008.

24. V. Jungnickel, L. Thiele, T. Wirth, M. Schellmann, V. Venkatkumar and T. Haustein, "Feedback Design for Multiuser MIMO Systems", *13th International OFDM-Workshop (InOWo)*, Hamburg, Germany, Aug. 2008.

25. M. Schellmann, L. Thiele and V. Jungnickel, "Predicting SINR conditions in mobile MIMO-OFDM systems by interpolation techniques", *42nd Asilomar Conference on Signals, Systems and Computers*, Monterey, USA, Oct. 2008.

26. Y. Hadisusanto, L. Thiele and V. Jungnickel, "Distributed Base Station Cooperation via Block-Diagonalization and Dual-Decomposition", *IEEE Global Telecommunications Conference (GLOBECOM)*, New Orleans, USA, Nov. 30 - Dec. 4, 2008.

27. M. Schellmann, L. Thiele and V. Jungnickel, "Low-complexity Doppler compensation in mobile SIMO-OFDM systems", *42nd Asilomar Conference on Signals, Systems and Computers*, Monterey, USA, Oct. 2008.

28. L. Thiele, M. Schellmann, T. Wirth and V. Jungnickel, "On the Value of Synchronous Downlink MIMO-OFDMA Systems with Linear Equalizers", *IEEE International Symposium on Wireless Communication Systems (ISWCS08)*, Oct. 2008.

29. L. Thiele, M. Schellmann, T. Wirth and V. Jungnickel, "Cooperative Multi-User MIMO based on Reduced Feedback in Downlink OFDM Systems", *42nd Asilomar Conference on Signals, Systems and Computers*, Monterey, USA, Oct. 2008.

30. V. Jungnickel, L. Thiele, M. Schellmann, T. Wirth, W. Zirwas, T. Haustein and E. Schulz, "Implementation Concepts for Distributed Cooperative Transmission", *42nd Asilomar Conference on Signals, Systems and Computers*, Monterey, USA, Oct. 2008.

31. L. Jiang, V. Jungnickel, S. Jaeckel, L. Thiele and A. Brylka, "Correlation Analysis of Multiple-Input Multiple-Output Channels with Cross-Polarized Antennas", *IEEE 14th Asia-Pacific Conference on Communications (APCC2008)*, Tokyo, Japan, IEEE, Oct. 2008.

32. L. Jiang, L. Thiele and V. Jungnickel, "On the Modelling of Polarized MIMO Channel", *13th European Wireless Conference*, Paris, France, Apr. 2007.

33. W. Zirwas, E. Schulz, M. Schubert, W. Mennerich, V. Jungnickel and L. Thiele, "Cooperative Antenna Concepts for Interference Mitigation", *13th European Wireless Conference*, Paris, France, Apr. 2007.

34. M. Schellmann, L. Thiele, V. Jungnickel and T. Haustein, "A Fair Score-Based Scheduler for Spatial Transmission Mode Selection", *41st Asilomar Conference on Signals, Systems and Computers, Monterey*, USA, IEEE, Nov. 2007.

35. L. Thiele, M. Schellmann, W. Zirwas and V. Jungnickel, "Capacity Scaling of Multiuser MIMO with Limited Feedback in a Multicell Environment", *41st Asilomar Conference on Signals, Systems and Computers*, Monterey, USA, IEEE, Nov. 2007, invited.

36. L. Thiele and V. Jungnickel, "Out-of-Cell Channel Statistics at 5.2 GHz", *European Conference on Antennas and Propagation (EuCAP 2006)*, Nice, France, Nov. 2006.

37. V. Jungnickel, S. Jaeckel, L. Thiele, U. Krüger, A. Brylka and C. v. Helmolt, "Capacity Measurements in a Multicell MIMO System", *IEEE Global Telecommunication Conference (GLOBECOM 2006)*, San Francisco, California, Nov. 2006.

38. L. Thiele, M. Peter and V. Jungnickel, "Statistics of the Ricean K-Faktor at 5.2 GHz in an Urban Macro-Cell Scenario", *IEEE 17th Intern. Symp. on Personal, Indoor and Mobile Radio Communications (PIMRC 2006)*, Helsinki, Finland, Sept. 2006.

Patents

1. "Resolving channel state information outdating," W. Zirwas, L. Thiele and V. Jungnickel, US 20120250557, Oct. 2012.

2. "Channel-Adaptive Transmission in a Distributed Coordinated Multi-Point Transmission System," W. Zirwas, L. Thiele, T. Wirth, T. Haustein, M. Schellmann and V. Jungnickel, US 20120207092, Aug. 2012.

3. "Controlling Scheduling Decisions in a Distributed Cooperation System," W. Zirwas, L. Thiele, T. Wirth and T. Haustein, US 20120155366, Jun. 2012

4. "Method and Device for Data Processing in a Communication Network," L. Thiele, T. Wirth, T. Haustein, V. Jungnickel, M. Schellmann, E. Schulz and W. Zirwas, US 20120113897, May 2012.

5. "Method for network co-ordination in a mobile communications system and Apparatus thereof," A. Forck, T. Haustein, V. Jungnickel, M. Schellmann, E. Schulz, L. Thiele, T. Wirth and W. Zirwas, US 20110305195, Dec. 2011.

6. "Transmitting a First and a Second Channel Quality Information Between Two Network Elements," A. Forck, T. Haustein, V. Jungnickel, M. Schellmann, L. Thiele and T. Wirth, US 20110305154, Dec. 2011.

7. "Multi-Cell Channel Estimation in 3G-LTE Based Virtual Pilot Sequences," T. Haustein, V. Jungnickel, M. Schellmann, S. Schiffermüller, L. Thiele, T. Wirth and W. Zirwas, US 20110122789, May 2011.

8. "Verfahren und Vorrichtung zur Datenübertragung," W. Zirwas, J. Eichinger, A. Ibing, L. Thiele, V. Jungnickel and T. Haustein, DE 102008007497A1, Aug. 2009.

and 3 further patents pending.

B

Abbreviations

3GPP	Third Generation Partnership Project
64 QAM	64 quadrature amplitude modulation (QAM)
ACF	autocorrelation function
AoA	angel of arrival
AWGN	additive white Gaussian noise
AVC	arbitrarily varying channel
BC	broadcast channel
BD	block diagonalization
BLER	block error rate
BMWi	German Ministry of Economics
BS	base station
CCI	co-channel interference
CDF	cumulative distribution function
CoMP	coordinated multi-point
CP	cyclic prefix
CQI	channel quality indicator
CSI	channel state information
CSIR	channel state information at the receiver
CSIT	channel state information at the transmitter
CRS	common reference signals
CU	central unit
DAS	distributed antenna system
DFT	discrete Fourier transform
DRC	discrete Fourier transform receive combining

DPC	dirty paper coding
DS	delay spread
EBP	equal per beam power
EESM	exponential effective SINR mapping
EGT	equal gain transmission
EMSE	excess mean square error
EOC	eigenmode-aware optimum combining
ERC	eigenmode-aware receive combining
FDD	frequency division duplex
FDM	frequency division multiplex
FEC	forward error correction
FFT	fast Fourier transform
FLS	fully loaded system
GoB	grid of beams
GPS	global positioning system
GRA	greedy rate approximation
GSCM	geometry-based stochastic channel model
HARQ	hybrid automatic repeat request
ICI	inter-carrier interference
i.i.d.	independent identically distributed
IRC	interference rejection combining
ISI	inter-symbol interference
JT	joint transmission
KPI	key performance indicator
L2S	link-to-system
LDPC	low density parity check
LOS	line-of-sight
LBS	last bounce scatterer
LSP	large-scale parameter
LTE	Long Lerm Evolution
LTE-A	Long Term Evolution - Advanced
MAC	medium access control
MCS	modulation and coding scheme
MET	multi-user eigenmode transmission
MIMO	multiple-input multiple-output
MISO	multiple-input single-output
MMSE	minimum mean square error

MPC	multi-path components
MRC	maximum ratio combining
MSE	mean square error
MU	multi-user
MU-MIMO	multi-user MIMO
NLOS	non line-of-sight
NLMS	normalized least-mean-squares
OC	optimum combining
OFDM	orthogonal frequency division multiplex
OFDMA	orthogonal frequency division multiple access
OSDMA	opportunistic SDMA
PAPC	per antenna power constraint
PAPR	peak-to-average power ratio
PDF	probability distribution function
PHY	physical
PLS	partially loaded system
PMI	precoding matrix indicator
PRB	physical resource block
PRS	pseudo-random scrambling sequence
PSS	primary synchronization signal
PU2RC	per user unitary and rate control
QuaDRiGa	quasi-deterministic radio channel generator
QAM	quadrature amplitude modulation
QPSK	quadrature phase shift keying
QRD	QR-decomposition
RB	resource block
RE	resource element
RET	remote electrical tilt
RI	rank indicator
RLS	recursive least squares
rMSE	relative mean square error
RS	reference signal
RSRP	reference signal received power
RVQ	random vector quantization
SCM	spatial channel model
SCME	spatial channel model extended
SDIV	spatial diversity

SDMA	spatial division multiple access
SF	shadow fading
SINR	signal-to-interference-and-noise ratio
SIR	signal-to-interference ratio
SISO	single-input single-output
SMUX	spatial multiplexing
SNR	signal-to-noise ratio
SU-MIMO	single-user MIMO
SVD	singular value decomposition
TDD	time division duplex
TDMA	Time Division Multiple Access
THP	Tomlinson-Harashima precoding
TPC	total power constraint
TTI	transmission time interval
UE	user equipment
ULA	uniform linear array
WDN	wireless distributed network
WiMAX	Worldwide Interoperability for Microwave Access
WIM2	WINNER Phase II model
WIM+	WINNER+ model
WINNER	Wireless World Initiative New Radio
WF	water filling
X2 interface	X2 interface
XPR	cross-polar ratio
ZF	zero-forcing

C

Nomenclature

$\mathbf{A}^{1/2}$ element-wise square root of matrix $\mathbf{A}$

$\mathbf{a}(\xi)$ array response with respect to a given angle of arrival/departure

$\mathcal{B}$ codebook, i.e. set of precoding matrices

$\boldsymbol{\beta}$ one element in the codebook, i.e. $\boldsymbol{\beta} \in \mathcal{B}$

$\mathcal{B}_{mask}$ set of masking matrices

$\boldsymbol{\beta}_{mask}$ masking matrix for selection of precoding columns

$\mathbf{B}$ precoding matrix

$\mathbf{b}$ precoding vector

C subsets of clusters

$\boldsymbol{\Delta}_k$ offset matrix of k-th user

δ_k offset vector of k-th user

η frequency reuse factor

$\mathbf{H}$ MIMO channel matrix

$\mathbf{h}$ MISO channel vector

$\mathbf{I}$ is the identity matrix

$\mathcal{K}$ set of UEs in all M cells

$\mathcal{K}_m$ set of UEs in m-th cells

$\mathcal{K}_c$ set of UEs assigned to cluster c

$\mathcal{K}_{c,m}$ set of UEs assigned to cluster c with highest channel gain to BS m

$\mathcal{M}$ set of all BSs

M number of all BSs

$\mathcal{M}_c$ set of cells included in a cluster c

$\mathcal{M}_{c,k}$ set of cells included in a cluster c seen at user k

$|\mathcal{M}_c|$ number of cells in cluster c

$\mathbf{n}$ noise vector

N_t number of transit antennas at BS side

N_r number of receive antennas at UE side

Ω directivity pattern of an specific antenna array

$\boldsymbol{\omega}$ optimal weight vector, channel prediction

$\mathbf{P}$ power allocation matrix

P_m total transmit power budget of m-th base station

$\boldsymbol{\Psi}$ projection matrix

σ_n^2 noise power

$R_{bh,m}$ backhaul rate at BS m

R_c data rate in c-th cluster

$R_{fb,k}$ feedback rate at user k

$\mathbf{R}_{yy}$ received covariance matrix

ϱ relative gain

$\mathbf{S}$ matrix containing precoded user data

$\mathbf{s}$ vector containing precoded user data

σ_n^2 noise power

T_c coherence time is considered as the inverse of the maximal Doppler component, i.e. $T_c = 1/f_D$

$\mathbf{\Phi}$ transmit covariance matrix

$\mathcal{T}$ set of spatial layers

$\mathcal{T}_{\overline{k}}$ set of available spatial layers at user k

$\mathcal{T}_k$ set of reported spatial layers at user k

$\mathcal{T}_K$ set of spatial layers reported from all user in $\mathcal{M}_c$

$\mathcal{T}_s$ set of selected spatial layers for instantaneous downlink service in c-th cluster

$\mathcal{T}_{s,k}$ set of selected spatial layers for instantaneous downlink service at user k

$\boldsymbol{\vartheta}_{k,t}$ Intra-cell interference

$\mathbf{\Theta}_{k,t}$ Received intra-cell interference covariance matrix

$\mathbf{W}$ equalization matrix

$\mathbf{w}$ equalization vector

$\mathbf{z}_k$ Inter-cell interference

$\mathbf{Z}_k$ Received inter-cell interference covariance matrix

$\mathbf{Z}_{k,t}$ Received overall interference covariance matrix

References

[3GP] 3GPP TS 36.214 V9.2.0, Tech. Rep.

[3GP03] 3GPP TR 25.996 V6.1.0, "Spatial channel model for multiple input multiple output (MIMO) simulations (Release 6)," Tech. Rep., Sep. 2003. [Online]. Available: http://www.tkk.fi/Units/Radio/scm/

[3GP07a] 3GPP TR 25.996 V7.0.0, "Spatial channel model for multiple input multiple output (MIMO) simulations (Release 7)," Tech. Rep., Jul. 2007. [Online]. Available: http://www.tkk.fi/Units/Radio/scm/

[3GP07b] 3GPP TS 36.211 V8.0.0, "E-UTRA - physical channels and modulation (Release 8)," Tech. Rep., Sep. 2007.

[3GP10] 3GPP TS 36.211 V9.1.0, "E-UTRA - physical channels and modulation (Release 9)," Tech. Rep., Mar. 2010.

[3GP11] 3GPP TR 25.996 V10.0.0, "Spatial channel model for multiple input multiple output (MIMO) simulations (Release 10)," Tech. Rep., Mar. 2011. [Online]. Available: http://www.tkk.fi/Units/Radio/scm/

[3GP12] 3GPP TS 36.213 V10.6.0, "Evolved Universal Terrestrial Radio Access (E-UTRA); Physical layer procedures (Release 10)," Tech. Rep., Jun. 2012.

[AAB+05] A. Alexiou, D. Astély, K. Brüninghaus, P. Coronel, M. Döttling, M. Fuchs, J. Giese, and M. Haardt, "IST-2003-507581 WINNER, D2.7 ver 1.1: Assessment of Advanced Beamforming and MIMO Technologies," Information Society Technologies, Belgium, Tech. Rep., 2005.

[ABW12] D. Aziz, F. Boccardi, and A. Weber, "System-level performance study of interference alignment in cellular systems with base-station coordination," *23rd IEEE Intern. Symp. on Personal, Indoor and Mobile Radio Communications (PIMRC 2012)*, Sep. 2012.

[ACH07] J. Andrews, W. Choi, and R. Heath, "Overcoming interference in spatial multiplexing MIMO cellular networks," *IEEE Wireless Communications*, vol. 14, no. 6, pp. 95–104, Dec. 2007.

[BBS12] I. Bjelaković, H. Boche, and J. Sommerfeld, "Capacity results for arbitrarily varying wiretap channels," *CoRR*, vol. abs/1209.5213, 2012, accepted for publication in the LNCS Volume in Memory of Rudolf Ahlswede. Some of the results were presented at the ITW 2012.

[BDJT12] K. Börner, J. Dommel, S. Jaeckel, and L. Thiele, "On the requirements for quasi-deterministic radio channel models for heterogeneous networks," in *International Symposium on Signals, Systems and Electronics (ISSSE'12)*, Oct. 2012, pp. 1–5.

[BH06] F. Boccardi and H. Huang, "Zero-forcing precoding for the MIMO broadcast channel under per-antenna power constraints," in *IEEE 7th Workshop on Signal Processing Advances in Wireless Communications, SPAWC '06*, Jul. 2006, pp. 1 –5.

[BH07a] ——, "Limited downlink network coordination in cellular networks," in *IEEE 18th International Symposium on Personal, Indoor and Mobile Radio Communications, PIMRC 2007*, Sep. 2007, pp. 1–5.

[BH07b] ——, "A near-optimum technique using linear precoding for the MIMO broadcast channel," *IEEE International Conference on Acoustics, Speech and Signal Processing (ICASSP)*, vol. 3, pp. III–17–III–20, Apr. 2007.

[BHA08] F. Boccardi, H. Huang, and A. Alexiou, "Network MIMO with reduced backhaul requirements by MAC coordination," in *42nd Asilomar Conference on Signals, Systems and Computers*, Oct. 2008, pp. 1125–1129.

[BHS05] D. Baum, J. Hansen, and J. Salo, "An interim channel model for beyond-3G systems: extending the 3GPP spatial channel model (SCM)," in *IEEE 61st Vehicular Technology Conference (VTC 2005-Spring)*, vol. 5, May 2005, pp. 3132 – 3136 Vol. 5.

[BHT07] F. Boccardi, H. Huang, and M. Trivellato, "Multiuser eigenmode transmission for MIMO broadcast channels with limited feedback," *IEEE 8th Workshop on Signal Processing Advances in Wireless Communications, SPAWC 2007*, pp. 1–5, Jun. 2007.

[BMWT00] P. Baier, M. Meurer, T. Weber, and H. Troger, "Joint transmission (JT), an alternative rationale for the downlink of time division CDMA using multi-element transmit antennas," *Spread Spectrum Techniques and Applications, 2000 IEEE Sixth International Symposium on*, vol. 1, pp. 1–5 vol.1, 2000.

[Bon04] T. Bonald, "A score-based opportunistic scheduler for fading radio channels," *5th European Wireless Conference*, pp. 1–7, Feb. 2004.

[BS03] O. Besson and P. Stoica, "On parameter estimation of MIMO flat-fading channels with frequency offsets," *IEEE Transactions on Signal Processing*, vol. 51, no. 3, pp. 602–613, Mar. 2003.

[BSC+11] T. Biermann, L. Scalia, C. Choi, B. Karl, and W. Kellerer, "Improving CoMP cluster feasibility by dynamic serving base station reassignment," in *IEEE 22nd International Symposium on Personal Indoor and Mobile Radio Communications (PIMRC)*, Sep. 2011, pp. 1325 –1330.

[BSM+05] D. S. Baum, J. Salo, M. Milojevic, P. Kyösti, and J. Hansen, "MATLAB implementation of the interim channel model for beyond-3G systems (SCME)," May 2005. [Online]. Available: http://www.tkk.fi/Units/Radio/scm/

[BTC06] F. Boccardi, F. Tosato, and G. Caire, "Precoding schemes for the MIMO-GBC," *IEEE International Zurich Seminar on Communications*, Feb. 2006.

[BZ71] C. A. Baird and C. L. Zahm, "Performance criteria for narrowband array processing," *IEEE Conference on Decision and Control*, vol. 10, pp. 564–565, 1971.

[CDG00] S. Catreux, P. Driessen, and L. Greenstein, "Simulation results for an interference-limited multiple-input multiple-output cellular system," *IEEE Communications Letters*, vol. 4, pp. 334 – 336, Nov. 2000.

[CDG01] ——, "Attainable throughput of an interference-limited multiple-input multiple-output (MIMO) cellular system," *IEEE Transactions on Communications*, vol. 49, pp. 1307 – 1311, Aug. 2001.

[CJ08] V. Cadambe and S. Jafar, "Interference alignment and degrees of freedom of the k -user interference channel," *IEEE Transactions on Information Theory*, vol. 54, no. 8, pp. 3425 –3441, Aug. 2008.

[CJCU08] P. Castro, M. Joham, L. Castedo, and W. Utschick, "Robust MMSE linear precoding for multiuser MISO systems with limited feedback and channel prediction," in *IEEE 19th International Symposium on Personal, Indoor and Mobile Radio Communications (PIMRC)*, Sep. 2008, pp. 1 –5.

[Cla05] H. Claussen, "Efficient modelling of channel maps with correlated shadow fading in mobile radio systems," in *IEEE 16th International Symposium on Personal, Indoor and Mobile Radio Communications, PIMRC 2005*, vol. 1, Sep. 2005, pp. 512 –516.

[CLH+04] S. T. Chung, A. Lozano, H. C. Huang, A. Sutivong, and J. M. Cioffi, "Approaching the MIMO capacity with a low-rate feedback channel in V-BLAST," *EURASIP Journal on Applied Signal Processing*, vol. 5, pp. 762–771, 2004.

[CM04] L.-U. Choi and R. Murch, "A transmit preprocessing technique for multiuser MIMO systems using a decomposition approach," *IEEE Transactions on Wireless Communications*, vol. 3, no. 1, pp. 20 – 24, Jan. 2004.

[CMIH08] C.-B. Chae, D. Mazzarese, T. Inoue, and R. Heath, "Coordinated beamforming for the multiuser MIMO broadcast channel with limited feedforward," *IEEE Transactions on Signal Processing*, vol. 56, no. 12, pp. 6044 –6056, Dec. 2008.

[CO08] N. Czink and C. Oestges, "The cost 273 MIMO channel model: Three kinds of clusters," in *IEEE 10th International Symposium on Spread Spectrum Techniques and Applications (ISSSTA '08)*, Aug. 2008, pp. 282 –286.

[Cos83] M. Costa, "Writing on dirty paper (corresp.)," *IEEE Transactions on Information Theory*, vol. 29, no. 3, pp. 439–441, 1983.

[CS03] G. Caire and S. S. (Shitz), "On the achievable throughput of a multiantenna Gaussian broadcast channel," *IEEE Transactions on Information Theory*, vol. 49, no. 7, pp. 802–811, Jun. 2003.

[DS05] G. Dimić and N. Sidiropoulos, "On downlink beamforming with greedy user selection: performance analysis and a simple new algorithm," *IEEE Transactions on Signal Processing*, vol. 53, no. 10, pp. 3857 – 3868, oct. 2005.

[DUD11] A. Dotzler, W. Utschick, and G. Dietl, "Efficient zero-forcing based interference coordination for MISO networks," in *IEEE 73rd Vehicular Technology Conference (VTC Spring)*, May 2011, pp. 1 –5.

[ETS98] "TR 101 112 V3.2.0," European Telecommunications Standards Institute, Tech. Rep., 1998.

[FDGH07] M. Fuchs, G. Del Galdo, and M. Haardt, "Low-complexity space-time-frequency scheduling for MIMO systems with SDMA," *IEEE Transactions on Vehicular Technology*, vol. 56, no. 5, pp. 2775 –2784, Sep. 2007.

[FGH06] M. Fuchs, G. D. Galdo, and M. Haardt, "Low complexity spatial scheduling ProSched for MIMO systems with multiple base stations and a central controller," in *International ITG/IEEE Workshop on Smart Antennas (WSA), (Guenzburg, Germany)*, Mar. 2006.

[FHK+05] G. J. Foschini, H. Huang, K. Karakayali, R. A. Valenzuela, and S. Venkatesan, "The value of coherent base station coordination," *Conference on Information Sciences and Systems*, Mar. 2005.

[GA10] J. Giese and M. Amin, "Performance upper bounds for coordinated beam selection in LTE-Advanced," in *International ITG Workshop on Smart Antennas (WSA)*, Feb. 2010, pp. 280 –285.

[GJJV03] A. Goldsmith, S. Jafar, N. Jindal, and S. Vishwanath, "Capacity limits of MIMO channels," *IEEE Journal on Selected Areas in Communication*, vol. 21, no. 5, pp. 684–702, Jun. 2003.

[GKGi07] D. Gesbert, S. Kiani, A. Gjendemsj, and G. ien, "Adaptation, coordination, and distributed resource allocation in interference-limited wireless networks," *Proceedings of the IEEE*, vol. 95, no. 12, pp. 2393 –2409, dec. 2007.

[GKH+07] D. Gesbert, M. Kountouris, R. Heath, C.-B. Chae, and T. Salzer, "Shifting the MIMO paradigm," *IEEE Signal Processing Magazine*, vol. 24, no. 5, pp. 36–46, Sep. 2007.

[Gre] [Online]. Available: http://www.greentouch.org/

[Gud91] M. Gudmundson, "Correlation model for shadow fading in mobile radio systems," *Electronics Letters*, vol. 27, no. 23, pp. 2145 –2146, Nov. 1991.

[GUD09] C. Guthy, W. Utschick, and G. Dietl, "A user grouping method for maximum weighted sum capacity gain," in *IEEE International Conference on Communications (ICC)*, Jun. 2009, pp. 1 –5.

[GV96] G. H. Golub and C. F. Van Loan, *Matrix Computations*, 3rd ed. John Hopkins University Press, 1996.

[GV97] A. Goldsmith and P. Varaiya, "Capacity of fading channels with channel side information," *IEEE Transactions on Information Theory*, vol. 43, no. 6, pp. 1986 –1992, Nov. 1997.

[HAH09] K. Huang, J. Andrews, and R. Heath, "Performance of orthogonal beamforming for SDMA with limited feedback," *IEEE Transactions on Vehicular Technology*, vol. 58, no. 1, pp. 152 –164, Jan. 2009.

[HCPR11] H. Huh, G. Caire, H. C. Papadopoulos, and S. A. Ramprashad, "Achieving "Massive MIMO" spectral efficiency with a not-so-large number of antennas," *CoRR*, vol. abs/1107.3862, 2011.

[HP05] R. Heath and A. J. Paulraj, "Switching between diversity and multiplexing in MIMO systems," *IEEE Transactions on Communications*, vol. 53, no. 6, 2005.

[HS09] H. Huang and D. Samardzija, "Determining backhaul bandwidth requirements of Network MIMO," *17th Euopean Signal Processing Conference (EUSIPCO2009)*, Aug. 2009, invited.

[HT98] S. Hanly and D. Tse, "Multiaccess fading channels. II. Delay-limited capacities," *IEEE Transactions on Information Theory*, vol. 44, no. 7, pp. 2816 –2831, Nov. 1998.

[HtBD11] J. Hoydis, S. ten Brink, and M. Debbah, "Massive MIMO: How many antennas do we need?" *CoRR*, vol. abs/1107.1709, 2011.

[HTH+09] H. Huang, M. Trivellato, A. Hottinen, M. Shafi, P. Smith, and R. Valenzuela, "Increasing downlink cellular throughput with limited network MIMO coordination," *IEEE Transactions on Wireless Communication*, vol. 8, no. 6, pp. 2983 –2989, Jun. 2009.

[HV04] H. Huang and S. Venkatesan, "Asymptotic downlink capacity of coordinated cellular networks," *Thirty-Eighth Asilomar Conference on Signals, Systems and Computers*, vol. 1, pp. 850–855, 2004.

[HVKS03] H. Huang, S. Venkatesan, A. Kogiantis, and N. Sharma, "Increasing the peak data rate of 3G downlink packet data systems using multiple antennas," *The 57th IEEE Semiannual Vehicular Technology Conference, VTC 2003-Spring*, vol. 1, pp. 311–315 vol.1, Apr. 2003.

[HWKS11] R. Heath, T. Wu, Y. H. Kwon, and A. Soong, "Multiuser MIMO in distributed antenna systems with out-of-cell interference," *IEEE Transactions on Signal Processing*, vol. 59, no. 10, pp. 4885 –4899, Oct. 2011.

[IDM+11] R. Irmer, H. Droste, P. Marsch, M. Grieger, G. Fettweis, S. Brueck, H.-P. Mayer, L. Thiele, and V. Jungnickel, "Coordinated multipoint: Concepts, performance, and field trial results," *IEEE Communications Magazine*, vol. 49, no. 2, pp. 102 –111, Feb. 2011.

[IST07] IST-4-027756 WINNER II – D2.2.3, "Modulation and coding schemes for the WINNER II system," Information Society Technologies, Belgium, Tech. Rep., Nov. 2007.

[JBT12] S. Jaeckel, K. Börner, and L. Thiele, "QuaDRiGa: a multicell channel model to predict system-level performance using time evolving broadband channels," *IEEE Transactions on Vehicular Technology*, pp. 1–11, 2012, submitted.

[JBTJ12] S. Jaeckel, K. Börner, L. Thiele, and V. Jungnickel, "A Geometric Polarization Rotation Model for the 3D Spatial Channel Model," *IEEE Transactions on Antennas and Propagation*, pp. 1–11, 2012, accepted.

[JCUC12] M. Joham, P. Castro, W. Utschick, and L. Castedo, "Robust precoding with limited feedback design based on precoding MSE for MU-MISO systems," *IEEE Transactions on Signal Processing*, vol. 60, no. 6, pp. 3101 –3111, Jun. 2012.

[JFJ+10] V. Jungnickel, A. Forck, S. Jaeckel, F. Bauermeister, S. Schiffermüller, S. Schubert, S. Wahls, L. Thiele, T. Haustein, W. Kreher, J. Müller, H. Droste, and G. Kadel, "Field Trials using Coordinated Multi-Point Transmission in the Downlink," in *Proc. 3rd International Workshop on Wireless Distributed Networks (WDN), Held in Conjunction with IEEE PIMRC 2010*, Istanbul, Turkey, Sep. 2010.

[JHJ+01] V. Jungnickel, T. Haustein, E. Jorswieck, V. Pohl, and C. von Helmolt, "Performance of a MIMO system with overlay pilots," *IEEE Global Telecommunications Conference, GLOBECOM '01*, vol. 1, pp. 594–598 vol.1, 2001.

[JHJvH02] V. Jungnickel, T. Haustein, E. Jorswieck, and C. von Helmolt, "On linear preprocessing in multi-antenna systems," in *IEEE Global Telecommunications Conference*, vol. 1, Nov. 2002, pp. 1012 – 1016 vol.1.

[Jin06] N. Jindal, "MIMO broadcast channels with finite-rate feedback," *IEEE Transactions on Information Theory*, vol. 52, no. 11, pp. 5045–5060, Nov. 2006.

[JJJ+09] S. Jaeckel, L. Jiang, V. Jungnickel, L. Thiele, C. Jandura, G. Sommerkorn, and C. Schneider, "Correlation properties of large and small-scale parameters from multicell channel measurements," in *European Conference on Antennas and Propagation (EuCAP 2009)*, Berlin, Germany, 2009, invited.

[JJT+09] V. Jungnickel, S. Jaeckel, L. Thiele, L. Jiang, U. Krüger, A. Brylka, and C. von Helmolt, "Capacity measurements in a cooperative MIMO network," *IEEE Transactions on Vehicular Technology*, vol. 58, no. 5, pp. 2392–2405, Jun. 2009.

[JMT+09] V. Jungnickel, K. Manolakis, L. Thiele, T. Wirth, and T. Haustein, "Handover sequences for interference-aware transmission in multicell MIMO networks," in *International ITG Workshop on Smart Antennas (WSA 2009)*, Berlin, Germany, Feb. 2009, pp. 1–4.

[Jon41] R. C. Jones, "A new calculus for the treatment of optical systems, i. description and discussion of the calculus," *Journal of the Optical Society of America*, vol. 31, pp. 488–493, 1941.

[JRV+05] N. Jindal, W. Rhee, S. Vishwanath, S. Jafar, and A. Goldsmith, "Sum power iterative water-filling for multi-antenna Gaussian broadcast channels," *IEEE Transactions on Information Theory*, vol. 51, no. 4, pp. 1570 –1580, Apr. 2005.

[JST+09] V. Jungnickel, M. Schellmann, L. Thiele, T. Wirth, T. Haustein, O. Koch, W. Zirwas, and E. Schulz, "Interference-aware scheduling in the multiuser MIMO-OFDM downlink," *IEEE Communicaions Magazine*, Jun. 2009.

[JTB+09] S. Jaeckel, L. Thiele, A. Brylka, L. Jiang, V. Jungnickel, J. Heft, and C. Jandura, "Intercell interference measured in urban areas," *IEEE International Conference on Communications (ICC)*, 2009.

[JTS+08] V. Jungnickel, L. Thiele, M. Schellmann, T. Wirth, W. Zirwas, T. Haustein, and E. Schulz, "Implementation concepts for distributed cooperative transmission," *42nd Asilomar Conference on Signals, Systems and Computers*, Oct. 2008.

[JTW+09] V. Jungnickel, L. Thiele, T. Wirth, T. Haustein, S. Schiffermüller, A. Forck, S. Wahls, S. Jaeckel, S. Schubert, C. Juchems, F. Luhn, R. Zavrtak, H. Droste, G. Kadel, W. Kreher, J. Mueller, W. Stoermer, and G. Wannemacher, "Coordinated multipoint trials in the downlink," in *Proc. 5th IEEE Broadband Wireless Access Workshop (BWAWS), co-located with IEEE GLOBECOM 2009*, Honolulu, Hawai, Nov. 2009.

[JVG04] N. Jindal, S. Vishwanath, and A. Goldsmith, "On the duality of Gaussian multiple-access and broadcast channels," *IEEE Transactions on Information Theory*, vol. 50, no. 5, pp. 768–783, 2004.

[JWS+08] V. Jungnickel, T. Wirth, M. Schellmann, T. Haustein, and W. Zirwas, "Synchronization of cooperative base stations," *IEEE International Symposium on Wireless Communication Systems 2008 (ISWCS2008)*, Oct. 2008.

[KFV06] M. Karakayali, G. Foschini, and R. Valenzuela, "Network coordination for spectrally efficient communications in cellular systems," *IEEE Wireless Commun. Mag.*, vol. 13, pp. 56–61, 2006.

[KG08] S. Kiani and D. Gesbert, "Optimal and distributed scheduling for multicell capacity maximization," *Wireless Communications, IEEE Transactions on*, vol. 7, no. 1, pp. 288 –297, jan. 2008.

[KM99] T. Klingenbrunn and P. Mogensen, "Modelling cross-correlated shadowing in network simulations," in *IEEE 50th Vehicular Technology Conference (VTC 1999 - Fall)*, vol. 3, 1999, pp. 1407 –1411 vol.3.

[KMH+07] P. Kyöstisti, J. Meinilä, L. Hentilä, X. Zhao, T. Jämsä, C. Schneider, M. Narandzić, M. Milojević, A. Hong, J. Ylitalo, V.-M. Holappa, M. Alatossava, R. Bultitude, Y. de Jong, and T. Rautiainen, "IST-4-027756 WINNER II D1.1.2 V1.2: WINNER II channel models," Tech. Rep., 2007.

[KPLK07] I. H. Kim, S. Y. Park, D. Love, and S. J. Kim, "Partial channel state information unitary precoding and codebook design for MIMO broadcast systems," in *IEEE Global Telecommunications Conference, GLOBECOM '07*, Nov. 2007, pp. 1607 –1611.

[LH03a] D. J. Love and R. W. Heath, "Equal gain transmission in multiple-input multiple-output wireless systems," *IEEE Transactions on Communications*, vol. 51, no. 7, pp. 1102–1110, Jul. 2003.

[LH03b] D. Love and J. Heath, R.W., "Limited feedback precoding for spatial multiplexing systems," *IEEE Global Telecommunications Conference, GLOBECOM '03*, vol. 4, pp. 1857–1861 vol.4, 2003.

[LH05] ——, "Limited feedback unitary precoding for spatial multiplexing systems," *IEEE Transactions on Information Theory*, vol. 51, no. 8, pp. 2967–2976, 2005.

[LHL+08] D. Love, R. Heath, V. Lau, D. Gesbert, B. Rao, and M. Andrews, "An overview of limited feedback in wireless communication systems," *IEEE Journal on Selected Areas in Communications*, vol. 26, no. 8, pp. 1341 –1365, Oct. 2008.

[LHZ09] J. Lee, J.-K. Han, and J. Zhang, "MIMO Technologies in 3GPP LTE and LTE-Advanced," *EURASIP Journal on Wireless Communications and Networking*, vol. 2009, no. 302092, May 2009.

[LSB+11] J. Li, T. Svensson, C. Botella, T. Eriksson, X. Xu, and X. Chen, "Joint scheduling and power control in coordinated multi-point clusters," in *IEEE Vehicular Technology Conference (VTC Fall)*, Sep. 2011, pp. 1 –5.

[Mar10] T. Marzetta, "Noncooperative cellular wireless with unlimited numbers of base station antennas," *IEEE Transactions on Wireless Communications*, vol. 9, no. 11, pp. 3590 –3600, Nov. 2010.

[MF07] P. Marsch and G. Fettweis, "A decentralized optimization approach to backhaul-constrained distributed antenna systems," in *16th IST Mobile & Wireless Communications Summit (IST Summit'07)*, Budapest, Hungary, Jul. 2007.

[MF11] ——, "Static clustering for cooperative multi-point (CoMP) in mobile communications," in *IEEE International Conference on Communications (ICC)*, Jun. 2011, pp. 1 –6.

[MKH+10] J. Meinilä, P. Kyösti, L. Hentilä, T. Jämsä, E. Suikkanen, E. Kunnari, and M. Narandžić, "CELTIC / CP5-026: D5.3: WINNER+ Final Channel Models," Tech. Rep., Jun. 2010.

[MKP07] M. Morelli, C.-C. Kuo, and M.-O. Pun, "Synchronization techniques for orthogonal frequency division multiple access (OFDMA): A tutorial review," *Proceedings of the IEEE*, vol. 95, no. 7, pp. 1394–1427, Jul. 2007.

[MTO+11] K. Manolakis, L. Thiele, C. Oberli, T. Haustein, and V. Jungnickel, "Impairment modeling for joint transmission CoMP," in *IEEE 2nd International Conference on Wireless Communications, Vehicular Technology, Information Theory and Aerospace & Electronic System Technology (Wireless VITAE)*, Chennai, India, Mar. 2011, invited.

[NEHA08] B. L. Ng, J. Evans, S. Hanly, and D. Aktas, "Distributed downlink beamforming with cooperative base stations," *IEEE Transactions on Information Theory*, vol. 54, no. 12, pp. 5491–5499, Dec. 2008.

[NMK+07] M. Noda, M. Muraguchi, T. G. Khanh, K. Sakaguchi, and K. Araki, "Eigenmode tomlinson-harashima precoding for multi-antenna multi-user mimo broadcast channel," in *6th International Conference on Information, Communications Signal Processing*, 10-13 2007, pp. 1 –5.

[OCD+12] C. Oestges, N. Czink, P. D. Doncker, V. Degli-Esposti, K. Haneda, W. Joseph, M. Liénard, L. Liu, J. Molina-García-Pardo, M. Narandžić, J. Poutanen, F. Quitin, and E. Tanghe, *Pervasive Mobile and Ambient Wireless Communications (COST Action 2100)*. Springer, 2012, ch. Ch. 3: Radio Channel Modeling for 4G Networks, pp. 67–147.

[OL05] A. Osseiran and A. Logothetis, "Closed loop transmit diversity in WCDMA HS-DSCH," in *61st IEEE Vehicular Technology Conference (VTC 2005-Spring)*, vol. 1, May 2005, pp. 349 – 353 Vol. 1.

[Orf88] S. J. Orfanidis, *Optimum Signal Processing*, 2nd ed. McGraw-Hill, 1988. [Online]. Available: http://www.ece.rutgers.edu/~{}orfanidi/osp2e/

[PF05] D. P. Palomar and J. R. Fonollosa, "Practical algorithms for a family of waterfilling solutions," *IEEE Transactions on Signal Processing*, vol. 53, no. 2, Feb. 2005.

[PGH08] A. Papadogiannis, D. Gesbert, and E. Hardouin, "A dynamic clustering approach in wireless networks with multi-cell cooperative processing," *IEEE International Conference on Communications*, 2008.

[PHG09] A. Papadogiannis, E. Hardouin, and D. Gesbert, "Decentralising multi-cell cooperative processing on the downlink : a novel robust framework," *EURASIP Special Issue on Broadband Wireless Access, Journal on Wireless Communications and Networking*, Aug. 2009.

[PHS05] C. B. Peel, B. M. Hochwald, and A. L. Swindlehurst, "A vector-perturbation technique for near-capacity multi-antenna multi-user communication - part I: channel inversion and regularization," *IEEE Transactions on Communication*, vol. 53, pp. 195 – 202, Jan. 2005.

[PNJvH03] V. Pohl, P. Nguyen, V. Jungnickel, and C. von Helmolt, "Limits of the achievable symbol rate in flat fading MIMO systems," in *Proc. 14th IEEE Intern. Symposium on Personal, Indoor and Mobile Radio Commun. (PIMRC)*, vol. 3, Bejing, China, Sep. 2003, pp. 2548–2552.

[PNJvH05] V. Pohl, P. H. Nguyen, V. Jungnickel, and C. von Helmolt, "Continuous flat-fading MIMO channels: achievable rate and optimal length of the training and data phases," *IEEE Transactions on Wireless Communications*, vol. 4, no. 4, pp. 1889–1900, Jul. 2005.

[RC00] W. Rhee and J. Cioffi, "Increase in capacity of multiuser OFDM system using dynamic subchannel allocation," in *IEEE 51st Vehicular Technology Conference Proceedings, VTC 2000-Spring*, vol. 2, 2000, pp. 1085 –1089 vol.2.

[RHV09] V. Raghavan, M. Honig, and V. Veeravalli, "Performance analysis of RVQ-based limited feedback beamforming codebooks," in *IEEE International Symposium on Information Theory (ISIT)*, Jul. 2009, pp. 2437 –2441.

[Say08] A. H. Sayed, *Adaptive Filters*. Wiley-Interscience, 2008.

[SB04] M. Schubert and H. Boche, "Solution of the multiuser downlink beamforming problem with individual SINR constraints," *IEEE Transactions on Vehicular Technology*, vol. 53, no. 1, pp. 18–28, 2004.

[Sch09] M. Schellmann, "Multi-user MIMO-OFDM in practice: Enabling spectrally efficient transmission over time-varying channels," Ph.D. dissertation, Technische Universität Berlin, Jun. 2009.

[SFFM99] M. Speth, S. Fechtel, G. Fock, and H. Meyr, "Optimum receiver design for wireless broad-band systems using OFDM. I," *IEEE Transactions on Communications*, vol. 47, no. 11, pp. 1668–1677, Nov. 1999.

[SH05] M. Sharif and B. Hassibi, "On the capacity of MIMO broadcast channels with partial side information," *IEEE Transactions on Information Theory*, vol. 51, no. 2, pp. 506–522, Feb. 2005.

[SHC+10] A. Simonsson, B. Hagerman, J. Christoffersson, L. Klockar, C. Koutsimanis, and P. Cosimini, "LTE downlink inter-cell interference assessment in an existing GSM metropolitan deployment," in *IEEE 72nd Vehicular Technology Conference Fall (VTC 2010-Fall)*, Sep. 2010, pp. 1 –5.

[SJSC06] M. Schellmann, V. Jungnickel, A. Sezgin, and E. Costa, "Rate-maximized switching between spatial transmission modes," *IEEE 40st Asilomar Conference on Signals, Systems and Computers*, pp. 1635–1639, Nov. 2006.

[SSH04] Q. H. Spencer, A. Swindlehurst, and M. Haardt, "Zero-forcing methods for downlink spatial multiplexing in multiuser MIMO channels," *IEEE Transactions on Signal Processing*, vol. 52(2), pp. 461–471, Feb. 2004.

[ST08] C. Suh and D. Tse, "Interference alignment for cellular networks," in *46th Annual Allerton Conference on Communication, Control, and Computing*, Sep. 2008, pp. 1037 –1044.

[STHJ10] M. Schellmann, L. Thiele, T. Haustein, and V. Jungnickel, "Spatial transmission mode switching in multiuser MIMO-OFDM systems with user fairness," *IEEE Transactions on Vehicular Technology*, vol. 59, no. 1, pp. 235 –247, Jan. 2010.

[STJH07] M. Schellmann, L. Thiele, V. Jungnickel, and T. Haustein, "A fair score-based scheduler for spatial transmission mode selection," *IEEE 41st Asilomar Conference on Signals, Systems and Computers*, pp. 1961–1966, Nov. 2007.

[STW+09] M. Schellmann, L. Thiele, T. Wirth, T. Haustein, and V. Jungnickel, "Resource Management in MIMO-OFDM systems," *OFDMA: Fundamentals and Applications*, 2009.

[SW97a] S. Shamai and A. Wyner, "Information-theoretic considerations for symmetric, cellular, multiple-access fading channels I," *IEEE Transactions on Information Theory*, vol. 43, no. 6, pp. 1877 –1894, Nov. 1997.

[SW97b] ——, "Information-theoretic considerations for symmetric, cellular, multiple-access fading channels II," *IEEE Transactions on Information Theory*, vol. 43, no. 6, pp. 1895 –1911, Nov. 1997.

[SW12] J. Schreck and G. Wunder, "Interference alignment over limited dimensions for cellular networks: Feasibility and algorithms," in *International ITG Workshop on Smart Antennas (WSA)*, Mar. 2012, pp. 352 –358.

[SYT10] S. Szyszkowicz, H. Yanikomeroglu, and J. Thompson, "On the feasibility of wireless shadowing correlation models," *IEEE Transactions on Vehicular Technology*, vol. 59, no. 9, pp. 4222 –4236, Nov. 2010.

[SZ01] S. Shamai and B. Zaidel, "Enhancing the cellular downlink capacity via co-processing at the transmitting end," *IEEE Vehicular Technology Conference, VTC 2001 Spring*, vol. 3, pp. 1745 –1749 vol.3, 2001.

[TBB+10] L. Thiele, F. Boccardi, C. Botella, T. Svensson, and M. Boldi, "Scheduling-assisted joint processing for CoMP in the framework of the WINNER+ project," in *Future Network Mobile Summit (Florence, Italy)*, Jun. 2010.

[TBH08a] M. Trivellato, F. Boccardi, and H. Huang, "On transceiver design and channel quantization for downlink multiuser MIMO systems with limited feedback," *IEEE Journal on Selected Areas in Communications*, vol. 26, no. 8, pp. 1494–1504, Oct. 2008.

[TBH08b] ——, "Zero-forcing vs. unitary beamforming in multiuser MIMO systems with limited feedback," *IEEE 19th International Symposium on Personal, Indoor and Mobile Radio Communications, PIMRC 2008*, pp. 1–6, Sep. 2008.

[TBT07] M. Trivellato, F. Boccardi, and F. Tosato, "User selection schemes for MIMO broadcast channels with limited feedback," *IEEE 65th Vehicular Technology Conference, 2007. VTC2007-Spring.*, pp. 2089–2093, Apr. 2007.

[TH98] D. Tse and S. Hanly, "Multiaccess fading channels. I. Polymatroid structure, optimal resource allocation and throughput capacities," *IEEE Transactions on Information Theory*, vol. 44, no. 7, pp. 2796 –2815, Nov. 1998.

[TJ08] L. Thiele and V. Jungnickel, "Adaptive transmission in a realistic multicell scenario," *IEEE Radio and Wireless Symposium*, Jan. 2008.

[TJH10] L. Thiele, V. Jungnickel, and T. Haustein, "Interference management for future cellular ofdma systems using coordinated multi-point transmission," *IEICE Transactions on Communications*, vol. E93.B, no. 12, pp. 3228–3237, Dec. 2010, invited.

[TR 09] TR 36.814 V1.0.0, "Evolved universal terrestical radio access (E-UTRA); further advancements for (E-UTRA) physical layer aspects," Feb. 2009.

[TSSJ08] L. Thiele, M. Schellmann, S. Schiffermüller, and V. Jungnickel, "Multi-cell channel estimation using virtual pilots," *IEEE 67th Vehicular Technology Conference VTC2008-Spring*, pp. 1211–1215, May 2008.

[TSW+09] L. Thiele, M. Schellmann, T. Wirth, V. Jungnickel, F. Boccardi, and H. Huang, "DFT-based vs. cooperative MET-based MU-MIMO in the downlink of cellular OFDM systems," *International ITG Workshop on Smart Antennas (WSA 2009)*, Feb. 2009.

[TSWJ08] L. Thiele, M. Schellmann, T. Wirth, and V. Jungnickel, "On the value of synchronous downlink MIMO-OFDMA systems with linear equalizers," *IEEE International Symposium on Wireless Communication Systems (ISWCS08)*, pp. 428–432, Oct. 2008.

[TSWJ09] ——, "Interference-aware scheduling in the synchronous cellular multi-antenna downlink," *IEEE 69th Vehicular Technology Conference VTC2009-Spring, Barcelona, Spain*, Apr. 2009, invited.

[TSZJ07] L. Thiele, M. Schellmann, W. Zirwas, and V. Jungnickel, "Capacity scaling of multi-user MIMO with limited feedback in a multi-cell environment," *41st Asilomar Conference on Signals, Systems and Computers*, Nov. 2007, invited.

[TWB+09] L. Thiele, T. Wirth, K. Börner, M. Olbrich, V. Jungnickel, J. Rumold, and S. Fritze, "Modeling of 3D Field Patterns of Downtilted Antennas and Their Impact on Cellular Systems," *International ITG Workshop on Smart Antennas (WSA 2009)*, Feb. 2009.

[TWH+09] L. Thiele, T. Wirth, T. Haustein, V. Jungnickel, E. Schulz, and W. Zirwas, "A unified feedback scheme for distributed interference management in cellular systems: Benefits and challenges for real-time implementation," *17th Euopean Signal Processing Conference (EUSIPCO2009)*, Aug. 2009, invited.

[TWS+09] L. Thiele, T. Wirth, M. Schellmann, Y. Hadisusanto, and V. Jungnickel, "MU-MIMO with localized downlink base station cooperation and downtilted antennas," in *IEEE International Workshop on LTE Evolution*, Dresden, Germany, Jun. 2009.

[TWS+11] L. Thiele, T. Wirth, M. Schellmann, T. Haustein, and V. Jungnickel, *Coordinated Multi-Point in Mobile Communications - From Theory to Practice*. Cambridge University Press, Jul. 2011, ch. Downlink Multi-User Beamforming with Interference Rejection Combining.

[VHLV09] S. Venkatesan, H. Huang, A. Lozano, and R. Valenzuela, "A WiMAX-based implementation of network MIMO for indoor wireless systems," *EURASIP Journal on Advances in Signal Processing (Special Issue on Multiuser MIMO Transmission with Limited Feedback, Cooperation, and Coordination)*, 2009.

[VJG03] S. Vishwanath, N. Jindal, and A. Goldsmith, "Duality, achievable rates, and sumrate capacity of Gaussian MIMO broadcast channels," *IEEE Transactions on Information Theory*, vol. 49, no. 10, p. 2658Ű2668, Oct. 2003.

[VRH09] C. Van Rensburg and P. Hosein, "Interference coordination through network-synchronized cyclic beamforming," in *70th IEEE Vehicular Technology Conference Fall (VTC 2009-Fall)*, Sep. 2009, pp. 1 –5.

[VT03] P. Viswanath and D. Tse, "Sum capacity of the vector Gaussian broadcast channel and uplink-downlink duality," *IEEE Transactions on Information Theory*, vol. 49, no. 8, pp. 1912–1921, 2003.

[VTL02] P. Viswanath, D. Tse, and R. Laroia, "Opportunistic beamforming using dumb antennas," *IEEE Transactions on Information Theory*, vol. 48, no. 6, pp. 1277–1294, 2002.

[VVH03] H. Viswanathan, S. Venkatesan, and H. Huang, "Downlink capacity evaluation of cellular networks with known-interference cancellation," *IEEE Journal on Selected Areas in Communications*, vol. 21, no. 5, pp. 802 – 811, Jun. 2003.

[WB11] M. Wiese and H. Boche, "The arbitrarily varying multiple-access channel with conferencing encoders," *CoRR*, vol. abs/1105.0319, 2011, submitted to IEEE Transactions on Information Theory, partially appeared in IEEE International Symposium on Information Theory (ISIT 2011).

[WB12a] ——, "Strong secrecy for multiple access channels," *CoRR*, vol. abs/1209.4557, 2012.

[WB12b] R. F. Wyrembelski and H. Boche, "Impact of interference in coexistingwireless networks with applications to arbitrarily varying bidirectional broadcast channels," *Entropy*, vol. 14, pp. 1357–1398, 2012.

[WB12c] R. Wyrembelski and H. Boche, "Physical layer integration of private, common, and confidential messages in bidirectional relay networks," *IEEE Transactions on Wireless Communications*, vol. 11, no. 9, pp. 3170 –3179, Sep. 2012.

[WB12d] ——, "Strong secrecy in compound broadcast channels with confidential messages," in *IEEE International Symposium on Information Theory Proceedings (ISIT)*, Jul. 2012, pp. 76 –80.

[WBB10] R. F. Wyrembelski, I. Bjelaković, and H. Boche, "Bidirectional relaying in wireless networks-impact of degree of coordination," in *IEEE International Conference on Acoustics Speech and Signal Processing (ICASSP)*, march 2010, pp. 3234 –3237.

[WBBJ11] M. Wiese, H. Boche, I. Bjelaković, and V. Jungnickel, "The compound multiple access channel with partially cooperating encoders," *IEEE Transactions on Information Theory*, vol. 57, no. 5, pp. 3045 –3066, May 2011.

[WFHE04] I. C. Wong, A. Forenza, R. W. Heath, and B. L. Evans, "Long range channel prediction for adaptive OFDM systems," in *Thirty-Eighth Asilomar Conference on Signals, Systems and Computers*, vol. 1, 2004, pp. 732–736.

[WGS+11] R. Weber, A. Garavaglia, M. Schulist, S. Brueck, and A. Dekorsy, "Self-organizing adaptive clustering for cooperative multipoint transmission," in *IEEE 73rd Vehicular Technology Conference (VTC Spring)*, May 2011, pp. 1 –5.

[Wil83] F. Willems, "The discrete memoryless multiple access channel with partially cooperating encoders," *IEEE Transactions on Information Theory*, vol. 29, no. 3, pp. 441 – 445, May 1983.

[Win84] J. Winters, "Optimum combining in digital mobile radio with cochannel interference," *IEEE Journal on Selected Areas in Communications*, vol. 2, no. 4, pp. 528–539, 1984.

[WMS+02] T. Weber, I. Maniatis, A. Sklavos, Y. Liu, E. Costa, H. Haas, and E. Schulz, "Joint transmission and detection integrated network (JOINT), a generic proposal for beyond 3G systems," *9th International Conference on Telecommunications (ICT'02), Beijing*, vol. 3, pp. 479 – 483, Jun. 2002. [Online]. Available: citeseer.ist.psu.edu/weber02joint.html

[WSG94] J. Winters, J. Salz, and R. Gitlin, "The impact of antenna diversity on the capacity of wireless communication systems," *IEEE Transactions on Communications*, vol. 42, no. 234, pp. 1740–1751, 1994.

[Wyn94] A. Wyner, "Shannon-theoretic approach to a gaussian cellular multiple-access channel," *IEEE Transactions on Information Theory*, vol. 40, no. 6, pp. 1713 –1727, Nov. 1994.

[YG06] T. Yoo and A. Goldsmith, "On the optimality of multiantenna broadcast scheduling using zero-forcing beamforming," *IEEE Journal on Selected Areas in Communication*, vol. 24, no. 3, pp. 528 – 541, Mar. 2006.

[YL05] C. K. A. Yeung and D. Love, "Performance analysis of random vector quantization limited feedback beamforming," in *Thirty-Ninth Asilomar Conference on Signals, Systems and Computers*, Nov. 2005, pp. 408 –412.

[YL07] W. Yu and T. Lan, "Transmitter optimization for the multi-antenna downlink with per-antenna power constraints," *IEEE Transactions on Signal Processing*, vol. 55, Dec. 2007.

[YR06] W. Yu and W. Rhee, "Degrees of freedom in wireless multiuser spatial multiplex systems with multiple antennas," *IEEE Transactions on Communications*, vol. 54, no. 10, pp. 1747–1753, Oct. 2006.

[ZD04] H. Zhang and H. Dai, "Cochannel interference mitigation and cooperative processing in downlink multicell multiuser MIMO networks," *Eurasip Journal on Wireless Communications and Networking*, vol. 2004, no. 2, pp. 222–235, 2004.

[ZGN+09] S. Zhou, J. Gong, Z. Niu, Y. Jia, and P. Yang, "A decentralized framework for dynamic downlink base station cooperation," in *IEEE Global Telecommunications Conference, GLOBECOM 2009*, Dec. 2009, pp. 1 –6.

[ZHC00] C. Zeng, L. Hoo, and J. Cioff, "Efficient water-filling algorithms for a gaussian multiaccess channel with ISI," *EEE 52nd Vehicular Technology Conference, VTC-Fall 2000*, vol. 3, pp. 1072–1077 vol.3, 2000.

[ZMS+09] W. Zirwas, W. Mennerich, M. Schubert, L. Thiele, V. Jungnickel, and E. Schulz, *Cooperative Transmission Schemes*. CRC Press, Taylor and Francis Group, 2009.

[ZSK+06] W. Zirwas, E. Schulz, J. H. Kim, V. Jungnickel, and M. Schubert, "Distributed organization of cooperative antenna systems," *European Wireless*, Apr. 2006.

[ZSSD11] M. Zhang, M. Shafi, P. J. Smith, and P. A. Dmochowski, "Precoding performance with codebook feedback in a MIMO-OFDM system," in *IEEE International Conference on Communications (ICC)*, Jun. 2011, pp. 1 –6.

[ZT03] L. Zheng and D. Tse, "Diversity and multiplexing: A fundamental tradeoff in multiple-antenna channels," *IEEE Transactions on Information Theory*, vol. 49, no. 5, pp. 1073–1096, May 2003.